Applications of Coarse-Graining Approaches: Volume Averaging, Macrotransport Theory and Scaling Concepts

by

Venkatraghavan Ganesan

B. Tech., Indian Institute of Technology, Madras (1995)

Submitted to the Department of Chemical Engineering
in partial fulfillment of the requirements for the degree of

Doctor of Philosophy in Chemical Engineering

at the

MASSACHUSETTS INSTITUTE OF TECHNOLOGY

September 1999

Author .....
Department of Chemical Engineering
July 28, 1999

Certified by .....
Howard Brenner
Willard H. Dow Professor of Chemical Engineering
Thesis Supervisor

Accepted by ....
Robert Cohen
St. Laurent Professor of Chemical Engineering
Chairman, Committee for Graduate Students

Applications of Coarse-Graining Approaches: Volume Averaging, Macrotransport Theory and Scaling Concepts

by

Venkatraghavan Ganesan

Submitted to the Department of Chemical Engineering
on July 28, 1999, in partial fulfillment of the
requirements for the degree of
Doctor of Philosophy in Chemical Engineering

Abstract

This thesis is concerned with the applications of several "multiscale" concepts to the description of systems wherein the accompanying physical phenomena afford a natural delineation of lengthscales. Explicitly, the thesis demonstrates the use and limitations of the different schemes by invoking specific examples appropriate to each.

The first part of the thesis illustrates the use of spatial averaging techniques to model two-phase flows through porous media. This exposition commences by reviewing and critiquing previous attempts at coarse-graining two-phase flows. Subsequently, we adopt a novel microscale viewpoint (termed the "diffuse interface approach") wherein the averaging procedure can be effected in a somewhat rigorous manner. Explicitly, the fine scale (microscale) equations are averaged to effect the corresponding coarse-grained (macroscale) description. Also illustrated is the use and role of linear irreversible thermodynamics in the context of obtaining the functional form of the constitutive equations at the coarse-grained scale. The proposed scheme possesses conceptual as well as computational and analytical advantages. On the conceptual side, we are able to clearly define and clarify the macroscale concept of capillary pressure, which in contemporary literature is incorrectly confounded with the well-known microscale, pore-level Laplace boundary condition at the curved interfaces between the immiscible phases. In this same context we offer insights into fundamental issues that have afflicted mixture theories involving 'interpenetrating continua.' Within this framework we formulate, in a rigorous manner, definitions of macroscale quantities, following which we identify the pertinent phase-specific Darcy's laws. Moreover, utilizing the outlined framework, one can, in principle, calculate the phenomenological coefficients appearing therein in terms of quadratures of the prescribed microscale data.

The second portion of the thesis demonstrates the utility of concepts abstracted from macrotransport theory to implement coarse-graining procedures in multiscale systems. The first example considered within this context illustrates the manner in which macrotransport theory can be employed to provide quantitative measures of transport rates in flow systems involving laminar chaotic processes. As an illustrative

example, thermal Taylor dispersion theory for time-periodic systems is used to study the extent of chaotic laminar heat transfer enhancement and axial thermal dispersion occurring during combined transverse and axial annular flow between two nonconcentric circular cylinders undergoing alternate rotations. Calculations are performed for three different cases: (i) Concentric cylinder rotation (for which case the resulting circular transverse flow has no effect upon the effective transport properties); (ii) Nonconcentric counter-rotating circular cylinders, each undergoing a steady rotation, thereby creating a time-independent transverse flow field; (iii) Nonconcentric counter- and co-rotating circular cylinders, each undergoing time-periodic alternate rotation while the other remains at rest. A 'regular' enhancement of the heat transfer rate over the concentric cylinder case is observed in case (ii), arising from the presence of a secondary-flow recirculation region. Enhancement due to chaotic advection is observed in case (iii) [about 50% more than that of case (ii) and more than double that of case (i), all other things being equal].

In the second example considered within this same section, calculations are presented for the long-time diffusivity and sedimentation velocity of *associating colloids*. Examples of the latter are micellar solutions and microemulsions. The analysis incorporates the role of reversible association-dissociation processes accompanying the physical-space transport of these clusters through the solution. This is accomplished without the need for pre-averaging by transforming the association-dissociation processes into equivalent 'size-space' diffusional processes, which are then embedded into the simultaneous physical-space transport processes occurring in three-dimensional space so as to obtain a four-dimensional convective-diffusion equation governing transport of the clusters in both the physical and size spaces. A generic 'projection' scheme framework based on generalized Taylor dispersion theory is then applied to the problem, thereby reducing the four-dimensional transport equation to a coarse-grained three-dimensional *physical-space* convective-diffusion equation. Effects arising from the existence of a distribution of cluster sizes are accounted for in the latter formulation governing the *mean* transport process by the appearance of three coarse-grained phenomenological coefficients whose values depend *inter alia* upon the cluster-size distribution. This section illustrates a novel aspect of "coarse-graining," viz., one wherein the space which is coarse-grained corresponds to the cluster size, rather than to the physical spatial scale, the usual circumstances encountered in other examples. This application serves to illustrate the broad generality of coarse-graining procedures beyond physical space homogenization schemes.

The final phase of the thesis illustrates the use of scaling concepts akin to those employed in the description of 'critical-phenomena,' so as to establish the functional form of physical quantities exemplifying the property of self-similarity. An explicit account is given of the nonlocal dynamics (in a quasistatic approximation) involved in two-phase fluid dynamics quantifying flow through porous media. The results obtained are then employed to derive the dynamical equation of motion of a Darcyscale interfacial fluid front. The resulting model of the physical displacement process is then utilized to glean insights into the self-similar scaling behavior (quantified in terms of depinning exponents) of the interfacial fronts observed in experiments on such systems. Invasion and imbibition phenomena are considered separately, and the

features responsible for the different depinning exponents observed in the two cases are pointed out. A Flory-type scaling analysis is also performed on this model, yielding a roughness exponent of $\alpha = 3/4$ in a range of intermediate length scales, in good agreement with experimental observations. Our model possesses a number of features absent in the model widely speculated to be applicable to this scenario, namely the Random Field Ising Model (RFIM). Among other things, our model incorporates physical phenomena existing in actual two-phase fluid flow phenomena that are not reflected in the RFIM model. Additionally, our model furnishes possible reasons for rationalizing discrepancies observed between theory and experiments.

Thesis Supervisor: Howard Brenner
Title: Willard H. Dow Professor of Chemical Engineering

This Thesis is Dedicated to

My family — Who believed that I could do it

Vibha — Who stood by me while I did it

All my professors — Who showed me how to do it

Prof. Howard Brenner — Who made me do it

It is that the sciences do not try to explain, they hardly even try to interpret, they mainly make models. By a model is meant a mathematical construct which, with the addition of certain verbal interpretation, describes observed phenomena. The justification of such a mathematical construct is solely and precisely that, it is expected to work, that is, correctly describe the phenomena from a reasonably wide area.

John von Neumann

"Method in the Physical Sciences,"

Collected Works, Vol. 6

Pergamon Press (1963).

Acknowledgments

In this hallowed tradition of thesis acknowledgements, it is apposite to commence by expressing my sincere gratitude to my dissertation advisor and mentor, Prof. Howard Brenner for his academic inputs, supervision, his warm and infectious sense of humor, and last but not least, his encouragement in allowing me to pursue my own research agenda. His persistent obsession with 'fundamentals,' and the unity of knowledge across fields, has been intimately responsible for inculcating within me the passion for pursuing "true science." I am indebted to him for spending time to serve as my mentor in almost all facets of my life.

I am also extremely grateful to Prof. Mehran Kardar, who spent a significant portion of his time helping me navigate during my flights of fancy on the realm of statistical physics, typically having to teach me from α to ω of a problem. His reservoir of knowledge, his clarity and intuitive ability in thinking, and his capability to convey the same to his audience has inspired me at a critical stage of my intellectual development to look to him as a role model and mentor for my future career. In this regard, I am also equally indebted to Profs. Balakrishnan, Ananth (IIT, Madras) and Prof. Arup Chakraborty (U.C. Berkeley) for initiating me to the fascinating field of statistical field theory and condensed matter physics.

I am also very grateful to Prof. Irwin Oppenheim for his efforts which went far beyond those of a thesis committee member. His efforts, especially to read and comment on my postdoctoral applications, suggesting appropriate persons to contact as well as the appropriate times to do so, truly laid the seeds for my future academic career.

Equally am I thankful to Profs. Deen, Nadim and Stone, my thesis committee members, for allocating time from their busy schedules to serve on my committee, thereby providing valuable inputs and intellectually sparkling discussions during the committee meetings.

I also acknowledge the role played by the Brenner group (most of whom had a transitory existence during my stay) of Michelle Bryden, Shimon Haber (and Miriam),

Udi Gavze (and Yael and Chuppi), Yoram Zimmels, Tony Davis and Carlos Rinaldi, for providing me the intellectual fodder during my stay in 66-569. Special thanks also goes to my friends Rava da Silveira, Dan Kamei, Jenny Fujii, Pat Walton, Ravi Radhakrishnan and Shankar Vaidhyaraman for their constant encouragement and willingness to put in a patient ear whenever I wanted to discuss my research. There are a number of other people who have had academic interactions with me during the course of this thesis and so have had direct or indirect influences upon this thesis. The following pages would not suffice to recount the entire roster of people I was privileged to know and share thoughts with.

On a personal side, I deeply appreciate the efforts of Arline Benford and Joan Chisholm in putting up with me and for making the 5th floor of Building 66 a real pleasure in which to live. Their activities, extending beyond conventional secretarial duties, served to dispel any feelings of homesickness which descended upon me unbidden at fleeting moments.

Lastly, I wish to acknowledge the role played by my parents and my sister. Without their encouragement and patience in dealing with my tantrums and eccentricities, my doctorate would have been a nonstarter. Of course, no words would suffice to express my appreciation for the efforts and encouragement of my wife, Vibha, especially for being there when I needed her most.

No acknowledgement is complete without an explicit mention of the source of my sustenance while at MIT. This work was financially supported by the Office of Basic Energy Sciences of the U.S. Department of Energy as well as by a "Grand Challenge Award" from the Mathematical, Information and Computational Sciences Division within the Office of Computational and Technology Research of the Office of Energy Research of the DOE.

Contents

List of Figures

List of Tables

Chapter 1

Overview

This chapter provides an overview of the specific issues and the examples considered in this thesis. This chapter commences with a brief exposition on the features of multiscale systems, particularly emphasizing the manifestation of coarse-grained behavior. Subsequently, we provide an outline of the different portions of the thesis, emphasizing their explicit relationship to the broader theme of the whole undertaking. This chapter concludes with a brief discussion on the organization and format of the thesis.

1.1 Multiscale Systems

This thesis is concerned almost exclusively with unique aspects encountered in describing multiscale systems. Studies pertaining to multiscale systems are especially important, embodying both fundamental and practical ramifications. This privileged importance arises from the ubiquity of such systems in Nature, as well as from the intellectual challenges they evoke in the course of homogenizing such systems. Probably the most basic example of a multiscale system is constituted by the atoms which comprise all the known living and nonliving entities in the universe. Each chemical entity termed an atom is itself comprised of more fundamental units, designated as

electrons, protons, etc.[1] The motion and the behavior of these fundamental units is embodied within the quantum mechanical probability density of these entities. However, despite the incredibly vast amount of information required to quantify the quantum-probabilistic description of these entities, the macroscopic behavior of the atom manifests but a few generic physical properties — the magnitude of each being however, intimately related to and derived from the probability density distribution of the fundamental entities constituting the atom. This conception provides one of most fundamental manifestations of 'multiscale' behavior. While at the *fine scale*, the description of the systems is enabled by a quantum mechanical description of all the entities, the *macroscopic behavior* is described (and governed) by the physical properties of the atom, which represents a *coarse-grained* representation of the fine-scale behavior.

More examples of multiscale behavior can also be envisioned. One of the classic examples is constituted by the abstract conception of 'life' and its relationship to the fundamental entities constituting it. At the fine scale we have the elements and molecules which constitute the biologically fundamental entities like genes etc., while the organized behavior of the same biologically fundamental entities like genes constitute the macroscale or coarse-grained behavior. In this case however, the complete resolution of the relationship between the macroscale behavior to the microscale behavior is yet to be achieved. This question was first raised (in a formal manner), by the quantum theorist Schrodinger [1]. While he has been proved to be incorrect in the context of a number of ideas which he put forth claiming to be the solution of this issue, nevertheless the fundamental recognition of the multiscale manifestation still retains its validity.

While the above constitute fundamental examples wherein the multiscale behavior is evident, practical examples aplenty also manifest multiscale behavior. The equilibrium and nonequilibrium properties exhibited by fluids and solids are examples of the macroscale manifestation of the innumerous microscale interactions between

[1]Fundamental units like electrons might themselves be composed made of yet more fundamental units like quarks.

the molecules constituting the fluid or solid. Such equilibrium and nonequilibrium properties constitute the brain of most of chemical and other technological processes, thereby rendering studies on multiscale systems important and imperative.

The objectives of this thesis are quite modest in comparison to the grandiose issues raised in the above discussion. In essence, the underlying question constituting the entire thesis can be stated as follows: "If the fine scale knowledge of a system can be embodied within a reasonable microscale model, can we say anything about the macroscale behavior of the system, explicitly the model applicable thereto ?" The generality of this question would evidently invite a resounding "yes" for an answer. However, a moment of reflection on the question and the accompanying answer serves to clarify that the issue in multiscale systems is not the recognition that the macroscale behavior constitutes a manifestation of the microscale behavior, but rather, the explicit and possibly quantitative identification of such a relationship. Towards this objective, the thesis deals with relevant physical examples wherein such an identification can, with ingenuity, be determined. It is to be clarified at this juncture that this thesis does not deal with development of general techniques for coarse-graining. Rather, in most cases it employs methods which have been developed or implicitly assumed in other contexts. The achievements of this thesis can be identified as comprising *novel formulations of several microscale-level problems serving to enable application of appropriate coarse-graining techniques to identify the corresponding macroscale behavior.*

A vast number of coarse-graining (homogenization) techniques have been developed explicitly and implicitly within different contexts. However, despite the presence of the requisite tools, neither the exact relationship of the macroscale attributes of an arbitrary system to its comparable microscale attributes, nor the coarse-graining technique to be applied to glean such information, is generally self-evident. This thesis concerns itself with applications of coarse-graining techniques to four distinct examples, each embodying quite distinct characteristics. We undertake in the following sections a brief exposition, describing the salient features and the specific achievements within the examples considered in this thesis. Concomitantly, we outline the

explicit 'coarse-graining' involved in each of the examples considered. Furthermore, we also elucidate a brief outline of the organization of each of the different parts of the thesis.

1.2 Part 1: A Diffuse Interface Model of Two Phase Flows in Porous Media

A single-phase, two-component mixture Darcyscale model characterized by a diffuse interface is proposed as a rational alternative to the conventional singular interface Darcyscale empirical model currently employed for analyzing two-phase flows of immiscible fluids through porous media. The proposed scheme possesses conceptual as well as computational and analytical advantages. On the conceptual side, we are able to clearly define the macroscale concept of capillary pressure, which in contemporary literature is incorrectly confounded with the well-known microscale, pore-level Laplace boundary condition at the curved interfaces between the immiscible phases. In this same context we offer insights into fundamental issues that have afflicted mixture theories involving 'interpenetrating continua.' This is accomplished in part by clarifying the distinction between whether the continua being referred to constitute *phases* (consisting of 'immiscible' multiphase continua) or *species* (present in an inhomogeneous single-phase continuum). In particular, we show that the issue devolves upon the *scale* at which the phenomenon is viewed. On the computational and analytic sides our scheme offers the advantages of dealing with *continuous* fields rather than with *discontinuous* fields, the latter necessitated in contemporary literature by the existence of singular (mobile) phase boundaries, namely interfaces. Also on the analytical side, our scheme permits a formal physico-mathematical transition from the diffuse microscale to the coarser singular-surface scale view, by using singular perturbation techniques to achieve the requisite change in scale. Within this framework we formulate, in a rigorous manner, definitions of macroscale quantities, following which we identify the pertinent phase-specific Darcy's laws. Moreover, one can, in principle,

calculate the phenomenological coefficients appearing therein in terms of quadratures of the prescribed microscale data. Our macroscale framework treats the Darcyscale continuum as a multicomponent mixture (referred to as the 'diffuse Darcyscale' view) rather than adopting the more commonly-employed coarse-grained picture embodied in interpenetrating continua models or singular-surface Darcyscale models. This fine-scale viewpoint is directed towards the foundational aspects of two-phase flows at both the micro- and macroscales — especially with regard to the existence and interpretation of phase-specific Darcy's laws, including capillary pressure as a macroscale field variable. Eventually, we implement this framework with a simplified linear example to substantiate our thesis. Our study embodies several distinct investigations, logically intertwined by the common objective of erecting rational foundations for describing and quantifying two-phase flows through porous media.

This part of the thesis implements the most common of the coarse-graining approaches to multiscale systems, namely the volume averaging technique. Such an approach is utilized to implement the transition from the microscale viewpoint to the coarse-grained, macro- or Darcyscale viewpoint. Concomitantly, we elucidate the issues which typically need to be accounted in defining a volume averaging procedure. These issues transcend mathematical details, and embody the physical definitions of the macro- (or coarse-) scale physical quantities themselves. Subsequent to our criticism of earlier theories ('singular' interface models), we invoke the 'diffuse' interface viewpoint to outline the physical definitions of the macroscale quantities which satisfy the constraints imposed by the physical meaning of these fields. As is common with the execution of most volume averaging (and statistical averaging) techniques, we encounter issues relating to the closure of the macroscale equations. This part of the thesis also elucidates a specific tool by which such issues can be resolved, enabling us to propose possible functional forms of the macroscale constitutive equations.

This part of the thesis is organized as follows: Chapter 2 provides a brief introduction to the theory of multiphase flows in porous media. We review and critique some of the previous researches, and thereby simultaneously outline the motivations for our own research. Subsequently, chapter 3 provides an exposition of the novel framework

(diffuse interface model) used to model two-phase flows in porous media. In chapter 4 we outline a coarse-graining procedure for implementing the transition from the microscale to the macroscale level, within the framework embodied by the diffuse interface model. Chapter 5 concerns the explicit identification of the phase-specific quantities at the macroscale level. Finally, in chapter 6 we utilize considerations derived from nonequilibrium thermodynamics to glean insights into the functional form of the macroscale constitutive equations.

1.3 Part 2: Applications of Macrotransport Theory

This part of the thesis deals with the explicit application of macrotransport theory (or generalized Taylor dispersion theory) to two novel applications, enabling us thereby to quantify the macroscale transport and dispersion properties encountered in these systems. Macrotransport theory constitutes a generalized Taylor dispersion theory, which furnishes a rigorous coarse-grained description of the convective-diffusion transport of a 'Brownian tracer.' (Chapter 8 elucidates the precise manner in which the concept of a Brownian tracer can be generalized). At the fine scale the transport of the Brownian tracer occurs within two orthogonal spaces, termed the "local" and the "global" spaces respectively. The coarse-grained description of the transport of the averaged Brownian tracer (averaging being accomplished over the local space) embodies the convective-diffusive transport of the tracer occurring exclusively within the global space, albeit with effective transport coefficients. These coarse-grained, global-space transport coefficients embody the transport process occurring within the local space in an averaged manner, whereby, the quantitative magnitudes of these coefficients, along with their physical *Lagrangian* definitions (refer to chapter 8) provide a measure of the transport processes occurring within the local space. This conception is utilized in a novel manner in the examples considered in this part of the thesis, thereby providing a nontrivial quantitative measure of the transport processes

occurring within the local space.

This part of the thesis is subdivided into two chapter, each of which individually concerns the application of the macrotransport theory to the specific example considered therein. These chapters follow subsequent to a brief elucidation of the salient concepts of macrotransport theory. Explicit details are furnished in chapter 8.

1.3.1 Chaotic Heat Transfer Enhancement in Rotating Eccentric Cylinder Configuration

Thermal Taylor dispersion theory for time-periodic systems is used to study the extent of chaotic laminar heat transfer enhancement and axial thermal dispersion occurring during combined transverse and axial annular flow between two nonconcentric circular cylinders undergoing alternate rotations. A local Newton's 'law of cooling' heat transfer boundary condition is used on the outer cylinder, whereas the inner cylinder is supposed insulated. The effective heat transfer coefficient $\bar{H}^*$, describing the global rate of heat loss from the system (differing in general from the true microscale Newton's law heat transfer coefficient h on the outer cylinder), is calculated as a function of the system parameters, thereby serving to quantify the extent of chaotic heat transfer enhancement. The axial thermal Taylor dispersivity provides an independent measure of the effects of chaotic mixing, as too does the axial thermal velocity. Calculations are performed for three different cases: (i) Concentric cylinder rotation (for which case the resulting circular transverse flow has no effect upon the effective transport properties); (ii) Nonconcentric counter-rotating circular cylinders, each undergoing a steady rotation, thereby creating a time-independent transverse flow field; (iii) Nonconcentric counter- and co-rotating circular cylinders, each undergoing time-periodic alternate rotation while the other remains at rest. A 'regular' enhancement of the heat transfer rate over the concentric cylinder case is observed in case (ii), arising from the presence of a secondary-flow recirculation region. Enhancement due to chaotic advection is observed in case (iii) [about 50% more than that of case (ii) and more than double that of case (i), all other things being equal]. Concomitant

values of the axial thermal Taylor dispersivity and axial thermal velocity confirms the existence of enhanced transverse transport due to chaotic advection. It is observed that the functional dependence of the enhanced heat transfer rate upon the system parameters does not consistently display the same trends as are qualitatively suggested by the 'degree of chaoticity' of the comparable Poincaré plots. This observation signals the need for caution in simply assuming that the greater the degree of chaotic 'mixing' implicit in the Poincaré plot the greater will be the corresponding global transport rate. By a simple redefinition of the symbols used in the present research, our energy transport results may be re-interpreted so as to apply to the case of reactive-species transport involving a first-order irreversible chemical reaction occurring on the outer-cylinder surface; explicitly, the Nusselt number quantifying the local heat transfer coefficient rate is simply replaced by a comparable Damköhler number quantifying the local kinetics of the surface reaction.

1.3.2 Long-time Non-preaveraged Diffusivity and Sedimentation Velocity of Clusters: Applications to Micellar Solutions

Calculations are presented for the long-time diffusivity and sedimentation velocity of *associating colloids*. Examples of the latter are micellar solutions and microemulsions. The analysis incorporates the role of reversible association-dissociation processes accompanying the physical-space transport of these clusters through the solution. This is accomplished without the need for pre-averaging by transforming the association-dissociation processes into equivalent 'size-space' diffusional processes, which are then embedded into the simultaneous physical-space transport processes occurring in three-dimensional space so as to obtain a four-dimensional convective-diffusion equation governing transport of the clusters in both the physical and size spaces. A generic 'projection' scheme framework based on generalized Taylor dispersion theory is then applied to the problem, thereby reducing the four-dimensional transport equation to a coarse-grained three-dimensional *physical-space* convective-diffusion equation. Effects

arising from the existence of a distribution of cluster sizes are accounted for in the latter formulation governing the *mean* transport process by the appearance of three coarse-grained phenomenological coefficients whose values depend *inter alia* upon the cluster-size distribution. These 'macrotransport' coefficients include a mean sedimentation velocity vector arising from the action of external forces (if any), a mean molecular diffusivity dyadic, and an additional diffusive-type contribution to the diffusivity corresponding to a convective ('Taylor') dispersivity. The latter contribution arises as a consequence of the spread in settling velocities of the differently-sized clusters. The generic framework developed is illustrated by applications to two classes of micellar solutions: (*i*) solutions comprised of spherical micelles; (*ii*) solutions comprised of cylindrical or worm-like micelles (so-called 'living polymers'). Each spherical micelle is modeled as an impenetrable rigid sphere whose radius is determined by its aggregation number. The living polymers are modeled by the Debye-Bueche theory, wherein a coiled macromolecular chain is regarded as a Brownian 'sponge-like' porous sphere through whose interior solvent percolates. Calculations of the resulting macrotransport coefficients, including their scaling relationships, are presented for both cases, and their physical significance discussed in terms of the underlying microscale physics.

1.4 Part 3: Dynamics of Two-Phase Fluid Interfaces in Random Porous Media

This part of the thesis concerns the phenomenological behavior of self-similar systems. The analysis of systems exhibiting the property of self-similarity is much simplified owing to the fact that the physical properties of interest remain unchanged in functionality under the operation of coarse-graining. Such a property establishes an intimate connection between self-similar behavior and power law characteristics. Utilizing this relationship conjointly with the physical implications of self-similarity enables the explicit determination of the scaling exponents describing the behavior of

the self-similar physical property.

This part of the thesis commences (chapter 12) with an exposition on the phenomenon of self-similarity, both in deterministic and statistical context, and their explicit relationship to power-law behavior. Subsequently, we expound upon the salient concepts of self similarity in the context of interfacial fluctuations. Such concepts are utilized in chapter 13 to analyze the problem of interest.

In chapter 13, explicit account is given of the nonlocal dynamics (in a quasistatic approximation) involved in two-phase fluid dynamics quantifying flow through porous media. The results are then used to derive the dynamical equation of motion of a Darcyscale interfacial fluid front. Such a model is then utilized to glean insights into the self-similar scaling behavior (quantified in terms of depinning exponents) of the interfacial fronts experimentally observed in such systems. We consider the cases of invasion and imbibition separately, and point out the features responsible for the different depinning exponents observed in the two cases. A Flory-type scaling analysis is also performed on this model, and yields a roughness exponent $\alpha = 3/4$ in a range of intermediate length scales — in good agreement with experimental observations. Our model possesses a number of features absent in the model widely speculated to be applicable to this scenario, namely the Random Field Ising Model (RFIM). Among other things, it incorporates physical phenomena existing in two-phase fluid flow phenomena that are not reflected in the RFIM model. Additionally, our model furnishes possible reasons for rationalizing discrepancies observed between experiments and theory.

1.5 Conclusions

The exposition of the previous sections outlines specific issues considered in the several chapters of the thesis. While their common theme reflects our emphasis on 'multiscale' modeling, the explicit achievements of any specific example transcend this commonality. Therefore, in the different sections of the text we specifically allude to the 'coarse-graining' aspect invoked, only after detailing the conclusions arising from

the specific achievements. However, based on the above exposition together with the physical description accompanying the specific examples, the explicit identification of the 'multiscales' and the 'coarse-graining' is rendered self-evident in the different examples.

The above discussion in conjunction with the discussion preceding each of the different examples considered in this thesis serves to underline the importance and the ubiquitousness of multiscale systems in nature. From a practical viewpoint, it has become imperative to discover the explicit relationship of the macroscale behavior to the precursor microscale phenomena, thereby enabling one to facilitate control of the macroscale behavior by appropriately tuning the microscale properties. This thesis serves to illustrate some of the techniques available to glean such information.

1.6 Format of Thesis

In view of the diverse nature of the very distinct applications considered, this thesis is organized in a manner which attempts to optimize its comprehensibility. For instance, to ease the efforts requisite to cross-referencing, separate list of references is provided at the end of each chapter. A roster of all the figures and tables of this thesis initiate the textual content of the thesis. Further, each of the three distinct parts of the thesis begins with an introduction, which expounds the specific issues considered therein, emphasizing the salient concepts utilized in the analysis of that issue. Following the introduction, we effect the analysis of the particular issue of interest. The salient features and achievements of each example are recapitulated in the section concluding the analysis. This section also outlines possible future directions pertinent to the specific example analyzed. Such an exposition eschews the need for an overall conclusion to this thesis. Indicated within the different portions of the thesis is the relationship to coarse-graining and multiscales; however, we do not lapse into a detailed discussion of the same. The underlying reasons for such an attitude lies in the exposition of the above sections, considered together with our objective of emphasizing the specific achievements rather than those consistent with

the broader theme. Finally, in applicable cases, we also indicate at the outset the literature citation of the publication which the text embodies.

References

[1] E. Schrodinger, *What is life ? : The physical aspect of the living cell*, Cambridge University Press, New York (1945).

Part 1: A Diffuse Interface Model of Two Phase Flows in Porous Media

Chapter 2

Introduction

Reference: Venkat Ganesan and Howard Brenner, "A diffuse interface model of two-phase flow in porous media," *Proc. R. Soc. Lond. A*, In press (1999).

2.1 Flows in Porous Media

A plethora of natural phenomena and engineered processes involve the flow of immiscible fluids through porous media. For example, the movement of water and air through soils, relevant to the field of hydrology [39], has long been studied from both theoretical and experimental perspectives beginning with the pioneering work of Buckingham [10]. In the field of petroleum engineering, the secondary[1] and tertiary stages of oil recovery constitute economically important examples of biphasic flows in porous media. Examples of bi- and multi-phase flows relevant to industrial applications are far too numerous and well known to require review here. An overall introduction relevant to applications is provided by Marle [34].

Theoretical analysis of biphasic flows through a porous matrix, which constitutes the main focus of this part of the thesis, is extremely complicated owing, *inter alia*, to the complex geometric configuration of the pore space. Realistic porous-medium geometries constitute a virtually intractable configuration, even for single-phase flows.

[1] In the secondary stage of oil recovery, crude oil is often displaced from the interstices of the rock by injecting water.

In fact, complete experimental characterization of the skeletal structure of an actual porous medium is itself an extremely difficult geometric proposition [2].

Given these circumstances, and motivated by both hydrological and petroleum engineering applications, it has proved expedient heretofore to formulate theoretical analyses of fluid flow phenomena through porous media at an observable scale (the Darcyscale or macroscale) through the use of averaged pore-scale (i.e., microscale) fields. Fundamental to this notion is the assumption that to each macroscale 'point' there corresponds a microscale volume element encompassing a representative sample of the local (instantaneous or time-averaged) contents of the porous medium in the neighborhood of that point [4]. This dual scale 'micro-macro' modeling is justified under the assumption that there exists a wide disparity in linear dimensions between the pore and observable scales, whence microscale lengths appear as infinitesimals at the macroscale. The porous rock formations present in naturally-occurring oil recovery wells exemplify such disparate length scales. While on the one hand the pore level is characterized by length scales of the orders of millimeters, with pore sizes of the order of microns, on the other hand the Darcyscale or macroscale is characterized by changes occurring on the lengthscales of meters — thereby facilitating such a 'macro' approach [cf. Fig. (2-1) for an illustration of the 'micro-macro' viewpoint].

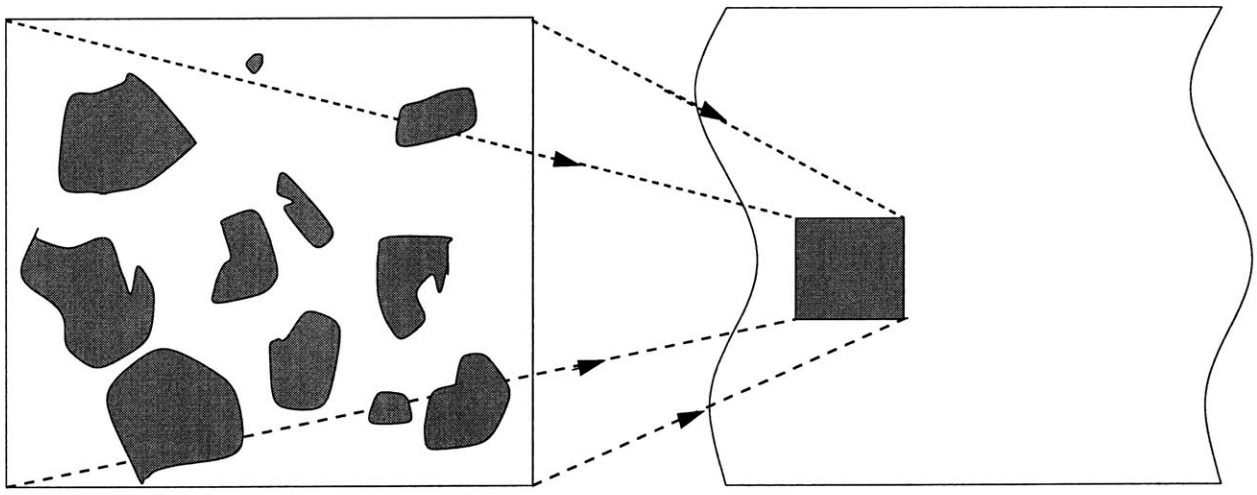

Figure 2-1: The "micro-" (or pore-level) and the "macro-" (or Darcy level) scale of a porous medium.

Under such a micro-macro modeling approach, and for single-phase flows, Darcy's law governs the slow, monophasic flow of a Newtonian fluid through a porous medium under the animating effects of gravity and/or externally imposed pressure gradients [36]. The essence of Darcy's law is the relationship between the macroscopic pressure gradient $\bar{\nabla}\overline{p}$ and the macroscopic (superficial) velocity vector $\overline{\mathbf{v}}$. (Notation for the macroscopic quantities is clarified in a later section):

$$\overline{\mathbf{v}} = -\frac{\mathbf{K}}{\mu} \cdot (\bar{\nabla}\overline{p} - \overline{\rho}\mathbf{g}), \tag{2.1}$$

where μ and $\overline{\rho}$ respectively denote the viscosity and the density of the interstitial fluid, $\mathbf{g}$ is the gravity vector, and $\mathbf{K}$ the permeability tensor. The latter phenomenological coefficient encapsulates all of the macroscopically unobservable microscale phenomena. For a macroscopically inhomogeneous flow the above relationship is conventionally assumed to hold at each macroscale point $\overline{\mathbf{R}}$ in the porous medium.

Though proposed empirically based on experimental observations [14], the single phase Darcy's law (2.1) has subsequently been proved by rigorous theoretical arguments [2, 4, 6, 7, 36]. Such theoretical efforts have primarily focussed on the volume averaging of the microscale equations utilizing realistic assumptions regarding the geometrical nature of the porous medium. In general, such studies can be divided into two categories depending on the particular assumption employed to model the geometry of the porous medium. Studies belonging to the first category employ a periodic model of the microscale level [2, 6, 7], whereas those belonging to the latter category employ a disordered, statistical model of the microscale geometry [4, 36]. Both approaches have been shown to yield predictions which accord semi-quantitatively with observed experimental facts.

In modeling multiphase flows, Darcy's law has been interpreted as applying to each phase separately, this multiphase analog of Darcy's law being proposed on an empirical basis [34]. Explicitly, with $\overline{\mathbf{v}}_\alpha$ the superficial or seepage velocity vector of

phase α relative to the fixed pores, the two-phase form of Darcy's law is taken to be

$$\overline{\mathbf{v}}_\alpha = -\frac{1}{\mu_\alpha} K \mathbf{K}_{r\alpha} \cdot (\bar{\nabla} \overline{p}_\alpha - \overline{\rho}_\alpha \mathbf{g}) \qquad (\alpha = 1, 2), \tag{2.2}$$

where $\mathbf{K}_{r\alpha}$ represents the relative permeability of phase α. The latter is defined as

$$\mathbf{K}_{r\alpha} = \mathbf{K}_\alpha / \|\mathbf{K}\|,$$

with $\mathbf{K}_\alpha$ the permeability of the porous medium to phase α, and $\|\mathbf{K}\|$ a norm of the single-phase permeability of the porous medium (assumed to be a strictly geometrical quantity, possessing the same value for each phase) [cf. eq. (2.1)]; $\overline{\rho}_\alpha$ denotes the macroscopic density of phase α (i.e., the mass of phase α per unit of macroscopic interstitial volume). The presence of more than one phase is conventionally quantified through the saturation s_α ($s_1 + s_2 = 1$), the latter denoting the macroscopic volume fraction of phase α. $\mathbf{K}_{r\alpha}$ is assumed to be dependent only on the saturations. Furthermore, $\overline{p}_1 - \overline{p}_2 = P_c[s_1]$ defines the capillary pressure, assumed to be a function only of the saturation.

In contrast to the experimental and the theoretical success of single phase Darcy's law, the biphasic analog (2.2) has defied a complete understanding. The following sections reviews and critiques some of the aspects which previous theoretical researches on multiphase flows have focused their efforts upon.

2.2 Review of Prior Studies

Table 2.1 presents a brief literature review of some of the previous researches and the specific issues addressed therein. The three major fundamental aspects of multiphase flows towards which prior researches have primarily been directed are as follows:

(i) Many studies (e.g., [16, 32, 34]) have focused on the dynamics of displacement fronts in two-phase systems, modeling the resulting phenomena using the multiphase form (2.2) of Darcy's law. Conservation equations for the respective saturations

s_1 and s_2, namely

$$\frac{\partial s_1}{\partial t} + \nabla \cdot (s_1 \mathbf{v}_1) = 0; \qquad \frac{\partial s_2}{\partial t} + \nabla \cdot (s_2 \mathbf{v}_2) = 0, \tag{2.3a,b}$$

supplement (2.2) — with closure of the system of equations effected by the relationships $P_c = P_c[s_1]$ and $\mathbf{K}_{r\alpha} = \mathbf{K}_{r\alpha}[s_1]$, the explicit functional relationship being assumed known from experiments.

Researches on this particular aspect of multiphase flow has been pioneered by Buckley & Leverett [11] and others (refer table 2.1). A majority of these studies are concerned with the analysis of the explicit nature of the solutions arising from the set of differential equations constituted by (2.3a,b) and the two-phase Darcy's laws (2.2).

(ii) Percolation theories [9] have been used as simplistic models of the complex pore-level flow phenomena [29]. These theories, which concentrate on universal behavior invariant to the quantitative geometrical details of the system (as well as to the physical properties of the flowing fluids), are usually used to model transitions occurring between gross types of system behavior. Some such characteristic features studied by employing such models include the 'critical' transitions observed during the drainage and wetting processes in two-phase flows. Within the context of percolation theories, such transitions are claimed to be a manifestation of a percolation transition occurring with the system. However, the exact relationship between such discrete models (employing a lattice structure to characterize the porous medium) and the actual flow phenomena taking place in porous media has not been rationally established [1].

(iii) A third aspect of research, pursued primarily by continuum mechanicians [22, 33], attempts to establish the credibility of the macroscale equations (2.2) to (2.3a,b), by averaging the 'pore-level' Navier-Stokes and continuity equations underlying them, albeit generally by different schemes specific to each investigator. Such studies are of fundamental importance since, in contrast to the situation accompanying single-phase flows, the two-phase Darcy's laws have not been firmly established

Table 2.1: A brief literature review of previous researches on two phase flows.

◯ Darcy's law to two-phase flows
- Muskat, Wyckoff, Botset and Myres [35]
- Douglas, Blair and Wagner [19]
- Fayers and Perrine [21]

◯ Buckley-Leverett approach to two-phase flows
- Buckley and Leverett [11]
- Cardwell [13]
- Fayers and Perrine [21]
- Schmidt, Soo and Radke [43]

◯ Displacement of interfacial fronts
- Douglas, Blair and Wagner [19]
- Rachford [42]
- Yortsos and Fokas [48]

◯ Percolation theories
- Lenormand [30, 31]
- deGennes [16, 17]
- Larson, Scriven and Davis [29]

◯ Viscous fingering instability
- van Meures and van der Poel [45]
- Rachford [41]
- Homsy [24]

◯ Derivation of two phase Darcy's laws
- Whitaker [46]
- Gray and Hassanizadeh [22, 23]
- Marle [33]
- Auriault [3]

either on theoretical or experimental grounds. A rigorous derivation of the macroscale equations for two phase flows, would possibly elucidate the regime of validity of the Darcy's laws and the other macroscale concepts employed in the description of two phase flows.

Our own contribution in this work falls into the third category listed above, although from a unique perspective which involves viewing the fluid-fluid interfaces in a porous medium as diffuse, continuous transition regions, rather than as singular surfaces separating immiscible phases. It should however be noted that even the past singular interface efforts [22, 33, 38, 46], aimed at rationally effecting this micro-macro transition, have generally resulted in only partial (and in some cases even contradictory) answers, thus embedding the bi-(and multi-) phasic Darcy's law as yet only within an empirical framework. However, it has long been argued [23] that empirical approaches to modeling multiphase flows based on assumed analogies with single-phase flows might be invalidated either by theory, experiments, or both. We expound below on what we believe to be some of the accepted shortcomings of such an empirical extension. Eventually, this critique provides the motivation for our own works:

2.3 Critique of Previous Researches

(a) Whereas Darcy's law for single-phase flow can be proved rigorously [27, 36] beginning with a microscale model of the pertinent flow phenomena, the rational extension of this approach to multiphase flows has not yet been achieved. Even the choices for the appropriate variables to describe such multiphase flows (saturation s_1, capillary pressure P_c) have yet to rigorously justified [1]. Furthermore, the fundamental assumption that the seepage velocity of each phase should depend functionally only upon the pressure gradient existing in that phase has been called into question [16, 26].

(b) A natural fallout arising from the traditional choice of independent variables is the presence of the capillary pressure P_c, which is usually branded as an 'experimental' quantity [16, 34]. The physical interpretation of this variable has proved a

major deterrent to many theoretical analyses of multiphase flows for manifold reasons — the primary obstacle being the commonly-observed hysteretic phenomena occurring in experimental capillary pressure vs saturation curves [Fig. (2-2)], depending on whether drainage (displacement of the wetting fluid) or imbibition (displacement of the nonwetting fluid) is involved. Though normally represented by two distinct curves, it is not universally recognized that the capillary pressure may also take on any value intermediate between the two. Yet to be explained is the fundamental reason for expecting such a 'phase equilibrium' type of relationship to exist between the macroscopic pressures in the two flowing phases — neither of which phases exists in a state of equilibrium, much less with one another. In addition, the experimental capillary pressure curves are obtained by allowing the multiphase mixture to attain static equilibrium. It is questionable whether use of the same *static* data is appropriate for modeling the inherently *dynamical* phenomena occurring during flow through porous media, though that is what is frequently done.

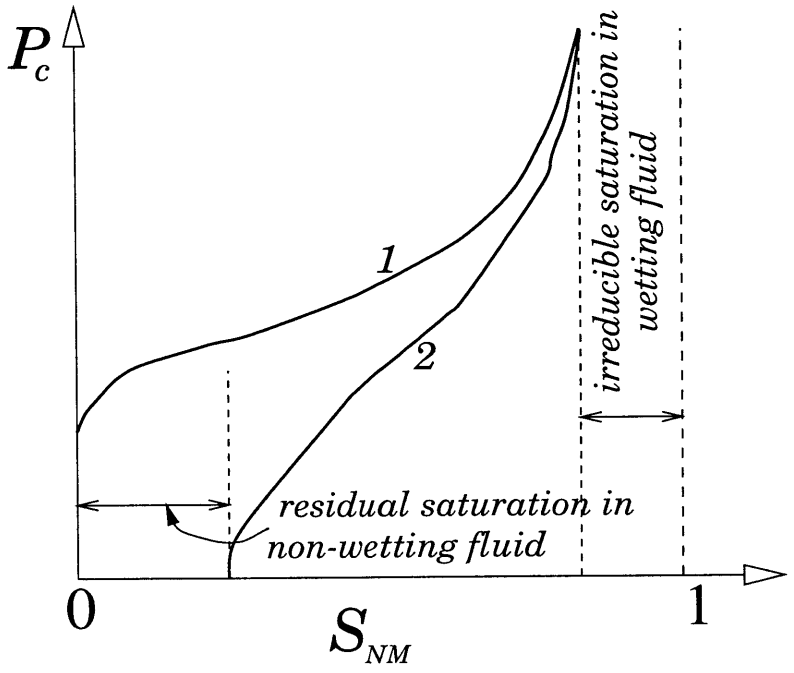

Figure 2-2: Capillary pressure vs saturation relationship. S_{NM} represents the saturation of the nonwetting fluid [adapted from Marle (1981)]. Refer chapter 6 for a description, and a possible explanation of this plot.

Our major criticism of prior approaches to multiphase flow modeling lies in their failure to clearly distinguish conceptually between what constitutes a 'phase' and what constitutes a 'component' (or 'species') [5]. The confusion is compounded by loose usage of the concept of interpenetrating continua [22]. Such interpenetrating continuum (IPC)-type theories of immiscible mixtures were originally formulated in the context of fluid-*solid* particle mixtures [37], wherein such a viewpoint seemed intuitively appropriate, especially when no material was exchanged between the solid and the fluid phases. Among other distinguishing features of this special class of mixtures is the fact that which of the two phases constitutes the *continuous* phase is never in doubt. However, mixture theories for immiscible fluid-fluid systems possess manifestly contrasting features [5, 18], primarily as a result of the interfacial boundary conditions as well as of the question of which of the two phases is the continuous phase (not even addressing the issue of 'bicontinuous' mixtures [15], where neither phase can be uniquely classified as constituting the continuous or discontinuous phase). Recently, the interfacial boundary conditions were themselves also averaged [22], thereby creating additional field equations involving new physical variables. The additional 'macroscale' interfacial equations arising from this interfacial averaging scheme then need to be solved conjointly with the above singular Darcyscale equations. However, the physical interpretation to be ascribed to such additional interfacial field variables seems obscure in the context of the IPC picture. Moreover, as indicated below, the existence of two *ad hoc* tenets underlying the philosophy of mixture theories has diminished the practical utility of its predictions:

(a) The spirit of the mixture theories is to accept the macroscale equations (obtained by suitable averaging of the microscale equations) as fundamental, and to propose constitutive relations for the various macroscale fields appearing therein as functions of a select set of independent variables (chosen so as to satisfy suitable general criteria) [22]. The sentiment is to compare the resulting mathematical predictions (after complete quantitative calculations of the requisite macroscale field variables) of such a model with experimental observations so as to authenticate the model — a step rarely achieved fully in practice owing to the complexity of the governing equations

as well as of the experimental difficulties in effecting the requisite measurements.

(b) The manner in which mixture theories treat constitutive equations as fundamental entities has eventually obscured the physical interpretation of the singular Darcyscale fields in terms of their precursor singular-interface microscale fields. For instance, Hassanizadeh & Gray [23] state that: 'The pressures present in the capillary pressure relationships are not the averages of the (respective) microscopic pressures but instead are to be determined from a macroscopic constitutive equation for the Helmholtz free energy A.' However, the precise relationship of the macroscale free energy $\overline{A}$ to its microscale counterpart A is never clarified.

2.4 Outline and Summary of Approach

What follows is not a comprehensive program aimed at reformulating the theory of mixtures as a whole based on the diffuse interface model. Rather, attention is focused explicitly on the more limited goal of modeling slow biphasic flows through porous media. Nevertheless, some of the concepts advanced are believed to possess relevance within the more general context of mixture theory. The philosophy used in our modeling approach differs from that underlying conventional theories of multiphase flow through porous media in the following ways:

(a) The central notions of immiscibility, species, and phases at both the micro- and macro-levels are clarified, invoking a viewpoint different from that employed in traditional (singular Darcy) approaches to multiphase fluid flow phenomena. Simultaneously, those aspects involving interfacial balance conditions are accounted for in a consistent manner. Purely formal axiomatic continuum-mechanical theories are eschewed in favor of the physical aspects of the phenomena. For example, rational mechanical treatments of mixtures establish appropriate thermodynamic identities through use of the *equilibrium* version of the Coleman-Noll inequality (cf. [22] and the references cited therein). In contrast, here it is *assumed* that those classical intensive thermodynamic identities which are locally valid pointwise for inhomogeneous microscale continua hold equally well at the macroscale (diffuse Darcyscale). Given

the simplistic nature of the description afforded by our treatment, we believe that such a hypothesis would be borne out from the Coleman-Noll inequality too.

(b) Our identification of appropriate macrofields is based upon their rigorous *physical, scale-invariant* definitions rather than upon simple *ad hoc* volume averaging of the corresponding microfields. For instance (see section 4.5), the continuum-level Darcyscale mass-average seepage velocity vector $\overline{\mathbf{v}}$ at a given point $\overline{\mathbf{R}}$, say, is *defined* as that field which when scalarly multiplied by an arbitrarily directed Darcyscale surface element $d\overline{\mathbf{s}}$ situated at $\overline{\mathbf{R}}$ together with the Darcyscale mass density $\overline{\rho}$ gives the physical mass rate of flow,

$$d\overline{\dot{m}} = \overline{\rho} d\overline{\mathbf{s}} \cdot \overline{\mathbf{v}}, \tag{2.4}$$

at which fluid crosses $d\overline{\mathbf{s}}$ in the direction of $\mathbf{n}$ (the normal to $d\overline{\mathbf{s}}$). This continuum-mechanical definition of $\overline{\mathbf{v}}$ contrasts with the usual definition of $\overline{\mathbf{v}}$ as being the volume-average of the microfield $\mathbf{v}$ taken over some representative volume element V centered at $\overline{\mathbf{R}}$:

$$\overline{\mathbf{v}} = \frac{1}{V} \int_V \mathbf{v} dV.$$

Similarly, the Darcyscale continuum stress field $\overline{\mathbf{P}}$ is defined so as to satisfy the physical, Cauchy, continuum-mechanical definition

$$d\overline{\mathbf{F}} = d\overline{\mathbf{s}} \cdot \overline{\mathbf{P}}, \tag{2.5}$$

where (with the usual convention) $d\overline{\mathbf{F}}$ is the vector force exerted across $d\overline{\mathbf{s}}$ by the fluid situated on one side of the surface upon the fluid lying on the opposite side. At appropriate points in the subsequent text, similar physically-based macroscale definitions will be enunciated relevant to the other pertinent fields there being introduced. Such considerations are of prime importance since they relate directly to the manner in which an experimental probe, with its appropriately sized aperture, properly registers the local values of the dynamical variables it purports to measure. Conventional theories, which utilize a mathematical volume averaging of the microscale

fields to define their respective macroscale counterparts, generally fail to provide such a physical interpretation of the macroscale fields [46, 47].

(c) The diffuse Darcyscale fields appearing in the macroscale conservation equations governing the pertinent transport phenomena are explicitly defined through their microcontinuum counterparts, as they are – after all – a manifestation of the underlying microscale phenomena viewed on a different length scale. In any rational theory, operational definitions of the macroscale quantities calculable in principle (from solutions of the governing microscale equations) need to be explicitly provided for those willing to expend the computational resources necessary to literally perform these calculations based on these 'recipes'. This philosophy is similar to that underlying the statistical mechanics of transport processes (the foundations of which were legitimatized and rendered rigorous by Kirkwood [28]). In particular, that scheme provides microscopic, molecularly-based expressions for the magnitudes of macroscopic transport coefficients like viscosity, etc., despite the fact that the constitutive equations themselves were already known on the basis of macroscopic experiments independently of the values of the macroscopic phenomenological coefficients appearing therein. In our analogy we are in some sense, albeit imperfectly, likening: (i) the discrete molecular, microscale view with the discrete nature of the particle- (or equivalent pore-) level view of the porous medium; (ii) the continuum-level manifestation of this discrete molecular view, with our continuum Darcyscale view.

Important conceptual differences exist between conventional *two-component* systems and *two-phase* systems, especially with respect to the temporal configurational evolution of the pertinent fields, where the concept of a 'micro-macro' time scale needs to be identified and quantified. Our contribution appears to be the first wherein a rigorous foundational basis is indicated for a time-averaging scheme (see also [25]). Eventually, rigorous, unambiguous, *physically-based* definitions are adopted for spatially- and time-averaged diffuse Darcyscale fields in terms of their microscale field counterparts. Subsequently, these macroscale definitions are used to derive the Darcyscale field conservation equations from their pore-level precursors.

Within the proposed framework of a *multicomponent mixture* description of flow

at the Darcyscale, the concept of *phase-specific* pressures is identified with *species-specific* pressures, and a relationship for the capillary pressure derived in terms of appropriately-defined microcontinuum fields. Such an analysis serves to clarify the relationship between our fine-scale, diffuse Darcyscale model and conventional, coarser-scale, singular-surface Darcyscale models (see section 5.1). Discussion following the derivation of the capillary pressure relationship in section 5.2 leads to several significant observations. As an example illustrating the application of our model in practice, in section 6.3 we use a phenomenological set of pore-level constitutive equations to show how the previously empirical two-phase Darcy's law formulation can be derived from first principles via a set of linearizing assumptions. Explicitly, the diffuse two-component Darcyscale field equations are subjected to a singular perturbation analysis, enabling us to derive the conventional, otherwise empirical, singular-surface, Darcyscale equations commonly employed in practice. This illustrates the fact that the novel framework erected in this paper can serve a dual purpose — namely, to provide insights into the forms of macroscopic constitutive equations as well as to derive the more generic macroscale transport equations into which such constitutive relations are to be embedded.

It is important to delineate the major assumptions involved in the subsequent analysis so as to both identify the scope of our work and to spur future extensions thereof. We concentrate on a simple geometric model of a porous medium, namely a spatially periodic skeletal array [7, 8] (described in section 4.1). Such a definite geometrical construct, which may at first appear overly restrictive, has been shown to serve as a good theoretical model for a number of phenomena to date, especially single-phase flows through porous media [6]. Deterministic models of this nature (in contrast to statistical models) enable one to define in a completely rigorous manner all of the macroscopic fields appearing in the Darcyscale description of the several transport processes, while simultaneously furnishing definitive error estimates arising in the eventual continuum description resulting from the spatial and temporal homogenization of the discrete microscale system. Describing the flow and transport in such model porous media leads to a consideration of what are termed 'homogeneous

multiphase flows,' defined as follows [40, 47]:

'A porous medium is homogeneous with respect to a given process and averaging volume when the effective transport coefficients in the volume-averaged equations are independent of position. If the porous medium is not homogeneous, it is heterogeneous.'

Results based on strictly spatially periodic fields can also be expected to apply in circumstances wherein a slow spatial modulation is superposed on the spatial periodicity (common models for homogenization theories [3, 6]). One might also hope that results gleaned from this modulated model could also be used for the macroscopic modeling of displacement fronts — by arguing that the macroscopic front is, in reality, a diffuse transition region extending over a significant microscale distance (embodying many unit cells of the spatially periodic medium, but nevertheless still small compared with the overall length of the porous medium in the direction of net flow). The phenomenon of solid-liquid contact lines [20], both static and dynamic, as well as issues of wettability of the porous medium are omitted in this initial foray. Though very relevant to practical flows in porous media, this area remains extremely controversial. Its role in multiphase flow phenomena is still widely debated to the extent that even the boundary-condition equations governing the microscale fluid motions are not yet fully established.[2]

Finally, with regard to the thermodynamics of these diffuse 'multiphase' systems, we make the crucial assumption in the subsequent development that it is permissible to employ standard thermodynamic identities at *both* the micro- and macroscales. This assumption appears reasonable in view of the *multicomponent mixture* model (see also [26, 33, 38]) subsequently proposed in chapter 3 as the conception underlying diffuse Darcyscale phenomena. For instance, we hypothesize that a macroscale thermodynamic chemical potential $\overline{\mu}$ can be defined within our diffuse Darcy frame-

[2]Issues pertaining to wettability can perhaps be incorporated into our work by modeling the presence of the solid surface through an interaction potential (see [12] and [44]).

work as

$$\overline{\mu} \stackrel{\text{def.}}{=} \frac{\partial \overline{F}}{\partial \overline{\rho}}, \tag{2.6}$$

given the existence of a macroscopic free energy density function $\overline{F}$ and a macroscopic density $\overline{\rho}$, each being derived (in a manner to be discussed) from the respective comparable continuum microscale fields F and ρ by well-defined spatial and temporal averages of the latter.

While a complete explanation of the panoply of multiphase flow phenomena accompanying flow through a porous medium of arbitrary configuration is the eventual goal of our diffuse interface approach, such an effort is overly ambitious at present. Porous rock formations encountered in oil recovery wells are neither homogeneous nor possesses a periodic microstructure. Further, the wetting properties of the liquids play an important role in determining the microscale flow patterns. Moreover, flows in real rock formations may be characterized by highly nonequilibrium phenomena like Haynes jumps, etc., representative of high Reynolds number flows. Our assumptions, outlined in the previous paragraph and subsequently elaborated in the text, eschew these complications with the aim of developing a mathematically tractable model of a porous medium so as to uncover key insights which would hopefully prove applicable to real flows through the irregular formations encountered in nature.

In essence, this section of the thesis is divided into two distinct complementary parts. The first part is represented by chapter 3, while the latter part is constituted by chapters 4, 5 and 6. Chapter 3 provides a self-contained generic introduction to the diffuse interface model without reference to its subsequent application to porous medium flows. Chapters 4 – 6 entails specific applications of the generic framework created in Chapter 3 to situations involving flows through porous media.

Chapter 3 reviews the diffuse interface model embodying our own perspective for describing immiscible flows, using what we have chosen to call the 'multicomponent mixture' framework. This approach successfully overcomes many of the difficulties outlined above that have been encountered in prior analyses. Section 3.1 begins with

an introduction to the equations and boundary conditions encountered in the conventional or the singular interface model for describing two-phase flows. Section 3.2 reviews the spirit of the diffuse interface model, along with a repertoire of comparable conservation equations encountered within this framework. Section 3.3 outlines the constitutive forms for the various fields present in the conservation equations outlined in the previous section. Section 3.4 is devoted to clarifying issues relating to immiscibility, and to the manner in which it is supported within our diffuse interface framework. Finally, in section 3.5 we illustrate (using singular perturbation techniques) the precise manner in which the diffuse interface equations reduce to the singular-interface multiphase flow equations. This section also serves simultaneously to clarify the generic mathematical framework within which the diffuse interface model needs to be utilized in order to effect analytical calculations of practical fluid-mechanical problems, viz., through a sequential, successively improvable, singular perturbation approach.

Chapter 4 begins with a brief introduction to the geometrical characteristics of the spatially periodic model of a porous medium, placing special emphasis on the notation and definitions subsequently used in the text. Sections 4.2 and 4.3 consider the appropriate microscale conservation equations applicable within the binary mixture framework model. Using physically-based definitions outlined in section 4.4 we execute a rigorous transition from the diffuse microscale to the diffuse Darcyscale to derive the 'diffuse' Darcyscale equations in section 4.5.

Chapter 5 is concerned the explicit identification of the phase specific quantities at the macroscale. Such an identification permits the transition from the finer, diffuse Darcyscale to the coarser, singular Darcyscale. Section 5.1 defines phase-specific quantities based upon diffuse Darcyscale fields. In section 5.2 we propose a rational definition of capillary pressure, arising as a natural consequence of the transition from the diffuse Darcyscale to the singular Darcyscale. Up until section 5.3 the analysis completely eschews use of the constitutive equations outlined in section 3.3. In sections 5.3 and 5.4 we utilize the constitutive equations outlined in section 3.3 to provide a number of new insights into the observed hysteresis phenomena occurring

during capillary pressure vs saturation experiments. This discussion is supplemented in section 5.5 with an exposition of results gleaned from the constitutive equations governing the nonequilibrium conservation equations.

In chapter 6, concepts drawn from irreversible thermodynamics are used in section 6.1 to suggest and illustrate possible forms for the macroscale constitutive relations. We also analyze a simple linear example in section 6.3 to verify some of the predictions obtained through the framework of irreversible thermodynamics.

Finally, chapter 7 summarizes our work, pointing out possible future research directions. Several appendices and footnotes, elaborating details that are glossed over in the text, complete the analysis.

References

[1] P. M. Adler and H. Brenner, "Multiphase flow in porous media," *Ann. Rev. Fluid Mech.*, **20**, 35 (1988).

[2] P. M. Adler, *Porous Media: Geometry and Transports*, Butterworth-Heinemann, Boston (1992).

[3] J. L. Auriault, "Nonsaturated deformable porous media: Quasistatics," *Transp. Porous Media*, **2**, 45 (1987).

[4] J. Bear and Y. Bachmat, "Transport phenomena in porous media - Basic equations," *Fundamentals of Transport Phenomena in Porous Media* (eds. J. Bear & M. Y. Corapciglu), pp. 3–61, NATO ASI Series E, Applied Science, Martinus Nijhoff, Boston (1984).

[5] A. Bedford and D. S. Drumheller, "Recent advances: Theories of immiscible and structured mixtures," *Int. J. Engng Sci.*, **21**, 863 (1983).

[6] A. Bensoussan, J. L. Lions, and G. Papanicolaou, *Asymptotic Analysis for Periodic Structures*, North-Holland, New York (1978).

[7] H. Brenner, "Elements of Transport Processes in Porous Media," 9 folios of unpublished notes (1972).

[8] H. Brenner and D. A. Edwards, *Macrotransport Processes*, Butterworth-Heinemann, Boston (1993).

[9] S. R. Broadbent and J. M. Hammersly, "Percolation processes: 1. Crystals and mazes," *Proc. Camb. Philos. Soc.*, **53**, 629 (1957).

[10] E. Buckingham, "Studies on the movement of soil mixtures," *Bulletin*, U. S. Dep. of Agric., Vol. 38, Washington, D. C (1907).

[11] S. E. Buckley and M. C. Leverett, "Mechanissm of fluid displacement in sands," *Trans. AIME*, **146**, 107 (1942).

[12] J. W. Cahn, "Critical point wetting," *J. Chem. Phys.*, **66**, 3667 (1974).

[13] T. Cardwell, "The meaning of triple value in noncapillary Buckley-Leverett theory," *Trans. AIME*, **216**, 271 (1959).

[14] H. Darcy, *Les fontaines publiques de la ville Dijon*, Dalmont, Paris (1856).

[15] H. T. Davis, *Statistical Mechanics of Phases, Interfaces, and Thin films*, VCH, New York (1995).

[16] P. G. deGennes "Theory of slow biphasic flows in porous media," *PhysicoChem. Hydrodyn.*, **4**, 175 (1983).

[17] P. G. deGennes and E. Guyon, "Lois generales pour l'injection d'un fluide dans un milieu poreux," *J. Mechanique*, **17**, 403 (1978).

[18] F. Dobran, "Constitutive equations for multiphase mixtures of fluids," *Int. J. Multiphase Flow*, **10**, 273 (1984).

[19] J. Douglas, P. M. Blair and R. J. Wagner, "Calculation of linear waterflood behavior including the effects of capillary pressure," *Pet. Trans. AIME*, **213**, 96 (1958).

[20] V. E. B Dussan, "On the spreading of liquids on solid surfaces: Static and dynamic contact lines," *Ann. Rev. Fluid Mech.*, **11**, 371 (1979).

[21] F. J. Fayers and R. L. Perrine, "Mathematical description of detergent flooding in oil reservoirs," *Trans. AIME*, **216**, 277 (1959).

[22] W. G. Gray and S. M. Hassanizadeh, "Mechanics and thermodynamics of multiphase flow in porous media including interphase boundaries," *Adv. Water Resour.*, **13**, 169 (1990).

[23] S. M. Hassanizadeh and W. G. Gray, "Thermodynamic basis of capillary pressure in porous media," *Water Resour. Res.*, **29**, 3389 (1993).

[24] G. M. Homsy, "Viscous fingering in porous media," *Ann. Rev. Fluid Mech.*, **19**, 271 (1987).

[25] M. Ishii, *Thermo-Fluid Dynamic Theory of Two-Phase Flows*, Eyrolles, Paris (1975).

[26] F. Kalaydjian, "A macroscopic description of multiphase flow in porous media involving spacetime evolution of fluid/fluid interface," *Transp. Porous Media*, **2**, 537 (1993).

[27] J. B. Keller, "Darcy's Law for flow in porous media and the two-space method," *Lecture Notes in Pure and Applied Mathematics - Vol. 102, Physical Mathematics and Nonlinear Partial Differential Equations* (eds. J. H. Lightbourne and S. M. Rankin), pp. 429-443, NATO ASI Series E, Applied Science, M. Decker, Boston (1985).

[28] J. G. Kirkwood, *Selected Topics in Statistical Mechanics*, Gordon & Breach, New York (1967).

[29] R. G. Larson, L. E. Scriven and H.T. Davis, "Percolation theory of residual phases in porous media," *Nature*, **268**, 409 (1977).

[30] R. Lenormand, C. Zarcone and A. Sarr, "Mechanisms of the displacement of one fluid by another in a network of capillary ducts," *J. Fluid Mech.*, **135**, 337 (1983).

[31] R. Lenormand and C. Zarcone, "Invasion percolation in an etched network: Measurement of fractal dimension," *Phys. Rev. Lett.*, **54**, 2226 (1985).

[32] M. C. Leverett, "Capillary behavior in porous media," *Trans. AIME.*, **142**, 152 (1941).

[33] C. M. Marle, "On macroscopic equations governing multiphase flow with diffusion and chemical reactions in porous media," *Int. J. Engng Sci.*, **20**, 643 (1977).

[34] C. M. Marle, *Multiphase Flow in Porous Media*, Gulf, Houston (1981).

[35] M. Muskat, R. D. Wyckoff, H. G. Botset and M. W. Myres, "Flow of gas-liquid mixtures through sands," *Trans. AIME*, **123**, 69 (1937).

[36] S. P. Neumann, "Theoretical derivation of Darcy's Law," *Acta. Mechanica.*, **25**, 153 (1977).

[37] R. I. Nigmatulin, "Spatial averaging in the mechanics of heterogeneous and dispersed systems," *Int. J. Multiphase Flow.*, **5**, 353 (1979).

[38] D. Pavone, "Macroscopic equations derived from space averaging for immiscible two-phase flow in porous media," *Rev. I. Fr. Petrol.*, **44**, 29 (1989).

[39] J. R. Philip, "Flow in porous media," *Ann. Rev. Fluid Mech.*, **2**, 177 (1970).

[40] M. Quintard and S. Whitaker, "Two-phase flow in heterogeneous porous media: The method of large scale averaging," *Transp. Porous Media.*, **3**, 357 (1988).

[41] H. H. Rachford, "Instability in water flooding oil from water-wet porous media containing connate water," *Soc. Pet. Eng. J.*, **4**, 133 (1964).

[42] H. H. Rachford, "Numerical calculation of immiscible displacement by a moving reference point method," *Soc. Pet. Eng. J.*, **6**, 87 (1966).

[43] D. P. Schmidt, H. Soo and C. J. Radke, "Linear oil displacement by the emulsion entrapment process," *Soc. Pet. Eng. J.*, **24**, 351 (1984).

[44] G. F. Teltezke, L. E. Scriven, and H. T. Davis, "Gradient theory of wetting transitions," *J. Colloid and Interface Sci.*, **87**, 550 (1982).

[45] P. van Meures and C. van der Poel, "A theoretical description of water-drive processes involving viscous fingering," *Trans. AIME*, **213**, 103 (1958).

[46] S. Whitaker, "Flow in porous media: 2. The governing equations for immiscible Two-Phase flow," *Transp. Porous Media*, **1**, 105 (1986).

[47] S. Whitaker, *The Method of Volume Averaging*, Boston: Kluwer (1999).

[48] Y. C. Yortsos and A. S. Fokas, "An analytical solution for linear waterflood including the effects of capillary pressure," *Soc. Pet. Eng. J.*, **23**, 115 (1983).

Chapter 3

Diffuse Interface Model

This chapter provides a brief introduction and review of the salient aspects of the diffuse interface model. The main objective of this chapter is to demonstrate the approach embodied within the diffuse interface model in the context of modeling dynamical phenomena in 'multiphase' flows. Such a discussion also serves to clarify the relationship of the diffuse interface model to the singular interface viewpoint which is conventionally used in modeling multiphase flows. To accomplish the latter objective we employ the formal techniques of matched asymptotic expansions to thereby clarify the asymptotic equivalence of the two seemingly contrasting viewpoints. This chapter also outlines the constitutive forms of various physical quantities that appear within the governing transport equations. Such an explicit identification enables the possible application of numerical techniques to the solutions of the governing microscale equations. The resulting solutions can then be embedded within the rigorous framework erected in the subsequent chapter to thereby accomplish the transition from the microscale to the macroscale level. The conception accompanying the diffuse interface viewpoint is employed in the subsequent chapters to derive and clarify the multiphase flow equations and concepts at the macroscale level.

An interface has traditionally been viewed [14] as a singular surface separating two immiscible bulk fluids or phases. In equilibrium situations these bulk phases are regarded as being separately homogeneous, although each will generally be inhomogeneous in nonequilibrium states. Each bulk phase is separately characterized by its

own material properties which, while continuous within the individual bulk phases, may display a sharp jump in magnitude across the interface. This singular interfacial surface is itself endowed with and characterized by its own material properties, such as interfacial tension, shear and dilatational viscosities, etc. [23]. Traditional microscale descriptions of two-phase flows (in the absence of the porous medium) involve conservation field equations written for each of the two bulk phases, together with corresponding matching conditions imposed on the respective values of the bulk fields at the interfacial surface — the latter matching conditions being derived by considering the pertinent transport phenomena occurring across and within the interface [cf. (3.1) and (3.2)], the latter entailing new, interfacial fields [9, 23].

This two-dimensional, singular view of the interface has, however, long been recognized as representing only an *asymptotic* mathematical approximation of the true physical state of affairs [17, 26]. In reality, when viewed on a sufficiently fine length scale the interfacial region between two immiscible fluids is a highly inhomogeneous three-dimensional transition region (even at equilibrium) over which rapid changes in continuum-mechanical fields and concomitant material properties may occur [10, 15] [cf. Fig. (3-1)]. In this three-dimensional diffuse view of the interface, the relevant continuum-mechanical phenomenological properties vary continuously throughout the entire fluid domain, with some fields experiencing extremely steep gradients within the interfacial region in a direction normal to the 'interface.' Examples of such rapidly varying fields include the pressure field and, when a surfactant is 'adsorbed' within the interfacial region, the three-dimensional mass density field ρ_i of the surfactant species i [24].

Although the traditional singular-surface view of an interface proves specially convenient in many practical contexts, some applications require a finer-scale continuum view of the interfacial region. Such microscale perspectives have primarily been used for two different purposes:

(a) Theoretical investigation of transport processes involving moving and deforming interfaces [10, 15, 19]: These works concentrate on the distinction between the true, diffuse picture of the interface and its approximate representation as a singular

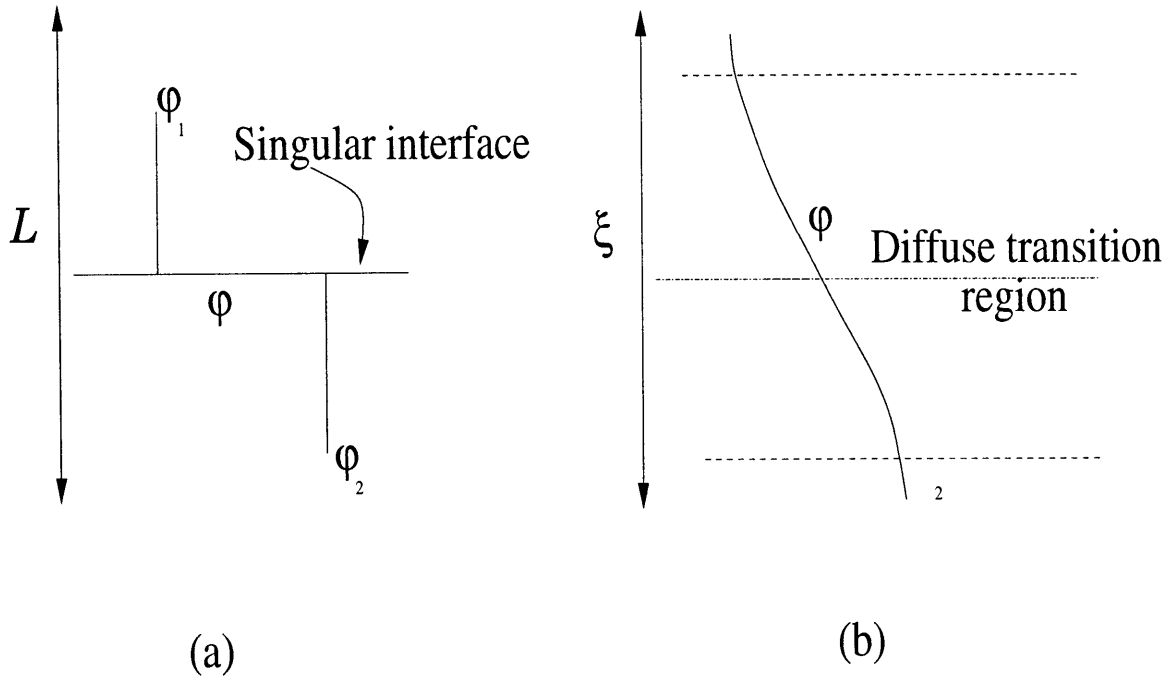

Figure 3-1: The (a) singular and (b) diffuse viewpoints of an interface. φ denotes a generic physical property, like for instance, density, viscosity, etc. In the singular view (wherein the relevant lengthscale is embodied by the lengthscale of the apparatus, denoted L), φ exemplifies a sharp discontinuity at the interface, signifying the distinct physical properties possessed by the two phases. In the diffuse view (the relevant lengthscale is now embodied by the interfacial thickness ξ), φ displays a steep, nevertheless continuous transition across the interface.

surface. Such theories attempt a reconciliation of the continuous, diffuse-interface view, which admits large inhomogeneities in material properties over a narrow transition region, with the more conventional singular-surface view of the interface, which lumps the inhomogeneities into so-called 'surface-excess' quantities. One such application, emphasized in the work of Mavrovouniotis & Brenner [19], deals with the distinction between material and nonmaterial interfaces.

(b) More recently, the diffuse view of interfaces has gone beyond simply clarifying the physical meaning of surface-excess quantities. Phenomenological constitutive equations have been proposed that enable one to work directly with the finer-scale continuous, three-dimensional, inhomogeneous fluid. This is in lieu of working separately with the bulk fluids lying on either side of the singular interface together with the corresponding matching conditions imposed at that interface. These approaches, which owe their origin to the seminal work of Cahn & Hilliard [7], have been revived and popularized by Caginalp and coworkers [3, 4], and others. The present investigation entails one further, albeit novel, application of this approach.

3.1 Singular Interface Equations

The singular interface approach exemplifies the discrete nature of the bulk fluids or phases of a two-phase system. Such a discrete structure is inherent in the governing microscale conservation equations [9], which can be written separately for each of the two phases in the generic form (refer to table 3.1 for specific identifications)

$$\frac{\partial \psi}{\partial t} + \nabla \cdot (\mathbf{v}\psi) + \nabla \cdot \mathbf{J} = \pi + \zeta, \tag{3.1}$$

to which are appended matching conditions at the interface embodying the generic interfacial transport equation:

$$\frac{\delta_s \psi^s}{\delta t} - \mathbf{u} \cdot \nabla_s \psi^s - \nabla_s \cdot (\mathbf{I}_s \cdot \mathbf{v}\psi)^s + \nabla_s \cdot (\mathbf{I}_s \cdot \mathbf{J}^s) - \pi^s - \psi^s = -\mathbf{n} \cdot [[(\mathbf{v} - \mathbf{u})\psi + \mathbf{J}]]. \tag{3.2}$$

Physical property, $\mathcal{P}$	Volumetric density, ψ	Areal-flux density, $\mathbf{J}$	Volumetric rate of production, π	Volumetric rate of supply by external sources, ζ
Mass	ρ	$\mathbf{0}$	$\mathbf{0}$	$\mathbf{0}$
Species i	ρ_i	$\mathbf{J}_D$	$\mathbf{0}$	$\mathbf{0}$
Linear momentum	$\rho\mathbf{v}$	$-\mathbf{P}$	$\mathbf{0}$	$\rho\mathbf{F}$

Table 3.1: Identification of the volumetric and areal flux density terms appearing in the generic conservation equation (3.1) for the transport property $\mathcal{P}$.

In the latter the superscript s denotes surface-excess quantities ascribed to the singular interface, whereas $\mathbf{n}$ represents the unit normal to the interface, $\mathbf{I}_s \equiv \mathbf{I} - \mathbf{nn}$ the surface idemfactor, $\nabla_s \equiv \mathbf{I}_s \cdot \nabla$ the surface gradient operator, and $\mathbf{u}$ the velocity of the interface [which in the general case of nonmaterial interfaces can differ from the bulk velocities $\mathbf{v}$ (i.e., $\mathbf{v}^+, \mathbf{v}^-$) on either side of the interface]; $[[\ldots]]$ denotes the jump in the value of the argument across the interfacial surface. Quantification of the surface-excess mass balance is achieved through the surface-excess mass density ρ^s, which is conventionally assumed to be zero. Adsorbed surfactant species at the interface correspond to non-zero values of ρ_i^s $(i = 1, 2, \ldots)$. Furthermore, $\delta_s/\delta t$ denotes the interfacial convected time derivative [9, 19].

3.2 Diffuse Interface Model

Theoretical analyses which treat the interface as a region characterized by a continuous variation of physical properties owe their genesis to the phenomenological constitutive model proposed by Cahn & Hilliard [7]. The latter can be also be viewed as a variant of the dynamical Landau-Ginzburg theory of critical phenomena [16]. This model allows for the coexistence of two phases by representing the free energy

of the interfacial system as a sum of two terms: (a) a free energy function (dependent on the component concentrations) describing the miscibility behavior; (b) a term dependent on the gradients (commonly truncated at the second order) of the component concentrations, serving to model interfacial tension and other capillary effects (cf. section 3.3). This approach is widely used to model spinodal decomposition and nucleation phenomena [5, 6]. While it is generally cautioned that such models intrinsically possess a restricted range of validity [7], being strictly applicable only near the critical point (or the consolute point, in the case of binary liquid mixtures), great success has nevertheless been achieved in using this model for studying noncritical behavior in several other contexts, including the equilibrium thermodynamics of microstructures [8] as well as the dynamics of solid melts [3]. It is generally believed that the approximations inherent in using this model for noncritical mixtures do not result in excessively large errors when applied to binary liquid mixtures [27].

In this section we outline the general form of the two-phase equations, valid for incompressible and immiscible two-phase mixtures. Discussion of the constitutive equations required therein, for which we use variants of the Cahn-Hilliard model, is postponed until the next section.

It is imperative before proceeding further to imbibe the spirit of the diffuse interface model by recognizing that at this fine-scale level of description there no longer exists a discontinuous or singular surface separating two bulk phases. Rather, the system is envisioned as being an inhomogeneous single-phase multicomponent mixture, more precisely a solution (the number of components being chosen here as two), locally described by conventional, spatially varying composition variables [7]. The governing conservation transport equations are then simply the classical mass conservation equations for each of the two species, together with the momentum conservation equation for the mixture as a whole; explicitly,

$$\frac{\partial \rho_1}{\partial t} + \nabla \cdot (\rho_1 \mathbf{v_1}) = 0; \qquad \frac{\partial \rho_2}{\partial t} + \nabla \cdot (\rho_2 \mathbf{v_2}) = 0, \tag{3.3a,b}$$

$$\frac{\partial(\rho \mathbf{v})}{\partial t} + \nabla \cdot (\rho \mathbf{v}\mathbf{v}) = -\nabla p + \nabla \cdot \boldsymbol{\tau}_v + \nabla \cdot \boldsymbol{\tau}_c + \sum \rho_i \mathbf{F}_{ie}, \tag{3.4}$$

where $\rho_i, \mathbf{v}_i$ and $\mathbf{F}_{ie}$ $(i = 1, 2)$ respectively denote the species-specific mass density, velocity, and external force fields.[1] As usual, p denotes the pressure field, $\boldsymbol{\tau}_v$ the viscous deviatoric stress tensor, ρ the mass density of the mixture ($\rho = \rho_1 + \rho_2$), and $\mathbf{v}$ the mass-average velocity of the mixture [cf. (3.7)]. The continuous microscale vector field $\nabla \cdot \boldsymbol{\tau}_c \equiv \mathbf{F}_p$, say, represents the precursor of the macroscale physicochemical capillary or interfacial forces, arising as a consequence of the steep species concentration gradients $\partial \rho_i / \partial n$ existing within the diffuse interfacial region in a direction n normal to the 'interface'. The implicit macroscale interfacial tension and related nonequilibrium capillary effects traditionally associated with the presence of a singular surface (which includes interfacial viscosities[2]) are thus explicitly accounted for in our model by the appearance of this force field. As such, the physicochemical volumetric force density field $\mathbf{F}_p$ constitutes a central feature of our diffuse interface model, and the ultimate success of this model depends upon our ability to provide a rational constitutive equation for $\mathbf{F}_p$ — an issue deferred until the next section [cf. (3.18)].

We assume at the outset that the mixture as a whole is incompressible. This assumption allows the microscale pressure field p to be treated as an independent dynamical variable rather than as a dependent variable, functionally dependent upon temperature, composition, etc. Further, upon supposing that the law of additive volumes applies to the mixture, the relation between the density ρ of the mixture and

[1]The presence of a body-force field $\mathbf{F}_{ie}$, e.g., a gravity field, ultimately precludes the scenario of spatially-periodic microscale fields envisioned in later sections in cases where the immiscible phases possess different densities. However, to maintain generality of the exposition, we eschew that constraint until section 6.3.

[2]In the singular interface model, interfacial viscosities are associated with the adsorption of surfactant species on the 'interfacial surface.' In our diffuse model of the interface, the presence of a surfactant species in the two-phase mixture would constitute a ternary system. Though most of our arguments in subsequent sections remain valid in this ternary case, we do not formally delve into the complexities of such situations in this preliminary report, wherein we confine ourselves exclusively to binary systems.

the densities ρ_i^o of the pure components is given simply by the linear relation [1],

$$\rho = \rho_1^o c + \rho_2^o (1 - c), \tag{3.5}$$

where c denotes the volume fraction of component 1. The latter concentration is henceforth taken as the relevant composition variable when characterizing our binary system. The assumption of incompressibility shows that at the microscale only one composition variable is relevant, namely, the volume fraction c [since $\rho_1 = c\rho_1^o$, and $\rho_2 = (1 - c)\rho_2^o$]. This observation also makes the number of scalar equations defined by (3.3a,b) - (3.4), namely five, consistent with the corresponding number of unknown scalar variables embodied in c, p and $\mathbf{v}$.

Equations (3.3a,b) may be rewritten as

$$\frac{\partial \rho_1}{\partial t} + \nabla \cdot (\rho_1 \mathbf{v}) = -\nabla \cdot \mathbf{J}_1; \qquad \frac{\partial \rho_2}{\partial t} + \nabla \cdot (\rho_2 \mathbf{v}) = -\nabla \cdot \mathbf{J}_2, \tag{3.6a,b}$$

wherein the mass-average velocity $\mathbf{v}$ is defined by the relation

$$\rho \mathbf{v} = \rho_1 \mathbf{v}_1 + \rho_2 \mathbf{v}_2, \tag{3.7}$$

and the respective diffusion fluxes $\mathbf{J}_1$ and $\mathbf{J}_2$ as

$$\mathbf{J}_1 = \rho_1 (\mathbf{v}_1 - \mathbf{v}); \qquad \mathbf{J}_2 = \rho_2 (\mathbf{v}_2 - \mathbf{v}). \tag{3.8a,b}$$

[In view of the definition (3.7) of the mixture velocity $\mathbf{v}$, the two diffusion fluxes are related by the identity $\mathbf{J}_1 + \mathbf{J}_2 = \mathbf{0}$, whence we can choose to denote $\mathbf{J}_1 = -\mathbf{J}_2 \equiv \mathbf{J}$, say, and so by adding equations (3.3a,b) obtain the conventional equation of continuity for the mixture:

$$\frac{\partial \rho}{\partial t} + \nabla \cdot (\rho \mathbf{v}) = 0, \tag{3.9}$$

together with a diffusion equation for one of the species, say 1:

$$\frac{\partial c}{\partial t} + \nabla \cdot (c\mathbf{v}) = -\nabla \cdot \mathbf{J}. \tag{3.10}$$

While this index-free notation representation will be the form employed in the next section when dealing with constitutive equations, considerations of invariance afforded by the interchangeability of the arbitrary labels identifying species "1" and "2" suggest that for the present we opt for the individual species-specific forms, namely (3.6a,b).]

Equations (3.6a,b) and (3.4) together with appropriate boundary conditions dictated by geometrical and kinematical considerations constitute a complete set of conservation equations serving to determine the diffuse microscale fields $c, p, \mathbf{v}$. These equations are identical to the conventional multicomponent equations used to describe the flow of *miscible*, single-phase, binary mixtures (solutions) except for the appearance of the additional term $\mathbf{F}_p$, representing the microscale precursor of the macroscopic capillary forces. In the next section it will be shown that the sole difference between the respective miscibility and immiscibility cases arises *in toto* from the forms of the constitutive equations chosen for $\mathbf{F}_p$ and $\mathbf{J}$ $(= \mathbf{J}_1 \equiv -\mathbf{J}_2)$. This seemingly subtle feature is the main thrust of our hypothesis. It shows how even immiscible *two-phase* systems may be alternatively regarded as two-component, *single-phase* systems when the system description is appropriately supplemented by constitutive equations for the diffusive flux $\mathbf{J}$ and capillary force field $\mathbf{F}_p$ [11]. The fact that such constitutive equations can be provided and embedded in physical context renders our work novel beyond its classification as a mere academic exercise. Section 3.3, which follows, thereby constitutes in a fundamental sense a prescription for performing explicit two-phase flow calculations using the diffuse interface model. Furthermore, it shows in an explicit manner how the traditional equations governing the singular interface model can be recovered from the diffuse model through the natural apparatus available for identifying and effecting such microscale/macroscale equivalences, namely, singular perturbation analysis [19]. Though some related aspects of the subsequent analysis have been dealt with in prior studies by others, we take pains to

clarify the subtleties involved in such an exercise, enabling us thereby to transcend the purely numerical or mathematical details of the scheme.

3.3 Microscale Constitutive Equations

This section utilizes the respective forms (3.9) and (3.10) of the diffusion and continuity equations in place of the precursor pair (3.6a,b). Moreover, constitutive expressions for $\mathbf{J}$ and $\mathbf{F}_p$ are discussed.

Constitutive equation for $\mathbf{J}$

The assumption of linear response theory together with the assumed absence of coupling between the fluxes requires that

$$\mathbf{J} = -\frac{\Lambda}{kT}\nabla\mu, \tag{3.11}$$

where μ denotes the difference in chemical potential between the two species, and kT is the Boltzmann factor. The mobility coefficient Λ is, in general, a second-rank tensor and may also depend upon c. However, consistent with the nature of the present work, stressing only on the simplest physical elements, we eschew both generalizations. Thus, we assume Λ to be a concentration-independent scalar constant. For the chemical potential μ we have by definition that

$$\mu = \frac{\delta F}{\delta c}, \tag{3.12}$$

with F is the free energy density of the mixture and $\delta/\delta c$ the functional derivative with respect to c. The constitutive form of F is assumed to be that proposed in [7], namely

$$F = \int d^3\mathbf{r}\,\left[f(c) + \frac{1}{2}K(\nabla c)^2\right], \tag{3.13}$$

where $f(c)$ denotes the excess volumetric free energy density of the mixture[3] and K is a dimensionless phenomenological coefficient, related to the equilibrium direct correlation function between the two species [8, 12]. Though K may be a function of concentration, it is here assumed to be a constant. In this work we use a modified form of the above equation to explicitly incorporate the interfacial 'thickness' ξ, the latter representing the characteristic linear dimension of the interfacial transition zone:

$$F = \frac{1}{\xi}\int d^3\mathbf{r}\left[f(c) + \frac{1}{2}K\xi^2(\nabla c)^2\right]. \tag{3.14}$$

Thus, $\mathbf{J}$ takes the form

$$\mathbf{J} = -\frac{\Lambda}{kT}\frac{1}{\xi}\nabla\Big(\frac{\partial f}{\partial c} - K\xi^2\nabla^2 c\Big). \tag{3.15}$$

Substitution into the diffusion equation (3.10) yields

$$\frac{\partial c}{\partial t} + \nabla\cdot(\mathbf{v}c) = \frac{1}{\xi}\frac{\Lambda}{kT}\nabla^2\Big(\frac{\partial f}{\partial c} - K\xi^2\nabla^2 c\Big) \tag{3.16}$$

for the microscale convective-diffusion equation [see also [11] and [1]]. The constitutive form of $f(c)$ is taken up subsequently.

Constitutive equation for $\mathbf{F}_p$

An appropriate constitutive relationship for $\mathbf{F}_p$ has been suggested by a number of researchers, frequently starting from the virtual work principle [11, 25, 1], as well as

[3] The actual free energy density of the mixture is of the form:

$$f' = f(c) + f_{\text{id}} + \frac{1}{2}K(\nabla c)^2,$$

where $f_{\text{id}} = cf_1(\text{pure}) + (1-c)f_2(\text{pure})$ denotes the free energy density of an ideal mixture, and f' denotes the microscale volumetric free energy density. However, in most applications we are concerned only with $\nabla\mu$, rather than μ itself. As such, f_{id} proves irrelevant.

other arguments.[4] We adopt the following constitutive expression for $\boldsymbol{\tau}_c$:

$$\boldsymbol{\tau}_c = \xi K \left[(\nabla c)(\nabla c) - |\nabla c|^2 \mathbf{I}\right], \tag{3.17}$$

whence from the definition $\nabla \cdot \boldsymbol{\tau}_c = \mathbf{F}_p$ of the physicochemical force density we obtain

$$\mathbf{F}_p = \xi K \, \nabla \cdot \left[(\nabla c)(\nabla c) - |\nabla c|^2 \mathbf{I}\right]. \tag{3.18}$$

Constitutive equation for $\boldsymbol{\tau}_v$

In view of the fact that the interfacial transition region is strongly inhomogeneous in a direction normal to the interface, the viscous stress tensor is expected to be transversely isotropic [10, 15]. However, consistent with our desire to focus attention primarily on the physicochemical (rather than rheological) aspects of the dynamics, we adopt the usual simple isotropic Newtonian form for $\boldsymbol{\tau}_v$, namely

$$\boldsymbol{\tau}_v = 2\mu \left[\mathbf{D} - \frac{1}{3}(\mathbf{I} : \mathbf{D})\mathbf{I}\right], \tag{3.19}$$

with

$$\mathbf{D} = \frac{1}{2}\left[(\nabla v) + (\nabla v)^\dagger\right] \tag{3.20}$$

---

[4]Though conventionally derived from a variational formulation, we can heuristically justify the expression (3.17) for $\boldsymbol{\tau}_c$ in the following manner: Define a pressure

$$p_c \stackrel{\text{def.}}{=} c\frac{\delta F}{\delta c} - F$$

in analogy to the thermodynamic definition

$$p = c\frac{\partial f}{\partial c} - f.$$

This enables a separation of ∇p_c into the sum $\nabla p + \nabla \cdot \boldsymbol{\tau}_c$, with $\nabla p = \nabla\left(c\frac{\partial f}{\partial c} - f\right)$, wherein $\boldsymbol{\tau}_c$ is given as above.

the deformation gradient and $\mu \equiv \mu(c)$ the local viscosity of the mixture (solution), which by definition satisfies the relation[5]

$$\mu \longrightarrow \begin{cases} \mu_1^o \text{ as } c \longrightarrow 1, \\ \mu_2^o \text{ as } c \longrightarrow 0. \end{cases} \tag{3.21}$$

Upon using the above identifications, the momentum equation (3.4) adopts the form

$$\frac{\partial(\rho \mathbf{v})}{\partial t} + \nabla \cdot (\rho \mathbf{v}\mathbf{v}) = -\nabla p + \nabla \cdot \boldsymbol{\tau}_v + \xi K \nabla \cdot \left[(\nabla c)(\nabla c) - |\nabla c|^2 \mathbf{I} \right] + \rho \mathbf{g}. \tag{3.22}$$

Form of $f(c)$

Conventional theories of dynamical critical phenomena [wherein our model is equivalent to that of Model H of [16]] adopt a double-well potential for the free energy density $f(\psi)$, where ψ represents an order parameter. In a binary liquid system the order parameter is usually taken to denote the difference in composition between the two species. Thus, we choose

$$f(\psi) \sim (1 - \psi^2)^2, \tag{3.23}$$

where

$$|\psi| = |1 - 2c|.$$

Consequently, the following form is adopted here for $f(c)$:

$$f(c) = AK(1 - c)^2 c^2, \tag{3.24}$$

[5]Though we will have no need here for an explicit functional relationship between μ and c, if necessary one could, in order to satisfy (3.21), simplistically *assume* μ to be linearly related to the respective viscosities μ_1^o and μ_2^o of the pure species by the expression

$$\mu = \mu_1^o c + \mu_2^o (1 - c).$$

where A is a dimensionless constant and K is the same phenomenological constant introduced earlier. Note that $f(c) \to 0$ as $c \to 0$ and 1; this dual property will later prove crucial in identifying the compositions of coexisting phases.

This section dealt with the constitutive equations accompanying the diffuse interface viewpoint of an immiscible two phase system. The next section clarifies the manner in which the above constitutive equations explicitly distinguishes between a miscible and an immiscible system.

3.4 Immiscibility

This section is devoted to clarifying the notion of immiscibility in the present context of *species* rather than *phases*, especially the manner in which immiscibility is supported by the above equations. To achieve this objective we start with a brief discussion pertinent to the existence of phase-separated solutions of the modified diffusion equation (3.16). At the outset, we provide a physical argument commenting on the approach to equilibrium to thereby justify the existence of a phase separated solution of the diffusion equation. Subsequently, we provide a more detailed exposition of the thermodynamical features embodied within the excess free energy function $f(c)$. Eventually, in the following section we perform a singular perturbation analysis of the governing equations, thereby explicitly demonstrating that our diffuse interface model does indeed furnish an appropriate pair of 'bulk-phase' equations (*outer* equations) as well as yielding 'interfacial' transport equations (*matching conditions*) connecting these two bulk fields at the 'interface.' And it is these bulk field regions that constitute the 'immiscible phases' in the macroscale view.

3.4.1 Diffusion Equation

In the interests of simplicity we temporarily ignore hydrodynamical considerations as well as effects arising from the presence of K in the expression (3.14) for $F(c)$. Figures (3-2a) and (3-2b) respectively show the general configurations of the concentration-dependent forms of the excess free energy density function $f(c)$ appearing in (3.24)

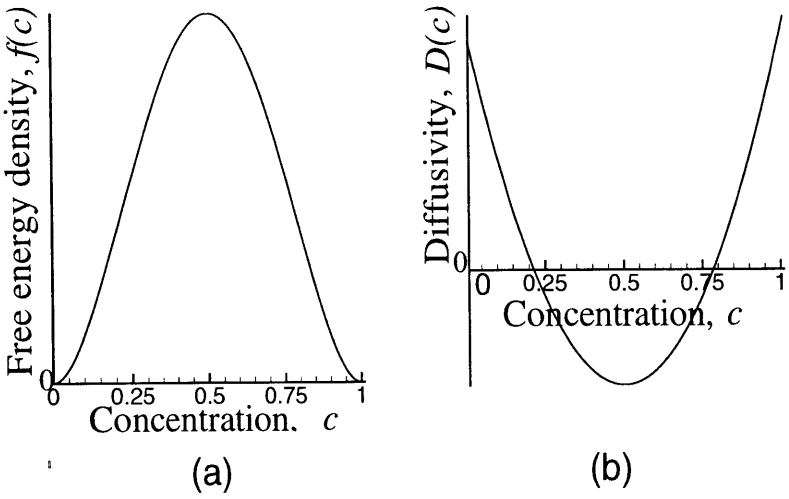

Figure 3-2: Double-well potential form for: (a) Free-energy density $f(c)$; (b) Diffusivity $D(c)$.

as well as the diffusion coefficient $D(c)$, the latter being the term appearing in the resulting 'diffusion' equation,

$$\frac{\partial c}{\partial t} = D\nabla^2 c, \tag{3.25}$$

and defined as

$$D \stackrel{\text{def.}}{=} \frac{\Lambda}{kT}\frac{\partial^2 f}{\partial c^2}. \tag{3.26}$$

Since $\Lambda > 0$ as a consequence of the Second Law of Thermodynamics, we observe from (3.25) and (3.24) that there exists a range of concentrations over which $D(c) < 0$ [representing a thermodynamically unstable region, wherein an initially homogeneous mixture (solution) of composition $0 < c < 1$ spontaneously separates into two distinct 'phases' of respective compositions $c = 0$ and 1]. In contrast, for a completely miscible mixture, $D(c) > 0 \ \forall c$, whence an initially homogeneous mixture remains homogeneous for all time! This observation forms the basis of our two-component mixture model as supporting phase-separated stable solutions of the modified diffu-

sion equation.

3.4.2 Thermodynamic Considerations

Considerations pertaining to the thermodynamical equilibrium state enable us to glean further insights into the notions of miscibility vs immiscibility. Explicitly, the equilibrium state corresponds to the situation wherein the free energy F is stationary (as well as a minimum for a stable equilibrium) with respect to infinitesimal variations in the governing physical properties, i.e.

$$\left.\frac{\delta F}{\delta c}\right|_{\text{equilibrium}} = 0. \tag{3.27}$$

Employing the constitutive form (3.13) for F (as stated earlier, we neglect the effects of the concentration gradients) we obtain

$$\frac{\partial f}{\partial c_{\text{eq}}} = 0, \tag{3.28}$$

which corresponds to the classical equilibrium condition requiring that the excess free energy of the mixture be an extremum with respect to variations in the composition.

To illustrate the concepts of miscibility and immiscibility within the context of the above equilibrium condition (3.28) we employ a generalized version of the free energy function $f(c)$ earlier proposed in eq. (3.24):

$$f(c) = \frac{A(T)}{2}x^2 + \frac{B}{4}x^4, \tag{3.29}$$

where, x denotes the difference in concentrations between the two species, i.e. $x \equiv 1 - 2c$. In the above expression the physical constant A is assumed to be a function of temperature, and is chosen in the present discussion to be the simple linear form, $A(T) \sim a(T - T_c)$, with a a positive constant. It is pertinent to note here that the above expression for the free energy is identical to Van der Waal's equation of state

for fluids.[6]

Invoking the equilibrium condition (3.28) for a fluid obeying the equation of state (3.29) yields the following compositions corresponding to the equilibrium scenario:

$$x_{\rm eq} = 1 - 2c_{\rm eq} = \begin{cases} 0 & (T > T_c), \\ 0, \pm\sqrt{-A(T)/B} & (T < T_c). \end{cases}$$

In the above equation $x_{\rm eq}$ and $c_{\rm eq}$ denote the values corresponding to the equilibrium situation. The above identification implies that the equilibrium composition requiring $c = 0.5$ uniformly everywhere (a homogeneous mixture) constitutes the equilibrium scenario for temperatures T exceeding T_c. Below T_c the equilibrium scenario might either correspond to a phase separated system with bulk concentrations $x_{\rm eq} = \pm\sqrt{A(T)/B}$, or to the scenario corresponding to a homogeneous mixture with $x = 0$.[7] The choice of the observed equilibrium solution invokes the considerations relating to the relative stability of these solutions, and in this case requires the phase separated solution to be manifested below T_c.

The preceding analysis of the free energy function thereby clarifies the fact that completely miscible mixtures correspond to a system above its consolute temperature (T_c). If the consolute temperature possesses an extremely low magnitude, then a binary liquid system appears to be miscible for practically all ranges of temperature. However, the existence of a high consolute temperature would necessarily be manifested as partial miscibility.[8] Furthermore, dual considerations of stability and equilibrium compositions determine the kinetic rate of approach to equilibrium, which, in turn is governed by the diffusion equation. As such, if the equilibrium situation corresponds to a phase-separated system, the effective diffusion coefficient for a homogeneous system then acquires a negative value, thereby tending to equilibrate the system to one wherein the equilibrium compositions correspond to the

[6]The extraneous factors 2 and 4 present in the above expressions are introduced to enable simpler algebraic factors in the subsequent discussion. As such, they possess no physical significance.

[7]Constraints imposed by conservation of mass preclude equilibrium compositions of solutions like $x = 0, \sqrt{A(T)/B}$.

[8]Note that immiscible mixtures correspond to equilibrium compositions of $c_{\rm eq} = 0$ and $c_{\rm eq} = 1$, respectively, and may be considered as an extreme case of partial miscibility.

phase-separated situation.

This preceding discussion was meant to provide a brief overview for readers unfamiliar with the work of Cahn & Hilliard [7]. Excellent reviews and details can be found in [13] and [18]. However, our work is not concerned with the *dynamics* of phase separation, but rather assumes at the outset that a phase-separated mixture already exists at the microscale, one whose dynamics can be described via the above system of equations.

Some comments are in order regarding the form of F set forth in (3.14): (i) The factor $1/\xi$ appearing as the multiplier of F is obtained by normalizing the volume over which F is nonzero; ξ is expected to be small for immiscible systems; (ii) while the above equations appear to be superficially similar to those possibly encountered for miscible systems, the contrasting phase behavior of the two systems arises from the different forms of the excess free energy function f appearing in F above. While the form of f illustrated in eq. (3.23) supports a phase-separated equilibrium scenario, the corresponding functional form of f for a miscible system necessarily describes an equilibrium scenario with partial miscibility; (iii) the factor K and the second gradient present in the expression for F account for interfacial tension effects [7].

The next section is devoted to effecting a singular perturbation analysis of the preceding system of microscale equations so as to provide a rational derivation of the conventional macroscale two-phase equations, (3.1) and (3.2), together with appropriate matching conditions. This section also serves to clarify the precise manner in which analytical calculations of practical fluid-mechanical problems need to be effected when using the diffuse interface model. Such a procedure necessarily involves the use of singular perturbation techniques to determine the governing equations and their solutions at every order of the perturbation analysis.

3.5 Singular Perturbation Analysis

Below, we nondimensionalize the variables appearing in (3.16) and (3.22). To avoid a proliferation of symbols the same unadorned symbols will be used to denote both

dimensional quantities and their nondimensional counterparts, imagining that the preceding dimensional symbols had previously been augmented by an asterisk:

$$\mathbf{v} = \frac{\mathbf{v}^*}{U},\ \mathbf{r} = \frac{\mathbf{r}^*}{L},\ \nabla = L\nabla^*,\ \rho = \frac{\rho^*}{\rho_o},\ p = \frac{p^*L}{\mu_o U},\ \boldsymbol{\tau}_v = \frac{\boldsymbol{\tau}_v^* L}{\mu_o U},\ \Lambda = \frac{\Lambda^* \tau_D}{L^2}.$$

Here, U, L, ρ_o and μ_o respectively represent a characteristic velocity, length, density and viscosity, whereas τ_D represents a characteristic diffusion time scale. In terms of these dimensionless variables, equations (3.9), (3.16) and (3.22) respectively become

$$\frac{\partial \rho}{\partial t} + \nabla \cdot (\rho \mathbf{v}) = 0, \tag{3.30}$$

$$\mathrm{Re}\left[\frac{\partial(\rho \mathbf{v})}{\partial t} + \nabla \cdot (\rho \mathbf{v}\mathbf{v})\right] = -\nabla p + \nabla \cdot \boldsymbol{\tau}_v + \mathrm{Ca}^{-1}\delta \nabla \cdot \left[(\nabla c)(\nabla c) - |\nabla c|^2 \mathbf{I}\right] + \rho \mathbf{g} \tag{3.31}$$

and

$$\delta \tau_D \frac{U}{L}\left[\frac{\partial c}{\partial t} + \nabla \cdot (\mathbf{v}c)\right] = \Lambda \nabla^2 \Big(\frac{\partial f}{\partial c} - \delta^2 \nabla^2 c\Big), \tag{3.32}$$

where the following nondimensional parameters have been introduced:

$$\mathrm{Re} = \frac{\rho_o U L}{\mu},\quad \delta = \frac{\xi}{L},\quad \mathrm{Ca} = \frac{\mu U}{K},\quad \Lambda = \frac{\Lambda K}{LkT},$$

and where f is now given by the expression

$$f(c) = A(1-c)^2 c^2. \tag{3.33}$$

Re and Ca are, of course, the Reynolds and capillary numbers.

For the immiscible systems contemplated, τ_D is expected to be very small compared with the convective time-scale L/U. In this section, circumstances will be established as to how the above system of equations reduce to the conventional system of two-phase, singular interface equations. The motivation behind such an exercise

is to explain the spirit of the diffuse interface model. A description of the actual dynamics of phase separation [22] is beyond the scope of this work; in lieu of this we make an *a priori* assumption as to the existence of an interface characterized by a transition region with steep variations in physical properties.

The natural mathematical apparatus for extracting the bulk equations and matching interfacial conditions from the above system of equations is singular perturbation analysis, with the interfacial region representing a thin boundary layer sandwiched between two outer bulk regions (phases). To the best of our knowledge the only such interfacial analysis previously effected via this approach is embodied in the work of Starovitov [25] (see also [3] for an analysis with similar objectives, albeit in a different context). However, that analysis was restricted to a one-dimensional interface; moreover, a number of aspects of that work appear controversial. Here, we treat a moving material interface in three-dimensional space, characterized by a special metrical geometry specially chosen to avoid notational complexities. In this context the analysis of systems containing mobile interfaces is facilitated by parameterizing three-dimensional space via a semiorthogonal surface-fixed coordinate system (cf. Fig. 3), namely (q_1, q_2, q_3), with q_3 lying normal to the 'parent surface' [19, 9]. Since our aim is merely to illustrate the spirit of the diffuse interface model without performing an exhaustive and comprehensive investigation to rigorously justify the applicability of our results under very general circumstances, we consider a special kind of interface — one in which the interfacial transition region can be characterized by an orthogonal coordinate system possessing the metrical coefficient $h_3 = 1$ (the 'parallel surface' representation of Eliassen [10]). Additionally, the interfacial curvature will be assumed to be much greater than the interfacial thickness [and of $\mathcal{O}(1)$ relative to the small perturbation parameter δ].

As is conventional with diffuse interface models we identify the macroscopic interface with a so-called 'parent surface,' one whose precise location in the transition region to within an error of $\mathcal{O}(\delta)$ is not critical to the subsequent $\delta \ll 1$ asymptotic analysis. This parent surface is parameterized by the normal coordinate $q_3 = q_3^o$,

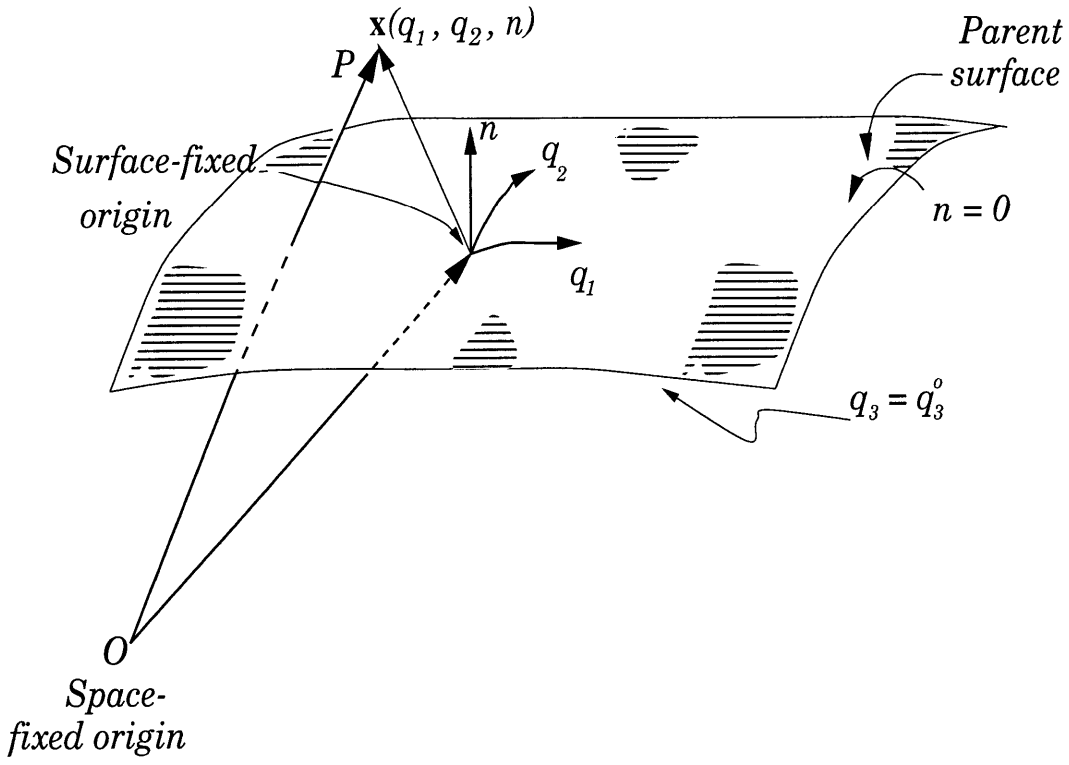

Figure 3-3: Parent surface and representation of the surface-fixed coordinate system; (q_1, q_2, n) represent the coordinates of a point in the outer region as measured from axes fixed on the parent surface.

whence the variable

$$n \stackrel{\text{def.}}{=} \int_{q_3^o}^{q_3} h_3 \, dq_3 = q_3 - q_3^o \tag{3.34}$$

denotes an algebraically-signed distance measured normal to interface. By definition, $n = 0$ on the parent surface. Given the presence of the small perturbation parameter δ in the equations governing the two-component transport process, one can anticipate the existence of disjoint inner and outer regions. Length scales in the two outer regions lying on either side of the 'interface' are taken to be macroscopic, with the magnitudes of physical quantities and their gradients in these regions assumed to be everywhere of $\mathcal{O}(1)$.

In the outer regions we assume, subject to *a posteriori* verification, that each physical variable (here denoted generically by $\boldsymbol{\psi}$) admits a regular perturbation expansion of the form

$$\boldsymbol{\psi}(q_1, q_2, n, t; \delta) = \boldsymbol{\psi}_0(q_1, q_2, n, t) + \delta \boldsymbol{\psi}_1(q_1, q_2, n, t) + \ldots . \tag{3.35}$$

In contrast, in the inner region, whose thickness is of $\mathcal{O}(\delta)$, these physical quantities may display steep gradients. Accordingly, distances in the inner region are normalized with δ, thereby magnifying them. Explicitly, the independent inner variable,

$$\tilde{n} \stackrel{\text{def.}}{=} \frac{(q_3 - q_3^o)}{\delta}, \tag{3.36}$$

represents an algebraically-signed scaled distance in the inner region, normal to the 'interface.' Concomitant expressions for $\tilde{\nabla}$ and $\tilde{\nabla}^2$ need to be explicitly rewritten in terms of $(q_1, q_2, \tilde{n})$. Furthermore, subject to *a posteriori* verification, the generic physical variables are each assumed to possess an inner expansion of the form

$$\tilde{\boldsymbol{\psi}}(q_1, q_2, \tilde{n}, t; \delta) = \tilde{\boldsymbol{\psi}}_0(q_1, q_2, \tilde{n}, t) + \delta \tilde{\boldsymbol{\psi}}_1(q_1, q_2, \tilde{n}, t) + \ldots . \tag{3.37}$$

Matching conditions imposed on the respective outer and the inner fields, $\boldsymbol{\psi}_i$ and $\tilde{\boldsymbol{\psi}}_i$,

have been established by Caginalp & Fife [4], albeit in a different context, as

$$\lim_{|\tilde{n}|\longrightarrow\infty} \tilde{\psi}_0(q_1, q_2, \tilde{n}, t) = \psi_0(q_1, q_2, n = 0, t) \tag{3.38}$$

and

$$\lim_{|\tilde{n}|\longrightarrow\infty} \tilde{\psi}_1(q_1, q_2, \tilde{n}, t) = \psi_1(q_1, q_2, n = 0, t) + \tilde{n}\frac{\partial \psi_0(q_1, q_2, n, t)}{\partial n}\bigg|_{n=0}. \tag{3.39}$$

Higher-order matching conditions may also be easily derived; however, the need for such additional conditions does not arise in the present work as a consequence of the fact that our theory is strictly asymptotic [19] rather than being serially sequential. As such, only the leading- and first-order terms of the respective expansions are involved in the subsequent analysis.

Outer equations

This section addresses the leading-order outer fields. Affixes $\pm$ will be used to denote the respective regions lying on either side of the interface. Upon substituting the outer expansion into (3.32), the $\mathcal{O}(1)$ diffusion equation is found to be of the form

$$\nabla^2\left[\frac{\partial f}{\partial c}\right]_0^{\pm} = 0, \tag{3.40}$$

where the subscript zero denotes the zeroth-order field. Since a soliton solution of the above equation is anticipated, we assume subject to *a posteriori* verification that the appropriate solution of the above equation is

$$\left[\frac{\partial f}{\partial c}\right]_0^{\pm} = 0.$$

As noted earlier, $f(c) \rightarrow 0$ and $\partial f/\partial c \rightarrow 0$ as $c \rightarrow (0, 1)$. Consequently, we find that $c_0 = (0, 1)\ \forall\ n$ lying on either side of the interface. This is consistent with our physical picture of the two outer regions as constituting immiscible bulk phases. For

definiteness, we arbitrarily choose $c_0^+ = 1$ and $c_0^- = 0$.

At $\mathcal{O}(1)$ the equation of continuity becomes

$$\frac{\partial \rho_0^\pm}{\partial t} + \nabla \cdot (\rho_0^\pm \mathbf{v}_0^\pm) = 0. \tag{3.41}$$

In view of the preceding solution for c_0 on either side of the interface, it follows that

$$\nabla \cdot \mathbf{v}_0^\pm = 0. \tag{3.42}$$

The $\mathcal{O}(1)$ momentum equation here takes the form

$$\mathrm{Re}\left[\frac{D(\rho_0 \mathbf{v}_0)}{Dt}\right]^\pm = -\nabla p_0^\pm + \nabla \cdot \boldsymbol{\tau}_{v0}^\pm + \rho_{i0}^\pm \mathbf{g}. \tag{3.43}$$

Equations (3.42) and (3.43) represent the outer equations in the respective regions lying on either side of the interface. These equations accord with the usual bulk-phase equations employed in conventional singular surface, two-phase models of interfacial phenomena. Considerations pertaining to the inner equations will be shown to lead to appropriate matching conditions imposed on these outer fields at their common interface.

Inner equations

In the inner region the normal-distance coordinate n needs to be rescaled via the transformation (3.36). Relevant rescalings of the operators thereby obtained, along with the leading- and the first-order terms that arise, are indicated in Appendix A. Here, we note that the dynamical evolution of the interface leads to the following rescaling of the time-derivative [4]:

$$\left(\frac{\partial}{\partial t}\right)_n = \left(\frac{\partial}{\partial t}\right)_{\tilde{n}} - \frac{\dot{q}_3^o}{\delta}\left(\frac{\partial}{\partial \tilde{n}}\right)_t \qquad (q_1, q_2 = \text{ const.}), \tag{3.44}$$

where, $\dot{q}_3^o$ denotes the normal velocity of the parent surface, $\tilde{n} = 0$. Furthermore, the metrical coefficients $\tilde{h}_1(q_1, q_2, \tilde{n})$ and $\tilde{h}_2(q_1, q_2, \tilde{n})$ admit inner expansions of the

respective forms,

$$\tilde{h}_1(q_1, q_2, \tilde{n}) = h_{10}(q_1, q_2, q_3^o, t) - \delta h_{10}(q_1, q_2, q_3^o, t)\kappa_1(q_1, q_2, \tilde{n}, t)\tilde{n} + ..., \tag{3.45}$$

$$\tilde{h}_2(q_1, q_2, \tilde{n}) = h_{20}(q_1, q_2, q_3^o, t) - \delta h_{20}(q_1, q_2, q_3^o, t)\kappa_2(q_1, q_2, \tilde{n}, t)\tilde{n} + ..., \tag{3.46}$$

where the definitions (A.4) and (A.5) has been used. Higher-order contributions prove unnecessary in the subsequent analysis.

At the leading order the continuity equation becomes

$$-\dot{q}_3^o \frac{\partial \tilde{\rho}_0}{\partial \tilde{n}} + \frac{\partial(\tilde{\rho}_0 \tilde{v}_{30})}{\partial \tilde{n}} = 0. \tag{3.47}$$

Integration of the latter at constant (q^1, q^2) gives,

$$\tilde{\rho}_0(\tilde{v}_{30} - \dot{q}_3^o) = g(q_1, q_2), \tag{3.48}$$

where $g(q_1, q_2)$ is an integration function. However, since $\tilde{v}_{30} = \dot{q}_3^o$ at $\tilde{n} = 0$ owing to the material nature of the interface, it follows that

$$\tilde{v}_{30} = \dot{q}_3^o \quad \forall \tilde{n}. \tag{3.49}$$

Since $\dot{q}_3^o$ is independent of $\tilde{n}$, this implies that

$$\frac{\partial \tilde{v}_{30}}{\partial \tilde{n}} = 0. \tag{3.50}$$

Moreover, the matching conditions (3.38) require that

$$v_{30}^{\pm}(n = 0) = \dot{q}_3^o, \tag{3.51}$$

whence

$$[[v_{30}]] = 0, \tag{3.52}$$

where we have used the jump operator $[[\ldots]]$ of [9] to denote the discontinuity, if any, in the value of the argument across the parent surface.

At the leading order, the inner form of the diffusion equation yields

$$\frac{\partial f}{\partial c} - \frac{\partial^2 \tilde{c}_0}{\partial \tilde{n}^2} = 0. \tag{3.53}$$

Multiplying the above equation by $\partial \tilde{c}_0/\partial \tilde{n}$ and integrating with respect to $\tilde{n}$ gives

$$f - \frac{1}{2}\left(\frac{\partial \tilde{c}_0}{\partial \tilde{n}}\right)^2 = 0, \tag{3.54}$$

where the facts that both $\partial \tilde{c}_0/\partial \tilde{n}$ and $f \to 0$ as $\tilde{n} \to \pm\infty$ have been used. Into the above expression one can substitute the explicit form of f given in (3.33), subsequently integrating the resulting equation to obtain the leading-order inner concentration profile as

$$\tilde{c}_0 = \frac{\exp(2\tilde{n}\sqrt{A})}{1 + \exp(2\tilde{n}\sqrt{A})}. \tag{3.55}$$

(Note that $\tilde{c}_0 \to 0$ as $\tilde{n} \to -\infty$ and $\tilde{c}_0 \to 1$ as $\tilde{n} \longrightarrow \infty$.)

The leading-order inner components appearing in the momentum equation are

$$-\frac{\partial \tilde{p}_{-1}}{\partial \tilde{n}}\mathbf{i}_3 + \mathbf{i}_1 \frac{\partial}{\partial \tilde{n}}\left(\mu \frac{\partial \tilde{v}_{10}}{\partial \tilde{n}}\right) + \mathbf{i}_2 \frac{\partial}{\partial \tilde{n}}\left(\mu \frac{\partial \tilde{v}_{20}}{\partial \tilde{n}}\right) + \mathbf{i}_3 \frac{\partial}{\partial \tilde{n}}\left(\frac{4}{3}\mu \frac{\partial \tilde{v}_{30}}{\partial \tilde{n}}\right) = \mathbf{0}, \tag{3.56}$$

where $(\mathbf{i}_1, \mathbf{i}_2, \mathbf{i}_3)$ respectively denote unit vectors along the coordinate axes (q^1, q^2, q^3). Additionally, $\tilde{p}_{-1}$ denotes the $\mathcal{O}(\delta^{-1})$ inner pressure field. Using (3.50) together with the fact that $\tilde{v}_{10}$ and $\tilde{v}_{20}$ are finite as $\tilde{n} \to \pm\infty$ gives

$$\tilde{v}_{10} = \nu(q_1, q_2), \tag{3.57}$$

$$\tilde{v}_{20} = \eta(q_1, q_2), \tag{3.58}$$

$$\tilde{p}_{-1} = 0, \tag{3.59}$$

in which ν and η denote integration functions. The first pair of the preceding equations require that

$$\frac{\partial \tilde{v}_{10}}{\partial \tilde{n}} = \frac{\partial \tilde{v}_{20}}{\partial \tilde{n}} = 0, \tag{3.60}$$

whence

$$[[v_{10}]] = [[v_{20}]] = 0. \tag{3.61}$$

In combination with (3.52) we thereby obtain

$$[[\mathbf{v}_0]] = \mathbf{0}, \tag{3.62}$$

which is equivalent to (A.13). As such, our considerations of the leading-order terms of the inner equations lead to the expected jump condition (3.62) imposed on the velocity field for the case of material interfaces [9].

At the next order the inner form of the continuity equation requires that

$$\tilde{v}_{31}\frac{\partial \tilde{\rho}_0}{\partial \tilde{n}} + \tilde{\rho}_0 \chi = 0, \tag{3.63}$$

where (3.49) and (3.50) have been used, and wherein χ is as defined in (A.11). Consider the $\tilde{n} \to \pm\infty$ limit of the above equation. Since, as a consequence of (3.5) and (3.55), $\partial\tilde{\rho}_0/\partial\tilde{n} \to 0$ exponentially as $\tilde{n} \to \pm\infty$, it follows that

$$\chi \to 0 \qquad \text{as } \tilde{n} \to \pm\infty. \tag{3.64}$$

Using (A.10) and (A.12) the momentum equation at first order reads

$$\frac{\partial}{\partial\tilde{n}}\left[\mu\left(\frac{\partial\tilde{v}_{11}}{\partial\tilde{n}}+h_{10}\frac{\partial\tilde{v}_{30}}{\partial q_1}-\tilde{v}_{10}\kappa_1\right)\right]=0, \tag{3.65}$$

$$\frac{\partial}{\partial\tilde{n}}\left[\mu\left(\frac{\partial\tilde{v}_{21}}{\partial\tilde{n}}+h_{20}\frac{\partial\tilde{v}_{30}}{\partial q_2}-\tilde{v}_{20}\kappa_2\right)\right]=0, \tag{3.66}$$

$$-\frac{\partial\tilde{p}_0}{\partial\tilde{n}}+\frac{\partial}{\partial\tilde{n}}\left(2\mu\frac{\partial\tilde{v}_{31}}{\partial\tilde{n}}\right)-\frac{2}{3}\frac{\partial(\mu\chi)}{\partial\tilde{n}}+\mathrm{Ca}^{-1}\left[(\kappa_1+\kappa_2)\left(\frac{\partial\tilde{c}_0}{\partial\tilde{n}}\right)^2\right]=0. \tag{3.67}$$

Integrate (3.65) and (3.66), and use the matching condition

$$\lim_{\tilde{n}\longrightarrow\infty}\frac{\partial\tilde{\psi}_1(q_1,q_2,\tilde{n},t)}{\partial\tilde{n}}=\frac{\partial\psi_0(q_1,q_2,n=0,t)}{\partial n} \tag{3.68}$$

together with (3.57) and (3.58) to obtain the jump conditions

$$\left[\left[\mu\left(h_{10}\frac{\partial v_{30}}{\partial q_1}+\frac{\partial v_{10}}{\partial n}-v_{10}\kappa_1\right)\right]\right]=0 \tag{3.69}$$

and

$$\left[\left[\mu\left(h_{20}\frac{\partial v_{30}}{\partial q_2}+\frac{\partial v_{20}}{\partial n}-v_{20}\kappa_2\right)\right]\right]=0. \tag{3.70}$$

Integration of (3.67) yields

$$-\tilde{p}_0+\left(2\mu\frac{\partial\tilde{v}_{31}}{\partial\tilde{n}}\right)-\frac{2}{3}\mu\chi+\ \mathrm{Ca}^{-1}\left[(\kappa_1+\kappa_2)\int d\tilde{n}\left(\frac{\partial\tilde{c}_0}{\partial\tilde{n}}\right)^2\right]=\zeta(q_1,q_2), \tag{3.71}$$

where the right-hand term represents an integration function.

Consider the limit as $\tilde{n}\ \rightarrow\ \pm\infty$ together with the fact that $\chi\rightarrow 0$ as $\tilde{n}\rightarrow\pm\infty$.

This yields

$$\left[\left[-p_0 + 2\mu \frac{\partial v_{30}}{\partial n} \right]\right] = -2\sigma\mathcal{H}, \tag{3.72}$$

with the mean curvature $\mathcal{H}$ defined as in (A.16), and the macroscopic interfacial tension σ defined (nondimensionally) in terms of the continuous microscale field $\tilde{c}_0$ as

$$\sigma = \mathrm{Ca}^{-1} \int_{-\infty}^{+\infty} d\tilde{n} \left(\frac{\partial \tilde{c}_0}{\partial \tilde{n}} \right)^2. \tag{3.73}$$

The latter expression represents a classical result, one which has been derived innumerable times for equilibrium situations [7, 12], albeit by perhaps less formal procedures. However, our analysis appears to be the first to systematically treat the complete *dynamical* situation case, so as to also derive the interfacial matching conditions imposed on the stress and velocity fields. Though we have ignored possible surface rheological effects arising from the presence of an adsorbed surfactant, it would be straightforward to incorporate these into the above model by using appropriate constitutive equations and scalings, and by extending our analysis to include ternary systems (with the surfactant representing the third species).[9] Moreover, by retaining higher-order terms in the perturbation scheme it is possible to proceed along similar lines to derive the well-known effects of curvature on interfacial tension [2, 21]. However, in the interests of focusing only on the fundamentals of diffuse interfaces we do not embark on such extensions in the present contribution.

In summary, the diffuse interface model provides a complete physicochemical identification of the bulk equations and interfacial boundary conditions employed in conventional singular interface models, albeit one that eschews both interfacial rheology and large curvature effects. The present section was devoted to rationalizing the admissibility of incorporating two-phase immiscible systems into the framework of a two-component mixture model of interpenetrating continua. The microscale constitutive equations introduced were shown to reduce to the conventional singular interface

[9]For instance, the viscosity would no longer be of $\mathcal{O}(1)$ within the interfacial zone, but might rather display very large values, eventually leading to nonzero interfacial viscosities [10, 15, 9, 20].

model through the use of physical scaling arguments accompanied by an asymptotic singular perturbation scheme. In accomplishing this demonstration, we have also simultaneously illustrated the manner in which analytical solution of problems can be effected using the diffuse interface model. Such a procedure entails use of singular perturbation techniques concurrently with prescribed constitutive equations to obtain solutions accurate to the required degree of approximation.

Henceforth, the diffuse interface model will be used exclusively in the subsequent analysis to treat multiphase flows at the *microscale* level, appropriate to pore-level interstitial transport processes, in lieu of the traditional singular interface pore-level model. However, until the stage where section 5.3 is reached, the subsequent analysis will be seen to be invariant to the explicit choice of constitutive equations.

Sections 4.3 to 6.3 serve to apply the preceding *single-phase (diffuse), two-component*, interstitial microscale description of macroscopically multiphase systems to problems involving their flow through porous media. Such two-phase flow processes have conventionally been regarded as governed at the (singular surface) microscale level by equations (3.1) and (3.2) together with appropriate boundary conditions imposed at the bed-particle surfaces. Our alternative *diffuse* interface model, however, requires that we instead concern ourselves with the continuous equations (3.4) and (3.6a,b) together with appropriate bed-particle boundary conditions imposed on the fields appearing in these equations. These equations form the basis of our analysis of biphasic flows in porous media. This multicomponent description at the diffuse microscale leads naturally to a multicomponent description at the diffuse macroscale, and hence ultimately to an assignation of distinct macroscale pressures to each of the two 'species' (i.e., 'bulk phases'). The relationship between these two bulk-phase pressures is shown, in turn, in Section 5.2 to be the formal equivalent of the usual capillary pressure relationship connecting these 'phase-specific' pressures. The entire analysis which follows is performed in a manner such as to admit completely general functional forms for the constitutive equations governing $\mathbf{J}$ and $\mathbf{F}_p$. However, in sections 5.3 – 5.5 we use the constitutive equations outlined above to provide a number of new and fundamental insights into the physical basis of capillary pressure as well

as into the dynamical equations currently used in the modeling of two-phase flows in general.

References

[1] L. K. Antanovskii, "Phase field model of capillarity," *Phys. Fluids* A **7**, 747 (1995).

[2] F. P. Buff and H. Saltsburg, "Curved fluid interfaces 2. The generalized Neumann formula," *J. Chem. Phys.*, **26**, 23 (1957).

[3] G. Caginalp,, "An analysis of a phase field model of a free boundary," *Arch. Rat. Mech. Anal.*, **92**, 206 (1986).

[4] G. Caginalp and P. C. Fife, "Dynamics of layered interfaces arising from phase boundaries," *SIAM J. Appl. Math.*, **48**, 506 (1988).

[5] J. W. Cahn, "Phase separation by spinodal decomposition in isotropic systems" *J. Chem. Phys.*, **42**, 93 (1965).

[6] J. W. Cahn and J. E. Hilliard, "Free energy of a nonuniform system: 3. Nucleation in a two-component incompressible fluid," *J. Chem. Phys.*, **31**, 688 (1959).

[7] J. W. Cahn and J. E. Hilliard, "Free energy of a nonuniform system: 1. Interfacial free energy," *J. Chem. Phys.*, **28**, 258 (1958).

[8] H. T. Davis and L. E. Scriven, "Stress and structure in fluid interfaces," *Adv. Chem. Phys.*, **49**, 357 (1982).

[9] D. A. Edwards, H. Brenner and D. T. Wasan *Interfacial Transport Processes and Rheology*, Butterworth-Heinemann, Boston (1991).

[10] J. D. Eliassen, *Interfacial Mechanics*, Ph. D. thesis, University of Minnesota, Minneapolis (1963).

[11] M. Fixman, "Viscosity of critical mixtures," *J. Chem. Phys.*, **36**, 310 (1962).

[12] P. D. Fleming, A. J. M. Yang, and J. H. Gibbs, "A molecular theory of interfacial phenomena in multicomponent systems," *J. Chem. Phys.*, **65**, 7 (1976).

[13] J. D. Gunton, M. San Miguel and P. S. Sahni, "The dynamics of first-order phase transitions," *Phase Transitions and Critical Phenomena* (eds. M. S. Green & C. Domb), Volume 8, pp. 267–466, Academic, New York.

[14] J. W. Gibbs, *The Collected works of J. Willard Gibbs*, Yale University Press, New Haven (1957).

[15] F. C. Goodrich, "The theory of capillary excess viscosities," *Proc. R. Soc. Lond. A.*, **374**, 341 (1981).

[16] P. C. Hohenberg and B. I. Halperin, "Theory of dynamic critical phenomena," *Rev. Mod. Phys.*, **49**, 43 (1977).

[17] J. G. Kirkwood and F. P. Buff, "The statistical mechanical theory of surface tension," *J. Chem. Phys.* , **17**, 338 (1949).

[18] J. S. Langer, "Metastable states," *Physica*, **73**, 61 (1974).

[19] G. M. Mavrovouniotis and H. Brenner, "A micromechanical investigation of interfacial transport processes: 1. Interfacial conservation equations," *Phil. Trans. R. Soc. Lond.* A **345**, 165 (1993).

[20] G. M. Mavrovouniotis, H. Brenner, D. A. Edwards and L. Ting, " Micromechanical investigation of interfacial transport processes: 2. Interfacial constitutive equations," *Phil. Trans. R. Soc. Lond.* A **345**, 209 (1993).

[21] S. Ono and S. Kondo, "Molecular theory of surface tension in liquids," *Encyclopedia of Physics* (ed. S. Flugge), Vol. 10, pp. 134–280, Springer, Berlin.

[22] R. L. Pego, "Front migration in the nonlinear Cahn-Hilliard equation," *Proc. R. Soc. Lond.* A **422**, 261 (1989).

[23] L. E. Scriven, "Dynamics of a fluid interface. Equation of motion for Newtonian surface fluids," *Chem. Engng Sci.*, **12**, 98 (1960).

[24] J. C. Slattery, "Kinematics of diffusion in a heterogeneous surface" *Chem. Engng Sci.*, **6**, 453 (1964).

[25] V. N. Starovitov, "A model of motion of a two-component liquid with effect of capillary forces," *Zh. Prikl. Mekh. Tekhn. Fiz.*, **35**, 86 (1994).

[26] R. C. Tolman, "The superficial density of matter at a liquid-vapor boundary," *J. Chem. Phys.*, **17**, 118 (1949).

[27] L. A. Turski and J. S. Langer, "Dynamics of a diffuse liquid-vapor interface," *Phys. Rev.* B **22**, 2189 (1980).

Chapter 4

Biphasic Flows in Porous Media: Diffuse Darcyscale

This chapter concerns the specific application of the diffuse interface framework to biphasic flows in porous media. The ensuing discussion restricts itself in implementing the spirit of the diffuse interface model only to the extent of eschewing the explicit use of the constitutive equations outlined in section (3.3). In essence, this chapter deals with the development of the theoretical framework so as to enable the transition from the microscale to the macroscale level description of the porous medium flow phenomena. We commence with an elucidation of the physically-based definitions of the macroscale quantities. Subsequent to such an exposition, we derive the macroscale equations governing the flow through porous media using the preceding framework. Chapter 4 restricts itself to the derivation of the generic physical quantities and macroscale equations existing within the diffuse Darcyscale level.[1] The explicit identification of the phase specific quantities like phase velocities, capillary pressure, etc. is deferred to Chapter 5.

[1] At the diffuse Darcyscale, the flow is envisioned to be that of a binary mixture. In contrast, it is at the singular Darcyscale level corresponds to the physico-spatial scale at which the 'phase'-specific physical quantities and equations (biphasic Darcy's law) manifest.

4.1 Geometry of Unbounded Spatially Periodic Porous Media

4.1.1 Microscale

A spatially periodic fixed bed-particle configuration and a corresponding (instantaneously) spatially- and time-periodic mobile interstitial fluid velocity field is proposed as a tractable geometrical model of multiphase flow through a porous medium. Owing to its deterministic configuration, this specific geometrical microcontinuum model permits a rigorous mathematical analysis of the pertinent physical phenomena using standard mathematical tools, including Fourier series, Bloch functions [2], and homogenization techniques [3]. Such models have already been used for computational purposes with regard to emulsions, suspensions, etc. (cf. [12] and the references cited therein), albeit at the *singular surface* microscale level. We are explicitly concerned here with macroscopically *homogeneous* multiphase flows, where time-averaged macroscale quantities like saturation, velocity, pressure gradient, etc. are spatially and temporally uniform throughout the porous medium. However, we will also briefly indicate the more general forms of equations that would result for circumstances in which a slow spatial macroscale variation is superposed on the otherwise spatially periodic configuration (for which our rigorous macroscopic definitions hold *locally*). While the model of a spatially periodic medium might appear unnecessarily restrictive in view of the fact that the entire porous medium is assumed generated by replication of the unit cell contents (in contrast with the disordered media usually encountered in practice), it is to be pointed out here that such media do not however exclude a complex *disordered unit cell* as the template [4].

Reviews of the properties of spatially periodic media are available elsewhere [1, 4, 5, 6, 7] and will not be repeated here. Rather, we restrict ourselves in what follows to a brief summary of the notation to be used. Moreover, attention is focused exclusively on unit cells characterized by planar faces. Extension to curvilinear cells is straightforward [12].

Spatially periodic systems are characterized by an associated lattice system embodying the translational symmetries of the medium. The complete lattice is generated from a single lattice point (the origin) by discrete displacements of the form

$$\mathbf{R}_n = n_1\mathbf{l}_1 + n_2\mathbf{l}_2 + n_3\mathbf{l}_3, \tag{4.1}$$

where $\{n_1, n_2, n_3\} \equiv \mathbf{n}$ is a triplet of integers $(n_1, n_2, n_3 = 0, \pm 1, \pm 2, \pm 3, \ldots)$, and $(\mathbf{l}_1, \mathbf{l}_2, \mathbf{l}_3)$ a triad of non-coplanar vectors, termed basic lattice vectors. As in the references cited in the preceding paragraph, the position vector $\mathbf{R}$ of a point denotes the displacement of the point from a space-fixed origin, whereas $\mathbf{r} = \mathbf{R} - \mathbf{R}_n$ denotes the intracellular position vector measured from the lattice point $\mathbf{R}_n$, the latter being taken as a local intracell origin. Furthermore, as regards a unit cell, $\partial\tau_o$ denotes the areal domain encompassing the totality of all six faces bounding the cell, whereas τ_f and τ_o denote the respective volumetric domains of the interstitial fluid and superficial cell [Fig. (4-1)]. Within a unit cell the solid particles comprising the porous medium are stationary. Fluid velocities are to be measured with respect to these fixed particles. The wetted surfaces of the fixed bed particles within a cell are designated collectively as s_p.

4.1.2 Macroscale

In order that a continuum macroscale description of the microscale phenomena be valid, there needs to exist a wide disparity in the magnitudes of the characteristic lengths (and times) separating the micro- and macroscales. Most theories of multiphase flow in porous media [8, 9, 10, 12] assume the existence of an intermediate length scale lying between the two — thereby serving to identify a macroscale 'point' with a nonzero microscale skeletal-space volume. Similarly, a macroscale 'differential volume' element is infinitesimal only in macroscale terms; in reality it needs to be sufficiently large to enclose a 'statistically representative' sample of the local skeletal geometry (as well as its contents). Quantitative details regarding the errors involved in homogenizing the microscale phenomena by this scheme are set forth in the work

of Nitsche & Brenner [12], with special emphasis on the kinematical aspects of the flow phenomena.

Since interest centers in this paper only on the physical aspects of two-phase flows in porous media, we concentrate on a rudimentary description of the micro-macro transition, as expounded by Brenner [5] (see also [7]). In this description a 'macroscopic point' (whose macroscopic position vector will be denoted by $\overline{\mathbf{R}}$) refers to a conveniently chosen reference lattice point located within the microscale unit cell $\mathbf{R}_n$ (e.g. at its centroid):

$$\overline{\mathbf{R}} \equiv \mathbf{R}_n. \tag{4.2}$$

While the lattice points $\mathbf{R}_n$ denote a *discrete*, infinitely denumerable set of points at the microscale, the macroscopic description treats $\overline{\mathbf{R}}$ as a *continuum* of vectors, with the 'infinitesimal' displacement vector defined as

$$d\overline{\mathbf{R}} = \mathbf{l}_\mathbf{k}, \tag{4.3}$$

wherein $\mathbf{l}_k$ $(k = 1, 2, 3)$ denotes a basic lattice vector. More explicitly, to remove any confusion between the equivalence of the *continuous* vector field $\overline{\mathbf{R}}$ and the *discrete* set of vectors $\mathbf{R}_n$, in place of (4.2) we heuristically write $\overline{\mathbf{R}} = \mathbf{R}_n + \mathcal{O}(\|l\|)$, where l denotes the characteristic linear dimension of a unit cell.

The macroscopic differential directed areal surface element is identified with any one of the six directed surface areas of the cell faces:

$$d\bar{\mathbf{s}}_\nu = \mathbf{s}_k, \tag{4.4}$$

with $\mathbf{s}_{-k} = -\mathbf{s}_k$ $(k = \pm 1, \pm 2, \pm 3)$, and where the index ν connotes the direction of the normal vector to the face. Henceforth, however, we will resort to the notation $d\bar{\mathbf{s}}$ to represent the macroscopic areal element, unless a specific need exists for explicitly identifying the particular face in question. (Proof of the facts that $d\overline{\mathbf{R}}$ and $d\bar{\mathbf{s}}$ respectively constitute acceptable definitions for the infinitesimal displacement vector and

areal element at the macroscale [explicitly, that both can be chosen to be of *arbitrary* magnitude and orientation in a macrosense] is discussed by Brenner [5] and Nitsche & Brenner [12]).

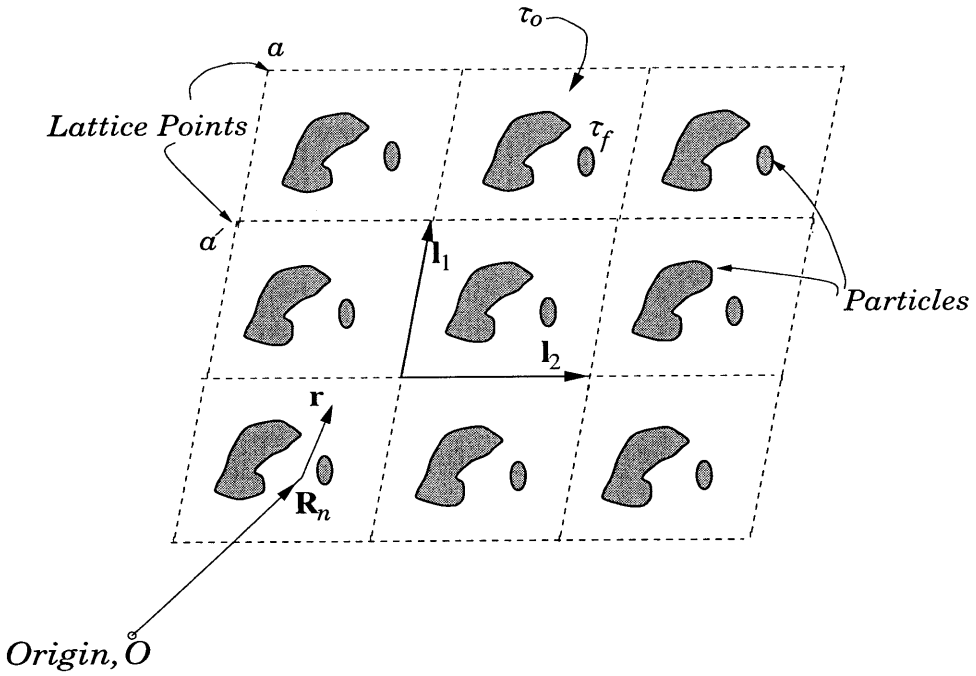

Figure 4-1: Spatially periodic medium (two-dimensional projection) comprised of particles of arbitrary shape. O refers to the lattice origin, $\mathbf{R}_n$ the centroid of the cell, and $\mathbf{r}$ a point within a unit cell as measured from the centroid; a, a' denote representative lattice points, whereas τ_f, τ_O respectively denote the domains of the interstitial fluid and the unit cell.

The macroscopic infinitesimal volume element is taken to be the superficial volume of the unit cell:

$$d^3\overline{\mathbf{R}} = \tau_o,$$

a fact consistent with (4.3) in conjunction with the relation $\tau_o = \mathbf{l}_1 \times \mathbf{l}_2 \cdot \mathbf{l}_3$. It follows from (4.3) and (4.4), together with the identity

$$\tau_o = \mathbf{l}_k \cdot \mathbf{s}_k$$

(valid for $k = 1, 2$ or 3), that

$$d^3\overline{\mathbf{R}} = d\overline{\mathbf{s}} \cdot d\overline{\mathbf{R}}.$$

4.2 Microscale Fields

Due to the spatially periodic geometry of the porous medium, the instantaneous microscale fields ρ, c and $\mathbf{v}$ can be expected to be spatially periodic with periods $\{\mathbf{l}_1, \mathbf{l}_2, \mathbf{l}_3\}$ along the three lattice directions. In such a scenario, we have using (4.1), the generic relation

$$\boldsymbol{\psi}(\mathbf{r} + \mathbf{R}_n, t) = \boldsymbol{\psi}(\mathbf{r}, t) \quad \forall\, \mathbf{r} \in \tau_f, \tag{4.5}$$

where $\boldsymbol{\psi}$ collectively denotes the fields $(c, \rho, \mathbf{v})$ as well as ρ_i. As a specific application of the above formula we have that:

$$\|\boldsymbol{\psi}\| = \mathbf{0}, \tag{4.6}$$

where $\|\boldsymbol{\psi}\|$ denotes the (algebraically-signed) jump in the value of $\boldsymbol{\psi}$ at equivalent points lying on opposite cell faces.[2] The microscale spatial periodicity condition embodied in (4.6) eventually enables us to define macroscopic quantities as averages over a unit cell, a procedure carried out in the next section.

Under the assumption that $\boldsymbol{\tau}_v$ and $\boldsymbol{\tau}_c$ are functions at most only of: (i) the velocity $\mathbf{v}$, (ii) the concentration c, and (iii) their respective gradients, we have

$$\boldsymbol{\tau}_v(\mathbf{R} + \mathbf{R}_n, t) = \boldsymbol{\tau}_v(\mathbf{R}, t) \tag{4.7}$$

and

$$\boldsymbol{\tau}_c(\mathbf{R} + \mathbf{R}_n, t) = \boldsymbol{\tau}_c(\mathbf{R}, t). \tag{4.8}$$

[2]This unit cell face operator $\|\ldots\|$ should be carefully distinguished from the interfacial jump operator $[[\ldots]]$ defined following equation (3.2).

In view of the above facts it follows from (4.12) that the pressure gradient is also spatially periodic:

$$\nabla p(\mathbf{R} + \mathbf{R}_n, t) = \nabla p(\mathbf{R}, t). \tag{4.9}$$

The time-dependence of the various microscale fields requires special comment. On the whole, microscale issues regarding the temporal evolution of two-phase flow fields are rarely discussed in the literature, especially in circumstances where the *mean* fields are themselves time independent. The implicit assumption of quasi-stationarity thereby implied tends to be all pervasive. *Ad hoc* 'volume-averaging' is usually applied to some 'random quasistatic configuration,' the latter taken to denote some 'representative' time-averaged geometric configuration. However, at the (singular surface) microscale level, two-phase flows of the respective fields inherently involve time evolution of the pertinent fields due to the relative motion of the two-phases with respect to one another, as well as with respect to the fixed particles comprising the porous medium (see also [11, 12], and the comments therein). The corresponding macroscale flow may either be steady (the common assumption under which the multiphase Darcy's law is employed) or unsteady. In the former case, the manner in which a *microscopically unsteady* motion can result in a *macroscopically steady* motion leads in our analysis to the formal concept of a 'micro-macro' timescale. To the best of our knowledge this feature has not previously been explicitly identified in the context of biphasic flows, though various arguments have been proposed for operationally performing the requisite time averaging [13]. Further concerns regarding the evolution of the system in relation to the ergodicity of the spatial averages, often used to justify the time-averaging hypothesis, are indicated in the work of Nitsche & Brenner [12]. However, even such measure-preserving flows as those we envision in a unit cell (equivalent to flows on a torus) can exhibit a wide range of droplet behavior, including periodic evolution, almost periodic evolution, and even chaotic motion [14]. Accordingly, it is virtually impossible to state anything of general validity about the time dependence of the singular surface microscale field variables in spatially-periodic

porous media (whose time dependence arises from the gross motions of the droplets relative to fixed bed particles). Here, we make the following plausible assumption regarding the time dependence of the diffuse microscale field variables for a flow which is specified to be macroscopically steady (albeit unsteady at the microscale level):

ASSUMPTION 1 *Let f be any bounded function inside the unit cell, i.e. on a suitable norm,*

$$\|f\| \leq C,$$

where C is a constant. We assume *that $\exists$ a T such that*

$$\frac{1}{T}\|f(t+T) - f(t)\| \leq \mathcal{O}(T) \quad \forall t. \tag{4.10}$$

Though formally stated above in a perhaps pontifical aphysical manner, the fact that the functions f are assumed to be dependent upon time only through the instantaneous location and configuration of the 'droplets' requires the latter to return to, or at least approach very closely, their original configurations after a time T. (Of course, in using coarse-scale words like 'droplets' in our diffuse microscale description we are speaking loosely, since such terminology is strictly appropriate only at the singular microscale view.) This time periodic (or *almost* time periodic [15]) assumption represents the dynamical constraint analogous to the geometrical constraint imposed by spatial periodicity. However, while an explicit length scale exists for the porous medium (viz. L) to compare with l, the variable T presents no such explicit choice in view of the steadiness of the macroscale fields. Thus, T can be considered infinitesimal compared with the relaxation time of the measuring instruments employed at the macroscale. Accordingly, the above assumption assures the requisite smoothness (on the time scales of measuring instruments) of the macroscale temporal derivatives.

The quantity T, which is of course finite at the microscale, will be identified later as constituting an *infinitesimal* macroscale time element $d\bar{t}$, whence the group of terms

appearing on the left-hand side of equation (4.10) will be identified as representing the definition of the *macroscopic time derivative.* Furthermore, the identification of T defines the time interval over which the physical variables need to be time averaged in order to complement the spatial averaging. Both are needed to derive expressions for the macroscale fields from their microscale counterparts.

4.3 Microscale Conservation Equations

This section discusses the conservation equations governing the microscale-level (diffuse interface) transport processes.

At the pore-space (microscale) level of description our biphasic flows are modeled from a diffuse interface viewpoint. The conservation equations governing species transport at the microscale correspond to the convective-diffusion and linear momentum equations outlined in section 3.2. They are summarized here, along with the corresponding microscale transport equations for both energy and moment-of-momentum.

Diffusion equations:

$$\frac{\partial \rho_1}{\partial t} + \nabla \cdot (\rho_1 \mathbf{v}) = -\nabla \cdot \mathbf{J}_1; \qquad \frac{\partial \rho_2}{\partial t} + \nabla \cdot (\rho_2 \mathbf{v}) = -\nabla \cdot \mathbf{J}_2. \tag{4.11a,b}$$

Momentum equations:

(a) Linear momentum[3]

$$\frac{\partial (\rho \mathbf{v})}{\partial t} + \nabla \cdot (\rho \mathbf{v}\mathbf{v}) = -\nabla p + \nabla \cdot \boldsymbol{\tau}_v + \nabla \cdot \boldsymbol{\tau}_c + \sum_{i=1}^{2} \rho_i \mathbf{g}_i, \tag{4.12}$$

[3]To be consistent with the spatially periodic interstitial-fluid field model of a porous medium here envisioned, gravity forces cannot strictly be included within this framework since the concentration of the individual species (and hence ρ_i) vary over the unit cell. However, as will be made clear during the subsequent exposition, the spatially periodic model serves as a backbone for constructing rigorous, physically-based definitions of the macroscale fields in terms of the microscale fields. The final forms of the macroscale transport equations, namely (4.53a,b) - (4.56), are expected to be independent of this strict periodicity assumption. In line with such an approach, we ignore the inconsistency arising from the inclusion of gravity forces within the spatially periodic model. Alternatively, the inconsistency can be removed by setting the gravity terms to zero.

where $\mathbf{g}_i$ is the external body force per unit mass exerted on species i.

(b) Moment-of-momentum: Define $\boldsymbol{\tau} \stackrel{\text{def.}}{=} \boldsymbol{\tau}_v + \boldsymbol{\tau}_c$ and assume the fluid to be non-polar. In such circumstances we have that [16]

$$\boldsymbol{\tau} = \boldsymbol{\tau}^{\dagger}. \tag{4.13}$$

Energy equation [17]:

$$\frac{\partial[\rho(e + \frac{1}{2}\mathbf{v}^2)]}{\partial t} + \nabla \cdot \left[\rho(e + \frac{1}{2}\mathbf{v}^2)\mathbf{v} + \mathbf{q} + \mathbf{v}p - \mathbf{v}.\boldsymbol{\tau}\right] - \sum_{i=1}^{2}(\rho_i \mathbf{v} + \mathbf{J}_i) \cdot \mathbf{g}_i = 0, \tag{4.14}$$

where e denotes the volumetric internal energy density[4] and $\mathbf{q}$ the heat-flux vector.

The pore-level boundary conditions are dictated by the geometry of the system. At the surfaces of the bed particles we have: (i) the no-slip condition,

$$\mathbf{v} = \mathbf{0} \text{ on } s_p; \tag{4.15}$$

and (ii) the condition of no net normal flux, which together with the vanishing of the convective flux on the bed particles as implied by (4.15) requires that

$$\boldsymbol{\nu} \cdot \mathbf{J}_i = 0 \text{ on } s_p \quad (i = 1, 2), \tag{4.16}$$

with $\boldsymbol{\nu}$ the unit normal on the bed particles. Consistent with the diffuse interface model, no interfacial boundary conditions exist.

[4] For liquid mixtures as considered in this article, the difference between the internal energy density and the free energy density is expected to be negligible, thereby requiring that the volumetric density ρe be identical to f', whose definition was outlined in footnote 3.

4.4 Macroscale Definitions

4.4.1 Time Scales

As already observed in connection with the temporal evolution of the microscale fields accompanying the flow, the relative motion of the two 'phases' leads to an inherently unsteady phenomenon at the diffuse (as well as the singular) microscale — this despite the fact that the macroscale flow may itself be steady, that is time independent! In such circumstances one can identify the concept of a micro-macro time interval in accordance with the assumption of time-periodic or almost time-periodic flows, with T (Assumption 1) constituting an infinitesimal time interval $d\bar{t}$, say, at the macroscale. Consequently, time intervals of order T will be regarded as being differentials at the macroscale. The macroscale manifestation of the underlying microscale phenomena is observed only in a time-averaged sense at the macroscale, consistent with the continuum description. Therefore, we write

$$d\bar{t} = T, \tag{4.17}$$

where $\bar{t}$ constitutes the macroscale time. In analogy with the previous definition of macroscale lengths following (4.3), one can heuristically write $\bar{t} = t + \mathcal{O}(T)$. Furthermore, all subsequent definitions of macroscale fields will involve a time averaging of the comparable microscale fields of the generic form

$$\frac{1}{T}\int_{t-\frac{T}{2}}^{t+\frac{T}{2}}(\dots)dt. \tag{4.18}$$

For simplicity of notation, we henceforth use the succinct abbreviation

$$\frac{1}{T}\int_{t-\frac{T}{2}}^{t+\frac{T}{2}}(\dots)dt \equiv \int_{t}(\dots) \tag{4.19}$$

to denote the time-averaging operator.

The subsequent analysis focuses primarily on flows that are steady at the macroscale (i.e. satisfy Assumption 1). The ensuing macroscale equations are then generated

by appropriately space- and time-averaging the microscale equations. In view of the assumed spatial- and time-periodicity (or, less stringently, *almost* time-periodicity) of the microscale fields, space-averaging is equivalent to averaging over a unit cell τ_o, and time-averaging to averaging over one period T. Quantities of $\mathcal{O}(\|l\|)$ and $\mathcal{O}(T)$ are subsequently neglected,[5] consistent with the identification of such quantities as being infinitesimal at the macroscopic level. While the main focus of our work will be on flows that are steady at the macroscale, we will also indicate the manner in which the definitions of the macroscale fields can be extrapolated to include time-dependent macroscale fields as well, albeit only those macroscale fields which vary on a much longer time scale than their microscale counterparts. In such circumstances the above definitions can be assumed to hold at a particular macroscopic instant $\bar{t}$, with the averages allowed to be functions of the macrotime $\bar{t}$. Similar generalizations may be applied to slowly varying *spatial* phenomena, thereby allowing for the possibility of spatially inhomogeneous macroscale fields.

Notation: We distinguish macroscale fields and operators from their microscale counterparts by affixing an overbar to the latter. Examples include the macroscale position vector $\overline{\mathbf{R}}$, the phase-specific pressures $\overline{p}_1$, $\overline{p}_2$, and the macroscale gradient operator $\bar{\nabla} \equiv \partial/\partial\bar{\mathbf{R}}$.

4.4.2 Macroscale Physical Quantities

Macroscale physical quantities are defined 'pointwise' at the position $\bar{\mathbf{R}}$ and 'instantaneously' at the time $\bar{t}$ as being the respective volume averages of comparable microscale physical quantities. With ψ representing the volumetric density of a generic macroscale physical property, the definition of the corresponding *interstitial* macro-

[5] In the case of *almost* time-periodic functions, the definition [15]

$$\lim_{T' \longrightarrow \infty} \frac{1}{T'} \int_t^{t+T'} f(t)dt \stackrel{\text{def.}}{=} \hat{f},$$

of $\hat{f}$ is such that that the convergence to $\hat{f}$ occurs uniformly in t. As such, one can identify a finite time interval T sufficient to define a mean value of f that is independent of t to within an error of $\mathcal{O}(T)$. This permits one to define macroscopically steady values for almost time-periodic microscopic fields, since quantities of $\mathcal{O}(T)$ are considered infinitesimal at the macroscale.

scopic density is [cf. (4.48)]

$$\overline{\psi} \stackrel{\text{def.}}{=} \frac{1}{\tau_f} \int_t \int_{\tau_f} d^3\mathbf{r}\, \psi. \tag{4.20}$$

By integrating only over τ_f we have implicitly assumed that the bed particles are impermeable to transport through their interiors of the physical property in question. The definition (4.20) is consistent with the usual viewpoint adopted by a macroscopic observer in representing the total amount, $\int_t \int_{\tau_f} d^3\mathbf{r}\, \psi$, of a 'physical quantity' instantaneously present in a macroscopic differential (interstitial) volume as the product of a macroscopic volumetric density $\overline{\psi}$ and the magnitude τ_f of the 'differential' volume element. However, in view of the fact that only a fraction of the pore space is occupied by interstitial fluid, the volumetric density can also be defined equivalently to (4.20) as

$$\varepsilon \overline{\psi} = \frac{1}{\tau_o} \int_t \int_{\tau_f} d^3\mathbf{r}\, \psi, \tag{4.21}$$

where $\varepsilon \equiv \tau_f/\tau_o$ represents the interstitial void fraction or porosity of the porous medium. In the standard parlance of flow through porous media [5, 7], $\overline{\psi}$ represents the interstitial volumetric density and $\varepsilon\overline{\psi}$[6] the superficial volumetric density of the macroscale property in question.

The generic definitions outlined in Section 4.4 lead us to identify the following physical diffuse Darcyscale densities:

Mass density:

$$\varepsilon\, \overline{\rho} \stackrel{\text{def.}}{=} \frac{1}{\tau_o} \int_t \int_{\tau_f} d^3\mathbf{r}\, \rho; \tag{4.22}$$

[6] In the case where $\overline{\psi}$ is assumed to be spatially nonuniform (possessing weak gradients) the above definition of the macroscale physical quantities, together with the definition of their respective macroscale gradients, cf. eq. (4.49), requires l to be small compared with the length scale of the second derivatives in order to justify the neglect of second derivatives.

Mass density of species 1:

$$\varepsilon\,\overline{\rho}_1 \stackrel{\text{def.}}{=} \frac{1}{\tau_o}\int_t\int_{\tau_f} d^3\mathbf{r}\;\rho_1. \tag{4.23}$$

The latter enables us to define a macroscale volume fraction (or saturation) of phase 1 as

$$\varepsilon\,\overline{c} \stackrel{\text{def.}}{=} \frac{1}{\tau_o}\int_t\int_{\tau_f} d^3\mathbf{r}\;c, \tag{4.24}$$

so that $\overline{\rho}_1 = \rho_1^o\overline{c}$ and $\overline{\rho}_2 = \rho_2^o\overline{(1-c)} \equiv \rho_2^o(1-\overline{c})$. Hence, we find from (3.5) that

$$\begin{aligned}\overline{\rho} &= \overline{\rho}_1 + \overline{\rho}_2\\ &= \rho_1^0\overline{c} + \rho_2^0(1-\overline{c}),\end{aligned} \tag{4.25}$$

consistent with expectations. In view of the assumed incompressibility of the mixture at both the micro- and the macroscales, it is not surprising that the conventional definition of saturation appears as the natural choice for the physical composition variable in our continuous multicomponent description (of what is normally regarded as a two-phase system).

The definition of macroscale momentum density leads to the following definition of the macroscale interstitial velocity $\overline{\mathbf{v}}$ of the binary mixture (with $\varepsilon\,\overline{\mathbf{v}}$ representing the so-called superficial or seepage velocity of the mixture):

$$\varepsilon\,\overline{\rho}\,\overline{\mathbf{v}} \stackrel{\text{def.}}{=} \frac{1}{\tau_o}\int_t\int_{\tau_f} d^3\mathbf{r}\;\rho\mathbf{v}. \tag{4.26}$$

The velocity $\overline{\mathbf{v}}$ appearing in the above expression also constitutes the mass-average velocity (cf. Appendix C). In contrast with conventional two-phase theories of averaging, involving a singular interface Darcyscale description of the pertinent phenomena [8, 10], it will prove unnecessary for us to define *individual* phase velocities $\bar{\mathbf{v}}_1$ and $\bar{\mathbf{v}}_2$ at the macroscale. This innovation is consistent with our diffuse Darcyscale model, which utilizes a *multicomponent* (rather than *multiphase*) viewpoint account-

ing for the several species present, and where accordingly the only relevant velocity is the mixture velocity. Nevertheless, for the sake of comparison with existing theories of multiphase flow, individual macroscale diffusion fluxes of the two species will be defined in the next chapter, enabling us to indirectly identify *species* velocities (equivalent to so-called *phase* velocities). In turn, this will enable us to relate our fine-scale diffuse Darcyscale description to its more traditional, coarser-scale, singular Darcyscale counterpart.

It is important to emphasize the fact that the velocity $\overline{\mathbf{v}}$ plays a dual role as both: (i) the momentum density (per unit mass) in a dynamical context; and (ii) the mass flux vector in a kinematical context. Hence, our subsequent generic definition of the macroscopic fluxes in (4.32), when applied to the mass flux, should (and does) furnish an expression identical to (4.26) for the macroscopic velocity (see Appendix C).

Angular momentum density

For a polar microscale interstitial fluid continuum the total angular momentum density (per unit mass) will generally include an intrinsic pseudovector contribution $\mathbf{l}$ from the internal angular momentum in addition to the usual contribution arising from the moment of the linear momentum [18]. However, it is a consequence of our assumption regarding the nonpolar nature of the fluid at the microscopic level, that $\mathbf{l} = \mathbf{0}$. Nevertheless, the macroscale intrinsic angular momentum density will generally embody within it a nonzero contribution arising from external moment-of-momentum considerations in relation to the screw-symmetric nature of the particles comprising the skeletal porous medium [5, 19]. Thus,

$$\varepsilon\,\overline{\rho}\big(\overline{\mathbf{l}} + \overline{\mathbf{R}} \times \overline{\mathbf{v}}\big) = \frac{1}{\tau_o}\int_t\int_{\tau_f} d^3\mathbf{r}\;\rho\mathbf{R} \times \mathbf{v}. \tag{4.27}$$

Together with the definitions $\mathbf{R} = \mathbf{R}_n + \mathbf{r}$ and $\mathbf{R}_n \equiv \overline{\mathbf{R}}$, the latter reduces to the following expression whereby $\overline{\mathbf{l}}$ can be calculated from the microscale data as:

$$\varepsilon\,\overline{\rho}\overline{\mathbf{l}} \stackrel{\text{def.}}{=} \frac{1}{\tau_o}\int_t\int_{\tau_f} d^3\mathbf{r}\;\rho\mathbf{r} \times \mathbf{v}. \tag{4.28}$$

From the latter definition of $\overline{\mathbf{l}}$ one can discern that it is $\mathcal{O}(\|l\|)$. Accordingly, to

maintain consistency with the subsequent analysis $\bar{\mathbf{I}}$ will henceforth be neglected.

The macroscale energy density $\overline{e}$ per unit volume is defined by the relation

$$\varepsilon\,\overline{\rho}(\overline{e}+\frac{1}{2}\overline{\mathbf{v}}^2)=\frac{1}{\tau_o}\int_t\int_{\tau_f} d^3\mathbf{r}\;\rho(e+\frac{1}{2}\mathbf{v}^2), \tag{4.29}$$

which furnishes the following explicit expression for the internal energy density $\overline{e}$:

$$\varepsilon\,\overline{\rho}\,\overline{e}\overset{\text{def.}}{=}\frac{1}{\tau_o}\int_t\int_{\tau_f} d^3\mathbf{r}\;\rho(e+\frac{1}{2}\mathbf{v}\cdot\mathbf{v}'). \tag{4.30}$$

The latter integrand includes contributions from the microscale internal energy density e, as well as a kinetic energy contribution arising from the distinction between $\frac{1}{2}\overline{\mathbf{v}}^2$ and $\frac{1}{2}\overline{\mathbf{v}^2}$, with $\mathbf{v}'=\mathbf{v}-\overline{\mathbf{v}}$.[7] Furthermore, for reasons identical to those elucidated in footnote 4, the difference between the macroscale free energy density and the macroscale internal energy density is expected to be negligible. Thereby, we obtain

$$\varepsilon\,\overline{F}\overset{\text{def.}}{=}\frac{1}{\tau_o}\int_t\int_{\tau_f} d^3\mathbf{r}\;\rho(e+\frac{1}{2}\mathbf{v}\cdot\mathbf{v}'), \tag{4.31}$$

wherein $\overline{F}$ denotes the macroscale volumetric free energy density.

4.4.3 Macroscopic Fluxes

The following generic definition is adopted for superficial macroscale areal flux densities:

DEFINITION 1 *At a point* $\bar{\mathbf{R}}$ *of the porous medium, the macroscale flux-density tensor* $\overline{\mathbf{M}}\equiv\overline{\mathbf{M}}(\overline{\mathbf{R}})$[8] *of the comparable microscale flux density tensor* $\mathbf{M}\equiv\mathbf{M}(\mathbf{R},t)$

[7]This phenomenon, whereby the clear distinction between 'internal' and 'external' energies at one scale becomes blurred at a coarser scale, is analogous to comparable phenomena at the pre-continuum, discrete molecular scale, whereby, say, the kinetic energy of discrete molecules becomes a part of the internal energy of the system at the continuum scale (so that the sum of the kinetic energies of the molecules is not identical with the kinetic energy of the continuum) [20].

[8]Note that $\overline{\mathbf{M}}\equiv\overline{\mathbf{M}}(\overline{\mathbf{R}},\bar{t})$ in the case of a flow varying temporally on the macroscopic time scale.

is defined generically as

$$\mathbf{s}_k \cdot \overline{\mathbf{M}} \stackrel{def.}{=} \int_t \int_{\mathbf{s}_k\{\mathbf{n}\}} d\mathbf{s} \cdot \mathbf{M}. \tag{4.32}$$

Inasmuch as $\mathbf{s}_k \equiv d\bar{\mathbf{s}}$, the preceding expression constitutes a *Eulerian* definition of the macroscale flux provided that $\overline{\mathbf{M}}$ can be shown to be independent of the orientation $\mathbf{s}_k$ of the cell face. This fact is demonstrated by Brenner [5] (see also [12]) for spatially periodic fields $\mathbf{M}$, albeit without the temporal integration. This Eulerian definition eventually enables us to satisfy the physical requirements demanded of any proposed definition of a macroscale flux density, e.g., the stress tensor, since in this case, the right-hand side of the above equation respectively represents the force exerted on a mass flowing across an area which is 'infinitesimal' at the macroscale. The following results, proofs of which are furnished in Appendix B, are consequences of the definition (4.32).

THEOREM 1 *When the instantaneous gradient* $\nabla\mathbf{M}$ *of the microscale flux density* $\mathbf{M}$ *is spatially periodic, the macroscale flux density* $\overline{\mathbf{M}}(\overline{\mathbf{R}})$*, defined so as to possess the areal property (4.32) [albeit only to* $\mathcal{O}(\|l\|)$ *terms], is explicitly given by the expression*

$$\overline{\mathbf{M}} = \frac{1}{\tau_o} \int_t \oint_{\partial\tau_o} \mathbf{r} d\mathbf{s} \cdot \mathbf{M}. \tag{4.33}$$

Moreover, $\overline{\mathbf{M}}$ *defined in this way possesses a macroscale gradient, expressible as*

$$\bar{\nabla}\overline{\mathbf{M}} = \frac{1}{\tau_o} \int_t \oint_{\partial\tau_o} d\mathbf{s}\, \mathbf{M}. \tag{4.34}$$

Upon scalar contraction the latter yields

$$\bar{\nabla} \cdot \overline{\mathbf{M}} = \frac{1}{\tau_o} \int_t \oint_{\partial\tau_o} d\mathbf{s} \cdot \mathbf{M}. \tag{4.35}$$

The preceding properties possessed by $\overline{\mathbf{M}}$ enable us to explicitly identify the following superficial areal flux densities, each respectively associated with a different choice of physical property:

Mass flux-density vector:

$$\overline{\mathbf{J}}_M \stackrel{\text{def.}}{=} \frac{1}{\tau_o} \int_t \oint_{\partial\tau_o} \rho \mathbf{r} d\mathbf{s} \cdot \mathbf{v}. \tag{4.36}$$

Proof of the fact that the above definition is consistent with one's expectation that $\overline{\mathbf{J}}_M$ should be expressible in terms of the macroscale variables $\overline{\rho}$ and $\overline{\mathbf{v}}$ as $\overline{\mathbf{J}}_M = \varepsilon\, \overline{\rho}\, \overline{\mathbf{v}}$ is presented in Appendix C.

Diffusion flux-density vector:

$$\overline{\mathbf{N}}_1 \stackrel{\text{def.}}{=} \frac{1}{\tau_o} \int_t \oint_{\partial\tau_o} \mathbf{r} d\mathbf{s} \cdot \mathbf{N}_1, \tag{4.37}$$

where $\mathbf{N}_1 = \rho_1 \mathbf{v} + \mathbf{J}_1$. Here, $\overline{\mathbf{N}}_1$ denotes the net macroscale flux-density of species 1 (relative to the stationary porous medium) arising from both microscale convection and diffusion processes. Analogous to the comparable microscale decomposition appearing in the diffuse interface description, one can separate $\overline{\mathbf{N}}_1$ into a sum of convective and diffusive fluxes:

$$\overline{\mathbf{N}}_1 = \varepsilon\, \overline{\rho}_1 \overline{\mathbf{v}} + \overline{\mathbf{J}}_1, \tag{4.38}$$

where the macroscale diffusion flux $\overline{\mathbf{J}}_1$ is defined as

$$\overline{\mathbf{J}}_1 \stackrel{\text{def.}}{=} \frac{1}{\tau_o} \int_t \oint_{\partial\tau_o} \mathbf{r} d\mathbf{s} \cdot (\rho_1 \mathbf{v}' + \mathbf{J}_1), \tag{4.39}$$

and $\mathbf{v}'$ is defined following (4.30), being the deviation from the mean velocity. Similarly, one can define the macroscale *momentum flux-density* dyadic

$$\overline{\mathbf{P}}_M \stackrel{\text{def.}}{=} \varepsilon\, \overline{\rho}\, \overline{\mathbf{v}}\, \overline{\mathbf{v}} + \overline{\mathbf{P}}, \tag{4.40}$$

with the macroscale stress tensor $\overline{\mathbf{P}}$ defined as

$$\overline{\mathbf{P}} \stackrel{\text{def.}}{=} \frac{1}{\tau_o}\int_t \oint_{\partial\tau_o} \mathbf{r}d\mathbf{s}\cdot(\rho\mathbf{v}\mathbf{v}' + \mathbf{P}), \tag{4.41}$$

in which $\mathbf{P} \equiv -p\mathbf{I} + \boldsymbol{\tau}$ denotes the microscale stress tensor.

Appendix D discusses the manner in which $\overline{\mathbf{P}}$ as defined above can be expressed as the sum of a macroscale pressure $\overline{p}$ and a (generally asymmetric) macroscale deviatoric stress tensor $\overline{\boldsymbol{\tau}}$:

$$\overline{\mathbf{P}} = -\overline{p}\mathbf{I} + \overline{\boldsymbol{\tau}}, \tag{4.42}$$

wherein

$$\overline{p} \stackrel{\text{def.}}{=} -\frac{1}{3\tau_o}\int_t \oint_{\partial\tau_o} \mathbf{r}\cdot d\mathbf{s}\cdot(\rho\mathbf{v}\mathbf{v}' + \mathbf{P}) \tag{4.43}$$

and

$$\overline{\boldsymbol{\tau}} \stackrel{\text{def.}}{=} -\frac{1}{\tau_o}\int_t \oint_{\partial\tau_o} (\mathbf{r}\mathbf{I} - \frac{1}{3}\mathbf{I}\mathbf{r})\cdot d\mathbf{s}\cdot(\rho\mathbf{v}\mathbf{v}' + \mathbf{P}). \tag{4.44}$$

As further discussed in Appendix D, it is the macroscopic pressure gradient that is physically significant, rather than the macroscale pressure itself. Indeed, according to (D.8),

$$\bar{\nabla}\overline{p} = \frac{1}{\tau_o}\int_t \oint_{\partial\tau_o} d\mathbf{s}\, p. \tag{4.45}$$

Similarly, the net macroscale *energy flux-density* vector is defined as

$$\overline{\mathbf{J}}_e \stackrel{\text{def.}}{=} \varepsilon\,\overline{\rho}\,(\overline{e} + \frac{1}{2}\overline{\mathbf{v}}^2)\overline{\mathbf{v}} - \overline{\mathbf{P}}\cdot\overline{\mathbf{v}} + \overline{\mathbf{q}}, \tag{4.46}$$

with

$$\overline{\mathbf{q}} \stackrel{\text{def.}}{=} \frac{1}{\tau_o}\int_t \oint_{\partial\tau_o} \mathbf{r}d\mathbf{s}\cdot\left[\mathbf{q} + \rho(e + \frac{1}{2}\mathbf{v}^2)\mathbf{v}' - \mathbf{P}\cdot\mathbf{v}'\right] \tag{4.47}$$

identified as the macroscopic heat flux-density vector. This completes the definitions adopted for the diffuse Darcyscale fluxes pertinent to our analysis.

4.4.4 Macroscopic Source Terms

Macroscale source terms are defined as being the volume averages of the respective microscale source terms. Again, this is consistent with measurements that would be registered by a macroscale experimental probe; that is, a probe whose aperture is of the order of the cell size.

Upon using equation (4.23) defining $\varepsilon\,\overline{\rho_i}$, the momentum source term is given by $\sum_{i=1}^{2}\varepsilon\,\overline{\rho_i}\mathbf{g}_i$. The macroscopic energy dissipation due to the diffusive flux is given by, $\sum_{i=1}^{2}(\varepsilon\,\overline{\rho_i}\,\overline{\mathbf{v}}+\overline{\mathbf{J}}_i)\cdot\mathbf{g}_i$, where the definition (4.39) of $\overline{\mathbf{J}}_i$ has been used.

To effect the averaging procedure enabling the transition from microscale to macroscale we require use of the following generic definition of the macroscale gradient:

4.4.5 Macroscopic Gradients

DEFINITION 2 *For a function of volumetric density ψ whose macroscale value is defined as*

$$\varepsilon\overline{\psi}\overset{def.}{=}\frac{1}{\tau_o}\int_t\int_{\tau_o}d^3\mathbf{r}\;\psi, \tag{4.48}$$

the corresponding macroscopic spatial gradient is defined as

$$\bar{\nabla}\overline{\psi}\overset{def.}{=}\frac{1}{\tau_f}\int_t\oint_{\partial\tau_o}d\mathbf{s}\;\psi, \tag{4.49}$$

and the macroscale time derivative as

$$\frac{\partial\overline{\psi}}{\partial\bar{t}}\overset{def.}{=}T^{-1}\left\{\frac{1}{\tau_f}\int_{\tau_o}d^3\mathbf{r}\;\psi(t+\frac{T}{2})-\frac{1}{\tau_f}\int_{\tau_o}d^3\mathbf{r}\;\psi(t-\frac{T}{2})\right\}. \tag{4.50}$$

The latter is consistent with our time-element identification in (4.17). Functions $\overline{\psi}$

satisfying Assumption 1 possess a macroscopic time derivative that is identically zero:

$$\frac{\partial \overline{\psi}}{\partial \bar{t}} = \mathbf{0}. \tag{4.51}$$

However, in the general case where the flow is macroscopically unsteady, (4.50) translates as

$$\frac{\partial \overline{\psi}}{\partial \bar{t}} = \frac{1}{\tau_f} \int_t \int_{\tau_o} d^3\mathbf{r} \frac{\partial \psi}{\partial t}. \tag{4.52}$$

The above identifications permit derivation of the pertinent field equations governing transport at the macroscale starting from the corresponding microscale transport equations, a topic addressed in the following section.

4.5 Macroscale Equations

Averaging the microscale equations over time and space (the former over one time-period T and the latter over the unit cell τ_o), and using the preceding definitions of the macroscopic time derivative together with the expressions for the macroscopic flux densities and their divergences jointly with the boundary conditions (4.15), (4.16), yields the following diffuse Darcyscale field equations:

Diffusion equations:

$$\frac{\partial(\varepsilon\, \overline{\rho_1})}{\partial \bar{t}} + \bar{\nabla} \cdot (\varepsilon\, \overline{\rho_1}\, \overline{\mathbf{v}}) = -\bar{\nabla} \cdot \overline{\mathbf{J}}_1; \quad \frac{\partial(\varepsilon\, \overline{\rho_2})}{\partial \bar{t}} + \bar{\nabla} \cdot (\varepsilon\, \overline{\rho_2}\, \overline{\mathbf{v}}) = -\bar{\nabla} \cdot \overline{\mathbf{J}}_2. \tag{4.53a,b}$$

Momentum equation:

$$\frac{\partial(\varepsilon\, \overline{\rho}\, \overline{\mathbf{v}})}{\partial \bar{t}} + \bar{\nabla} \cdot (\varepsilon\, \overline{\rho}\, \overline{\mathbf{v}}\, \overline{\mathbf{v}}) = -\bar{\nabla} \overline{p} + \bar{\nabla} \cdot \overline{\boldsymbol{\tau}} + \sum_{i=1}^{2} \varepsilon\, \overline{\rho_i} \mathbf{g}_i + \hat{\mathbf{F}}, \tag{4.54}$$

where

$$\hat{\mathbf{F}} \stackrel{\text{def.}}{=} \int_t \int_{s_p} d\mathbf{s} \cdot \mathbf{P} \tag{4.55}$$

denotes the macroscopic volumetric force density arising from the immobility of the bed particles.[9]

Energy equation:

$$\frac{\partial\left[\varepsilon\,\overline{\rho}(\overline{e}+\frac{1}{2}\overline{\mathbf{v}}^2)\right]}{\partial\bar{t}}+\bar{\nabla}\cdot\left[\varepsilon\,\overline{\rho}\,(\overline{e}+\frac{1}{2}\overline{\mathbf{v}}^2)\overline{\mathbf{v}}-\overline{\mathbf{P}}\cdot\overline{\mathbf{v}}+\overline{\mathbf{q}}\right]-\sum_{i=1}^{2}(\varepsilon\,\overline{\rho_i}\,\overline{\mathbf{v}}+\overline{\mathbf{J}}_i)\cdot\mathbf{g}_i=0. \tag{4.56}$$

All quantities appearing in these diffuse Darcyscale field equations have been rigorously defined so as to maintain consistency with the physical measurements discernible to a macroscale observer. Moreover, they are operationally expressed entirely in terms of spatial and temporal quadratures of well-defined microscale fields. As the subsequent analysis will be primarily concerned with inertia-free and isothermal microscale flows, effects arising from the existence of the macroscopic stress tensor as well as from energy considerations are consequently irrelevant and hence will not be further pursued except insofar as they prove necessary in our generic discussion of macroscale irreversible thermodynamic principles.

4.6 Conclusions

In this chapter we erected the infrastructure prerequisite to a rigorous transition from the microscale to the macroscale level of the porous medium flow phenomena within the context of the diffuse interface model. Subsequent to a brief introduction expounding the assumption of the geometrical periodicity, we elucidated the physically-based definitions of the macroscale physical quantities. Thereby we derived the transport equations governing the temporal evolution of macroscale physical variables. The

[9]The genesis of $\hat{\mathbf{F}}$ lies in the no-slip condition on the solid particle surfaces. Slip or other forms of boundary conditions resulting from the presence of contact lines would presumably lead to different boundary conditions at the solid surfaces, and hence would also change the constitutive form of the force appearing in the final expression. However, there does not exist an analogous term in the macroscale energy equation (4.56) even for varying temperature fields. The underlying reason for this is that the force $\hat{\mathbf{F}}$ is of a physicochemical nature, arising from the stationarity of the particles, rather than being externally imposed. Were the latter the case, this force would then have necessarily appeared in the energy equation. This subtle feature plays a crucial role in determining the form of Darcy's law from considerations of irreversible thermodynamics, as is outlined in Section 6.1.

framework outlined in this chapter thus enables computation of the macroscale fields, therefore constituting an implicit ratification of the functional form of the macroscale equations. In principle, the rigorous framework outlined in this chapter enables the following dual purposes: (a) computation of the macroscale fields from the precursor microscale fields; (b) construction of the macroscale constitutive equations, pending the specification of the microscale constitutive equations.

The subsequent chapter implements the diffuse Darcyscale framework outlined in the present chapter so as to identify the phase-specific quantities and governing equations. We also provide significant insights into the the functional form of the macroscale physical quantities by utilizing the microscale constitutive equations outlined in chapter 3. (The entirety of our preceding discussion had explicitly avoided incorporating any specific form for the microscale constitutive equations.) The prescription of the microscale constitutive equations enable one, in principle, to derive the macroscale equations based on our framework. However, the constitutive equations outlined in the previous chapter are highly nonlinear in their functionality, thereby precluding the possibility of an analytical averaging procedure. Consequently, instead of directly utilizing the microscale constitutive equations to derive the comparable macroscale equations, we rationally 'guess' the forms of the macroscale constitutive equations based on considerations of irreversible (or nonequilibrium) thermodynamics. Such a procedure, effected in chapter 6, enables justifying the biphasic Darcy's laws and their generalizations. Eventually, we consider a simple linearized example to verify the functional forms suggested by our irreversible thermodynamic arguments.

References

[1] P. M. Adler, *Porous Media: Geometry and Transports*, Butterworth-Heinemann, Boston (1992).

[2] L. Brillouin, *Wave Propagation in Periodic Structures*, McGraw-Hill, New York (1946).

[3] A. Bensoussan, J. L. Lions, and G. Papanicolaou, *Asymptotic Analysis for Periodic Structures*, North-Holland, New York (1978).

[4] L. C. Nitsche, *Multiphase Flows Through Spatially-Periodic Models of Porous Media*, Ph. D. Thesis, Massachusetts Institute of Technology, Cambridge 1989).

[5] H. Brenner, "Elements of Transport Processes in Porous Media," 9 folios of unpublished notes (1972).

[6] H. Brenner, "Dispersion resulting from flow through spatially periodic porous media," *Phil. Trans. R. Soc. Lond.* A **297**, 81 (1980).

[7] H. Brenner and D. A. Edwards, *Macrotransport Processes*, Butterworth-Heinemann, Boston (1993).

[8] C. M. Marle, "On macroscopic equations governing multiphase flow with diffusion and chemical reactions in porous media," *Int. J. Engng Sci.*, **20**, 643 (1977).

[9] W. G. Gray and S. M. Hassanizadeh, "Mechanics and thermodynamics of multiphase flow in porous media including interphase boundaries," *Adv. Water Resour.*, **13**, 169 (1990).

[10] S. Whitaker, "Flow in porous media: 2. The governing equations for immiscible two-phase flow," *Transp. Porous Media*, **1**, 105 (1986).

[11] P. M. Adler, M. Zuzovsky and H. Brenner, "Spatially-periodic suspensions of convex particles in linear shear flows: 1. Description and kinematics," *Int. J. Multiphase Flow.*, **11**, 361(1985).

[12] L. C. Nitsche and H. Brenner, "Eulerian kinematics of flow through spatially-periodic models of porous media," *Arch. Rat. Mech. Anal.*, **107**, 225 (1989).

[13] M. Ishii, *Thermo-Fluid Dynamic Theory of Two-Phase Flows*, Eyrolles, Paris (1975).

[14] J. M. Ottino, *The Kinematics of Mixing: Stretching, Chaos and Transport*, Cambridge University Press, Cambridge (1989).

[15] H. Bohr, *Almost Periodic Functions*, Chelsea, New York (1947).

[16] R. Aris, *Vectors, Tensors, and the Basic Equations of Fluid Mechanics*, Prentice-Hall, New Jersey (1962).

[17] S. R. deGroot and P. Mazur, *Non-Equilibrium Thermodynamics*, Dover, New York (1984).

[18] J. S. Dahler and L. E. Scriven, "Theory of structured continua," *Proc. R. Soc. Lond.* A **275**, 504 (1963).

[19] H. Brenner, "Rheology of two phase systems," *Ann. Rev. Fluid Mech.*, **2**, 137 (1970).

[20] J. G. Kirkwood, *Selected Topics in Statistical Mechanics*, Gordon & Breach, New York (1967).

Chapter 5

Biphasic Flows in Porous Media: Singular Darcyscale

The preceding chapter was explicitly concerned with developing the macroscale framework accompanying the diffuse Darcyscale viewpoint, the conception of which entailed the flow of a binary 'mixture' at the Darcyscale. This physically-based framework, outlined therein, enables identification of the transport equations applicable at the diffuse Darcyscale. However, conventional efforts at modeling biphasic flows in porous media (cf. chapter 2 and the references cited therein) are typically concerned with 'phase-specific' quantities. Examples of such concepts include phase-specific pressures, velocities, Darcy constitutive laws, etc. Consequently, in order to make an explicit connection with the conventional modeling framework (which we term the "singular Darcyscale"), in this chapter we utilize the diffuse Darcyscale framework to identify the physical definitions of the phase-specific quantities and the equations governing them.

The following sections are concerned with a rigorous thermodynamic framework for identifying 'phase-specific' quantities at the singular Darcyscale from their precursor 'mixture' quantities describing the diffuse Darcyscale. Such an approach embodies the philosophy whereby one identifies 'phase-specific' quantities with the 'species-specific' quantities characterizing the mixture. We utilize this framework to derive relationships between the phase-specific quantities and their diffuse Darcyscale pre-

cursors. Such a procedure yields an explicit expression for the capillary pressure, which has hitherto confounded most macroscale researches in terms of its rational understanding. Furthermore, we utilize the microscale constitutive equations to provide new insights into the nature of the hysteresis observed in experimental measurements of capillary pressure. Subsequently, we argue that the macroscale energy equation needs to be incorporated within any macroscale modeling framework so as to enable closure of the dynamical equations requisite to modeling multiphase flows at the Darcyscale level.

5.1 Phase-Specific Quantities

This section provides an interpretation of the conventional empirical singular Darcyscale phase-specific quantities appearing in the ubiquitous two-phase Darcy flow equation (2.2). This is achieved by correlating these phase-specific fields with our two-component microscale quantities. The basis for accomplishing this lies in the diffuse two-component mixture formulation that we have adopted at both the micro- and macroscales. The approach used in this section involves relating phase-specific (or, more properly, species-specific) macroscale fields appearing in the singular Darcyscale description (2.2) to their diffuse Darcyscale counterparts. Thus, in contrast with many prior analyses [4, 6, 10], singular Darcyscale phase-specific quantities will not be defined as averages of their (singular interface) microscale counterparts — so that, for instance,

$$\overline{p}_1 \neq \frac{1}{\tau_o}\int_t\int_{\tau_o} d^3\mathbf{r}\, p_1. \tag{5.1}$$

Only inertialess (slow) and isothermal flows are addressed in the ensuing discussion.

5.1.1 Phase Velocities

The diffuse Darcyscale formulation that we have adopted serves to define $\overline{\mathbf{v}}$ and $\overline{\mathbf{J}}_i$ in a rigorous manner. A macroscale observer then discerns the individual 'phase velocities' $\overline{\mathbf{v}}_1$ and $\overline{\mathbf{v}}_2$ only indirectly, namely from measurements of $\overline{\mathbf{J}}_1$ and $\overline{\mathbf{J}}_2$, by pursuing the following argument: By definition,

$$\overline{\mathbf{J}}_1 = \overline{\rho}_1(\overline{\mathbf{v}}_1 - \overline{\mathbf{v}}); \qquad \overline{\mathbf{J}}_2 = \overline{\rho}_2(\overline{\mathbf{v}}_2 - \overline{\mathbf{v}}). \tag{5.2a,b}$$

Consequently,

$$\overline{\mathbf{v}}_1 = \frac{\overline{\mathbf{J}}_1}{\overline{\rho}_1} + \overline{\mathbf{v}}; \qquad \overline{\mathbf{v}}_2 = \frac{\overline{\mathbf{J}}_2}{\overline{\rho}_2} + \overline{\mathbf{v}}. \tag{5.3a,b}$$

It is readily established that the above definitions imply that

$$\varepsilon\,\overline{\rho}_1\overline{\mathbf{v}}_1 = \frac{1}{\tau_o}\int_t\int_{\tau_f} d^3\mathbf{r}\;\rho_1\mathbf{v}_1, \tag{5.4}$$

together with a comparable relation for species 2. However, our interpretation of $\overline{\mathbf{v}}_1$ and $\overline{\mathbf{v}}_2$ is independent of (5.4) *et seq.*, since at the diffuse interfacial microscale only the mixture velocity $\overline{\mathbf{v}}$ is physically relevant in the context of our model.

5.1.2 Phase-specific Pressures

Before dealing with the concept of phase-specific pressures (in the context of the singular Darcy description), and as a preliminary to the subsequent development, we define the following diffuse Darcyscale quantities:

• Macroscale chemical potential

Consistent with the assumption stated in the Introduction, we hypothesize that conventional thermodynamic identities among microscale quantities hold equally well when macroscale thermodynamic quantities (such as free energy) are involved. A similar assumption has been made by others [4, 6, 9], who likewise employed conventional thermodynamic identities at the macroscale. Thus, we define the macroscale

chemical potentials:

$$\overline{\mu}_1 \stackrel{\text{def.}}{=} \frac{\partial \overline{F}}{\partial \overline{\rho}_1}; \qquad \overline{\mu}_2 \stackrel{\text{def.}}{=} \frac{\partial \overline{F}}{\partial \overline{\rho}_2}. \tag{5.5a,b}$$

The indicated differentiations are to be performed while keeping constant all other physical variables other than species density.

• Phase-specific pressures

With the above considerations in mind we propose the following definitions for the singular Darcyscale phase-specific pressures:

$$\bar{\nabla}\overline{p}_1 = \frac{\overline{\rho}_1}{\overline{\rho}}\bar{\nabla}\overline{\mu}_1; \qquad \bar{\nabla}\overline{p}_2 = \frac{\overline{\rho}_2}{\overline{\rho}}\bar{\nabla}\overline{\mu}_2. \tag{5.6a,b}$$

These relations are exact for homogeneous (and weakly inhomogeneous) systems at thermodynamic equilibrium. Their extension to nonequilibrium situations, as in our case, is linked to the assumption of local equilibrium — discussed in section 6.1. In fact, Kirkwood & Bearman [5] in their discussion of transport processes in multicomponent mixtures propose identical relations, albeit for species-specific pressures. The above definitions do not incorporate effects arising from incompressibility. This restriction is incorporated into our work by a novel method first proposed by de-Gennes [2], although in a different context. Its implementation involves assuming that the incompressibility condition can be viewed as resulting from the action of fictitious physicochemical forces, represented here by the gradient of some macroscale potential $\hat{U}$. Explicitly,

$$\bar{\nabla}\overline{p}_1 = \frac{\overline{\rho}_1}{\overline{\rho}}\bar{\nabla}(\overline{\mu}_1 + \hat{U}); \qquad \bar{\nabla}\overline{p}_2 = \frac{\overline{\rho}_2}{\overline{\rho}}\bar{\nabla}(\overline{\mu}_2 + \hat{U}), \tag{5.7a,b}$$

where $\hat{U}$ is determined by imposing the incompressibility condition:

$$\bar{\nabla}\overline{p}_1 + \bar{\nabla}\overline{p}_2 = \bar{\nabla}\overline{p}. \tag{5.8}$$

Upon solving for $\hat{U}$ in the above equations and substituting the resulting expression

into (5.7a,b) one obtains:

$$\bar{\nabla}\overline{p}_1 = \frac{\overline{\rho}_1}{\overline{\rho}}\bar{\nabla}\overline{p} + \frac{\overline{\rho}_1\overline{\rho}_2}{\overline{\rho}^2}\bar{\nabla}(\overline{\mu}_1 - \overline{\mu}_2); \quad \bar{\nabla}\overline{p}_2 = \frac{\overline{\rho}_2}{\overline{\rho}}\bar{\nabla}\overline{p} + \frac{\overline{\rho}_1\overline{\rho}_2}{\overline{\rho}^2}\bar{\nabla}(\overline{\mu}_2 - \overline{\mu}_1). \tag{5.9a,b}$$

The latter pair of equations constitute the operational definitions of the singular Darcyscale phase-specific pressures. It is appropriate here to review the evolution that led to these definitions. In particular, these pressures have not been obtained by averaging respective phase-specific microscale pressures p_1 and p_2 arising in the singular interface view, as has been done in the past by other researchers. Indeed, such individual pressure fields have no existence in our diffuse, strongly inhomogeneous, single-phase view. Rather, in our diffuse microscale view, the pressure p of the mixture ('solution') as a whole was identified by its contribution to the linear momentum transport process. Rigorous definitions of the diffuse Darcyscale fluxes (in terms of the microscale fluxes) subsequently yielded the diffuse Darcyscale pressure of the mixture. Within this mixture, individual species (or 'phase-specific') macroscale pressures $\overline{p}_i$ were identified with the corresponding gradients $\bar{\nabla}\overline{\mu}_i$ in chemical potential, consistent with the local equilibrium assumption. Incompressibility was incorporated through fictitious physicochemical forces. This conceptual foundation underlying $\bar{\nabla}\overline{p}_1$ and $\bar{\nabla}\overline{p}_2$ is subsequently used in the next section to explain the phase-equilibrium-type of relationship postulated [3, 7] to exist between $\bar{\nabla}\overline{p}_1$ and $\bar{\nabla}\overline{p}_2$.

Note: In this and subsequent sections we will be concerned exclusively with slow, isothermal flows characterized by weak spatial gradients. The temperature dependence of the various physical quantities, especially the free energies, will not be explicitly displayed unless essential to the development.

5.2 Capillary Pressure

As noted in the Introduction, the singular Darcyscale description of multiphase flows, being based upon phase-specific Darcy's laws, requires knowledge of the so-called

capillary pressure $P_c[\overline{c}]$ to effect closure of the resulting system of equations [3, 7]. However, prior analyses have been unable to convincingly identify the fundamental source of the hypothesized capillary pressure–saturation relationship underlying such theories. While it has always been conjectured that the capillary pressure–saturation relationship represents a macroscale manifestation of the microscale singular-surface Laplace interfacial boundary condition [cf. (3.72)] [10], attempts to relate quantities like $\overline{p}_1$ and $\overline{p}_2$ — resulting from *volume* averaging — to microscale matching conditions, which are valid only at interfaces [3], are not wholly convincing. Moreover, the Laplace equation derives from equilibrium considerations, whereas the Darcy-flow case necessarily entails nonequilibrium processes! As such, prior theoretical arguments proposed for the existence of a capillary-saturation relationship are at best conjectural and incomplete.

In contrast, the present work adopts an innovative formalism for describing microscale two-phase flows, where one no longer deals with intrinsically macroscopic terms like 'interfaces.' As a consequence, the Laplace boundary condition no longer manifests itself in an explicit manner, thereby enabling rigorous operational definitions to be set forth for the diffuse Darcyscale pressure field $\overline{p}$ in terms of quadratures of microscale fields. In turn, knowledge of this macroscale pressure, together with use of other equally well-defined macroscale fields, has enabled us to derive singular Darcyscale phase-specific pressures $\overline{p}_1, \overline{p}_2$ through rigorous operational definitions of the latter. This led, in turn, to the expressions (5.9a,b) for $\bar{\nabla}\overline{p}_1$ and $\bar{\nabla}\overline{p}_2$.

Subtraction of the latter pair of equations yields

$$\frac{\overline{\rho}}{\overline{\rho}_1}\bar{\nabla}\overline{p}_1 - \frac{\overline{\rho}}{\overline{\rho}_2}\bar{\nabla}\overline{p}_2 = \bar{\nabla}(\overline{\mu}_1 - \overline{\mu}_2). \tag{5.10}$$

At equilibrium, when both $\bar{\nabla}\overline{\rho}_1$ and $\bar{\nabla}\overline{\rho}_2$ vanish identically, so that $\overline{\rho}_1$ and $\overline{\rho}_2$ (and hence $\bar{\rho}$) are each independent of position, it follows from the above that

$$\frac{\overline{\rho}}{\overline{\rho}_1}\overline{p}_1 - \frac{\overline{\rho}}{\overline{\rho}_2}\overline{p}_2 = \overline{\mu}_1 - \overline{\mu}_2. \tag{5.11}$$

The left-hand side of the above equation constitutes our proposed definition of the

heretofore elusive capillary pressure, namely[1]

$$P_c \stackrel{\text{def}}{=} \frac{\overline{\rho}}{\overline{\rho}_1}\overline{p}_1 - \frac{\overline{\rho}}{\overline{\rho}_2}\overline{p}_2. \tag{5.12}$$

The definition (5.12) constitutes the logical outcome of our designation of species- (or phase-) specific pressures, starting from the concept of the *total* pressure $\overline{p}$ of the mixture. The above equation also embodies a definitive scheme for calculating the capillary pressure from the microscale data, since $\overline{\mu}_1$ and $\overline{\mu}_2$ are eventually defined in terms of their relationship to microscale quantities. We believe that our investigation is the first to propose a rigorous, physically-based, operational definition of the capillary pressure as a true continuum field concept. In a deeply intuitive study, Hassanizadeh & Gray [3] hint at similar considerations; but in view of the absence of a suitable micro-macro homogenization scheme in their proposal, the physical basis for such a hypothesis is lacking.

Until now our discussion was completely independent of the choice of the microscale constitutive equations adopted for $\mathbf{J}_1, \mathbf{J}_2$ and $\boldsymbol{\tau}_c$ in equations (4.11a,b) and (4.12). In the following sections, namely 5.3 - 5.5, we adopt the constitutive equations outlined in section 3.3, enabling us thereby to provide a number of significant insights into macroscale concepts which have heretofore defied completely rational elucidation in previous investigations. In view of our rigorous definitions linking microscale and macroscale physical quantities, we are able to furnish exact statements regarding the functional dependencies of the macroscale physical quantities. These dependencies constitute the appropriate form of an *equation of state* for macroscale-level modeling. We also display the complete set of equations required for macroscale modeling which embody the variables consistent with such an equation of state. An experimentally determined equation of state, in conjunction with the complete set of macroscale equations, thereby provides a framework for a macroscale modeling scheme, one which is devoid of the need for actually computing the microscale solutions appropriate to

[1]This pressure is defined in a manner different from that advocated by others, who employ a volume-averaging procedure (cf. the review by Adler & Brenner [1])

the porous-medium geometry. Such a framework is developed in the following three sections.

5.3 Macroscale Free Energy Density

Preliminary to seeking insights into the physical basis of capillary pressure, a topic which is discussed in the next section, we first analyze the functional form of the macroscale free energy density.

Calculation of the capillary pressure via (5.19) rests upon knowledge of the macroscale chemical potentials, $\overline{\mu}_1$ and $\overline{\mu}_2$. However, the macroscale chemical potential is calculated via (5.5a,b) through the macroscale free energy density $\overline{F}$, which is defined in eq. (4.31):

$$\varepsilon \overline{F} \stackrel{\text{def.}}{=} \frac{1}{\tau_o} \int_t \int_{\tau_f} d^3\mathbf{r}\ \rho(e + \frac{1}{2}\mathbf{v} \cdot \mathbf{v}'). \tag{5.13}$$

We consider the constitutive form proposed in footnotes 3 and 4 for the definition of the internal energy density e required above, thereby allowing us to write (5.13) as

$$\varepsilon \overline{F} \stackrel{\text{def.}}{=} \frac{1}{\tau_o} \int_t \int_{\tau_f} d^3\mathbf{r}\ [f(c) + f_{\text{id}} + \frac{1}{2}K(\nabla c)^2 + \frac{1}{2}\rho \mathbf{v} \cdot \mathbf{v}']. \tag{5.14}$$

Note that the energy density $\overline{F}$ possesses contributions arising from three sources: (i) Microscale bulk internal energy; (ii) Microscale kinetic energy; and (iii) Gradient energy. Contributions from sources (i) and (ii) are present in the macroscale energy density in single-phase, binary mixture flows. However, the third contribution, representing gradient effects, arises exclusively as a consequence of the presence of the second phase. To facilitate the analysis of the respective functional dependence of the macroscale free energy upon each of these contributions, we divide the contributions into two groups, denoting by $\overline{F}_{\text{bulk}}$ the sum of the contributions (i) and (ii), and by $\overline{F}_{\text{grad}}$ that resulting from the gradient terms. Consequently,

$$\varepsilon \overline{F}_{\text{bulk}} = \frac{1}{\tau_o} \int_t \int_{\tau_f} d^3\mathbf{r}\ (f + f_{\text{id}} + \frac{1}{2}\mathbf{v} \cdot \mathbf{v}'). \tag{5.15}$$

The functional dependence of each of the terms appearing above may be analyzed as follows: (i) In view of the fact that $f(c) = 0$ for $c = 0$ and 1, $f(c)$ is nonzero only in the interfacial region. Furthermore, since $f(c)$ is of $\mathcal{O}(1)$ everywhere (even within the interfacial region, since there exists no explicit dependence of f upon gradients) the contribution of $f(c)$ to $\overline{F}_{\text{bulk}}$ is of $\mathcal{O}(\delta^{1/3})$ (δ denoting the width of the interfacial region). As such, the contribution of this term proves negligible compared with that of the other terms; (ii) The contribution of $f_{\text{id}} \equiv cf_1 + (1-c)f_2$ to $\overline{F}_{\text{bulk}}$ is functionally dependent only upon $\overline{c}$ (in addition to temperature); (iii) The contribution arising from the kinetic energy term can influence the macroscale free energy through the dependence of the latter upon the macroscale temperature, in a manner not unlike that of the contribution of molecular motion to the continuum-scale internal energy density. However, since subtle differences existing between the macroscale and microscale temperatures are peripheral to the focus of this article we eschew this complication by assuming that the contribution arising from the microscale kinetic energy term is negligible for the slow, low Reynolds number flows considered here.

The suggested functional dependencies of the individual contributions lead us to conclude that $\overline{F}_{\text{bulk}} \equiv \overline{F}_{\text{bulk}}(\overline{c}, T)$.

Consider the gradient contribution to the macroscale free energy:

$$\varepsilon\, \overline{F}_{\text{grad}} = \frac{1}{\tau_o}\int_t\int_{\tau_f} d^3\mathbf{r}\rho e_{\text{grad}} = \frac{1}{\tau_o}\int_t\int_{\tau_f} d^3\mathbf{r}\, \frac{1}{2}K(\nabla c)^2. \tag{5.16}$$

By definition, e_{grad} is nonzero only in diffuse interfacial regions. Using (3.73), relating the interfacial surface tension to the concentration gradient, it is easily seen that $\overline{e}_{\text{grad}}$ is identically equal to $\sigma\overline{a}$, where σ and $\overline{a}$ respectively refer to the interfacial tension and the specific surface area [2] (interfacial area per unit volume) between the phases.[3]

[2]The concept of interfacial area is absent when the diffuse interface microscale model is adopted. Since σ and $\overline{a}$ always appears as the product $\sigma\overline{a}$, a microscale researcher can calculate this quantity as

$$\frac{1}{\tau_o}\int_t\int_{\tau_f} d^3\mathbf{r}\, \frac{1}{2}K(\nabla c)^2$$

using his microscale solutions.

[3]Incorporation of wetting effects would necessarily involve the solid-fluid surface tensions and areas, neither of which is present in our expression since we eschewed such effects in our analysis.

Based upon this identification, we discern that $\overline{F}_{\text{grad}} \equiv \overline{F}(\overline{a})$.

In combination, the above results lead to the following functional dependence of the macroscale free energy density:

$$\overline{F} \equiv \overline{F}(\overline{c}, \overline{a}). \tag{5.17}$$

(The dependence of the latter upon the macroscale temperature T is not displayed explicitly, as in all prior cases.) The identification of $\overline{a}$ as a relevant variable in the macroscale description of two-phase flows is particularly significant. Hassanizadeh & Gray [3] also claim that $\overline{F}$ should depend upon $\overline{a}$. However, they offer neither a concrete proof of this fact (as we have done) nor is the basis for $\overline{F}$ (as required by the distinction between *species* and *phases*) provided in their work. Other researchers who have undertaken to model directly at the macroscale (with no concession to microscale considerations) have also intuitively recognized the fact that saturation alone might not constitute the only variable required for a complete macroscale description of the phenomena. In a sense, the above analysis constitutes a proof, albeit one based upon our constitutive assumptions, that the macroscale free energy $\overline{F}$ is functionally dependent not only upon saturation, but upon specific surface area as well.

Upon utilizing (5.5a,b) we further obtain

$$\overline{\mu}_i \equiv \overline{\mu}_i(\overline{c}, \overline{a}) \quad (i = 1, 2), \tag{5.18}$$

the significance of which is analyzed in the next section.

5.4 Capillary Pressure–Saturation Relationship

This section is explicitly concerned with the experimental measurements quantifying the capillary pressure–saturation relationship. Utilizing the results obtained in the preceding sections we provide significant insights regarding the nature and the cause of hysteresis observed in such experiments. However, prior to embarking on such an effort, in subsection 5.4.1 we indulge in clarifying some salient aspects of the

capillary pressure–saturation relationship by utilizing simplistic examples to illustrate the hysteresis observed in such experimental measurements. Eventually, in subsection 5.4.2 we combine results obtained in section 5.2, concerning the definition of the capillary pressure jointly with the results obtained in the previous section, relating to the functional dependencies of the macroscale free-energy density and chemical potentials. These are utilized to draw pertinent conclusions regarding the existence of a relationship between capillary pressure and saturation, as well as regards the likely source of the hysteresis repeatedly observed in such experiments.

5.4.1 Hysteresis in Capillary Pressure-Saturation Measurements

This section utilizes simple examples to illustrate the hysteresis phenomena observed in experimental measurements of the capillary pressure-saturation relationship. These examples invoke the distinct wetting properties of the fluids to account for the hysteresis phenomena. In the next subsection we outline novel insights into the functional form of the capillary pressure, wherein we reconsider these examples so as to demonstrate the plausibility of our hypothesis in explaining the observed hysteresis.[4]

Example 1

Figure (5-1a) is a pictorial representation of the system considered for our first example. The system contains a reservoir of a wetting fluid (R1) linked through a cylindrical capillary tube of radius R to a geometrically identical reservoir (R2) containing a nonwetting fluid.[5] Further, we assume that the reservoirs are connected to external pressure pumps which enable the maintenance of arbitrary pressure differences between the two reservoirs R1 and R2.

[4]The examples in this section were borne out of a discussion with Prof. Deen. The author is indebted to Prof. Deen for suggesting the outline of the following example, and also to Prof. Nadim for discussions pertaining to the same. A survey of the literature revealed that a similar example has also been considered by Muccino *et al.* [8].

[5]In the spirit of simplicity, we assume that the wetting fluid contact angle is $\theta = 0$, and the nonwetting fluid contact angle is $\theta = 180°$.

In the following we outline a thought experiment to discern the capillary pressure–saturation relationship. At the completion of each of the steps of the experiment, we monitor the equilibrium state of the system, quantified by the difference in the pressures of the two reservoirs, and the volume fraction (c_w) of the wetting phase. Figure (5-1b) portrays the equilibrium states of the system attained in the course of executing our thought experiment. We envision an initial state wherein the capillary tube is filled with the wetting fluid while the pressures are being maintained equal in the two reservoirs (corresponding to the state denoted "a" in the figure). Subsequently, we consider the effect of an increase in the pressure in reservoir R2 containing the nonwetting fluid. As such, this act does not produce any perceptible effect on the volume fraction of wetting fluid in the capillary until the juncture (state "b") wherein the pressure difference $p_{nw} - p_w$ between the reservoirs infinitesimally exceeds the value corresponding to equilibrium, namely $2\sigma/R$, where σ denotes the interfacial tension between the wetting and the nonwetting fluids. In such a scenario (state "c") the nonwetting fluid invades the capillary tube, thereby draining the wetting fluid ($c_w = 0$).

Now, we conceptualize a reversal of the above thought experiment, starting however from the state achieved at the end of the above experiment (state "c"). If the pressure in the nonwetting fluid p_{nw} is now reduced, no change is perceived in the volume fraction c_w until the pressure p_{nw} acquires a value such that $p_{nw} - p_w < 2\sigma/R$. Subsequent to such a scenario, the wetting fluid invades the interior of the capillary tube, thereby draining the nonwetting fluid (the direction of the arrows in the figure indicate the path of the thought experiment).

It is evident from the above thought experiment that the system described in this example possesses a manifestly regular, nonhysteretic capillary pressure-saturation relationship.[6] In the next section we consider a simple geometrical modification of the

[6]It is to be cautioned here that our usage of the term capillary pressure to denote the difference in the pressures between the two phases is not accurate within the implications of real two-phase flows in porous media. As such, capillary pressure denotes a macroscopic quantity, which is related to the microscale pressures by some coarse-graining procedure. The examples considered in this section, however, deals with the difference in the microscale pressures. Our misusage of the proper terminology can, however, be justified within the crude geometrical model of a porous medium

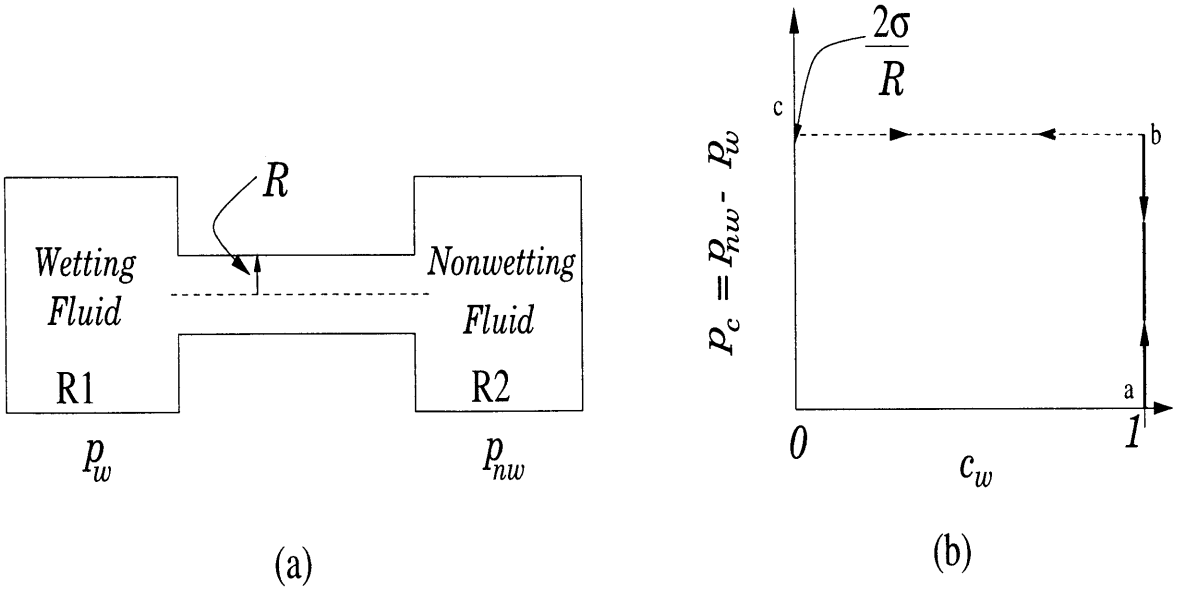

Figure 5-1: (a) Pictorial representation of the system considered in example 1; (b) Capillary-pressure-saturation behavior resulting from the thought experiment described in the text.

system considered in this example. Thereby we explicitly demonstrate the existence of hysteretic phenomena.

Example 2

Figure (5-2a) presents a schematic representation of the system considered in this second example. The feature that distinguishes this system from that considered in the first example resides in the presence of a second capillary tube (which, for simplicity has been assumed to be of radius $2R$). It is pertinent to indicate the presence of a wide body of literature pertaining to capillary models of porous media. These models represent the porous medium as a set of connected capillary tubes (of constant and/or varying diameters) within which the motion of the two fluids occur. In a sense, our examples constitute a rudimentary version of such models.

We envision effecting a thought experiment similar in spirit to that outlined in the previous example. Upon increasing the pressure in the nonwetting reservoir R2,

envisioned to consist of a single capillary tube.

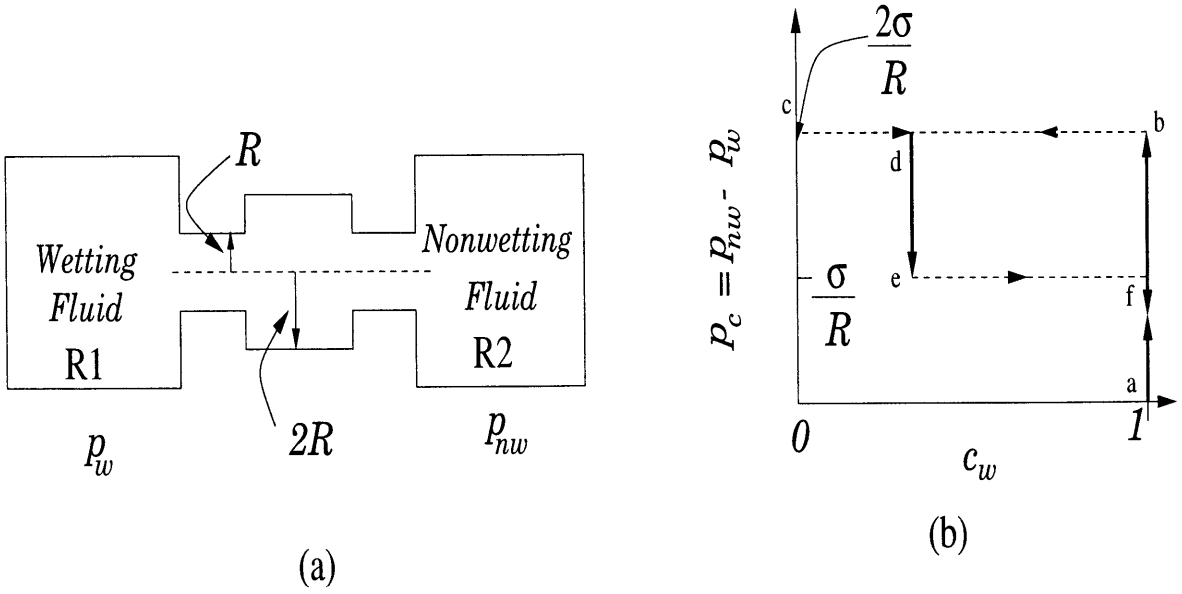

Figure 5-2: (a) Pictorial representation of the system considered in example 2; (b) Capillary-pressure saturation behavior for the thought experiment described in the text.

one observes behavior identical to that postulated in the previous section, namely that drainage of the wetting fluid occurs when the pressure in the nonwetting fluid exceeds that of the wetting fluid by $2\sigma/R$. However, upon reversing the experiment, we observe behavior qualitatively and quantitatively different from that envisioned in the previous example. Upon decreasing the pressure in reservoir R2, the first perceptible change again occurs at the stage wherein the pressures p_{nw} and p_w satisfy $p_{nw} - p_w < 2\sigma/R$. In such a scenario the wetting fluid again invades the capillary tube, but is however stopped at the neck representing the transition between the two capillary tubes (state "d"). At this juncture, the wetting fluid is unable to penetrate any further. This therefore, represents a state wherein the wetting and the nonwetting fluid coexist in the capillary tube (with a nontrivial value of c_w). Upon decreasing the pressure in R2 further, no perceptible change occurs in the volume fraction of the wetting fluid until the pressure in the nonwetting fluid satisfies $p_{nw} - p_w < \sigma/R$ (state "e"), beyond which the wetting invades the larger throat of the capillary tube, thereby draining the nonwetting fluid from the entirety of the capillary tubes (state

"f").

It is evident from our above discussion that the system considered here exhibits hysteresis in the functional form of the capillary pressure-saturation relationship. The 'phase-diagram' resulting from our thought experiment also qualitatively resembles that observed in the real experimental scenario [refer fig. (2-1)]. This simple example provides an illustration of the hysteretic phenomena observed in capillary pressure measurements. It seems remarkable that hysteretic behavior can be triggered by a mechanism as simple as the incorporation of an additional extra capillary tube. This observation rationalizes the existence of hysteresis observed in real porous media, which are constituted by innumerous capillary tubes of varying diameters and tortuosities. For instance, fig. (5-3b) depicts the path of the states in a system wherein there exists an capillary constriction of radius $4R$ in addition to the capillary tubes of radii R and $2R$. The qualitative resemblance of fig. (5-3b) to the real experimental measurements [depicted in fig. 2-1)] is striking.

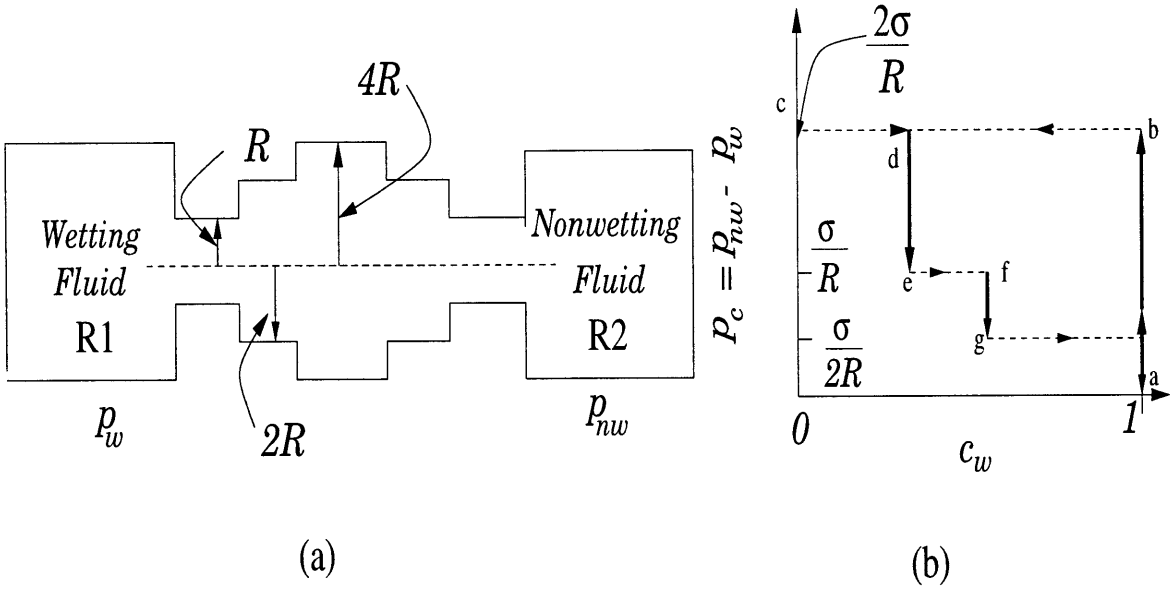

Figure 5-3: (a) Pictorial representation of the system considered in the discussion of example 3; (b) Capillary-pressure saturation behavior for the thought experiment; c_w designates the concentration of the wetting fluid.

It is pertinent to observe here that the above examples were however concerned

with a *microscale* interpretation of the hysteretic behavior. In contrast, in the following subsection, we provide a macroscale interpretation of hysteretic phenomena in capillary pressure measurements by utilizing our novel viewpoint for envisioning biphasic flows in porous media. Subsequent to this exercise, we return to the above examples in order to verify the consistency of our macroscale interpretations with the results obtained above.

5.4.2 Capillary Pressure-Saturation Relationship: Possible Reasons for Hysteresis

In this subsection we utilize the results obtained in sections 5.2 and 5.3 to elucidate the functional form of the macroscale capillary pressure. Such an exercise suggests the necessity of including the specific surface area as a macroscale variable in determining the capillary pressure. In turn, this result provides a plausible macroscale interpretation of the hysteresis observed in experimental measurements. Our discussion continues that initiated in section 5.2.

Upon combining equations (5.11) and (5.12) we obtain

$$P_c = \overline{\mu}_1 - \overline{\mu}_2. \tag{5.19}$$

This relation is responsible for the phase-equilibrium type of relationship existing between P_c and saturation $\overline{c}$, since both $\overline{\mu}_1$ and $\overline{\mu}_2$ are functions of $\overline{c}$. In our diffuse Darcyscale model, where the total pressure $\overline{p}$ and the macroscopic saturation $\overline{c}$ constitute the appropriate two-phase entities, the existence of a relationship between the macroscale pressures $\overline{p}_1, \overline{p}_2$ and $\overline{c}$ is not surprising. In contrast, however, other (singular) Darcyscale studies treat the microscale pressures p_1 and p_2 as being *independent* microscale variables. As such, their macroscale counterparts, namely $\overline{p}_1$ and $\overline{p}_2$, necessarily manifest themselves as being independent quantities. As a result, the existence of a functional relationship between $\overline{p}_1$ and $\overline{p}_2$, as embodied in the capillary pressure concept, appears to be not only *ad hoc*, but indeed mystifying.

In combination, equations (5.19) and (5.18), yield $P_c \equiv P_c(\overline{a}, \overline{c})$. *Thus, according*

to our analysis, the phenomenon of capillary pressure hysteresis arises from the non-uniqueness of $P_c(\overline{a}, \overline{c})$ under specification of only one of the two governing variables — namely, the saturation. Specification of $\overline{c}$ alone does not suffice to render the value of P_c unique. Since the variables $\overline{a}$ and $\overline{c}$ are wholly independent of one other, each being fixed appropriately by the solution of microscale problem, situations can arise wherein identical macroscale saturations involving different $\overline{a}$'s become possible.[7] Such circumstances would necessarily lead to different values of P_c, thereby explaining the **apparent** hysteresis loop as observed in P_c vs $\overline{c}$ curves. *In sum, our hypothesis is that this hysteresis is simply a result of the projection of the three-dimensional P_c - $\overline{c}$ - $\overline{a}$ surface onto the two-dimensional P_c - $\overline{c}$ plane* !

To verify the plausibility of our above arguments, we depict [cf. fig. (5-4)] the equation of state $P_c(\overline{a}, \overline{c})$ for the examples considered in the previous subsection [corresponding to figs. (5-2) and (5-3)]. In both cases, it can be observed that the generalized equation of state depicts a single-valued, nonhysteretic function. The projection of this function onto the space of reduced dimensionality constituted by the capillary pressure and saturation, exhibits hysteresis, identical to that displayed in figs. (5-2) and (5-3). This simple demonstration lends support to the plausibility of the arguments elucidated above. Further, numerical simulations embodying a larger number of capillary tubes, and in more exotic patterns, reported in [8] also lends credibility to our claim. Our diffuse interface framework thereby provides a rational explanation of the observed hysteresis by hypothesizing the existence of a generalized equation of state which quantifies the capillary pressure as a function of both specific surface area and saturation.

[7] One possible mechanism by which such a situation might occur corresponds to the scenario wherein the wetting properties of the fluids are taken into account.

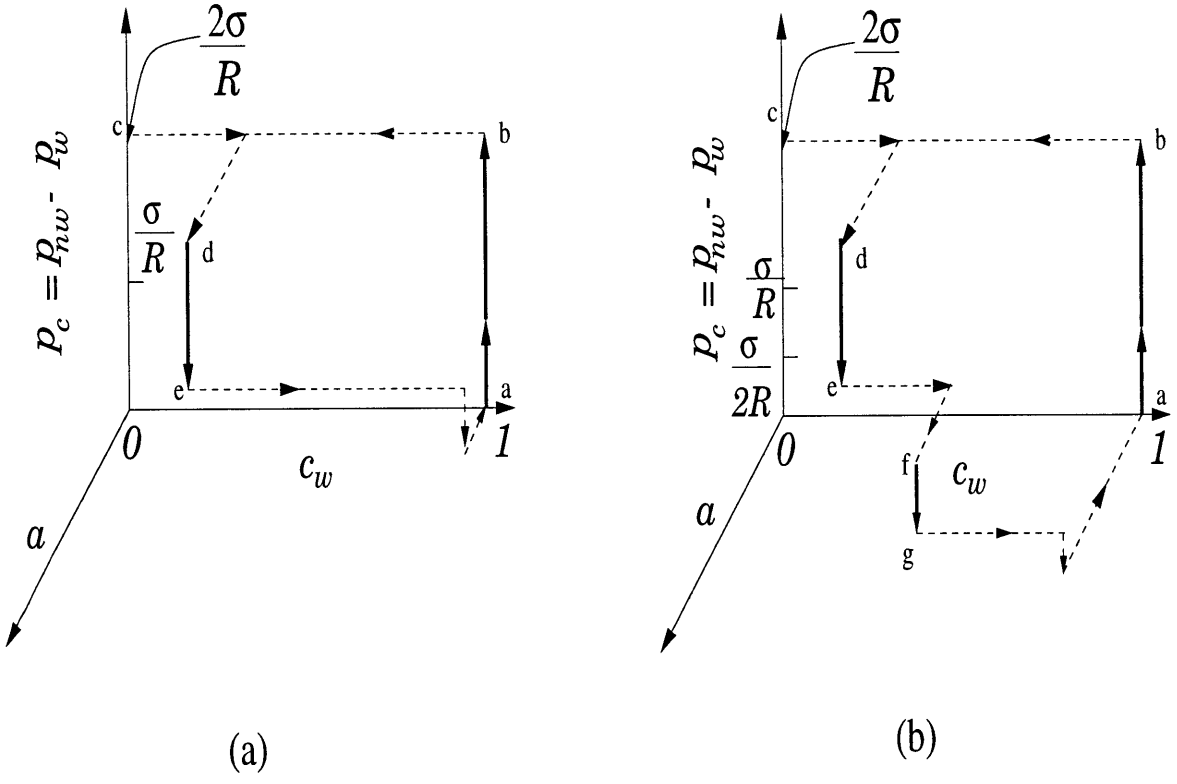

Figure 5-4: Generalized equation of state for the systems considered in: (a) example 2; (b) example 3.

5.5 Dynamical Equations for Macroscale Description

In the previous section we rationalized the nature of the hysteresis observed in experimental measurements of capillary pressure vs saturation experiments as being a direct consequence of the fact that the macroscale free energy density, and hence the capillary pressure is, in addition to the saturation, also a function of the specific surface area. In this section we complement the above result by expounding the argument that the mathematical modeling of multiphase flows needs to address the issue of macroscale energy transport in order to complete the set of equations governing two-phase flow phenomena.

As observed in the preceding section, a complete macroscale *equation of state* would necessarily involve the relationship of capillary pressure to both specific surface area and saturation. Such an equation of state complements Darcy's laws [derived in the next chapter — cf. eq. (6.8), (6.9)], and the diffusion equations (4.53a,b). However, these equations do not describe the evolution of the specific surface area $\overline{a}$, the latter constituting a variable wholly independent of the saturation. Consequently, a complete the set of equations purporting to describe the temporal evolution of the independent variables requires that we need to consider the macroscale equation governing energy transport.

Based upon the equivalence between the macroscale free energy density and the macroscale internal energy density, and utilizing the results of section 5.3 we find that

$$\overline{e}(\overline{c},\overline{a}) = \overline{e}_{\text{bulk}}(\overline{c}) + \sigma\overline{a}. \tag{5.20}$$

Under the assumption of slow, isothermal flows with weak gradients, such has pervaded the entirety of our discussion, the macroscale conservation equation for $\overline{e}$, namely (4.56), acquires the following form:

$$\frac{\partial(\varepsilon\,\sigma\overline{a})}{\partial\bar{t}} + \bar{\nabla}\cdot\left(\varepsilon\,\overline{\mathbf{v}}\sigma\overline{a}\right) = -\frac{\partial(\varepsilon\,\overline{e}_{\text{bulk}})}{\partial\bar{t}} + \sum_{i=1}^{2}\overline{\mathbf{J}}_i\cdot\mathbf{g}_i - \hat{\mathbf{F}}\cdot\overline{\mathbf{v}}, \tag{5.21}$$

where $\overline{\mathbf{J}}_i$ and $\hat{\mathbf{F}}$ obey the uncoupled version of the constitutive equations elucidated in section 6.1. The above equation serves as the governing equation for the evolution of the specific surface area $\overline{a}$. This evolution equation is nonconservative owing to the fact that interfacial area can be either created or destroyed by the respective breakup or coalescence of the droplets comprising the discontinuous phase.

The above equation complements the phase-specific Darcy's law, [cf. eqs. (6.8) - (6.9)], as well as the diffusion equations, (4.53a,b). Along with a capillary pressure equation of state $P_c(\overline{a}, \overline{c})$, *the resulting system of equations provides a complete description of slow, isothermal*[8] *biphasic flows through porous media.*

5.6 Conclusions

In this section we outlined the framework whereby the identification of the phase-specific quantities can be effected utilizing the diffuse Darcyscale physical fields. The implementation of this procedure enables the rigorous derivation of the functional form of the capillary pressure, and a possible explanation for the nature of hysteresis observed there within. The identification of the capillary pressure and its characteristics is one of the main achievements of our work. Such an accomplishment was enabled by our conception of the diffuse interface model at the microscale, and its comparable analog at the diffuse Darcyscale. Theoretical efforts of the past which lacked such a rigorous, physically based framework generally also fails to interpret the capillary pressure and its experimental manifestation.

Further, we argued the need for the consideration of the macroscale energy equation to enable the closure of the framework for macroscale modeling. The diffusion equations derived in the previous chapter [cf. (4.53a,b)] and the energy equation outlined in this chapter [cf. (5.21)] complement the phase-specific Darcy's law which

[8]For nonisothermal flows the above equation needs to be replaced by two species-specific energy equations together with the requirement of local thermal equilibrium in order to satisfy the mandated equivalence between the required number of equations and the number of independent variables. However, such issues take us far from the scope of the present work. As such, they will not be addressed here.

is derived in the next chapter [cf. eqs. (6.8) and (6.9)] to thereby furnish the complete set of equations to be utilized for the macroscale modeling of biphasic flows in porous media. Requisite to the solution of these equations is an equation of state which embodies capillary pressure as a function of its dependent variables, namely the saturation $\overline{c}$ and the specific surface area a.

In the next chapter, we utilize concepts from nonequilibrium thermodynamics to derive the macroscale constitutive equations. This framework is subsequently used to derive the phase specific Darcy's laws appropriate to the singular Darcyscale description of the transport. However, in contrast to the simple decoupled form of the Darcy's law conventionally used in two-phase flow modeling [cf. eq. (2.2)], we obtain a generalized version of the Darcy's law. Finally, we also consider a simplified example to illustrate the implementation of our complete framework within an analytical approach.

References

[1] P. M. Adler and H. Brenner, "Multiphase flow in porous media," *Ann. Rev. Fluid Mech.*, **20**, 35 (1988).

[2] P. G. deGennes, "Dynamics of fluctuations and spinodal decomposition in polymer blends," *J. Chem. Phys.*, **72**, 4756 (1980).

[3] S. M. Hassanizadeh and W. G. Gray, "Thermodynamic basis of capillary pressure in porous media," *Water Resour. Res.*, **29**, 3389 (1993).

[4] F. Kalaydjian, "A macroscopic description of multiphase flow in porous media involving spacetime evolution of fluid/fluid interface," *Transp. Porous Media*, **2**, 537 (1993).

[5] J. G. Kirkwood and R. J. Bearman, "Statistical mechanics of transport processes: 11. Equations of transport in multicomponent system," *J. Chem. Phys.*, **28**, 136 (1958).

[6] C. M. Marle, "On macroscopic equations governing multiphase flow with diffusion and chemical reactions in porous media," *Int. J. Engng Sci.*, **20**, 643 (1977).

[7] C. M. Marle, *Multiphase Flow in Porous Media*, Gulf, Houston (1981).

[8] J. C. Muccino, W. G. Gray and L. A. Ferrand, "Toward an improved understanding of multiphase flow in porous media," *Rev. Geophys.*, **36**, 401 (1998).

[9] D. Pavone, "Macroscopic equations derived from space averaging for immiscible two-phase flow in porous media," *Rev. I. Fr. Petrol.*, **44**, 29 (1989).

[10] S. Whitaker, "Flow in porous media: 2. The governing equations for immiscible Two-Phase flow," *Transp. Porous Media*, **1**, 105 (1986).

Chapter 6

Biphasic Flows in Porous Media: Macroscale Constitutive Equations

Preceding chapters outlined a framework for accomplishing the transition between the microscale and macroscale descriptions of the porous medium. This framework embodied rigorous, physically-based definitions of the macroscale quantities, both at the diffuse and the singular Darcyscales. Furthermore, such a framework also enabled the derivation of the respective (transport) equations governing the physical fields. Subsequent to the prescription of the microscale constitutive equations, this framework enables, in principle, establishing the functional form of the macroscale constitutive equations. However, implementation of this framework for the specific microscale constitutive equations outlined previously in section 3.3 proves to be analytically intractable.[1] Within such a scenario, nonequilibrium thermodynamics provides a rational route for *guessing* the possible forms of the macroscale constitutive equations within our diffuse Darcyscale viewpoint.

This section employs considerations abstracted from nonequilibrium thermodynamics so as to glean insights into the macroscale constitutive equations. Such an exercise is effected on the diffuse Darcyscale equations derived in section 4.5 to furnish the constitutive equations at the macroscale, albeit at the diffuse Darcyscale level.

[1]No such constraints manifest if, however, we implement the framework in a strictly numerical context.

Subsequently, utilizing the framework erected in the preceding chapter, we identify the 'phase-specific' constitutive equations. The constitutive equations at the diffuse Darcyscale yield the macroscale 'mixture' Darcy law, with the comparable equation for the singular Darcyscale embodied within the generalized 'phase-specific' Darcy's laws. In the final section, 6.3, we implement the complete micro-macro framework for a simple illustrative linearized example so as to explicitly display the computations entailed by the analytical framework. Such a procedure also enables verification of the heuristic constitutive equations proposed, based on considerations drawn from nonequilibrium thermodynamics.

6.1 Nonequilibrium Thermodynamics and Macroscopic Constitutive Equations

Nonequilibrium thermodynamics provides a convenient formalism for establishing the functional forms of the macroscale constitutive equations required in the macroscale field equations, at least in circumstances where these constitutive relations are linear. The methodology employed involves the identification of forces and fluxes in the entropy source term of the generalized entropy balance, subsequent to which one proposes a general linear relationship between these forces and fluxes [7]. The fundamental basis for constructing such an entropy balance lies in the assumption of local thermodynamic equilibrium, which posits that thermodynamic identities valid at equilibrium continue to remain locally valid in nonequilibrium circumstances. Although one can thereby identify the constitutive forms of the pertinent linear force-flux relationships within the framework of linear nonequilibrium thermodynamics, the formalism itself provides no insight into the magnitudes of the phenomenological coefficients appearing therein (with the possible exception of their algebraic signs), including whether coupling occurs between the different fluxes owing to the presence of nonzero phenomenological 'cross-coupling' coefficients. Furthermore, it is not possible to predict the functional dependence, if any, of the phenomenological coefficients upon

the (macroscale) physical properties. Despite such limitations, the success of linear nonequilibrium thermodynamics in providing valuable insights into the possible forms of constitutive equations cannot be denied. In this section we apply such concepts to the dependent macroscale field variables quantifying our 'two-phase' system.

In view of the relative simplicity of the preceding system of diffuse Darcy macroscale equations, the generalized entropy balance equation is easily obtained along the lines outlined by deGroot & Mazur [7]. For brevity we sketch only essential details.

The kinetic energy balance is obtained from the momentum equation (4.54) as

$$\frac{\partial\left(\frac{1}{2}\varepsilon\,\overline{\rho}\,\overline{\mathbf{v}}^2\right)}{\partial\bar{t}} + \bar{\nabla}\cdot\left(\frac{1}{2}\varepsilon\,\overline{\rho}\,\overline{\mathbf{v}}^2\overline{\mathbf{v}}\right) = \left(\bar{\nabla}\cdot\overline{\mathbf{P}}\right)\cdot\overline{\mathbf{v}} + \hat{\mathbf{F}}\cdot\overline{\mathbf{v}} + \sum_{i=1}^{2}\varepsilon\,\overline{\rho}_i\,\overline{\mathbf{v}}\cdot\mathbf{g}_i. \tag{6.1}$$

Upon performing an analysis predicated along the same lines as outlined by deGroot & Mazur [7], the following entropy transport equation is obtained (where the macroscopic volumetric entropy density $\overline{s}$ is defined as usual in terms of macroscopic thermodynamic quantities as $Td\overline{s} = d\overline{e} + \overline{p}d\overline{v}$,[2] with $\overline{v} = 1/\overline{\rho}$):

$$T\frac{d\left(\varepsilon\,\overline{\rho}\,\overline{s}\right)}{d\bar{t}} = -\bar{\nabla}\cdot\left(\overline{\mathbf{q}} - \sum_{k=1}^{2}\overline{\mu}_k\overline{\mathbf{J}}_k\right) - \frac{1}{T}\overline{\mathbf{q}}\cdot\bar{\nabla}T - \sum_{k=1}^{2}\overline{\mathbf{J}}_k\cdot\left(\bar{\nabla}\overline{\mu}_k - \mathbf{g}_k\right) - \hat{\mathbf{F}}\cdot\overline{\mathbf{v}} - \overline{\boldsymbol{\tau}}^s{:}\overline{\mathbf{D}}, \tag{6.2}$$

wherein $d/d\bar{t} \equiv \partial/\partial\bar{t} + \overline{\mathbf{v}}\cdot\bar{\nabla}$ represents the macroscale material derivative, and $\overline{\mu}_k$ the macroscale chemical potential of species k. Furthermore, $\overline{\mathbf{D}}$ denotes the macroscopic version of the deformation tensor [cf. (3.19)], and $\overline{\boldsymbol{\tau}}^s$ the symmetric part of the macroscopic deviatoric stress tensor. As the distinction between microscale temperature T and the macroscale temperature $\bar{T}$ is peripheral to the dynamical issues of interest, it is not further addressed here, whence we denote the macroscale temperature also by

[2]Strictly speaking, the mean pressure $\overline{p}$ is not the same as the thermodynamic pressure, whence one should define $\overline{\mathbf{P}} = -\overline{p}^T\mathbf{I} + \overline{\tau}'\mathbf{I} + \overline{\boldsymbol{\tau}}$, where $\overline{p}^T$ now refers to the thermodynamic pressure, with the difference $\overline{p} - \overline{p}^T$ denoted as $\overline{\tau}'$. The subsequent analysis requires knowledge of only that portion of $\overline{\mathbf{P}}$ excluding the thermodynamic pressure $\overline{p}^T$. Since the diagonal tensor $\overline{\tau}'\mathbf{I}$ contributes only to the symmetric part of $\overline{\mathbf{P}}$, we combine $\overline{\tau}'\mathbf{I}$ with $\overline{\boldsymbol{\tau}}^s$ and denote the sum also by $\overline{\boldsymbol{\tau}}^s$. However, the distinction between the thermodynamic and the mean pressures vanishes when $\bar{\nabla}\cdot\overline{\mathbf{v}} = 0$ [5], which condition applies to the class of flows eventually considered here.

Physical Entity	Generalized Force	Generalized Flux
Diffusion flux	$\overline{\mathbf{J}}_k$	$\bar{\nabla}\overline{\mu}_k - \mathbf{g}_k$
Body-force density	$\hat{\mathbf{F}}$	$\overline{\mathbf{v}} - \mathbf{U}$
Deviatoric stress (symmetrized)	$\overline{\boldsymbol{\tau}}^s$	$\overline{\mathbf{D}}$
Heat flux	$\overline{\mathbf{q}}$	$\bar{\nabla}T$

Table 6.1: Identification of the respective forces and fluxes in the entropy source terms appearing in the generalized entropy balance.

T.[3] Consistent with the assumptions of linear response theory, the respective forces and fluxes can be identified from the entropy source term (table 6.1). The above list constitutes only the nonequilibrium contributions to the fluxes. To remind readers of the reference frame in which $\overline{\mathbf{v}}$ is measured, these fluxes include the translational velocity $\mathbf{U}$ of the porous medium as a whole (measured relative to an inertial reference frame). This also renders the constitutive equations objective [17].

Based on the above identifications, together with the assumed absence of coupling between fluxes of tensorial orders differing by an odd integer, which holds true for a porous medium composed of centrally-symmetric particles [14], the following macroscopic constitutive equations are obtained:

$$\overline{\mathbf{J}}_k = \boldsymbol{\Lambda}_k^{\mathrm{I}} \cdot \left(\bar{\nabla}\overline{\mu}_k - \mathbf{g}_k\right) + \boldsymbol{\Lambda}_k^{\mathrm{II}} \cdot \overline{\mathbf{v}} \qquad (k = 1, 2), \tag{6.3}$$

$$\hat{\mathbf{F}} = \boldsymbol{\Lambda}^{\mathrm{III}} \cdot \overline{\mathbf{v}} + \sum_{k=1}^{2} \boldsymbol{\Lambda}_k^{\mathrm{IV}} \cdot \left(\bar{\nabla}\overline{\mu}_k - \mathbf{g}_k\right) \qquad (k = 1, 2), \tag{6.4}$$

[3] At issue here is the question of whether or not a continuum that is isothermal at the macroscale is also necessarily isothermal at the microscale, and, if so, is $T = \bar{T}$?

$$\overline{\boldsymbol{\tau}} = \boldsymbol{\Lambda}^{\mathrm{V}} : \bar{\nabla}\overline{\mathbf{v}}. \tag{6.5}$$

(Here, in contrast to the tabulation in table 6.1, we have reverted to our earlier convention of measuring velocities relative to the fixed porous medium, whence $\mathbf{U}$ has been set equal to zero.) The individual diffusive fluxes $\overline{\mathbf{J}}_1$ and $\overline{\mathbf{J}}_2$ are not independent variables since $\overline{\mathbf{J}}_1 + \overline{\mathbf{J}}_2 = \mathbf{0}$, whence only two of the four coefficients $\boldsymbol{\Lambda}_1^{\mathrm{I}}, \boldsymbol{\Lambda}_2^{\mathrm{I}}, \boldsymbol{\Lambda}_1^{\mathrm{II}}, \boldsymbol{\Lambda}_2^{\mathrm{II}}$ are independent. Furthermore, invocation of the Onsager reciprocity principle, assumed applicable at the macroscale [6, 9], leads to the observation that only three of the phenomenological coefficients, $\boldsymbol{\Lambda}_k^{\mathrm{I}}, \boldsymbol{\Lambda}_k^{\mathrm{II}}, \boldsymbol{\Lambda}^{\mathrm{III}}$ and $\boldsymbol{\Lambda}_k^{\mathrm{IV}} (k = 1, 2)$, are independent.

A major limitation of nonequilibrium thermodynamics lies in its inability to provide any indication of the magnitudes of these phenomenological coefficients, except possibly their algebraic signs. Moreover, the above relations are purely phenomenological, and hence do not constitute a self-contained theory. As a consequence, their applicability to the phenomena at hand needs to be ratified either through comprehensive experiments or a detailed microscale theory, or both. While the former verification mode is left to experimentalists, section 6.3 provides an illustrative analysis (albeit in the somewhat restricted context of quasistatic microscale behavior) of the manner in which the second mode of confirmation may be implemented.

Under the dual assumptions of slow flows and weak macroscale gradients in the mean velocity $\overline{\mathbf{v}}$, we may neglect effects arising in the macroscale equations from: (i) the presence of fluid inertia; (ii) the existence of a deviatoric stress tensor. Furthermore, neglect of coupling between the fluxes $\overline{\mathbf{J}}_k$ and the force $\hat{\mathbf{F}}$ leads, upon substituting the above relation for $\hat{\mathbf{F}}$ into (4.54), to the relation

$$\bar{\nabla}\overline{p} = \boldsymbol{\Lambda}^{\mathrm{III}} \cdot \overline{\mathbf{v}} + \sum_{i=1}^{2} \overline{\rho}_i \, \mathbf{g}_i, \tag{6.6}$$

which constitutes a diffuse, macroscale, *single-phase, multispecies* Darcy's law. In the case where $\mathbf{g}_1 = \mathbf{g}_2 \equiv \mathbf{g}$, say, where $\mathbf{g}$ is the acceleration of gravity, we find upon

inverting equation (6.6) that

$$\overline{\mathbf{v}} = (\mathbf{\Lambda}^{\mathrm{III}})^{-1} \cdot \left(\bar{\nabla}\overline{p} - \overline{\rho}\,\mathbf{g}\right). \tag{6.7}$$

It is not surprising that through linearized nonequilibrium thermodynamic arguments we have obtained a macroscale form of Darcy's law, which is itself a linear constitutive relation. A more rigorous derivation of (6.7) from first principles, is presented in section 6.3. Prior studies by others [9, 11] have also indicated how Darcy's law may be obtained by using constitutive relationships derived from nonequilibrium thermodynamics or some other basis. At a later stage [see equations (6.8), (6.9)] we address the more general case where coupling between the fluxes is included.

Sections 6.2 and 6.3, which follow, are devoted to clarifying the concept of phase-specific Darcy's laws in an effort to relate our work to more conventional singular, Darcyscale formulations of two-phase flow phenomena. By so doing, our two-component mixture framework renders rational the previously empirical two-phase Darcy field equations.

6.2 Phase-specific Darcy's laws

In this section we the definitions of the phase-specific quantities, previously in chapter 5, jointly with the constitutive equations obtained in section 6.1, to derive phase-specific Darcy laws underlying the singular Darcyscale description of multiphase flows. As such an exercise entails manifold algebraic manipulations, pertinent details are relegated to Appendix E. The final results obtained are

$$\overline{\mathbf{v}}_1 = (\mathbf{\Lambda}'_{11})^{-1} \cdot \left(\bar{\nabla}\overline{p}_1 - \varepsilon\,\overline{\rho}_1\mathbf{g}_1\right) + (\mathbf{\Lambda}'_{12})^{-1} \cdot \left(\bar{\nabla}\overline{p}_2 - \varepsilon\,\overline{\rho}_2\mathbf{g}_2\right), \tag{6.8}$$

$$\overline{\mathbf{v}}_2 = (\mathbf{\Lambda}'_{21})^{-1} \cdot \left(\bar{\nabla}\overline{p}_1 - \varepsilon\,\overline{\rho}_1\mathbf{g}_1\right) + (\mathbf{\Lambda}'_{22})^{-1} \cdot \left(\bar{\nabla}\overline{p}_2 - \varepsilon\,\overline{\rho}_2\mathbf{g}_2\right), \tag{6.9}$$

in which the dyadics (or, equivalently, 3×3 matrices) $\mathbf{\Lambda}'_{ij}$ are tensorial phenomenological coefficients. From our analysis it was established that only three of the above four tensor coefficients $\mathbf{\Lambda}'_{ij}\,(i,j = 1,2)$ are independent. However, we were unable establish any symmetries of the cross-coupling tensors [6, 9].

The forms of the pertinent constitutive equations obtained from nonequilibrium thermodynamic considerations, supplemented by our definitions of phase-specific quantities, thus yield the generalized two-phase form of Darcy's law, namely equations (6.8) and (6.9), hypothesized by a number of other researchers [6, 9, 15]. Fundamental to these singular Darcyscale laws is, however, the precursor multicomponent mixture, single-phase, Darcy's law (6.7) that we derived. This approach contrasts with that of other investigators, who treat the phase-specific Darcy's laws as fundamental entities, necessitating a closure relationship for the capillary pressure $P_c[\bar{c}]$ [2, 3]. Since our preceding phase-specific relationships were developed from mixture-based laws, we are as a consequence able to provide rational and explicit expressions for the capillary pressure as well as other elements appearing as *ad hoc* continuum-mechanical identities in singular Darcyscale theories (cf. section 5.2).

6.3 Illustrative Example

This final section explicitly illustrates how our microscale model can be used to rigorously derive and hence formally justify linear macroscale constitutive relations that accord with those previously postulated axiomatically on the basis of irreversible thermodynamic arguments. Additionally, it is shown explicitly how one may, in principle, calculate the Darcyscale phenomenological coefficients appearing therein from the specified microscale data. Section 6.1 illustrated the form of the constitutive equations, without however specifying the manner in which the phenomenological coefficients $\mathbf{\Lambda}'$ could be theoretically calculated. The analysis of the present section, designed to rectify this omission, is directed to the elementary case of two-phase flow through a spatially periodic model of a porous medium under the additional constraints of small capillary and Reynolds numbers. At the macroscale this de-

scription eventually leads to a *homogeneous* multiphase flow configuration, wherein macroscale quantities like saturation, velocity, and pressure gradient are all uniform throughout the porous medium [18]. Complete analytical treatment of the more general case presents insuperable difficulties owing to the severe nonlinearities present in the problem formulation, most notably in $\boldsymbol{\tau}_c$ and $F(c)$. However, at least in principle, numerical evaluation of the requisite macroscale phenomenological coefficients is made possible by their rigorous definitions in terms of the prescribed microscale data. In turn, this enables use of solutions of the microscale equations to confirm the predictions of linear irreversible thermodynamics, and concomitantly to determine the numerical values and parametric dependence of the phenomenological coefficients embodied in the various $\boldsymbol{\Lambda}'$s.

Physical description

In this section we elucidate the basic physics underlying the illustrative example accompanying the mathematical details elaborated in subsequent sections.

Consider the generic case of uniform two-phase flow through a porous medium animated by an external pressure gradient. This applied macroscopic pressure gradient generates a flow at the microscale, resulting in motion of the two species. In the following sections we analyze the governing microscale equations arising from this pressure gradient. An analytical solution of this problem would be extremely complicated owing to the underlying nonlinearities. These, in turn, are related to the classical nonlinearities appearing in the singular microscale approach, which result from having to satisfy interfacial boundary conditions on a surface whose unknown shape needs to be determined as a part of the solution of the problem.

However, in view of our prior arguments based on nonequilibrium thermodynamic concepts, it is to be expected that the two-phase Darcy's law will be applicable in some linear limit of the problem. Anticipating such a simplification, in what follows we analyze the microscale problem in the linear limit. This limit corresponds to the leading-order, small perturbation approach devised by G. I. Taylor [16], wherein the interfacial boundary conditions are initially enforced on a surface whose shape

is assumed known *a priori*. Departures from that assumed shape are then derived sequentially by employing the solutions of the governing equations (*sans* the normal stress interfacial boundary condition) at successively higher orders of approximation in the perturbation parameter.

We consider the microscale equations and boundary conditions outlined in section 4.3 together with the constitutive equations outlined in section 3.3, subject to the constraint that the macroscale pressure gradient be equal to the applied pressure gradient. Equation (4.43) suggests that this macroscale pressure gradient constraint is equivalent to a comparable constraint imposed on the microscale pressure gradient. The applied macroscopic pressure gradient thereby acts as an animating force driving the microscale flow, which can, in principle, be determined by the solving the governing microscale equations. The microscale velocity field generated in this manner is manifested as a uniform macroscale flow (at least for the case of homogeneous flows, under the assumed spatial and temporal flow characteristics outlined previously) — the dependence of which on the macroscale pressure gradient is subsequently proved to be linear, in accordance with the Darcy's laws. This section thereby constitutes an *ab initio* proof of the validity of the heretofore empirical two-phase Darcy's laws, albeit for the limited case wherein only the linear limit of the microscale equations is considered.

Microscale problem

The microscale equations appropriate to a quasisteady, zero Reynolds number, small capillary number description of multiphase flow is obtained by setting $\mathrm{Ca} = \delta$ and $\tau_D U/L = \delta$ $(\delta \ll 1)$. To simplify the analysis we ignore the effects of gravity, thereby obtaining the trio of equations

$$\frac{\partial \rho}{\partial t} + \nabla \cdot (\mathbf{v}\rho) = 0, \tag{6.10}$$

$$-\delta\nabla p+\delta\nabla\cdot\boldsymbol{\tau}_v+\delta\nabla\cdot\Big[(\nabla c)(\nabla c)-|\nabla c|^2\mathbf{I}\Big]=0, \tag{6.11}$$

$$\delta^2\Big[\frac{\partial c}{\partial t}+\nabla\cdot(\mathbf{v}c)\Big]=\boldsymbol{\Lambda}\nabla^2\Big(\frac{\partial f}{\partial c}-\delta^2\nabla^2 c\Big). \tag{6.12}$$

These equations are to be solved subject to the periodicity conditions (4.6) together with the no-slip and no-flux boundary conditions (4.15) and (4.16), respectively, on the bed particle surfaces. Furthermore, subject to *a posteriori* verification the following expansions are proposed for the relevant physical variables (corresponding expansions for the inner variables being obtained by imposing a tilde ornation):

$$p=\delta^{-1}p_{-1}(q_1,q_2,n,t)+p_0(q_1,q_2,n,t)+O(\delta), \tag{6.13}$$

$$\{\mathbf{v},c\}=\{\mathbf{v},c\}_0(q_1,q_2,n,t)+\delta\{\mathbf{v},c\}_1(q_1,q_2,n,t)+O(\delta^2). \tag{6.14}$$

The fluid motion is assumed to be driven by an externally-imposed, time-independent, macroscale pressure gradient $\bar{\nabla}\overline{p}$, taken to be uniform throughout the porous medium. This macroscopic pressure gradient, defined through (4.45), serves as a constraint on the solution of the above system of equations. While the solution of the complete dynamical problem subject to this constraint possesses nontrivial uniqueness properties, the fact that the dynamics in this section is assumed to involve a quasisteady response of the pressure field requires that an *instantaneous* version of 4.45) (that is, excluding the time averaging) be specified in order to assure uniqueness of the resulting solutions of the microscale equations. Thus, for purely mathematical reasons pertaining to uniqueness, we invoke a quasisteady analog of (4.45), namely that the instantaneous spatial average of the microscale pressure field constitute the macroscale configuration-specific pressure gradient:

$$\bar{\nabla}\overline{p}=\frac{1}{\tau_o}\oint_{\partial\tau_o}d\mathbf{s}\,p. \tag{6.15}$$

Inner and outer equations

We employ the same notation as in section 3. To leading order in δ, a quasisteady analysis requires *a priori* specification of the location of 'interface' (cf. [13] and the references cited therein). However, the shape of the interface also constitutes an unknown of the problem, which has to be determined concurrently with the solution of the equations of motion. The assumption of small Ca makes it possible for one to assign, at the leading order, a macroscopic interfacial configuration, one whose curvatures κ_1, κ_2 are independent of (q_1, q_2). This requires that a similar condition be satisfied by the normal component of the zeroth-order velocity field $\mathbf{v}_0$ at the interfacial surface. Continuation of the perturbation expansion to determine higher-order corrections to the interfacial shape is then carried out in a systematic manner similar to that of section 3, with the concentration field c used to establish corrections to the shape (say, by arbitrarily choosing the macroscale interface to coincide with the isoconcentration surface $c = 0.5$). Details of such an analysis are similar in spirit to those outlined in section 3.5, but quickly become algebraically unwieldy at higher order. Inasmuch as such extended calculations are not wholly relevant in this initial foray into the field, they are omitted here in the interests of brevity. Accordingly, we assume that the leading-order terms in the perturbation expansion suffice to adequately represent the required microscale fields. The resulting equations are summarized below.

• Outer equations

$$\nabla \cdot \mathbf{v}_0^{\pm} = 0, \tag{6.16}$$

$$\nabla p_0^{\pm} = \mu^{\pm} \nabla^2 \mathbf{v}_0^{\pm}. \tag{6.17}$$

These are to be solved subject to the following jump conditions imposed across the interface, such conditions being derived in a manner similar to those outlined in

section 3.4:

$$[[\mathbf{v}_0]] = \mathbf{0}, \tag{6.18}$$

$$[[\mathbf{n} \cdot \boldsymbol{\tau}_{v0}]] \cdot \mathbf{I}_s = \mathbf{0}, \tag{6.19}$$

$$\int_{I_{12}} d\mathbf{s} \cdot [[\mathbf{n} \cdot \boldsymbol{\tau}_{v0}]] = 0, \tag{6.20}$$

$$\mathbf{n} \cdot \mathbf{v}_0 = u. \tag{6.21}$$

Each of the above conditions is to be imposed at the parent surface, the unit normal to which is denoted by $\mathbf{n}$ (not to be confused with the cell number). Further, the integral condition (6.20) imposed on the stress is not a result of the singular perturbation analysis, but is rather a result of physical considerations accompanying the small Ca approximation [16]. The singular perturbation analysis results in the boundary conditions previously derived in section 3.5 [wherein equation (6.18) $\equiv$ (3.62) and (6.19) $\equiv$ (3.69) + (3.70)]. However, the normal stress condition (3.72) cannot be satisfied on the surface of the drop with an *a priori* shape assumed. Hence, based on physical considerations we impose the conditions (6.20) and (6.21) [13] to establish the higher-order corrections to the droplet shape.

• Inner equations

This section is concerned primarily with the normal component of the momentum equation in the inner region. Its purpose is to illustrate the fact that the microscale pressure gradient possesses a purely normal component in the interfacial region, whence its contribution to the macroscopic pressure gradient vanishes upon integration over the interfacial region contained within the unit cell. Perturbation analysis of both the concentration equation and the tangential component of the momentum equation are performed in a manner similar to that employed to establish

(3.55), (3.69) and (3.70) in section 3.5.

For the normal component, at the leading order it is found that

$$-\frac{\partial \tilde{p}_{-1}}{\partial \tilde{n}}+\left[(\kappa_1+\kappa_2)\left(\frac{\partial \tilde{c}_0}{\partial \tilde{n}}\right)^2\right]=0, \tag{6.22}$$

representing the Laplace condition imposed on the leading-order outer pressure fields, $p^{\pm}_{-1}$ [13]. At the next order in δ we find that

$$-\frac{\partial \tilde{p}_0}{\partial \tilde{n}}+\frac{\partial}{\partial \tilde{n}}\left(2\mu\frac{\partial \tilde{v}_{31}}{\partial \tilde{n}}\right)-\frac{2}{3}\frac{\partial(\mu\chi)}{\partial \tilde{n}}+2(\kappa_1+\kappa_2)\left(\frac{\partial \tilde{c}_0}{\partial \tilde{n}}\frac{\partial \tilde{c}_1}{\partial \tilde{n}}\right)=0, \tag{6.23}$$

where $\tilde{c}_1$ is the $\mathcal{O}(\delta)$ inner concentration term. Integration yields

$$-\tilde{p}_0+\left(2\mu\frac{\partial \tilde{v}_{31}}{\partial \tilde{n}}\right)-\frac{2}{3}\mu\chi+2\int(\kappa_1+\kappa_2)\left(\frac{\partial \tilde{c}_0}{\partial \tilde{n}}\frac{\partial \tilde{c}_1}{\partial \tilde{n}}\right)d\tilde{n}=\alpha(q_1,q_2), \tag{6.24}$$

where, as already noted,

$$\chi=h_1h_2\left[\frac{\partial}{\partial q_1}\left(\frac{\tilde{v}_{10}}{h_2}\right)+\frac{\partial}{\partial q_2}\left(\frac{\tilde{v}_{20}}{h_1}\right)+\frac{1}{h_2h_1}\frac{\partial \tilde{v}_{31}}{\partial \tilde{n}}+\tilde{v}_{30}\frac{\partial}{\partial \tilde{n}}\left(\frac{1}{\tilde{h}_2\tilde{h}_1}\right)\right]. \tag{6.25}$$

Upon taking the limit of the above expression as $\tilde{n}\to\pm\infty$, and using (3.57), (3.58) and (3.68), it is found that

$$\lim_{\tilde{n}\longrightarrow\infty}\chi\equiv h_1h_2\left[\frac{\partial}{\partial q_1}\left(\frac{\tilde{v}_{10}}{h_2}\right)+\frac{\partial}{\partial q_2}\left(\frac{\tilde{v}_{20}}{h_1}\right)+\frac{1}{h_2h_1}\frac{\partial v_{30}}{\partial n}+v_{30}\frac{\partial}{\partial \tilde{n}}(\kappa_1+\kappa_2)\right]\to 0. \tag{6.26}$$

The assumption that $\tilde{v}_{30},\kappa_1,\kappa_2$ are independent of (q_1,q_2), requires that

$$h_1h_2\left[\frac{\partial}{\partial q_1}\left(\frac{\tilde{v}_{10}}{h_2}\right)+\frac{\partial}{\partial q_2}\left(\frac{\tilde{v}_{20}}{h_1}\right)\right]\equiv\text{independent of }(q_1,q_2), \tag{6.27}$$

whence

$$\chi \equiv \text{independent of } (q_1, q_2). \tag{6.28}$$

These intermediate results are required in the next section.

Composite solutions

Solutions of the inner and the outer equations may be used to obtain a composite solution, defined generically as [12]

$$\boldsymbol{\psi}_{c0} = \boldsymbol{\psi}_0 + \tilde{\boldsymbol{\psi}}_0 - \boldsymbol{\psi}_{\text{m.c.}}, \tag{6.29}$$

where $\boldsymbol{\psi}_{\text{m.c.}}$ denotes the matching condition. However, in view of the fact that the boundary layer is of the intermediate layer kind, it is necessary to define *two* (rather than *one*) composite solutions:

$$\boldsymbol{\psi}^{\pm}_{c0} = \boldsymbol{\psi}^{\pm}_0 + \tilde{\boldsymbol{\psi}}_0 - \boldsymbol{\psi}^{\pm}_{\text{m.c.}}. \tag{6.30}$$

Note that these composite fields are continuous across the 'interface.' Thus, at the leading order we take the microscale fields in equations (4.21) - (4.29) to be represented by $\boldsymbol{\psi}^{\pm}_{c0}$. Further, we define the *continuous* composite field

$$\boldsymbol{\psi}_{c0} = \boldsymbol{\psi}^{+}_{c0} + \boldsymbol{\psi}^{-}_{c0}, \tag{6.31}$$

with $\boldsymbol{\psi}^{+}_{c0}, \boldsymbol{\psi}^{-}_{c0}$ respectively defined on either side of the interface, as appropriate, and set equal to zero on the other side.

Use of the above definitions together with the results (3.50) and (3.60) yields

$$\mathbf{v}^{\pm}_{c0} = \mathbf{v}^{\pm}_0, \tag{6.32}$$

whence

$$\mathbf{v}_{c0} = \mathbf{v}_0^+ + \mathbf{v}_0^-. \tag{6.33}$$

We also have that

$$c_{c0}^{\pm} = \tilde{c}_0, \tag{6.34}$$

$$\rho_{c0} = \rho_1^0 + (\rho_1^0 - \rho_2^0)\tilde{c}_0. \tag{6.35}$$

Moreover,

$$p_{c0}^{\pm} = p_0^{\pm} - 2\int_{\tilde{n}}^{\pm\infty}(\kappa_1 + \kappa_2)\left(\frac{\partial \tilde{c}_0}{\partial \tilde{n}}\frac{\partial \tilde{c}_1}{\partial \tilde{n}}\right)d\tilde{n} + \beta(\tilde{n}) + \zeta(\tilde{n}), \tag{6.36}$$

where (6.28) has been used to denote

$$2\mu\left(\frac{\partial \tilde{v}_{31}}{\partial \tilde{n}}\right) - 2\mu^+\left(\frac{\partial v_{30}^+}{\partial n}\right)_{q_3^0} - \frac{2}{3}\mu\chi \equiv \beta. \tag{6.37}$$

The fields $\tilde{p}_{-1}$ ($p_{-1}^{\pm}$ are constants), which are functions only of $\tilde{n}$, are denoted by $\zeta(\tilde{n})$ in the above. The development of the prior section is to be construed as preliminary to the observation that β is functionally dependent only upon $\tilde{n}$. In addition, we have that

$$p_{c0} = p_{c0}^+ + p_{c0}^-. \tag{6.38}$$

Macroscopic quantities

With equations (6.33) - (6.38) defining the continuous microscale fields, equation (4.26) furnishes the macroscopic velocity,

$$\varepsilon\overline{\rho}\,\overline{\mathbf{v}} = \frac{1}{\tau_o}\int_t\int_{\tau_f} d^3\mathbf{r}\,[\rho_1^0 - (\rho_1^0 - \rho_2^0)\tilde{c}_0]\,\mathbf{v}_{c0}. \tag{6.39}$$

The macroscopic pressure gradient is obtained as

$$\bar{\nabla}\overline{p} = \frac{1}{\tau_o}\oint_{\partial\tau_o} d\mathbf{s}\, p_1^+ + \frac{1}{\tau_o}\oint_{\partial\tau_o} d\mathbf{s}\, p_1^-. \tag{6.40}$$

[The extra terms in (6.36) result in a contribution to (6.15) of the form $\xi(\tilde{n})\mathbf{i}_3$ in the interfacial region. Integration of this purely normal component over the interfacial transition region results in no net contribution.]

The macroscopic diffusion flux $\overline{\mathbf{J}}_i$ is obtained from (4.39) as

$$\overline{\mathbf{J}}_1 = \frac{1}{\tau_o}\int_t\oint_{\partial\tau_o} \mathbf{r}d\mathbf{s}\cdot[\rho_1^0\tilde{c}(\mathbf{v}_{c0}-\overline{\mathbf{v}})], \tag{6.41}$$

where we have used the fact that $\tilde{\mathbf{J}}_1 = \mathbf{0}$ at leading order; $\overline{\mathbf{J}}_2$ is obtained from $\overline{\mathbf{J}}_1$ as

$$\overline{\mathbf{J}}_2 = -\overline{\mathbf{J}}_1. \tag{6.42}$$

Computations of the macroscale fields are seen to involve only the solutions of the outer equations, jointly with the solution for $\tilde{c}_0$. The solution for $\tilde{c}_0$ is completely determined once the location of the interface is specified via an appropriate constitutive equation for F [cf. (3.13) and (3.55)]. This solution is independent of the externally-applied macroscopic pressure gradient, $\bar{\nabla}\overline{p}$. However, the time-dependence of the microscale quantities in the above equations arises from the dynamical evolution of the interface, which depends nonlinearly on $\bar{\nabla}\overline{p}$ through the relation

$$\frac{dq_3^0}{dt} = u(\bar{\nabla}\overline{p}). \tag{6.43}$$

In the general case the latter equation implies that the macroscale quantities depend nonlinearly upon $\bar{\nabla}\overline{p}$. However, for the special dynamical evolution considered, viz., time periodic or almost time periodic motions, it is possible to replace the time averaging by a space-averaging procedure [1]. Consequently, we will henceforth utilize

the equivalence (refer to Fig. (6-1) for the definition of $\mathcal{L}$)

$$\int_t \equiv \int_{\mathcal{L}}. \tag{6.44}$$

As such, it is unnecessary to be concerned explicitly with the relationship between

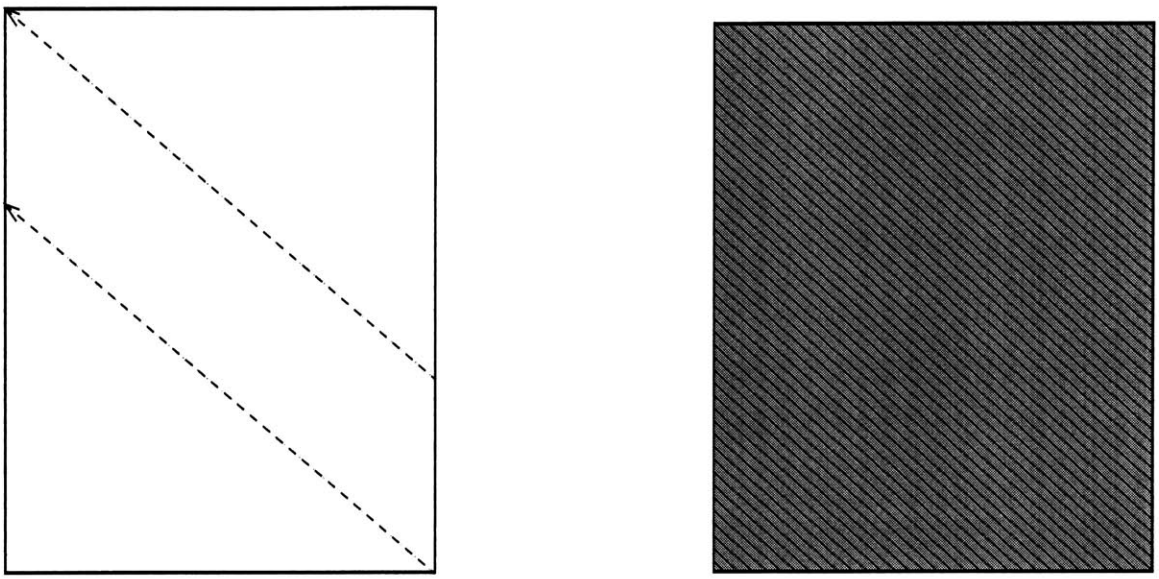

Figure 6-1: Space-averaging domain $\mathcal{L}$ for: (a) Periodic motions. Domain $\mathcal{L}$ is a straight line; (b) Almost-periodic motions. Due to the densely-filling ergodic motion, domain $\mathcal{L}$ constitutes the entire cell.

the dynamical evolution of the system and the macroscale pressure gradient $\bar{\nabla}\overline{p}$.

Linearity and Darcy's laws

The outer equations are *linear*, enabling solutions thereof to be obtained in terms of modified tensor fields $(\mathbf{V}, P, \boldsymbol{\mathcal{T}})$ defined as follows:

$$\{\mathbf{v}^{\pm}, p^{\pm}, \boldsymbol{\tau}^{\pm}\} = \{\mathbf{V}^{\pm}, P^{\pm}, \boldsymbol{\mathcal{T}}^{\pm}\} \cdot \bar{\nabla}\overline{p}. \tag{6.45a,b,c}$$

In terms of these modified fields the outer equations adopt the respective forms

$$\nabla \cdot \mathbf{V}_0^{\pm} = \mathbf{0}, \tag{6.46}$$

$$\nabla P_1^{\pm} = \mu^{\pm} \nabla^2 \mathbf{V}_0^{\pm}, \tag{6.47}$$

subject to the following jump conditions imposed across the interface:

$$[[\mathbf{V}_0]] = \mathbf{0}, \tag{6.48}$$

$$\mathbf{I}_s \cdot [[\mathbf{n} \cdot \boldsymbol{\mathcal{T}}_{v0}]] = \mathbf{0}, \tag{6.49}$$

$$\int d\mathbf{s} \cdot [[\mathbf{n} \cdot \boldsymbol{\mathcal{T}}_{v0}]] = \mathbf{0}, \tag{6.50}$$

$$\mathbf{I} = \frac{1}{\tau_o} \oint_{\partial \tau_o} d\mathbf{s}\, P_0^+ + \frac{1}{\tau_o} \oint_{\partial \tau_o} d\mathbf{s}\, P_0^-. \tag{6.51}$$

In the terminology of homogenization theories [2, 4], the above problem constitutes the 'unit cell' problem. Observe that the solution of the above quasisteady problem is independent of the macroscopic pressure gradient $\bar{\nabla}\overline{p}$.

With the identifications made in this and previous sections the Darcy multiphase flow laws can be obtained as follows: From (6.39),

$$\overline{\mathbf{v}} = \mathbf{K} \cdot \bar{\nabla}\overline{p}, \tag{6.52}$$

in which

$$\mathbf{K} = \frac{1}{\varepsilon \overline{\rho}} \int_{\mathcal{L}} \frac{1}{\tau_o} \int_{\tau_f} d^3\mathbf{r}\, [\rho_1^0 - (\rho_1^0 - \rho_2^0)\tilde{c}_0]\, \mathbf{V}_{c0}, \tag{6.53}$$

with $\mathbf{V}_{c0}$ defined in a manner similar to $\mathbf{v}_{c0}$. Since $\mathbf{V}_{c0}$ and $\tilde{c}_0$ are independent of $\bar{\nabla}\overline{p}$, the above equation constitutes the macroscopic mixture Darcy law. Moreover, equation (6.53) gives the prescription for calculating the phenomenological tensor coefficient $\mathbf{\Lambda}^{\mathrm{III}}$ appearing in (6.7) (namely, $\mathbf{\Lambda}^{\mathrm{III}} = \mathbf{K}^{-1}$), which was the objective of this section.

Furthermore, from (6.41),

$$\overline{\mathbf{J}}_1 = \mathbf{K}' \cdot \bar{\nabla}\overline{p}, \tag{6.54}$$

wherein

$$\mathbf{K}' = \int_{\mathcal{L}} \frac{1}{\tau_o} \oint_{\partial\tau_o} \mathbf{r} ds \cdot [\rho_1^0 \tilde{c}(\mathbf{V}_{c0} - \mathbf{K})]. \tag{6.55}$$

Using the above relations together with the definitions of the phase-specific macroscale quantities, one obtains the following phase-specific Darcy's laws:

$$\overline{\mathbf{v}}_1 = \left(\mathbf{K} + \frac{\mathbf{K}'}{\overline{\rho}_1}\right) \cdot \bar{\nabla}\overline{p}_1; \qquad \overline{\mathbf{v}}_2 = \left(\mathbf{K} - \frac{\mathbf{K}'}{\overline{\rho}_2}\right) \cdot \bar{\nabla}\overline{p}_2. \tag{6.56a,b}$$

In the simplified spatially periodic model analyzed above, $\bar{\nabla}\overline{\mu}_k = \mathbf{0}$ and $\bar{\nabla}\overline{c} = \mathbf{0}$, whence the capillary pressure adopts the simple form

$$P_c = \text{const.} \tag{6.57}$$

throughout the system. This spatial uniformity is consistent with the homogeneity of the macroscale fields.

Discussion

Calculations presented in this section have served to illustrate the formalism involved in computing the macroscale fields. The desire for analytical tractability forced us to choose an extremely simple example. Nevertheless, the analytical scheme leading to the multiphase Darcy law description is clearly nontrivial despite the apparent simplicity of the model. Numerical solutions of the unit cell problem also promise to be formidable. It needs to be emphasized here that despite the resemblance of the system of outer equations to the conventional singular interface equations, our formalism defines the pertinent macroscale fields in terms of the complete, continuous

fields, rather than in terms of the outer solutions alone. As such, it is likely that a schism will develop in more comprehensive studies between conventional singular interface analyses, where one deals with discontinuous fields, and our diffuse interface analysis, involving continuous fields. Moreover, in our simplistic case, the interfacial conditions played a subsidiary role in determining the solutions of the unit cell problem. In particular, it was unnecessary to deal with averaging these conditions at any stage in the analysis (in contrast with the treatments of Gray & Hassanizadeh [8] and Whitaker [18]). A useful exercise would be to illustrate the above formalism for other similar problems so as to highlight the conceptual advantages and the formalism embodied in our approach. However, such an effort entails manifold details, a number of which prove to be repetitive in terms of the examples addressed in this section and in section 3.5.

Outstanding issues regarding uniqueness of solutions of the outer equations are easily resolved by pursuing conventional uniqueness arguments, e.g., employing the energy dissipation theorem [10]. As such, further discussion of the uniqueness issue is omitted here. Questions pertaining to the symmetry properties of the phenomenological coefficients $\mathbf{K}, \mathbf{K}'$ are also omitted in the interests of brevity, except for the observation that these dyadics are not generally symmetric unless u in (6.21) is set to zero. This conclusion is consistent with that of other researchers [2, 18].

6.4 Conclusions

This chapter addresses the functional form of the macroscale constitutive equations. The macroscale constitutive equations thereby obtained were also verified subsequently by employing a simplified linear example, which served the dual purpose of illustrating the complete framework outlined in the preceding chapters.

The macroscale constitutive equations obtained were respectively identical to Darcy's law and its two-phase generalization Darcy's laws within the diffuse and the singular Darcyscales. Furthermore, our results cast doubts on the accuracy of claims concerning the symmetry properties of the cross-coupling permeability ten-

sors. The exercise effected in this chapter thereby renders rational the previously empirical two-phase Darcy field equations. Concomitantly, our framework furnishes valuable insights into the concepts of phase-specific quantities.

References

[1] P. M. Adler, M. Zuzovsky and H. Brenner, "Spatially-periodic suspensions of convex particles in linear shear flows: 1. Description and kinematics," *Int. J. Multiphase Flow.*, **11**, 361(1985).

[2] J. L. Auriault, "Nonsaturated deformable porous media: Quasistatics," *Transp. Porous Media*, **2**, 45 (1987).

[3] J. L. Auriault and E. Sanchez-Palencia, "Remarques sur la loi de Darcy pour les écoulements biphasiques en milieu poreux," *J. de Méch. Théorique et Appl.*, **Special**, 141 91986).

[4] A. Bensoussan, J. L. Lions, and G. Papanicolaou, *Asymptotic Analysis for Periodic Structures*, North-Holland, New York (1978).

[5] H. Brenner and A. Nadim, "The Lorentz reciprocal theorem for micropolar fluids," *J. Engng Math.*, **30**, 169 (1996).

[6] P. G. deGennes "Theory of slow biphasic flows in porous media," *PhysicoChem. Hydrodyn.*, **4**, 175 (1983).

[7] S. R. deGroot and P. Mazur, *Non-Equilibrium Thermodynamics*, Dover, New York (1984).

[8] W. G. Gray and S. M. Hassanizadeh, "Mechanics and thermodynamics of multiphase flow in porous media including interphase boundaries," *Adv. Water Resour.*, **13**, 169 (1990).

[9] F. Kalaydjian, "A macroscopic description of multiphase flow in porous media involving spacetime evolution of fluid/fluid interface," *Transp. Porous Media*, **2**, 537 (1993).

[10] J. B. Keller, L. A. Rubenfeld and J. E. Molyneux, "Extremum principles for slow viscous flows with applications to suspensions," *J. Fluid Mech.*, **30**, 97 (1967).

[11] R. G. Mokadam, "Thermodynamic analysis of the Darcy Law," *Trans. Amer. Soc. Mech. Engrs.*, **83**, 208 (1961).

[12] A. H. Nayfeh, *Perturbation Methods*, Wiley, New York (1973).

[13] L. C. Nitsche, *Multiphase Flows Through Spatially-Periodic Models of Porous Media*, Ph. D. Thesis, Massachusetts Institute of Technology, Cambridge 1989).

[14] J. F. Nye, *Physical Properties of Crystals: Their Representation by Tensors and Matrices*, Clarendon, Oxford (1985).

[15] D. Pavone, "Macroscopic equations derived from space averaging for immiscible two-phase flow in porous media," *Rev. I. Fr. Petrol.*, **44**, 29 (1989).

[16] G. I. Taylor, "The formation of emulsions in definable fields of flow," *Proc. R. Soc. Lond.* A **146**, 41 (1934).

[17] C. Truesdell, *Continuum mechanics 1. The Mechanical Foundations of Elasticity and Fluid Dynamics*, Gordon & Breach, New York (1966).

[18] S. Whitaker, "Flow in porous media: 2. The governing equations for immiscible two-phase flow," *Transp. Porous Media*, **1**, 105 (1986).

Chapter 7

Conclusions and Summary

The preceding analysis outlines a novel, generic framework for modeling multiphase fluid flow through porous media. Our perspective involves treating pore-scale flow phenomena from a *diffuse* interface point of view, in contrast to the more usual *singular* interface viewpoint. In our scheme, two-phase flows are likened to the Navier-Stokes flow of a *single-phase, two-component* mixture possessing steep gradients in physicochemical properties across the interfacial transition zone. Initially, to keep the arguments as simple as possible, we examined the admissibility of immiscible two-phase mixtures under the diffuse interface model in the absence of the porous medium. This involved a rigorous singular perturbation analysis to derive the conventional bulk-phase equations, as well as the kinematical and dynamical matching conditions — the latter yielding the usual Laplace interfacial tension boundary condition.

Using such a framework we shifted the focus to comparable flows in porous media, where we defined all macroscale (diffuse Darcyscale) quantities in a rigorous and physically plausible manner in terms of their microscale, Navier-Stokes counterparts. Special emphasis was placed on oft-neglected considerations regarding the time evolution of the pore-level fields [1]. Though the analysis was performed for a special geometric model of porous medium, namely one possessing a spatially periodic skeletal structure, we also indicated the existence of other cases to which we believe our scheme could be applied. Using physically-based definitions we derived the diffuse Darcyscale transport equations from their microscale counterparts. Ar-

guments from irreversible thermodynamics were also invoked to suggest linear forms for the macroscale constitutive equations connecting the dynamical and kinematical macroscale fields.

We believe that one of the main achievements of this work lies in clarifying the distinction between phase-specific and species-specific quantities. This identification was based upon a combination of physical and thermodynamic arguments. Such an interrelationship was shown to result from correlating the respective diffuse and singular Darcyscale approaches. This led us phenomenologically to the underlying basis for the existence of classical phase-specific Darcy's laws. In addition, our scheme furnished useful insights into both the definition and interpretation of capillary pressure as a continuum Darcyscale field concept. Eventually, we used a simple illustrative example, derived formally from our microscale equations by singular perturbation methods, to provide some justification for the linear macroscopic constitutive equations originally proposed purely phenomenologically on the basis of irreversible thermodynamics.

Our development invoked a number of simplifying assumptions at various stages of the analysis. It is useful to recall these, and hence the potential limitations thereby imposed, so as to concurrently point towards possible future research directions involving more realistic models of multiphase flows, albeit built upon the generic framework embodied in our diffuse interface approach. One of our main assumptions involved the neglecting the wetting properties of the two fluids. A wide variety of experimental observations [2] have demonstrated the relevance of wettability and contact-line phenomena to multiphase flow in porous media, neither of which phenomena falls under the purview of this thesis. Furthermore, we have restricted our attention exclusively to isothermal flows. In nonisothermal situations the averaging procedure, as well as the definition of macroscale temperature, can be expected to raise fundamental questions (although we believe these to be relatively unimportant in most applications). Moreover, no numerical results were cited to corroborate our macroscale theory. Model porous systems which facilitate numerical computations of the pertinent microscale problems, simultaneously suggesting comparable experimental observations, repre-

sent potential future research directions towards ratifying the theoretical framework presented here.

Our analysis deliberately straddled the boundary between physical concepts and mathematical rigor, albeit without straining too much into the latter, as is usual in such cases. We believe that the diffuse interface, mixture-theory model outlined in this paper has the potential to clarify a number of fundamental issues prerequisite to a deeper understanding of two-phase flow phenomena in porous media. At a practical level the model outlined herein can also be used to effect explicit numerical microcontinuum computations based upon representative geometric models of porous media. Such calculations are greatly facilitated by the fact that the major computational issue of temporally evolving 'interfaces,' together with their concomitant spatial discontinuities, is no longer explicitly present in our diffuse interface model (although it is, of course, implicitly present). Furthermore, our model can presumably be used to acquire useful insights into the forms of the pertinent constitutive equations as well as into the magnitudes of the phenomenological coefficients appearing therein.

This part of the thesis, constituting a major portion of text, serves to illustrate a number of issues encountered within the coarse-graining procedures, which we recapitulate below to highlight the path of our own framework. These issues are emphasized below by italic typeface. *The model chosen at the microscale level must be validated by the apparent agreement of its macroscale predictions with qualitative experimental observations.* Within such a philosophy, we adopted a novel, physically-based viewpoint for modeling the underlying microscale flows. Subsequent to the adoption of any microscale model, *the explicit relationship of the measurable macroscale quantities to their precursor microscale counterparts needs to be established.* This fact is fundamental to any rational theory of the phenomena. Such relationships must completely accord with the physical definitions of the macroscale quantities so as to enable an unambiguous interpretation of experimental measurements. In chapters 4 and 5 we outlined such a framework based upon our 'diffuse interface' conception. *Finally, the coarse-graining procedure needs to be effected, utilizing the microscale model together with the definitions of the macroscale quantities.* In some cases (one such instance rep-

resented by the example considered in the preceding chapters) the final step cannot be accomplished in an analytical manner, thereby forcing one to rely on approximations to determine the macroscale-level equations. Some of the common approximations employed in coarse-graining procedures include closure schemes, Taylor series expansions etc. In this context, we utilized the framework embodied in nonequilibrium thermodynamics to provide rational insights into the possible forms of the macroscale constitutive equations. A major limitation of irreversible thermodynamics lies in its inability to provide any indication of the magnitudes of these phenomenological coefficients, except possibly their algebraic signs. Moreover, the above relations are purely phenomenological, and hence do not constitute a self-contained theory. As a consequence, their applicability to the phenomena at hand needs to be ratified either through comprehensive experiments or a detailed microscale theory, or both. Similar issues confront most of the approximations effected at the macroscale level. We provided a partial justification of the predictions of nonequilibrium thermodynamics by employing a simplified linear example to verify the results obtained within the diffuse interface framework of the overall model.

In a sense, this portion of the thesis, justifiably the longest of the thesis, provides a detailed illustration of most of the procedures and the issues accompanying the implementation of a coarse-graining procedure. In subsequent parts of the thesis, we consider examples which possess certain special properties (elucidated at the appropriate junctures of the text), which enable the coarse-graining procedure to be effected in an exact manner, without introducing any *ad hoc* approximations.

References

[1] S. Whitaker, "Flow in porous media: 2. The governing equations for immiscible two-phase flow," *Transp. Porous Media*, **1**, 105 (1986).

[2] J. P. Stokes, D. A. Weitz, J. P. Gollub, A. Dougherty, M. O. Robbins, P. M. Chaikin and H. M. Lindsay, "Interfacial stability of immiscible displacement in a porous medium," *Phys. Rev. Lett.*, **57**, 1718 (1986).

Part 2: Applications of Macrotransport Theory

Chapter 8

Macrotransport Theory

In this part of the thesis we outline two novel applications of a multiscale coarse-graining technique referred to as macrotransport theory. In contrast to the other coarse-graining techniques outlined in different sections of this thesis, macrotransport theory constitutes a *generalized dispersion theory for characterizing the solute transport in continuous and discontinuous microscale systems.* The main feature that accompanies the class of generalized dispersion problems amenable to a 'macrotransport' (or coarse-grained) description is the presence of a *global* (unbounded) and a *local* (which can either be bounded or unbounded) phase-space within which solute transport occurs [3]. Within this broad context, macrotransport theory provides a paradigm for calculating the parameters characterizing the transport of the *local-space averaged solute concentration.* The transport of the 'mean' solute concentration is typically characterized by a mean solute velocity vector (denoted $\bar{\mathbf{U}}^*$) and a mean dispersivity dyadic[1] $\bar{\mathbf{D}}^*$ [14]. Situations can also arise which might entail the presence of a mean reaction coefficient (denoted $\bar{K}^*$) quantifying the microscale consumption of the solute due to bulk and surface reactions [13]. In the context of the nonreactive case, macrotransport theory thereby represents a generalized version of G. I. Taylor's dispersion analysis of a solute in a Poiseuille flow [14]. Therefore, macrotransport

[1]In contrast to the exact description of the solute transport which involves a 'diffusive' contribution to the transport, the mean solute concentration possesses a 'dispersive' contribution which embodies implicit contributions from both the the microscale diffusive and convective transport processes.

theory is also sometimes referred to as the generalized Taylor dispersion theory.

This chapter provides a brief introduction to the salient concepts which accompany the application of the 'macrotransport paradigm.' However, we eschew the elaboration of the details of the derivations that accompany the cited results, instead referring the reader to the book by Brenner & Edwards [4] (this book will be referred to as BE in subsequent sections of the text) which presents detailed derivations of the results as well as numerous applications thereof. A brief outline of this chapter is as follows: In section 8.1 we use simple physical examples to clarify the notation employed in the application of the macrotransport paradigm. Specifically, we focus on elucidating the concepts of a generalized Brownian tracer, and the meaning of local and global subspaces. Section 8.2 elaborates the transport equation governing the evolution of the probability density of the generalized Brownian tracer. In the case of a nonreactive Brownian solute, this equation is the conservation equation for the probability density, and embodies the transport due to convective and diffusive processes in both local and global spaces. For the case of a reactive Brownian solute the probability density is no longer conserved, whence requires a quantification of the consumption rate of the solute. In section (8.4 we highlight the typical form of the 'macrotransport equation,' and thereby simultaneously highlight the calculations that accompanies the utilization of the paradigm. Finally, we conclude the chapter with a discussion clarifying the physical basis of macrotransport theory in terms of the delineation of the timescales of the transport processes involved. This discussion also serves to clarify the possibilities for generalizing the macrotransport theory to encompass situations wherein some of the requirements imposed on the local and global subspaces might not be strictly satisfied.

8.1 Notation

8.1.1 Generalized Brownian Tracer

As we clarified in the Introduction, the theory of macrotransport process is concerned with the dispersion of a solute due to convective and diffusive processes. In macrotransport theory the transport of the solute is identified with the transport of the probability density field of an ideal Brownian particle.[2] The probability density of the Brownian particle is equivalent to the corresponding solute concentration field on the assumption that the system is sufficiently dilute to behave ideally in a physicochemical sense [8]. Conventionally, the Brownian tracer particle representing the solute does not possess an intrinsic structure, whereby enabling us to utilize the probability density of the center of the Brownian tracer to model the transport of solute particles. However, in the more general case, the solute particles can be expected to posses internal structure involving extra degrees of freedom for generalized displacements [2, 11]. In such a case, the Brownian tracer quantifying the solute particle also possesses internal structure which is kinematically and dynamically identical to that of the solute particles. In such a generalized scenario, the probability density field of the Brownian tracer particle is typically a function both of its internal degrees of freedom and the positional coordinate of its center of mass. Furthermore, in such a case the solute concentration field (the number density) would be identical to the projection of the probability density field onto the spatial coordinates (i.e. by integrating out the internal degrees of freedom). The use of a generalized Brownian tracer particle thereby enables us to obtain the coarse-grained or macrotransport description of systems wherein the positional solute diffusion equation embodies contributions arising from the internal degrees of freedom. Such a procedure is rendered formal by the identification that the internal degrees of freedom constitute the local space

[2] In this context, ideality refers to the situation wherein the non-equilibrium and comparable effects animating the Langevin description of the Brownian motion are absent — thereby allowing us to use the simple results accompanying the classical Einstein's theory of Brownian motion [8]. This requirement is to be carefully distinguished from the requirement that the pervading solvent be physicochemically an ideal solution.

and the positional coordinates of the Brownian tracer constitute the global space [see next section for a discussion on global and local subspaces]. Figure (8-1) depicts an example of a generalized Brownian tracer along with the identification of the local and the global spaces.

More exotic situations can also be envisaged wherein the tracer particle quantifies the transport of temperature or momentum rather than material solute. These generalized tracers are termed as 'thermions' [1] and 'momentons' [9] respectively. Further, the dispersion processes involving thermions and momentons can be handled in a manner analogous to the theory pertaining to the transport of the Brownian particle. Explicitly, the conservation equation governing the transport of the probability density of a thermion would be identical to the heat transport equation. Analogously, the transport of the momenton is governed by the momentum transport equation (Navier-Stokes equation or a comparable equation thereof). In the following chapter we encounter the application of macrotransport theory to thermion dispersion processes to thereby enable quantification of the macrotransport coefficients in a situation involving heat transport.

In the following sections we refer to the tracer particle consistently as a Brownian particle. The theoretical development corresponding to a thermion is completely analogous to the Brownian particle case and will not elaborated here. The dispersion theory for momentons is still under development. The rudiments of the theory can be found in BE [4].

8.1.2 Global and Local Spaces

The class of problems that are amenable to the application of macrotransport theory and a macrotransport description typically involve the existence of two distinctly different sets of independent coordinate variables characterizing the instantaneous 'position' of the Brownian solute particle. These variables are designated as the *global* and the *local* variables, and are denoted in the text by the symbols $\mathbf{Q}$ and $\mathbf{q}$ respectively. Each of these variables might themselves be scalars or vectors, and also possibly of different dimensionalities. Together, the vectors ($\mathbf{Q}$, $\mathbf{q}$) constitute a multidimensional

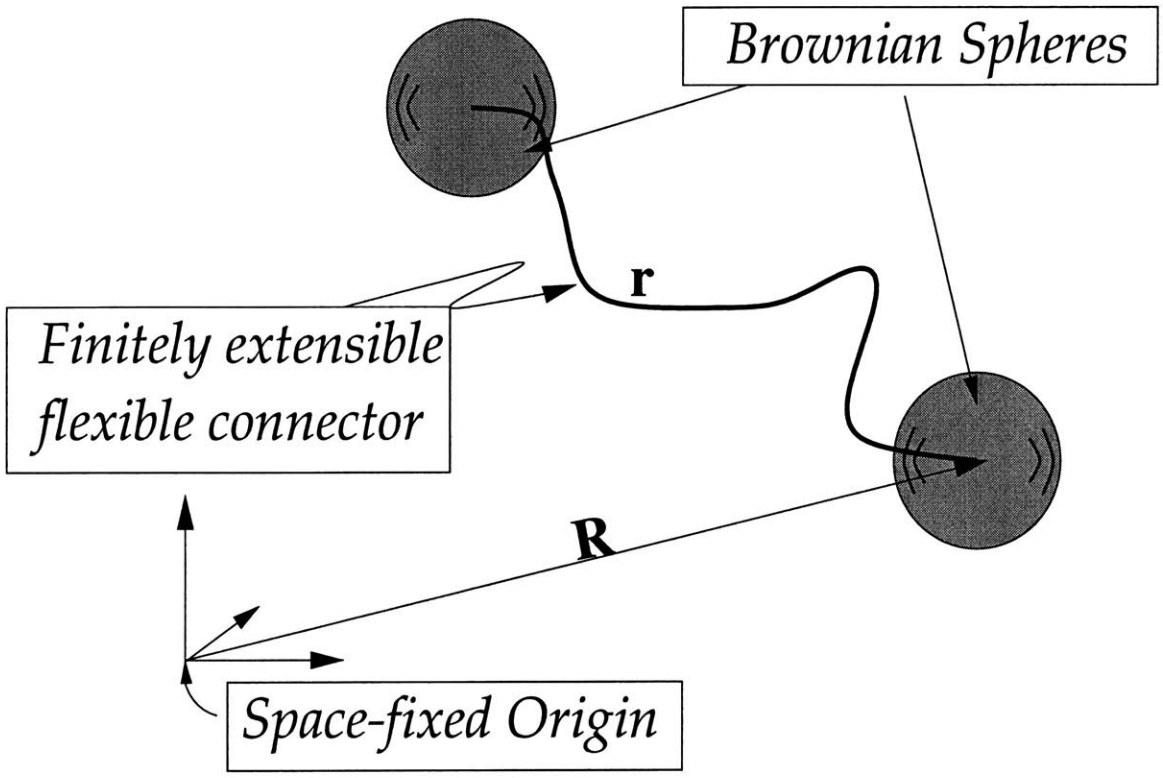

Figure 8-1: An example of a generalized Brownian tracer. The composite tracer particle is comprised of the two Brownian spheres along with the flexible string that connects them. The location of the Brownian tracer is identified by the position vector of one of the spheres (denoted $\mathbf{R}$) and the vector signifying the internal displacement $\mathbf{r}$. The finite extensibility of the string imposes the boundedness of the internal displacement vector $\mathbf{r}$. In this example, the unbounded vector $\mathbf{R}$ constitutes the global space coordinate $\mathbf{Q}$ and the bounded vector $\mathbf{r}$ constitutes the local space coordinate $\mathbf{q}$. This figure is adapted from Brenner & Edwards [4].

phase space (denoted $\mathbf{Q} \oplus \mathbf{q}$) within which the convective and diffusive solute-particle transport processes occur. The global space $\mathbf{Q}$ characterizing the solute transport will be assumed to be necessarily unbounded, in contrast to the local subspace of transport $\mathbf{q}$ which will be assumed to be bounded. Such an identification thereby renders the distinct delineation of global vs local spaces explicit. However, the above constraint posed on the topological compactness of the local subspace constitutes a strong and sufficient condition for the applicability of macrotransport paradigm. To enable the application of macrotransport theory to situations wherein such a strong condition might not be applicable, a weaker *necessary condition* is expounded in section 8.5 which thereby delineates the subspaces in terms of a temporal distinction. This condition subsequently enables the application of macrotransport theory to the issue considered in chapter 10 which possesses a local space with a noncompact support (unbounded). However, the focus of the rest of the development in this chapter is concerned with the case wherein the local space is bounded in extent, and thereby enables a geometrical distinction between the subspaces. The extension of the theory to situations involving unbounded local space is quite straightforward.

8.2 Evolution Equation for the Probability Density P

8.2.1 Conditional Probability Density

As expounded in the previous section, the convective and diffusive transport of the solute particles is modeled by the equivalent probability density field of a Brownian tracer particle. Let the nonnegative scalar $P(\mathbf{Q}, \mathbf{q}, t|\mathbf{Q}', \mathbf{q}', t')$ denote the conditional probability density that the Brownian particle is situated at ($\mathbf{Q}$, $\mathbf{q}$) at a time t, given that it was initially introduced into the system at the position $(\mathbf{Q}', \mathbf{q}')$ at a time $t' < t$. In almost all cases of interest, the conditional probability density of the Brownian particle is invariant to translational displacements along the global space coordinates (since the global space is assumed to be unbounded). Furthermore, in the

absence of exotic physicochemical effects,[3] the probability density of the Brownian particle is expected to be invariant to translations in time. The preceding two physical requirements constrain the conditional probability density to depend only on the relative global displacements $\mathbf{Q}-\mathbf{Q}'$ and the temporal displacement $t-t'$. Therefore, without loss of generality we can set $\mathbf{Q}'=\mathbf{0}$ and $t'=0$, thereby obtaining

$$P \equiv P(\mathbf{Q},\mathbf{q},t|\mathbf{q}'). \tag{8.1}$$

Further, the transport of a *nonreactive* Brownian tracer is characterized the conservation of the total solute concentration which equivalently requires the presence of the Brownian particle at some local and global space coordinate at any time $t>0$, i.e.

$$\int_{\mathbf{Q}_\infty} d\mathbf{Q} \int_{\mathbf{q}_\infty} d\mathbf{q} P = 1, \qquad t>0. \tag{8.2}$$

In the above equation $\mathbf{Q}_\infty$ and $\mathbf{q}_o$ denote the volumetric expanse of the global and the local spaces respectively. Moreover, to ensure that the constraints posed by causality are satisfied we require

$$P=0 \qquad \text{for } t<0. \tag{8.3}$$

8.2.2 Conservation Equation

The physicochemical transport of the solute particle is explicitly quantified by the convective-diffusive transport equation of the probability density $P(\mathbf{Q},\mathbf{q},t|\mathbf{q}')$. For the case of a nonreactive Brownian particle this equation acquires the form [10]

$$\frac{\partial P}{\partial t} + \nabla_Q \cdot \mathbf{J} + \nabla_q \cdot \mathbf{j} = \delta(\mathbf{Q})\delta(\mathbf{q}-\mathbf{q}')\delta(t). \tag{8.4}$$

[3]One such example involves the diffusion in glassy systems which exhibits aging characteristics.

In the above equation δ denotes the Dirac delta function. The terms on the right hand side of the equation quantifies the introduction of the Brownian tracer at $t = 0$ at the spatial coordinate $\mathbf{q} = \mathbf{q}'$ and $\mathbf{Q} = \mathbf{0}$. In the above equation $\mathbf{J}$ and $\mathbf{j}$ represents the fluxes of the probability density in the global and local spaces respectively. These fluxes embody within them *inter alia* the convective and the diffusive transport of the Brownian tracer in the global and local spaces respectively.

The constitutive equations for the fluxes present in the above conservation equation are assumed to be of the respective linearly additive forms,

$$\mathbf{J} = \mathbf{U}'(\mathbf{q})P - \mathbf{D}(\mathbf{q}) \cdot \nabla_Q P + \mathbf{M}(\mathbf{q}) \cdot \mathbf{F}(\mathbf{q})P \tag{8.5}$$

and

$$\mathbf{j} = \mathbf{u}(\mathbf{q})P - \mathbf{d}(\mathbf{q}) \cdot \nabla_q P + \mathbf{m}(\mathbf{q}) \cdot \mathbf{f}(\mathbf{q})P. \tag{8.6}$$

The above constitutive equations embody the following contributions: (i) convective fluxes arising from the global solute velocity $\mathbf{U}$ and the comparable local velocity $\mathbf{u}$; (ii) Fickian diffusive contributions to the global and the local spaces quantified by the respective diffusivity dyadics $\mathbf{D}$ and $\mathbf{d}$; (iii) Transport arising from animating external forces quantified by the contributions from global and local space forces $\mathbf{F}$, $\mathbf{f}$ and the respective mobilities $\mathbf{M}$, $\mathbf{m}$ in the subspaces.

In the above equations note that the convective and diffusive fluxes are assumed exclusively to be functions of the local space coordinates. Generalizations of macrotransport theory permit time-periodic [7] (with a single time-period T characterizing all unsteady functions) convective and diffusive transport mechanisms. In the next chapter of this thesis we encounter one such application of macrotransport theory, namely wherein the convective contributions are time-periodic. However, the development of the macrotransport paradigm enabling the treatment of more general time dependencies (like for instance, almost time-periodic functions etc.) are still as yet to be accomplished. More importantly, the theoretical development accompanying the paradigm of macrotransport theory as yet enables only treatment of situations

wherein the convective and diffusive-flux contributions are exclusive functions of local space variables (in addition to possibly being time-periodic). However, despite this constraint the macrotransport theory encompasses a number of wide-ranging examples, and thereby constitutes an important physical theory of coarse-graining (in this context see also an interesting work by Bryden & Brenner [5]).

Equation (8.6) embodies the conservation of the solute when concomitant convective and diffusive transport processes are present. Subsequent generalizations of macrotransport theory has enabled analysis of the case wherein a first order (bulk and/or surface) reaction accompanies the convective and diffusive transport processes. In such a case, the evolution equation of the conditional probability density P acquires the form

$$\frac{\partial P}{\partial t} + \nabla_Q \cdot \mathbf{J} + \nabla_q \cdot \mathbf{j} + KP = \delta(\mathbf{Q})\delta(\mathbf{q} - \mathbf{q}')\delta(t), \tag{8.7}$$

where $K \equiv K(\mathbf{q})$ (and possibly time-periodic) denotes the rate constant for the first order bulk reaction that depletes the solute.

The above equations (8.4) [or (8.7)] - (8.6) constitute the complete set of transport equations governing the probability density of the Brownian tracer particle. These equations are to be supplemented by the local and global space boundary conditions to enable the solution. These boundary conditions are considered in the next two sections.

8.2.3 q-space Boundary Conditions

In the absence of surface reactions, the local space flux is constrained to satisfy the absence of a normal flux component at the boundary of the local space. If we denote the boundary of the local space by $\partial\mathbf{q}_o$, this condition is mathematically quantified as

$$\mathbf{n} \cdot \mathbf{j} = 0 \quad \text{on } \partial\mathbf{q}_o, \tag{8.8}$$

wherein $\mathbf{n}$ denotes the surface normal to the boundary $\partial\mathbf{q}_o$.

The above equation permits the conservation of the Brownian tracer particle following its introduction into the system. However cases which involve the occurrence of surface reactions require modification of the above boundary condition to incorporate the consumption of the solute. The example considered in the next chapter belongs to this category of transport processes.

8.2.4 Q-space Boundary Conditions

The normalization condition embodied in (8.2) imposes constraints on the form of the probability density P to ensure convergence of the global space integral present therein. However, in the theoretical development of the macrotransport paradigm, one typically encounters similar normalization conditions imposed on the higher order global space moments of P. To enable such terms to converge, a slightly stronger condition is imposed on the probability density to thereby require that

$$|\mathbf{Q}|^m P \to 0 \text{ and } |\mathbf{Q}|^m \mathbf{J} \to 0 \text{ as } |\mathbf{Q}| \to \infty \tag{8.9}$$

for arbitrary nonnegative integers m.

8.3 Lagrangian Definitions of the Mean Solute Velocity and Dispersivity

Prior to outlining the macrotransport paradigm which furnishes the local-space averaged transport equation and the coefficients present therein, it is pertinent to clarify the physical meaning of the macrotransport coefficients which will appear in the macrotransport equation. In this section we adopt a Lagrangian viewpoint to define the mean solute velocity and the mean dispersivity of the Brownian tracer particle. The mathematical development accompanying the theory of macrotransport processes (the details of which can be found in BE [4]) involves the implementation of this Lagrangian approach to derive the macrotransport paradigm. This unique viewpoint,

which contrasts with the traditional Eulerian approach to defining the mean transport coefficients, subsequently (see the next two chapters) yields considerable physical insights into the nature of the transport processes that are manifest.

As a prelude to identifying the macrotransport coefficients, we define the following quantities:

(i) The mean displacement vector $\bar{\mathbf{Q}}$ of the Brownian tracer particle (released at $\mathbf{Q} = \mathbf{0}$ at time $t = 0$) at a time t is defined as

$$\bar{\mathbf{Q}} \stackrel{\text{def.}}{=} \int_{\mathbf{Q}_\infty} d\mathbf{Q} \int_{\mathbf{q}_o} d\mathbf{q}\, \mathbf{Q}\, P. \tag{8.10}$$

(ii) The mean-squared dyadic global displacement of the Brownian tracer particle measured from its mean global position $\bar{\mathbf{Q}}$ is defined as

$$\overline{(\mathbf{Q} - \bar{\mathbf{Q}})^2} \stackrel{\text{def.}}{=} \int_{\mathbf{Q}_\infty} d\mathbf{Q} \int_{\mathbf{q}_o} d\mathbf{q}\, (\mathbf{Q} - \bar{\mathbf{Q}})^2\, P. \tag{8.11}$$

In the above equation we have used the truncated notation $\mathbf{V}^2 \equiv \mathbf{VV}$ to denote dyadic products.

Based on the above definitions (8.10) and (8.11), the mean displacement vector $\bar{\mathbf{Q}}$ and the mean-squared displacement $\overline{(\mathbf{Q} - \bar{\mathbf{Q}})^2}$ can both be expected to be functions of the initial local space coordinate $\mathbf{q}'$ and the time t. However, within the framework of macrotransport theory, it has been proved that after the lapse of a sufficiently long time [see section 8.5 for a discussion pertaining to quantitative constraints on timescales] both $\bar{\mathbf{Q}}$ and $\overline{(\mathbf{Q} - \bar{\mathbf{Q}})^2}$ become independent of the initial local space coordinate $\mathbf{q}'$, and thereby depend only on time elapsed, t. Further, within the same limiting constraints imposed on the time t, it can be proved that both the mean displacement and the mean-squared displacement increases linearly with time. Based on the above facts, and the accompanying analogy with the theory of Brownian motion[4] we can define the mean global-space velocity $\bar{\mathbf{U}}^*$ and the dispersion dyadic $\bar{\mathbf{D}}^*$ by the

[4]In the theory of Brownian motion [6], the mean displacement and the mean-squared displacement of the Brownian particle varies linearly with time. The proportionality constants governing the relationship defines respectively the mean velocity and the diffusivity of the Brownian particle.

following asymptotic relations

$$\bar{\mathbf{Q}} = \bar{\mathbf{U}}^* t \tag{8.12}$$

and

$$\overline{(\mathbf{Q} - \bar{\mathbf{Q}})^2} = 2\bar{\mathbf{D}}^* t. \tag{8.13}$$

The latter definitions embody the *Lagrangian viewpoint definitions of the mean solute velocity and the mean solute dispersivity.*

The implementation of the definitions embodied in equations (8.10) - (8.13) on the microscale conservation equation (8.4) subsequently yields the macrotransport paradigm for calculating the mean-solute velocity $\bar{\mathbf{U}}^*$ and the dispersion dyadic $\bar{\mathbf{D}}^*$ in terms of microscale data and equations. It is a nontrivial task to prove that the mean velocity and the mean dispersivity characterizing the transport of the local-space averaged probability density is identical to the above Lagrangian definitions. The details elaborating the proof can be found in BE [4]. In the next section we outline the macrotransport paradigm or a recipe to obtain the above macrotransport coefficients in terms of more detailed microscale quantities.

8.4 Macrotransport Paradigm

In this section we outline the macrotransport description and the paradigm to evaluate the coefficients appearing therein. As an illustrative example, we consider the convective and diffusive transport of a nonreactive Brownian tracer in a steady or time independent scenario. The paradigms corresponding to time-periodic and reactive scenarios can be found in BE [4] and also in the next chapter.

In the asymptotic long time limit expounded in the previous section, the generic microscale transport equation (8.4) governing the conditional probability density $P(\mathbf{Q}, \mathbf{q}, t)$ can be coarse-grained to thereby obtain the macrotransport equation governing the coarse-grained macroscale probability density $\bar{P}(\mathbf{Q}, t)$ characterizing the

totality of the molecular solute species being transported, irrespective of the local-space coordinate in which the tracer molecule characterizing the chemical species being transported finds itself at any given instant of time. Mathematically, the coarse-grained probability density is obtained from the detailed fine-scale probability density by projecting out the degrees of freedom corresponding to the local-space coordinates, i.e.,

$$\bar{P}(\mathbf{Q},t) \overset{\text{asymptotic}}{\rightarrow} \int_{\mathbf{q}_o} d\mathbf{q} P(\mathbf{Q},\mathbf{q},t|\mathbf{q}') \tag{8.14}$$

The less detailed density distribution $\bar{P}(\mathbf{Q},t)$ quantifies the solute species transport process through the global or $\mathbf{Q}$-space, accounting for the transport in the local or $\mathbf{q}$-space in an appropriately averaged manner. This coarse-grained density is expected to evolve according to the macroscale, i.e., global-space convective-diffusive conservation equation [4]

$$\frac{\partial \bar{P}}{\partial t} + \bar{\mathbf{U}}^* \cdot \nabla_Q \bar{P} = \bar{\mathbf{D}}^* : \nabla_Q \nabla_Q \bar{P}, \tag{8.15}$$

wherein the time- and position-independent vector velocity $\bar{\mathbf{U}}^*$ and dispersion dyadic $\bar{\mathbf{D}}^*$ respectively quantify the coarse-grained convective and diffusive solute transport mechanisms in the fluid continuum. Implicitly embedded within these coefficients are the overall effects of the comparable microscale transport processes arising from the transport within the local space. The above equation is also referred to as the macrotransport equation or the macrotransport description corresponding to the microscale equation (8.4).

The macrotransport paradigm furnishes a recipe to evaluate the mean global-space velocity $\bar{\mathbf{U}}^*$ and the dispersion dyadic $\bar{\mathbf{D}}^*$ present in the above equation (8.15). To illustrate the manner in which the mean or macrotransport coefficients are to be obtained, we outline below the macrotransport paradigm which accompanies the evaluation of these quantities for the dispersive transport of a nonreactive Brownian tracer under the animating action of steady flow fields and forces. This exposition serves as an illustration of the details typically involved in the computations of the

macrotransport coefficients.

8.4.1 Macrotransport Coefficients

The macrotransport equation (8.15) governing the evolution of the coarse-grained probability density $\bar{P}(\mathbf{Q}, t)$ embodies convective and diffusive transport contributions quantified by the macrotransport coefficients $\bar{\mathbf{U}}^*$ and $\bar{\mathbf{D}}^*$ respectively. The macrotransport paradigm furnishes relations expressing these coefficients as a function of two independent, microscale fields $P_0^\infty(\mathbf{q})$ and $\mathbf{B}(\mathbf{q})$. Explicitly,

$$\bar{\mathbf{U}}^* = \int_{q_o} d\mathbf{q}\mathbf{U}(\mathbf{q})P_0^\infty(\mathbf{q}), \tag{8.16}$$

and

$$\bar{\mathbf{D}}^* = \bar{\mathbf{D}}^M + \bar{\mathbf{D}}^C, \tag{8.17}$$

where

$$\bar{\mathbf{D}}^M = \text{sym} \int_{q_o} d\mathbf{q}\, \mathbf{D}(\mathbf{q})\, P_0^\infty(\mathbf{q}) \tag{8.18}$$

represents the contribution of the molecular diffusivity, and

$$\bar{\mathbf{D}}^C = \text{sym} \int_{q_o} d\mathbf{q}\, P_0^\infty\, (\nabla_q \mathbf{B})^\dagger \cdot \text{sym}\, \mathbf{d} \cdot (\nabla_q \mathbf{B}) \tag{8.19}$$

represents the convective contribution to the dispersivity. In eq. (8.16) we have included within the global space solvent velocity the convective contributions arising from the animating actions of the global space forces, and have denoted the resulting sum as $\mathbf{U}$, i.e. $\mathbf{U} = \mathbf{U}' + \mathbf{M} \cdot \mathbf{F}$. In the above equations, the presence of '†' operator denotes the transposition of the dyad. Further, the operator 'sym' denotes that a symmetrizing operation is effected on that dyad, i.e., for an arbitrary dyad $\mathbf{V}$

$$\text{sym}\mathbf{V} = \frac{1}{2}[\mathbf{V} + \mathbf{V}^\dagger]. \tag{8.20}$$

The microscale field $P_0^\infty(\mathbf{q})$ present in the above equations represents the solution of the following microscale boundary value problem:

$$\nabla_q \cdot \mathbf{j}_0^\infty = 0, \tag{8.21}$$

where

$$\mathbf{j}_0^\infty(\mathbf{q}) = \mathbf{u}(\mathbf{q})P_0^\infty - \mathbf{d}(\mathbf{q}) \cdot \nabla_q P_0^\infty + \mathbf{m}(\mathbf{q}) \cdot \mathbf{f}(\mathbf{q})P_0^\infty, \tag{8.22}$$

subject to the boundary condition,

$$\mathbf{n} \cdot \mathbf{j}_0^\infty = 0 \quad \text{on } \partial\mathbf{q}_o. \tag{8.23}$$

and the normalization condition

$$\int_{\mathbf{q}_o} d\mathbf{q}\, P_0^\infty = 1. \tag{8.24}$$

On the other hand, the microscale field $\mathbf{B}(\mathbf{q})$ represents the solution of the following set of equations:

$$\frac{\partial(P_0^\infty \mathbf{B})}{\partial t} + \mathbf{j}_0^\infty \nabla_q \cdot \mathbf{B} - \nabla_q \cdot (P_0^\infty \mathbf{d} \cdot \nabla_q \mathbf{B}) = P_0^\infty(\mathbf{U} - \bar{\mathbf{U}}^*), \tag{8.25}$$

subject to the boundary condition

$$\mathbf{n} \cdot \mathbf{d} \cdot \nabla_q \mathbf{B} = \mathbf{0} \quad \text{on } \partial\mathbf{q}_o. \tag{8.26}$$

Solution of equation (8.25) presumes knowledge of the mean velocity $\bar{\mathbf{U}}^*$ which can be obtained using the solution of eqs. (8.21) - (8.24) in eq. (8.16).

This section was meant to clarify the procedure to obtain the macrotransport coefficients characterizing the transport of local space averaged solute concentration. Explicitly, it was demonstrated that in the simplest scenario (steady flows involving a nonreactive solute) the macrotransport coefficients are themselves given *inter alia*

in terms of two independent microscale fields P_0^∞ and $\mathbf{B}$ which are to be determined by solving microscale boundary value equations. The knowledge of these microscale fields furnishes the values acquired by the macrotransport coefficients for different values of the parameters present therein. The paradigm outlined in this section is utilized in the subsequent chapters in two distinct applications to determine the macrotransport coefficients in the respective cases. However, to maintain continuity within the text within each of the chapters we provide a self-contained description of the accompanying paradigm utilized there.

In the next section we clarify the fundamental physical basis of macrotransport theory by addressing the question: "when and why is it possible to provide a macrotransport description ?" The resolution of this question is explicitly accomplished by delineating the different time scales accompanying the convective and diffusive transport of the Brownian tracer. This exposition on the time scales also serve to quantitatively clarify the regime of validity of the macrotransport description.

8.5 Basis of Macrotransport Theory

In the previous sections we outlined the paradigm furnished by the macrotransport theory (or generalized Taylor dispersion theory) for deriving long-time asymptotic macroscale transport equations and the phenomenological coefficients appearing therein. This paradigm derives from the recognition that the microscale transport occurs in a phase space $(\mathbf{Q} \oplus \mathbf{q})$ composed of two orthogonal subspaces parameterized by the global coordinates $\mathbf{Q}$ and the local coordinates $\mathbf{q}$ respectively. As such, the existence of two time scales is already implicit in the underlying microscale conservation equation governing the conditional probability density P. Specifically, the transport of the Brownian tracer within the local and global spaces necessarily entails an individual time scale characterizing the former transport (through the local space) and a distinct time scale characterizing the latter transport processes (through the global space). Based on such an identification, the main principle underlying macrotransport theory can be stated as follows: *The local-space equilibration time should*

furnish the 'fast' time scale for transport, while the characteristic global time scale should furnish the 'slow' time scale intrinsic to the external space transport processes. Therefore, the necessary condition for a macrotransport description to be feasible requires that the time scales accompanying transport of the tracer in the local space should be significantly smaller than the time scales of transport in the global space. The fulfillment of this condition would thereby enable the Brownian tracer to reach a state of equilibrium with respect to transport within the local space in time intervals much less than comparable global-space transport times, thereby allowing a macro (or global scale) transport description of the Brownian tracer on time scales greater than the local space equilibration time scale.

Underlying the macrotransport theory was the assumption made at the outset requiring the existence of an unbounded global space and a bounded local space. This assumption implies that the time scales quantifying the transport in the former subspace is necessarily large compared to that of the latter. Whence, the ratio of the local equilibration time scale to the global time scales can be expected to be a small parameter. The mathematical framework of multiple time scale analysis constitutes a systematic perturbation procedure for the analysis of such temporal phenomena which are characterized by the presence of more than one time scale which differ amongst themselves significantly in their magnitudes. The formal perturbation theory accompanying the microscale conservation equation (8.4) has been effected by Pagitsas *et al.* [12] to obtain results completely equivalent to that obtained by a more intuitive procedure (the results are listed in the previous section and constitute the macrotransport paradigm). However, the formal mathematical framework concomitantly furnishes a procedure to extend the asymptotic leading order theory to higher orders, as well as to situations wherein the strict requirements on the boundedness of the spaces are not satisfied (cf. chapter 10). In the following we provide a brief quantitative discussion of the time scales characterizing the transport of the Brownian tracer. Thereby we identify the small parameter enabling the perturbation analysis. However, we eschew the details of the perturbation analysis and the identification of the macrotransport paradigm. The interested reader is referred to the

work of Pagitsas *et al.* [12].

The microscale conservation equation for the probability density P is embodied in eq. (8.4). For the sake of simplicity we assume the absence of external forces (in both local and global spaces) animating the transport of the Brownian particle. In such a scenario, the constitutive equations for the local and the global space fluxes adopt the following forms [cf. eqs. (8.5) and (8.6)]:

$$\mathbf{J} = \mathbf{U}'(\mathbf{q})P - \mathbf{D}(\mathbf{q}) \cdot \nabla_Q P \tag{8.27}$$

and

$$\mathbf{j} = \mathbf{u}(\mathbf{q})P - \mathbf{d}(\mathbf{q}) \cdot \nabla_q P. \tag{8.28}$$

The implementation of a perturbation analysis is preceded by the nondimensionalization of the equations to thereby identify the small parameter. The global space transport is nondimensionalized by utilizing a characteristic global space diffusivity D, a length scale l_Q and a velocity scale U. Implementing these scalings in eq. (8.27) we obtain,[5]

$$\mathbf{J} = \frac{U}{l_Q}[\mathbf{U}'(\mathbf{q})P - \mathrm{Pe}_Q^{-1}\mathbf{D}(\mathbf{q}) \cdot \nabla_Q P]. \tag{8.29}$$

In the above equation $\mathrm{Pe}_Q \equiv l_Q U/D$ represents the global space Péclet number. An analogous nondimensionalization of the local space fluxes quantified by eq. (8.28) is accomplished using a characteristic diffusivity d, a lengthscale l_q and a velocity scale u to thereby yield

$$\mathbf{j} = \frac{d}{l_q^2}[\mathrm{Pe}_q\mathbf{u}(\mathbf{q})P - \mathbf{d}(\mathbf{q}) \cdot \nabla_q P]. \tag{8.30}$$

In the above equation, the $\mathrm{Pe}_q \equiv l_q u/d$ denotes the local space Péclet number.

[5]To avoid excessive proliferation of symbols we have utilized the same notation to denote both the non-dimensional and the dimensional quantities.

Based on the above nondimensionalizations effected on the global and the local space flux equations, we can identify the presence of atleast four distinct time scales (more timescales could exist in cases where external forces contribute to the convective transport of the Brownian tracer) characterizing the transport of the Brownian tracer. These timescales respectively characterize the local space convective and diffusive transport, and the global space convective and diffusive transport. The presence of four distinct time scales enables the construction of three distinct ratios involving these time scales:

$$\mathrm{Pe}_q = \frac{l_q u}{d} = \frac{\text{Time scale for local space diffusion}}{\text{Time scale for local space convection}} \tag{8.31}$$

$$\mathrm{Pe}_Q = \frac{l_Q U}{D} = \frac{\text{Time scale for global space diffusion}}{\text{Time scale for global space convection}} \tag{8.32}$$

$$\epsilon = \frac{l_q^2 U}{d L_Q} = \frac{\text{Time scale for local space diffusion}}{\text{Time scale for global space convection}} \tag{8.33}$$

The global and local Péclet numbers respectively quantify the ratios of the time scales embodied in the convective and diffusive transports within a subspace. Whereas, the parameter ϵ in eq. (8.33) quantifies the ratio of the timescales of transport in the two different subspaces. As we expounded earlier in this section *we require the Brownian particle to reach equilibrium with respect to transport within the local space at a time much earlier than a comparable event in the global space. Physically, such an expectation would be satisfied under the mathematical requirement that* $\epsilon \ll 1$. Implicit in the delineation of these time scales is the assumption that the global and local Péclet numbers are $\mathcal{O}(1)$ to thereby enable the choice of a single timescale to characterize the transport in each subspace.

The above dual requirements quantify the qualitative statements outlined in the beginning of this section. The identification of the small parameter ϵ also enables the application of a macrotransport description to problems wherein some of our

earlier strict requirements on the boundedness of the respective spaces can fail. For instance, consider the following possible scenarios: (i) Global space is bounded (with a characteristic length scale l_Q) and the local space is bounded (with a characteristic length scale l_q): The macrotransport description is then applicable for the times t satisfying the inequality $l_q^2/d \ll t \ll l_Q/U$ [12]. (ii) Local space is unbounded and the global space is unbounded: The macrotransport description is applicable for the times $t \gg \tau_q$, where τ_q denotes a characteristic time scale for transport in the local space which might arise from other physicochemical constraints present within the local space (see chapter 10). (iii) Finally, when the local space is bounded and global space is unbounded (corresponding to the assumption underlying the majority of the preceding sections of the text): The macrotransport description is applicable for the times $t \gg l_q^2/d$.

This section quantitatively and qualitatively delineates the constraints which need to be necessarily satisfied by the appropriate physical processes to render a macrotransport description accurate. In the subsequent chapters we consider the application of macrotransport theory to two distinct examples to thereby derive the phenomenological macrotransport coefficients present within the macrotransport equation. Such a procedure when coupled with the physical meaning of these macrotransport coefficients furnishes significant insights regarding the coarse-grained transport processes occurring in these systems. The chapters embody a self-contained review of the macrotransport equations and the paradigm governing the particular example under consideration.

References

[1] R.P. Batycky *et al.*, "Internal energy transport in adiabatic systems. Thermal Taylor dispersion phenomena," *Int. J. Non-Linear Mech.* **29**, 639 (1994).

[2] H. Brenner, "Taylor dispersion in systems of sedimenting nonspherical Brownian particles. II. Homogeneous ellipsoidal particles," *J. Colloid Interface Sci.*, **80**, 548 (1981).

[3] H. Brenner, "A general theory of Taylor dispersion phenomena," *PhysicoChem. Hydrodyn.*, **1**, 91 (1990).

[4] H. Brenner and D.A. Edwards, *Macrotransport Processes*, Butterworth-Heinemann, Boston (1993).

[5] M. D. Bryden and H. Brenner, "Multiple-timescale analysis of Taylor dispersion in converging and diverging flows," *J. Fluid Mech.*, **311**, 343 (1996).

[6] S. Chandrasekhar, "Stochastic problems in physics and astronomy," *Rev. Mod. Phys.*, **15**, 1 (1943).

[7] L. H. Dill and H. Brenner, "A general theory of Taylor dispersion phenomena: V. Time-periodic convection," *PhysicoChem. Hydrodyn.*, **3**, 267 (1982).

[8] A. Einstein, *Theory of Brownian Motion*, Dover reprint, New York (1956).

[9] R. Mauri *et al.*, "The dispersion of momentum in periodic suspensions," Unpublished.

[10] P.M. Morse and H. Fesbach, *Methods of Theoretical Physics, Part 1* McGraw-Hill, New York (1953).

[11] A. Nadim and H. Brenner, "Long-time nonpreaveraged diffusion and sedimentation properties of flexible Brownian dumbbells," *PhysicoChem. Hydrodyn.*, **11**, 315 (1989).

[12] M. Pagitsas *et al.*, "Multiple time scale analysis of macrotransport processes," *Physica*, **135A**, 533 (1986).

[13] M. Shapiro and H. Brenner, "Chemically reactive generalized Taylor dispersion phenomena," *AIChe J.*, **33**, 1155 (1987).

[14] G. I. Taylor, "Dispersion of soluble matter in a solvent flowing slowly through a tube," *Proc. R. Soc. London*, **219A**, 186 (1990).

Chapter 9

Chaotic Heat Transfer Enhancement in Rotating Eccentric Cylinder Configuration

Reference: Venkat Ganesan, Michelle Bryden and Howard Brenner, "Chaotic heat transfer enhancement in rotating eccentric annular-flow systems," *Phys. Fluids A*, **9**, 1296 (1997).

This chapter deals with a novel application of the macrotransport paradigm outlined in the previous chapter. Specifically, we explicitly quantify the role of the chaotic advection in the enhancement of transport rates. As an illustrative model system, we consider the transport rate enhancements in an eccentric annular-flow configuration. We quantitatively demonstrate that the presence of chaotic advection leads to a significant enhancement in the heat transport rates. Explicitly, such a procedure is accomplished by utilizing the macrotransport paradigm for reactive thermal dispersion processes. We also contrast our quantitative results with more qualitative, pictorial kinematical measures of transport enhancement to demonstrate some of the shortcomings inherent in these other approaches.

This chapter begins with a brief introduction to the phenomenon of chaotic advection. Subsequent to this discussion, we motivate the application considered in this chapter. In section 9.2 we detail the geometry of the flow situation and the different

illustrative velocity protocols considered in our application. In section 9.3 we briefly discuss the concepts of micro and the macroscale equations (which has been elaborated in the previous chapter) in the specific context of thermal Taylor dispersion theory for time-periodic reactive systems. An analytical solution of the concentric cylinder protocol is presented in section 9.4, and is followed by a brief description of the numerical details pertinent to the other flow situations considered. The results for the concentric cylinder case serve as a 'ground state' for comparison of the results in the other cases. The results obtained for the other flow situations are presented in section 9.5. Overall conclusions are detailed in 9.6.

9.1 Chaotic Advection

Chaotic behavior in simple dynamical systems with area-preserving flows has generated considerable interest in recent years [11, 26]. In this context, laminar chaos (chaotic advection) in simple creeping flows constitutes a current focus of research activity. The existence of chaotic phenomenon in laminar flows seems surprising at first thought. Turbulent flows for example, possess a highly irregular velocity structure, typically defined by its statistics, and are purported (though not proved conclusively) to be a canonical example of a chaotic flow. In view of the typical 'regular' flow structures encountered in laminar flows, the occurrence of the phenomena of chaos (which is qualitatively synonymous with irregular or random) in laminar flows seems like an oxymoron. However, contrary to intuition, laminar chaos refers to *a kinematical phenomena* in which motion of the fluid particles is chaotic (in a Lagrangian sense) even though the velocity field is regular (i.e., nonchaotic). In contrast, 'turbulence' typically refers to the scenario wherein the fluid velocity itself possesses a chaotic or a random structure (Eulerian chaos).

To clarify the above statements consider the Lagrangian equation of motion of a fluid element whose center of mass is instantaneously at the position $\mathbf{x}$:

$$\frac{d\mathbf{x}}{dt} = \mathbf{u}(\mathbf{x}, t), \tag{9.1}$$

where $\mathbf{u}(\mathbf{x}, t)$ refers to the Eulerian velocity field at the position $\mathbf{x}$ and time t. The motion of the fluid elements themselves provide valuable insights into the mixing processes undergone by these material elements. In view of the fact that these mixing processes typically impact on transport rates within a system, the kinematical motion of the fluid elements in turn provides a *qualitative* measure of the transport rates occurring within the system. However, despite this relationship between the Lagrangian motion and the transport rates in the system, previous researches have not explicitly focussed on this quantification. The main reason for such an attitude is the ubiquitous presence of two-dimensional steady laminar flows which constrain the fluid elements to follow the innocuous regular patterns embodied in streamlines. This observation suggests the presence of other nonconvective transport mechanisms, like molecular diffusion, to enable cross-streamline transport and mixing. However, during the past decade, the situation underwent a dramatic change. Simple manipulations of steady flow fields were shown to lead to highly irregular or *chaotic motion of fluid elements, even in laminar flows*, thereby obviating the necessity for other transport mechanisms to enhance mixing of fluid elements [1, 9, 20]. This realization was founded upon the logic that the above equation (9.1), when stripped of its physical meaning, represents a set of ordinary differential equations which can exhibit chaotic phenomena depending on the functional form of the velocity field $\mathbf{u}$ [11, 26]. This suggested that enhancement of transport rates can possibly be achieved by tuning the kinematical features of the flow fields.

The pioneering studies of Aref [1], Ottino [20], and their co-workers, as well as others pointed attention towards the possibility of exploiting the enhanced mixing rates accompanying chaotic flows to increase transport rates in laminar flow systems. Since Lagrangian chaos can be achieved even under Stokes-flow conditions, the enhancement in heat (or mass) transport rates is not generally accompanied by corresponding increases in pressure drop or local shear rate, such as would be the case if turbulent flows were employed to enhance the rate. This makes such chaotic flow phenomena technologically attractive to contemplate — for example in the biotechnology industry, where laminar flows are necessary to minimize cell damage during

growth [13].

Efforts to quantitatively demonstrate the enhanced effectiveness achieved by chaotic mixing have yet to come to complete fruition, primarily because of the lack of simple quantitative measures of global mixing and transport rates in chaotic systems. Applications involving measures of transport rates involve dynamical aspects of chaotic advection through the different time-scales of transport by convective and diffusive mechanisms. Chaos, being purely kinematical in nature, impacts only in the convective aspects of dynamical transport processes, such as heat and mass transfer processes. However, dynamical processes also involve molecular transport, which possesses a time scale distinct from that of convection. (Indeed, at small Péclet numbers, where diffusive or conductive molecular transport dominates over convection, chaotic effects on global transport rates may be minimal.) Accordingly, in dynamical applications, calculations of Liapunov exponents, attractor dimensions, and Poincaré plots rarely provide more than a qualitative kinematical, and often asymptotic, description of the pertinent 'mixing' phenomena. (This limitation is corroborated *inter alia* by our results, which indicate that the observed values of the effective or global transport coefficients do not always manifest the same parametric trends as do the corresponding Poincaré plots.)

Several earlier studies do address quantitative aspects of the chaotic enhancement. Thus, Jana and Ottino [14] considered heat transfer in cavity flow and found significant enhancement within the chaotic flow regime. Closer to our own study, Ghosh *et al.* [10] investigated heat transfer between two nonconcentric counter-rotating cylinders when the cylinders were maintained at different temperatures. Their work, which was restricted to small eccentricities with no axial flow, confirmed the existence of significantly enhanced transport rates.

Most analyses performed to date have restricted themselves to two-dimensional, purely transverse flows, ignoring axial transport phenomena. While this may be acceptable in the context of verifying the existence of chaotic enhancement, it does not provide a good model of real continuous flow heat-exchanger performance. In contrast, the analysis of Bryden & Brenner [8] provides a quantitative measure of

mixing and transport in such systems, while also including axial flow. Their work considers transverse transport and axial flow accompanied by molecular diffusion during creeping flow in the annular space between two eccentrically-positioned circular cylinders which rotate alternately and periodically in the presence of an infinitely fast surface chemical reaction occurring on the outer cylinder. Our work differs from theirs primarily in the fact that their calculations were restricted to the limiting case where (in our heat transfer terminology) the local heat transfer coefficient h is effectively infinite. In contrast, we study here the effects of *finite* Nusselt numbers (which introduces another time scale of transport) upon the chaotic heat transfer, in addition to other related topics like co- vs counter-rotation, not systematically covered in their investigation.

The present work utilizes time-periodic thermal Taylor dispersion theory [4] together with the model of a prescribed microscale heat transfer coefficient h at the outer cylinder surface to determine the effective (macroscale) heat transfer coefficient $\bar{H}^*$ for the case of axial annular flow between non-concentric alternately rotating circular cylinders. This flow configuration is widely used to study Lagrangian chaos, partly because of the availability of an analytical solution for the transverse velocity field (in the Stokes-flow approximation) [3, 15], and partly because of the possibility of experimental verification of the calculated behavior [17, 25].

While methods like Melnikov theory [10], lobe dynamics [16], etc. do provide a quantitative measure of chaotic mixing, they are valid only for small time-dependent perturbations (or slow perturbations [16]) of the steady flow field. In contrast, our methods can be used for any arbitrary time-periodic flow fields. Moreover, the inclusion of an axial flow field adds to the applicability of both our specific results and general techniques to problems of potential industrial interest. The novelty of our generalized Taylor dispersion scheme [7] for calculating the effective macroscale system parameters from the prescribed microscale data lies in the fact that it obviates the need to solve the full three-dimensional energy equation for the microscale temperature field $T(\mathbf{q}, z, t)$ governing the heat transfer process. Rather, only a pair of two-dimensional equations [which are remarkably alike in structure – cf. eqs. (9.20a,b)]

need to be solved to obtain the macroscale transport coefficients. These coefficients serve to quantify the overall heat transfer process after an initial transient phase. The non-asymptotic transport processes occurring during this initial phase are incorporated into the macrotransport description through the use of a fictitious initial condition [represented by the field $A(\mathbf{q}, t)$ — cf. eq. (9.11)].

Three different classes of annular rotary flow fields are considered in our work to illustrate the modes of chaotic enhancement, as well as to demonstrate the general applicability of our methods in such disparate cases: (i) In the first case considered the cylinders are concentric, whence the transport is unaffected by the rotary transverse flow field; (ii) The second case is that of non-concentric counter-rotating cylinders in steady rotation, for which case only *regular* enhancement (over and above that of the concentric case) is present as a consequence of the transverse flow; (iii) Finally, the cases of time-periodic counter- and co-rotating flows are considered for the eccentrically-positioned configuration. In each case, the calculated relationship between the local (h) and overall ($\bar{H}^*$) heat transfer coefficients furnishes a quantitative global measure of the effectiveness of the transverse convective fluid motion ('mixing') in enhancing the overall rate of heat transfer from the system. Additionally, the resulting axial thermal Taylor dispersivities $\bar{\alpha}_T^*$ are calculated for each case to provide further data on the effectiveness of the kinematical mixing processes occurring in the annulus. Whereas convection transports energy over large distances, conduction involves processes occurring at the molecular scale. As such, the Taylor dispersivity provides information regarding the interplay between these different energy transport modes. The axial thermal velocity $\bar{U}^*$ displays qualitatively the same behavior as that of the axial thermal dispersivity due to similar controlling factors; accordingly, in the interests of brevity, the results obtained for this velocity are not explicitly presented here.

9.2 Geometry of Flow

As in Fig. (9-1), consider an infinitely long circular cylinder of radius R_i positioned eccentrically within a second cylinder of radius R_o, with e the center-to-center distance. Cylindrical bipolar coordinates [12] (η,ξ) are used in the subsequent analysis. A point within the annular space between the two cylinders is denoted by $(\mathbf{q}, z)$, with z the axial position and $\mathbf{q} \equiv \mathbf{q}(\eta, \xi)$ the transverse position vector in a plane perpendicular to the z axis. With these geometrical identifications the identification of the local and the global space coordinates becomes explicit. In the parlance of macrotransport theory outlined in the preceding chapter, the bounded cross sectional space identified by the cylindrical bipolar coordinates constitutes the local space, while the orthogonal unbounded space represented by the axial or the z coordinates constitute the global space.

When the cylinders are counter-rotated in a regular (i.e. steady, time-independent) manner the heat transfer rate is increased, over and above the pure conduction rate that would otherwise exist, due to the creation of a recirculation region in the annular gap (see Fig. (9-2c). The latter arises from a hyperbolic saddle point stemming from the intersection of two streamlines. This recirculation region produces *regular mixing* owing to reduction of the temperature gradient within the recirculation region. (Indeed, to a good approximation the temperature can be considered uniform within that region [10].) Outside of this recirculation region, conduction zones exist in which the heat transfer occurs primarily by molecular transport.

On the other hand, when the cylinders are rotated in a time-periodic manner, chaotic mixing occurs — allowing a material particle to be transported across the bounding streamlines of the recirculation region. Time-periodicity of the flow in our analysis is achieved by counter-rotating the inner and outer cylinders alternately for the same period $\mathcal{J}_a$ (the latter denoting the actual period of rotation, in contrast to the dimensionless period $\mathcal{J}$ defined later), albeit at generally different angular velocities Ω_i and Ω_o. The instantaneous quasisteady transverse velocity field thereby

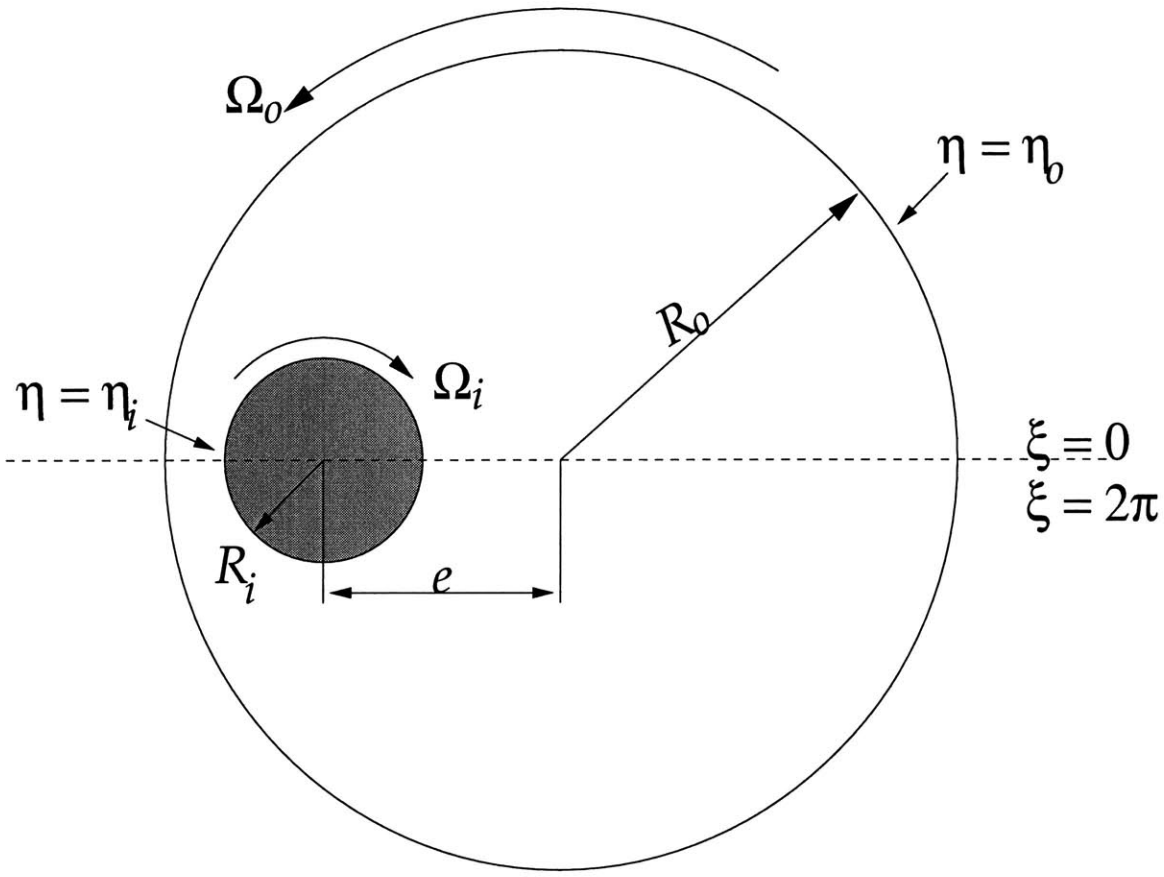

Figure 9-1: Geometry of the system. The axial coordinate z is directed into the plane of paper. The scalars Ω_o and Ω_i are each taken to be positive when the cylinders rotate in the directions indicated by the arrows.

generated is given by the expression :

$$\mathbf{u}(\mathbf{q},t) = \begin{cases} \mathbf{u}_i(\mathbf{q}), & 2n\mathcal{J}_a < t < (2n+1)\mathcal{J}_a, \\ \mathbf{u}_o(\mathbf{q}), & (2n+1)\mathcal{J}_a < t < (2n+2)\mathcal{J}_a, \end{cases} \tag{9.2}$$

$(n = 0, 1, 2, ...)$, where $\mathbf{u}_i$ and $\mathbf{u}_o$ represent the respective quasisteady transverse Stokes-flow velocity fields (expressed in bipolar coordinates [3]), resulting from rotation of the inner and outer cylinders. The Stokes-flow assumption is valid provided that the transverse Reynolds number $\mathrm{Re} = R_o^2\Omega/\nu$ is less than unity [22], with ν the kinematic viscosity and $\Omega = \max(\Omega_i, \Omega_o)$. Additionally, the quasisteady flow assumption is justified so long as the modulation period $\mathcal{J}_a$ is large compared with that of the viscous time scale, L^2/ν (i.e. the Strouhal number satisfies the inequality, $\mathrm{Sr} \equiv L^2/\nu\mathcal{J}_a \ll 1$), where L is a characteristic transverse length, say $R_o - R_i$. For regular mixing [case(ii)], the steady velocity field is given by[1]

$$\mathbf{u}(\mathbf{q}) = \frac{1}{2}\left[\mathbf{u}_i(\mathbf{q}) + \mathbf{u}_o(\mathbf{q})\right]. \tag{9.3}$$

Superposed on the above transverse field is a steady axial laminar velocity field $U(\mathbf{q})$ in the z direction. Expressions for this annular Poiseuille-like bipolar-coordinate field are given by Snyder and Goldstein [24] among others [21].

9.3 Macrotransport Equations

9.3.1 Microscale Equation

The temperature field $T(\mathbf{q}, z, t)$ is governed by the three-dimensional energy equation,

$$\rho C_p\left[\frac{\partial T}{\partial t} + U(\mathbf{q})\frac{\partial T}{\partial z} + \mathbf{u}(\mathbf{q},t)\cdot\nabla_q T\right] - k_T\left(\frac{\partial^2 T}{\partial z^2} + \nabla_q^2 T\right) = 0, \tag{9.4}$$

[1]We are grateful to one of the anonymous referees of our article for pointing out that a factor of 2 was necessary in the velocity field expression eq. (9.3) in order that the distance traversed by the cylinders in a period in the steady rotation case be identical to that for the time-periodic case.

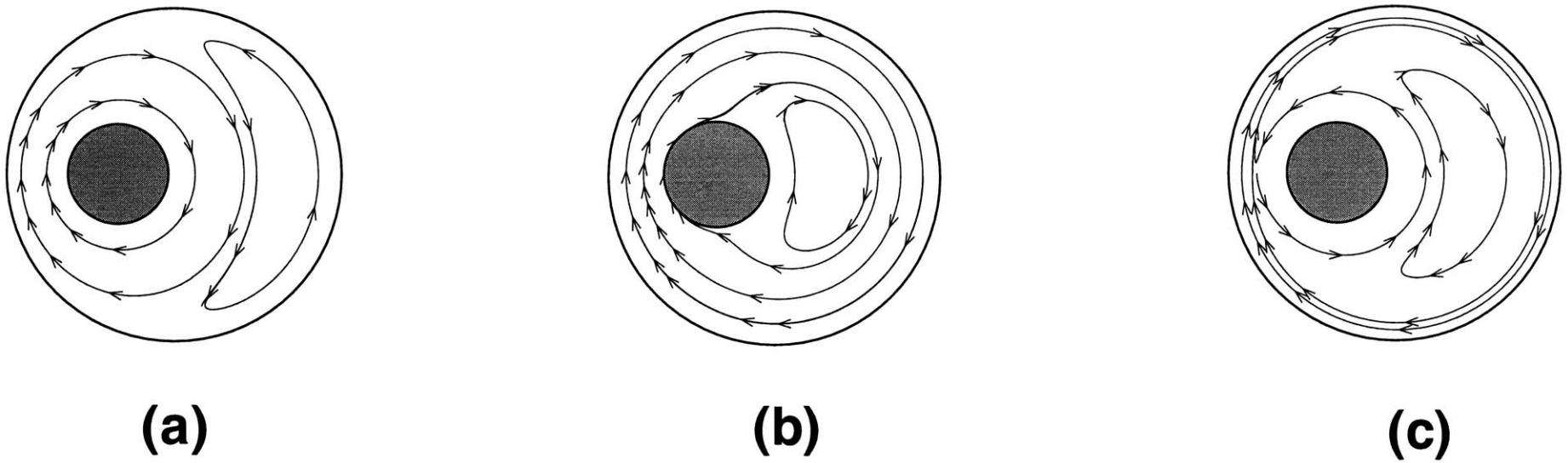

Figure 9-2: Typical transverse streamline profiles: (a) Inner cylinder alone rotates; (b) Outer cylinder alone rotates; (c) Steady counter-rotation of both cylinders (for $\Omega_i/\Omega_o = 6$)

satisfying the boundary conditions

$$k_T \mathbf{n} \cdot \nabla_q T + hT = 0 \qquad \text{on} \quad \partial q_o, \tag{9.5}$$

$$k_T \mathbf{n} \cdot \nabla_q T = 0 \qquad \text{on} \quad \partial q_i, \tag{9.6}$$

and subject to the arbitrarily prescribed initial temperature distribution

$$T(\mathbf{q}, z, 0) = T_o(\mathbf{q}, z). \tag{9.7}$$

To make explicit connection with the macrotransport concepts outlined in the previous chapter, the global (z) and the local ($\mathbf{q}$) transport variables have been separated in the above equations. In the above, $\nabla_q \equiv \partial/\partial\mathbf{q}$ denotes the transverse gradient operator, while ∂q_i and ∂q_o respectively denote the surfaces of the inner and outer cylinders, and $\mathbf{n}$ is the unit outer normal to a cylinder. In eq. (9.5) the heat is assumed transferred to an external ambient environment maintained at temperature $T = 0$. In the initial condition, eq. (9.7), it is supposed that $T_o(\mathbf{q}, \pm\infty) = 0$.

The Taylor macrotransport paradigm for reactive, time-periodic systems [7] will be used in the subsequent analysis to obtain the effective transport coefficients. In the case of thermal transport, a comparable nonmaterial tracer (designated a 'thermion' [4, 7]) is imagined to exist, and a micro/macro axial moment-matching scheme employed to calculate the transport coefficients appearing in the macrotransport equation,

$$\frac{\partial\langle\bar{T}\rangle}{\partial t} + \bar{U}^* \frac{\partial\langle\bar{T}\rangle}{\partial z} + \bar{H}^* \langle\bar{T}\rangle = \bar{\alpha}_T^* \frac{\partial^2\langle\bar{T}\rangle}{\partial z^2}, \tag{9.8}$$

governing the area- and time-averaged mean temperature field, $\langle\bar{T}\rangle(z,t)$ [cf. eqs. (9.12) and (9.13) for the respective definitions of these averages]. The three macrotransport coefficients $\bar{U}^*$, $\bar{H}^*$ and $\bar{\alpha}_T^*$ appearing above respectively denote the mean axial velocity at which heat is conveyed down the tube, the effective heat transfer loss coefficient,

and the effective axial thermal diffusivity — the latter being equivalent to $\bar{k}_T^*/\rho C_p$, with $\bar{k}_T^*$ the effective axial thermal conductivity and ρC_p taken to be constant.

Denote by $\rho C_p P(\mathbf{q}, z, t \,|\, \mathbf{q}', z', t')$ the conditional probability density for finding a thermion at position $(\mathbf{q}, z)$ at time t, given that it was introduced into the system at position $(\mathbf{q}', z')$ at time $t = t'$. Given the equality [18] between this probability density and the Green's function for the system of equations (9.4)-(9.7), we have that

$$T(\mathbf{q}, z, t) - T_r = \int_{V'_\infty} \rho C_p P(\, \mathbf{q}, z, t, |\mathbf{q}', z', t')[T(\mathbf{q}', z', t') - T_r] dV', \qquad (9.9)$$

where T_r is an arbitrary reference temperature and $dV \equiv d\mathbf{q}dz$ denotes a volume element of the annular space, with $d\mathbf{q}$ an areal element in the annular cross-sectional space. The domain of integration V'_∞ represents the infinite annular space, $(-\infty < z' < \infty,\ 0 \leq \xi' \leq 2\pi,\ \eta_o < \eta' < \eta_i)$.

The Green's function P constitutes the solution of a three-dimensional energy equation identical to (9.4), in which P now appears in place of T and in which an instantaneous unit heat source term, $\delta(z - z')\delta(\mathbf{q} - \mathbf{q}')\delta(t - t')$ with δ the Dirac delta function [equivalent to the introduction of a thermion into the system at $(\mathbf{q}', z', t')$], now appears on the right-hand side of (9.4) [also cf. eq. (8.4)]. Additionally, P satisfies boundary conditions identical to (9.5) and (9.6) in which T is replaced by P. Moreover, P satisfies the boundedness condition

$$|z - z'|^m P \longrightarrow 0 \qquad \text{as} \qquad z - z' \longrightarrow \pm\infty, \qquad (9.10)$$

the latter assuring convergence of the axial moments of P at all orders (required in the implicit micro/macro moment matching scheme [7]) [The above equation is equivalent to our abstract, general equation (8.9) wherein we have replaced $\mathbf{Q}$ by $z - z'$].

9.3.2 Macrotransport Formulation

By a moment-matching scheme [7, 5], for long times times t satisfying the inequality[2] $t \gg R_o^2/\alpha(\alpha = k_T/\rho C_p)$ the following macrotransport description of the mean transport process applies

$$\frac{\partial\langle\bar{P}\rangle}{\partial t} + \bar{U}^*\frac{\partial\langle\bar{P}\rangle}{\partial z} + \bar{H}^*\langle\bar{P}\rangle - \bar{\alpha}_T^*\frac{\partial^2\langle\bar{P}\rangle}{\partial z^2} = A(\mathbf{q}', t')\delta(z - z')\delta(t - t'). \tag{9.11}$$

The field $A(\mathbf{q}', t')$ appearing in the above equations [and explicitly defined in eqs. (9.20a,b)-(9.24a,b)] represents a 'fictitious' initial condition. Its presence takes account of the transport and concomitant heat loss from the system occurring at short times, $t \leq \mathcal{O}(R_o^2/\alpha)$, to which the asymptotic macrotransport equation (9.11) [as well as (9.8)] is inapplicable. This new feature contrasts with the paradigm pertaining to the nonreactive solutes outlined in the prior chapter. As a result of this new feature, the definition of the macrotransport coefficients explicitly include this ficticious initial condition [cf. eqns. (9.15) - (9.19)]. [For simplicity, in defining $\langle\bar{P}\rangle$ appearing in eq. (9.11), the factor ρC_p, which is assumed constant, has been combined with P, and the resulting product $\rho C_p P$ denoted here and henceforth by P as in the case of material tracers.] In the above we have used both areal and time averaging, with the respective averages defined as

$$\bar{g}(z, t) = \int_{S_q} d\mathbf{q}\, g(\mathbf{q}, z, t) \tag{9.12}$$

and

$$\langle g\rangle(\mathbf{q}, z, t) = \frac{1}{2\mathcal{J}_a}\int_t^{t+2\mathcal{J}_a} dt\, g(\mathbf{q}, z, t). \tag{9.13}$$

[2]Refer section (8.5) for a justification of the constraints on the timescales.

In the preceding, S_q denotes the areal annular domain ($0 \leq \xi \leq 2\pi,\ \eta_o < \eta < \eta_i$). Condition (9.10), requiring boundedness of the axial moments, here necessitates that

$$|z - z'|^m \langle \bar{P} \rangle \longrightarrow 0 \qquad \text{as} \qquad z - z' \longrightarrow \pm\infty. \tag{9.14}$$

In the subsequent analysis it will prove convenient to introduce the following nondimensional variables:

$$\tau = \frac{t\alpha}{R_o^2}, \quad \hat{\mathbf{q}} = \frac{\mathbf{q}}{R_o}, \quad \mathrm{Pe}_q = \frac{\bar{u}R_o}{\alpha}, \quad \mathrm{Pe}_z = \frac{\bar{V}R_o}{\alpha}, \quad \hat{\mathbf{u}} = \frac{\mathbf{u}}{\bar{\mathbf{u}}}, \quad \hat{U} = \frac{U}{\bar{V}}, \quad \varepsilon = \frac{e}{R_o - R_i},$$

$$\hat{\bar{U}}^* = \frac{\bar{U}^*}{\bar{V}}, \quad \hat{P}_o^\infty = P_o^\infty R_o^2, \quad \hat{A} = AR_o^2, \quad \hat{\nabla}_q = R_o \nabla_q, \quad \mathrm{Nu} = \frac{hR_o}{k_T}.$$

In the above,

$$\bar{u} = \Omega_o R_o,$$

$$\bar{V} = \frac{\int_{S_q} U(\mathbf{q}) d\mathbf{q}}{\int_{S_q} d\mathbf{q}}$$

and

$$\mathcal{J} = \mathcal{J}_a R_o^2/\alpha,$$

respectively denote the tangential speed of the outer cylinder, the average axial *fluid* velocity, and the nondimensional period of rotation. Pe_z and Pe_q respectively denote the axial and transverse Péclet numbers, and P_o^∞ denotes the long-time asymptotic zeroth-order axial moment of P [7] [also cf. eqs. (8.21) - (8.24)]. Additionally, $\int_{S_q} d\mathbf{q} = \pi(R_o^2 - R_i^2)$ denotes the cross-sectional annular area.

In terms of the above variables the corresponding nondimensional macrotransport coefficients appearing in eqs. (9.8) and (9.11) are to be computed as follows:

$$\frac{R_o}{\alpha}\bar{U}^* = \frac{\mathrm{Pe}_z}{2\mathcal{J}} \int_0^{2\mathcal{J}} d\tau \int_{S_q} d\hat{\mathbf{q}}\, \hat{U}(\hat{\mathbf{q}}) \hat{P}_o^\infty(\hat{\mathbf{q}}, \tau) \hat{A}(\hat{\mathbf{q}}, \tau), \tag{9.15}$$

$$\frac{\bar{H}^* R_o^2}{\alpha} = \mathcal{H} \tag{9.16}$$

and

$$\frac{\bar{\alpha}_T^*}{\alpha} = \frac{\bar{\alpha}_c^*}{\alpha} + 1, \tag{9.17}$$

wherein

$$\frac{\bar{\alpha}_c^*}{\alpha} = \frac{\mathrm{Pe}_z^2}{2\mathcal{J}} \int_0^{2\mathcal{J}} d\tau \int_{S_q} d\hat{\mathbf{q}}\, \hat{P}_o^\infty(\hat{\mathbf{q}},\tau)\hat{A}(\hat{\mathbf{q}},\tau)\hat{B}(\hat{\mathbf{q}},\tau)[\hat{U}(\hat{\mathbf{q}}) - \hat{\bar{U}}^*] \tag{9.18}$$

or, equivalently,

$$\frac{\bar{\alpha}_c^*}{\alpha} = \frac{\mathrm{Pe}_z^2}{2\mathcal{J}} \int_0^{2\mathcal{J}} d\tau \int_{S_q} d\hat{\mathbf{q}}\, \hat{P}_o^\infty(\hat{\mathbf{q}},\tau)\hat{A}(\hat{\mathbf{q}},\tau)\hat{\nabla}_q\hat{B}\cdot\hat{\nabla}_q\hat{B}. \tag{9.19}$$

The $\bar{\alpha}_c^*$ term represents the convective or Taylor contribution to the effective thermal dispersivity.

The $\hat{P}_o^\infty$ and $\hat{A}$ fields appearing in the above equations respectively represent the solutions of the following adjoint pair of eigenvalue problems, with $\mathcal{H}$ the corresponding eigenvalue [7, 5] common to the pair:

$$\left(\frac{\partial}{\partial\tau} + \mathrm{Pe}_q\hat{\mathbf{u}}\cdot\hat{\nabla}_q\right)\left\{\hat{P}_o^\infty,\hat{A}\right\} + \left(\hat{\nabla}_q^2 + \mathcal{H}\right)\left\{-\hat{P}_o^\infty,\hat{A}\right\} = 0, \tag{9.20a,b}$$

$$\left(\mathbf{n}\cdot\hat{\nabla}_q + \mathrm{Nu}\right)\left\{\hat{P}_o^\infty,\hat{A}\right\} = 0 \quad \text{on} \quad \partial q_o, \tag{9.21a,b}$$

$$\left(\mathbf{n}\cdot\hat{\nabla}_q\right)\left\{\hat{P}_o^\infty,\hat{A}\right\} = 0 \quad \text{on} \quad \partial q_i, \tag{9.22a,b}$$

$$\left\{\hat{P}_o^\infty,\hat{A}\right\}(\hat{\mathbf{q}},\tau+2\mathcal{J}) = \left\{\hat{P}_o^\infty,\hat{A}\right\}(\hat{\mathbf{q}},\tau), \tag{9.23a,b}$$

$$\frac{1}{2\mathcal{J}}\int_\tau^{\tau+2\mathcal{J}} d\tau \int_{S_q} d\hat{\mathbf{q}}\hat{P}_o^\infty\left\{1,\hat{A}\right\} = 1. \tag{9.24a,b}$$

The product field $\hat{P}_o^{\infty}\hat{B}$ required in (9.18) represents the solution of the inhomogeneous equation

$$\frac{\partial(\hat{P}_o^{\infty}\hat{B})}{\partial\tau} + \mathrm{Pe}_q\hat{\mathbf{u}}\cdot\hat{\nabla}_q(\hat{P}_o^{\infty}\hat{B}) - \hat{\nabla}_q^2(\hat{P}_o^{\infty}\hat{B}) - \mathcal{H}(\hat{P}_o^{\infty}\hat{B}) = \hat{P}_o^{\infty}(\hat{U} - \hat{\bar{U}}^*), \tag{9.25}$$

satisfying boundary and periodicity conditions identical to (9.21a,b) - (9.23a,b). Note that this field is uniquely determined only to within an arbitrary additive, position-independent, time-periodic function [7].

When the transverse velocity field is steady, the time derivatives appearing in (9.20a,b), and (9.25) drop out in the long-time limit.

9.4 Analysis of Different Protocols

9.4.1 Case (i) Concentric Cylinders ($\varepsilon = 0$)

We use cylindrical polar coordinates (r, θ) for this special case. Symmetry considerations dictate that the $\hat{P}_o^{\infty}$, $\hat{A}$ and $\hat{B}$ fields all be independent of the angular coordinate θ. Since the local velocity field is of the tangential form $\hat{\mathbf{u}} = u(r)\hat{\boldsymbol{\theta}}$, with $\hat{\boldsymbol{\theta}}$ a unit vector in the θ direction, the transverse convective contributions to the transport equations governing these fields vanish identically. For this same reason, these fields are also necessarily independent of time.

The equation (in non-dimensional form) for $\hat{P}_o^{\infty}(r)$ becomes

$$\frac{1}{r}\frac{d}{dr}(r\frac{d\hat{P}_o^{\infty}}{dr}) + \mathcal{H}\hat{P}_o^{\infty} = 0, \tag{9.26}$$

subject to the boundary conditions

$$\frac{d\hat{P}_o^{\infty}}{dr} + \mathrm{Nu}\hat{P}_o^{\infty} = 0 \quad \text{on} \quad r = 1, \tag{9.27}$$

$$\frac{d\hat{P}_o^{\infty}}{dr} = 0 \quad \text{on} \quad r = k, \tag{9.28}$$

with $k = R_i/R_o$, and where r has been rendered dimensionless with R_o. The general solution of eq. (9.26) in the annular space $k < r < 1$ simultaneously satisfying the boundary condition (9.28) on the inner wall is

$$\hat{P}_o^{\infty} = C_1\Big[J_0(r\sqrt{\mathcal{H}}) - \frac{J_1(k\sqrt{\mathcal{H}})}{Y_1(k\sqrt{\mathcal{H}})}Y_0(r\sqrt{\mathcal{H}})\Big], \tag{9.29}$$

with J_0 and Y_0 Bessel functions of order zero. Equation (9.27) thereby furnishes the following transcendental equation for the eigenvalue $\mathcal{H}$:

$$J_1(k\sqrt{\mathcal{H}})[\sqrt{\mathcal{H}}Y_1(\sqrt{\mathcal{H}}) - \mathrm{Nu}Y_0(\sqrt{\mathcal{H}})] = Y_1(k\sqrt{\mathcal{H}})[\sqrt{\mathcal{H}}J_1(\sqrt{\mathcal{H}}) - \mathrm{Nu}J_0(\sqrt{\mathcal{H}})]. \tag{9.30}$$

The $\bar{H}^*$ value calculated via (9.16) from the eigenvalue $\mathcal{H}$ above will be denoted as $\bar{H}_o^*$ in subsequent discussions.

The equations governing $\hat{A}(r)$ are identical to those for $\hat{P}_o^{\infty}$, whence we obtain a solution for $\hat{A}$ identical in form to (9.29) in which a new constant, E_1, appears in place of C_1.

The constants E_1 and C_1 are to be determined by use of the pair of normalization conditions (9.24a,b). Since only the product $\hat{P}_o^{\infty}\hat{A}$ is needed in subsequent applications, rather than $\hat{P}_o^{\infty}$ and $\hat{A}$ separately, it suffices to determine only the product E_1C_1. Using (9.24a,bb) we thereby obtain for this product

$$\begin{aligned}(E_1C_1)^{-1} =& \pi\Big\{r^2(J_0^2(r\sqrt{\mathcal{H}}) + J_1^2(r\sqrt{\mathcal{H}}) + \Lambda^2\Big[Y_0^2(r\sqrt{\mathcal{H}}) + Y_1^2(r\sqrt{\mathcal{H}}) \\ & - 2\Lambda(J_1(r\sqrt{\mathcal{H}})Y_1(r\sqrt{\mathcal{H}}) + J_0(r\sqrt{\mathcal{H}})Y_0(r\sqrt{\mathcal{H}}))\Big]\Big\}_k^1,\end{aligned} \tag{9.31}$$

wherein $\Lambda = J_1(k\sqrt{\mathcal{H}})/Y_1(k\sqrt{\mathcal{H}})$. The non-dimensional axial thermal velocity $\hat{\bar{U}}^*$

may be obtained from the expression

$$\hat{\bar{U}}^* = 2\pi \int_k^1 \hat{U}(r)\hat{P}_o^{\infty}(r)\hat{A}(r)rdr, \tag{9.32}$$

where for axial concentric annular Poiseuille flow the nondimensional velocity field reads: [6]

$$\hat{U}(r) = 2\left[1 - r^2 + \frac{(1-k^2)}{\ln(1/k)}\ln r\right] \Big/ \left[\frac{1-k^4}{1-k^2} - \frac{1-k^2}{\ln(1/k)}\right]. \tag{9.33}$$

In the present case eq. (9.25), together with the specified boundary and initial conditions governing the product field $\hat{P}_o^{\infty}\hat{B}$ in conjunction with (9.26) - (9.27) governing $\hat{P}_o^{\infty}(r)$, furnishes the following differential equation and pair of boundary conditions governing the $\hat{B}(r)$ field:

$$\frac{d^2\hat{B}}{dr^2} + \left(\frac{2}{\hat{P}_o^{\infty}}\frac{d\hat{P}_o^{\infty}}{dr} + \frac{1}{r}\right)\frac{d\hat{B}}{dr} = \hat{U} - \hat{\bar{U}}^*, \tag{9.34}$$

$$\frac{d\hat{B}}{dr} = 0 \quad \text{on} \quad r = 1 \text{ and } k. \tag{9.35a,b}$$

Here, $\hat{B}$ is uniquely determined only to within an arbitrary additive constant. A first integration of (9.34) with the help of the integrating factor $(\hat{P}_o^{\infty})^2 r$ followed by the use of (9.19) thereby yields

$$\frac{\bar{\alpha}_c^*}{\alpha} = 2\pi \int_k^1 \frac{dr}{r\hat{P}_o^{\infty}\hat{A}}\left[\int_k^r (\hat{U} - \hat{\bar{U}}^*)\hat{P}_o^{\infty}\hat{A}rdr\right]^2. \tag{9.36}$$

Except for the required quadratures, we have now effected the calculation of $\bar{H}_o^*$, $\hat{\bar{U}}^*$ and $\bar{\alpha}_c^*$ for the concentric cylinder case. [The $\bar{\alpha}_c^*$ value calculated above for the Nu = 0 case will be denoted in what follows as $(\bar{\alpha}_c^*)_o$.]

9.4.2 Case (ii) Steady Transverse Flow Field in a Nonconcentric Annulus

For the case of a steady transverse flow field $\hat{\mathbf{u}}$ imposed on the eccentrically-positioned cylinders the time derivatives disappear from (9.20a,b) and (9.25).

In cylindrical bipolar coordinates [12] (η, ξ) [Fig. (9-1)] the transverse velocity field $\hat{\mathbf{u}}(\eta, \xi)$ is given by the superposition of the respective velocity fields arising when each cylinder is rotated separately, whence

$$\hat{\mathbf{u}}(\eta, \xi) = \frac{1}{2}\left[\hat{\mathbf{u}}_i(\eta, \xi) + \hat{\mathbf{u}}_o(\eta, \xi)\right], \tag{9.37}$$

as in eq. (9.3). Streamline plots for this case are shown in Fig. (9-2c). A matched asymptotic analysis of $\hat{P}_o^{\infty}$ [physically equivalent to the temperature field $T(\mathbf{q}, t)$] for this steady-state case, with 'isothermal' wall boundary conditions appearing in place of (9.5) and (9.6) (and no axial flow) was performed by Ghosh *et al.* [10] for small eccentricities. Since one of our aims was to demonstrate the applicability of generalized Taylor dispersion theory [7] over a wide range of operating conditions, we solved the steady-state version of the system of equations (9.20a,b) - (9.25) numerically for an extensive parametric range (details being outlined in the next section). The $\hat{P}_o^{\infty}$, $\hat{A}$ and $\hat{B}$ fields thereby obtained were used to evaluate the three macrotransport coefficients. [An attempt to carry out a 'domain perturbation' expansion in ε so as to obtain some analytical results led to the recognition that the first-order correction to $\mathcal{H}$ is of $O(\varepsilon^2)$.]

9.4.3 Case (iii) Time-Periodic Flow Field in a Nonconcentric Annulus

Transport enhancement due to chaotic advection is expected in circumstances for which a time-periodic flow field is imposed in the form of alternate rotation of the cylinders, as in eq. (9.2). Due to the time-periodic modulation, the streamlines shift at the end of each period. As such, the streamlines at two successive instants of

time, immediately preceding and following the switchover from inner/outer cylinder rotation, appear to cross [Figs. (9-2a) and (9-2b)]. This constitutes one of the necessary conditions for a flow to produce a 'horseshoe map' [20]. It has been proposed [19] that the use of any wave form for the modulation would qualitatively produce the same effect, so long as the area under the angular speed vs time curve (i.e. the angular displacement) was the same. We concern ourselves here with the simplest configuration, namely the square-wave form. The transverse velocity field for this case is given by eq. (9.2) with $\hat{\mathbf{q}} \equiv (\eta, \xi)$. The equations governing $\hat{P}_o^\infty$, $\hat{A}$ and $\hat{B}$ are as set forth in (9.20a,b) - (9.25). A Melnikov analysis for the case of *continuous* time-periodic modulation has previously been carried out [10] for small eccentricities and large angular speeds. The latter work was important *inter alia* in establishing the existence of an optimal rotation period that maximized the heat transfer rate. However, such methods are necessarily highly restricted with respect to the parameter ranges that can be investigated. A semi-numerical analysis of this protocol was carried out by Atobe and Funakoshi [2]. These authors assumed that the area of the chaotic region (calculated numerically) could be directly correlated with the degree of transport enhancement. However, as shown by Bryden & Brenner [8] (as well as in the present work), this general assumption is not universally borne out by the facts.

A numerical solution of the above equations was effected using an implicit elliptic scheme with a finite-difference (centered-difference) mesh for the spatial coordinates and a backward Euler scheme for the temporal domain. $\hat{P}_o^\infty$ was transformed into a new variable p_o^∞ via the definition

$$p_o^\infty = \hat{P}_o^\infty \exp(-\mathcal{H}\tau) \tag{9.38}$$

in order to solve for the eigenvalue $\mathcal{H}$ of the problem from the equations governing $\hat{P}_o^\infty$. Thereby, eq. (9.20a,b) became

$$\frac{\partial p_o^\infty}{\partial t} + \mathrm{Pe}_q \hat{\mathbf{u}} \cdot \hat{\nabla}_q p_o^\infty - \hat{\nabla}_q^2 \, p_o^\infty = 0, \tag{9.39}$$

with a similar transformation applied to the $\hat{A}$ field in eq. (9.20a,b), namely $a =$

$\hat{A}\exp(\mathcal{H}\tau)$. The system of equations governing p_o^∞ and a were then solved with ever-increasing accuracy until convergence of the three macrotransport coefficients was secured, with the $\mathcal{H}$ value obtained from the expression

$$\mathcal{H} = \frac{1}{2\mathcal{J}} \ln \left[\frac{p_o^\infty(t+2\mathcal{J})}{p_o^\infty(t)} \right]. \tag{9.40}$$

In particular, it was found unnecessary to go beyond a 50×60 mesh in (η, ξ) coordinates. Large Péclet numbers, Pe_q, posed no apparent problems. Calculations were performed on a SUN Sparc 5 machine.

In addition to performing calculations for the counter-rotating case, we also obtained results for the comparable co-rotating case. As subsequently discussed, comparison between the two furnished useful insights into the limitations of qualitative methods like Poincaré maps for understanding chaotic enhancement phenomena.

9.5 Results and Discussion

9.5.1 Heat Transfer Coefficient

Energy transfer from the fluid to the environment involves two serially consecutive transport processes, namely heat transfer through the annular fluid to the wall and subsequently from the wall to the surroundings. As such, the global heat transfer coefficient necessarily embodies contributions representative of both transport mechanisms. Thus, the value of the effective heat transfer coefficient $\bar{H}^*$ increases with Nusselt number for small Nu, for which circumstances heat transfer from the wall to the surroundings constitutes the rate-limiting step. Eventually, an asymptotic value is attained at large Nu, for which circumstances transport of heat to the wall through the fluid becomes the limiting mechanism.

Figure (9-3) depicts the variation with both modulation period $\mathcal{J}$ and Nusselt number Nu of the normalized global heat transfer coefficient $\bar{H}^*/\bar{H}_o^*$, where $\bar{H}_o^*$ represents the heat transfer coefficient calculated for the case of concentric cylinders in

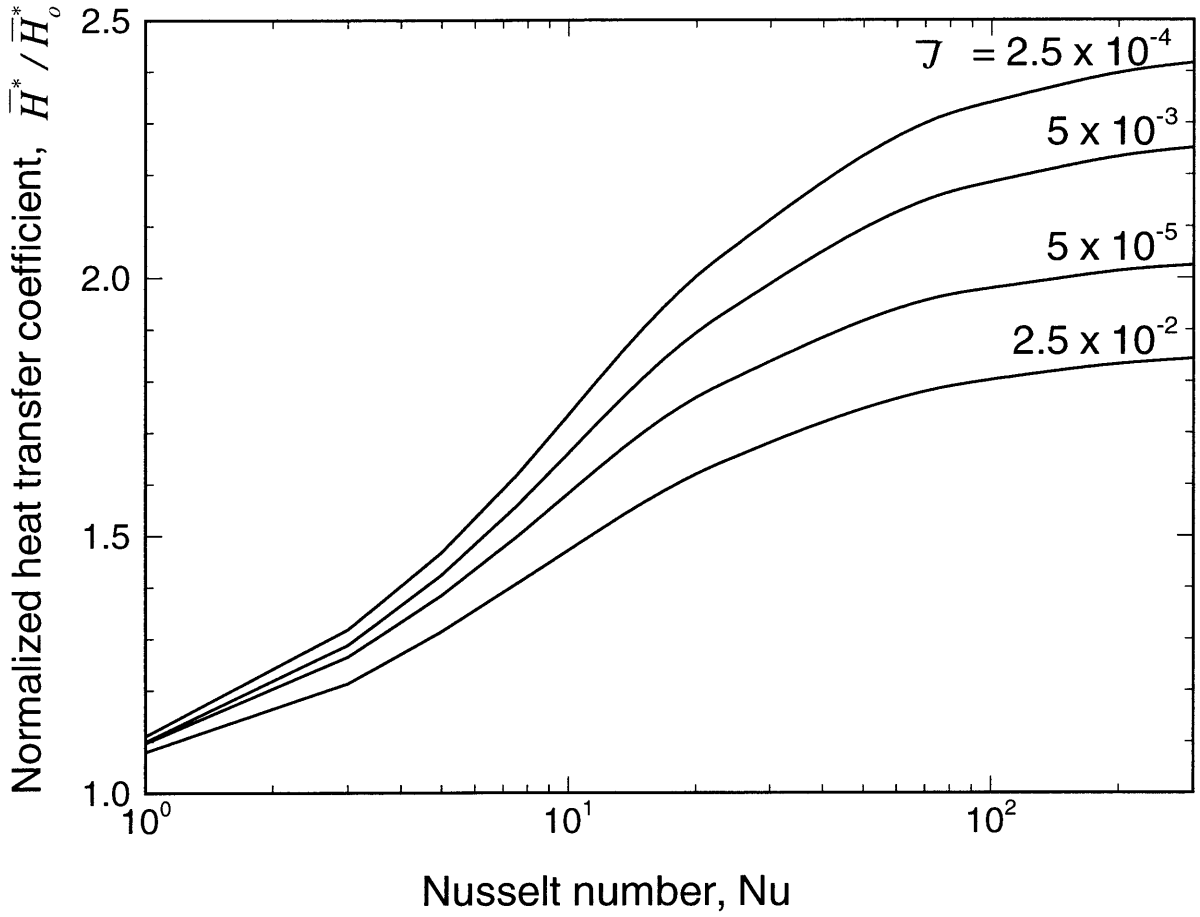

Figure 9-3: Effect of rotation period $\mathcal{J}$ on the normalized global heat transfer coefficient: $\mathrm{Pe}_q = 5,000$, $R_i/R_o = 0.3$, $\varepsilon = 0.5$, $\Omega_i/\Omega_o = 6$.

section (9.4.1). As expected, transport enhancement (i.e. $\bar{H}^*/\bar{H}_o^* > 1$) occurs over and above the concentric cylinder case. For a fixed Nu the degree of enhancement shows an initial increase with increasing time period, followed by a subsequent decrease. The same trend was observed by Bryden & Brenner [8] as well as by Ghosh *et al.* [10]. Whereas for small rotation periods the kinematical particle motion is unable to exploit fully the chaotic transport due to time-periodic modulation of the streamlines, large time periods result in a state of quasi-steady transport during each of the rotation cycles, whence there exists an optimum time-period of rotation. Different eccentricities were observed to yield different optimal time periods. It is interesting to note that the optimal time period was higher in the case where the cylinders were co-rotated than counter-rotated.

Figures (9-4a) and (9-4b) respectively show the variation of the normalized global heat transfer coefficient with inner/outer angular velocity ratio for the steady and time-periodic cases. Since the velocity field is obtained by superposition of the individual fields [3], the ratio of angular velocities constitutes a representation of the relative importance of the cylinder rotations. As Ω_i/Ω_o increases, for a prescribed Nu the normalized heat transfer coefficient is seen to increase for both the steady and chaotic-enhancement cases. For the steady rotation case our observations agree with those of Ghosh *et al.* [10]. In this case the observed behavior can be explained as resulting from the increased width of the recirculation region between the cylinders [Fig. (9-2c)]. This region, which has been characterized [10] as the 'well mixed' region, is one of the main factors responsible for regular enhancement. In the time-periodic case the observed behavior can be explained in terms of the location of the separation point arising from the inner cylinder rotation. Rotation of the inner cylinder creates a separation point on the outer wall, whence the fluid in proximity to that wall mixes with that from the central core of the annulus [Fig. (9-2a)]. Consequently, transport to the wall is enhanced.

Figures (9-5a) and (9-5b) depict the variation of the normalized heat transfer coefficient $\bar{H}^*/\bar{H}_o^*$ with the transverse Péclet number. For reasons that are intuitively obvious, an increase in Pe_q leads to an increase in the transverse transport rate, and

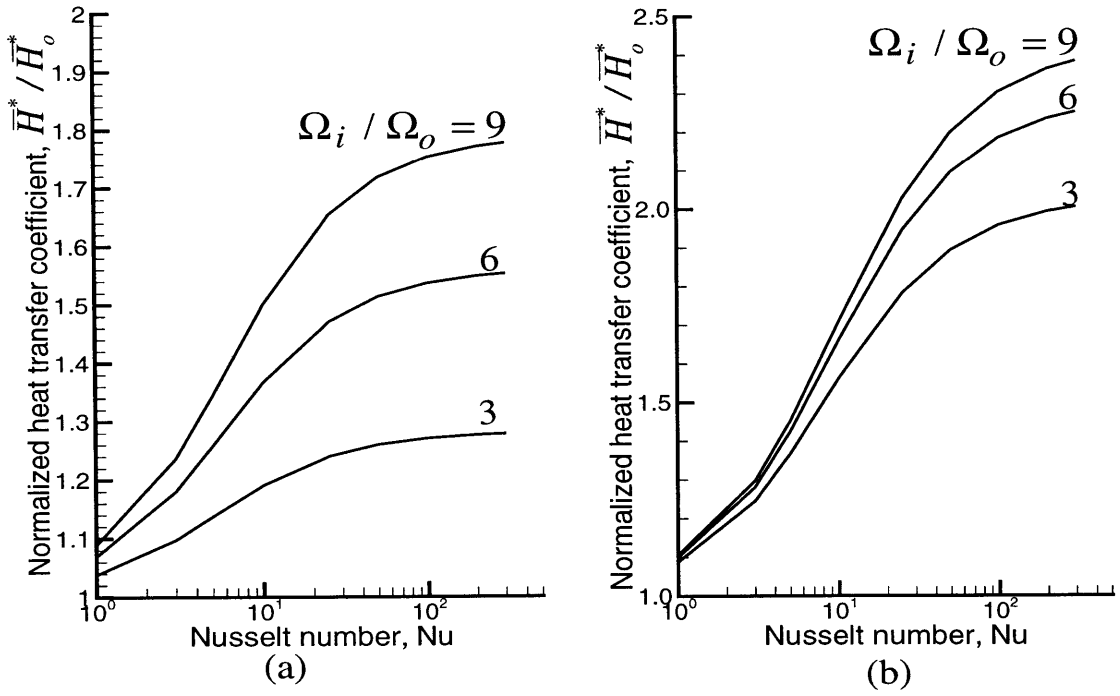

Figure 9-4: Dependence of the normalized heat transfer coefficient on the angular velocity ratio: $\mathrm{Pe}_q = 5,000$, $R_i/R_o = 0.3$, $\varepsilon = 0.5$. (a) Steady-flow case; (b) Time-periodic case. Note the different scales used for (a) and (b).

hence to a concomitant increase in the $\bar{H}^*$ as well. It is interesting to note that at small values of Pe_q, enhancement effects in the time-periodic case are minimal. In fact, surprisingly, the normalized heat transfer coefficient is slightly larger in the steady-flow case than in the time-periodic case for these small Péclet numbers. On the other hand, at the larger Péclet numbers the overall heat transfer coefficient in the time-periodic case is more than twice that realized in the comparable concentric cylinder case, and almost 50% more than that achieved in the regular enhancement case.

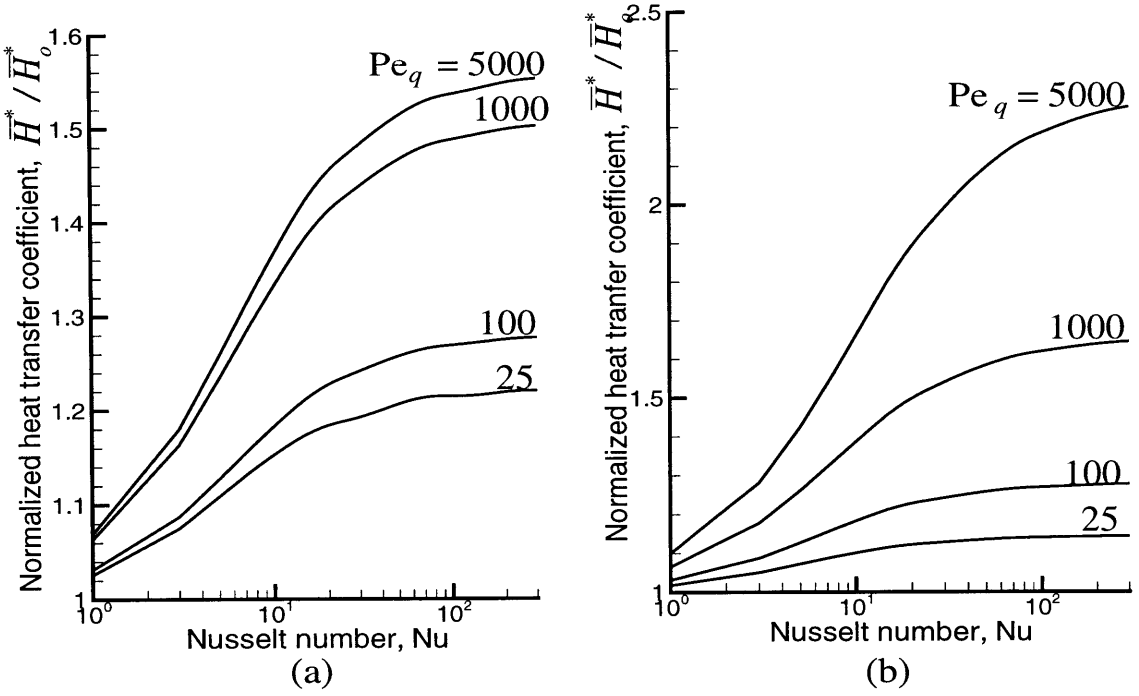

Figure 9-5: Effect of transverse Peclet number on the normalized global heat transfer coefficient: $R_i/R_o = 0.3$, $\varepsilon = 0.5$, $\Omega_i/\Omega_o = 6$. (a) Steady-flow case; (b) Time-periodic case. Note the different scales used for (a) and (b).

Figures (9-6a) and (9-6b) illustrate the variation of the normalized global heat transfer coefficient with eccentricity. In the steady rotation case the effective heat transfer rate is seen to initially increase with eccentricity. This may be regarded as a direct consequence of the increase in size of the recirculation region with increasing

eccentricity [3]; however, the occurrence of a maximum does not appear explicable by purely fluid-dynamical arguments. For the time-periodic rotation protocol, enhancement in the heat transfer rate is clearly evident. Moreover, this enhancement attains a maximum value at an intermediate eccentricity. This seems to be a significant observation, and may be a result of the nature of chaos itself. This is consistent with the results of Atobe and Funakoshi [2], where the numerically calculated area of the chaotic region achieved a maximum with eccentricity (and for some specific parameter values, even two maxima).

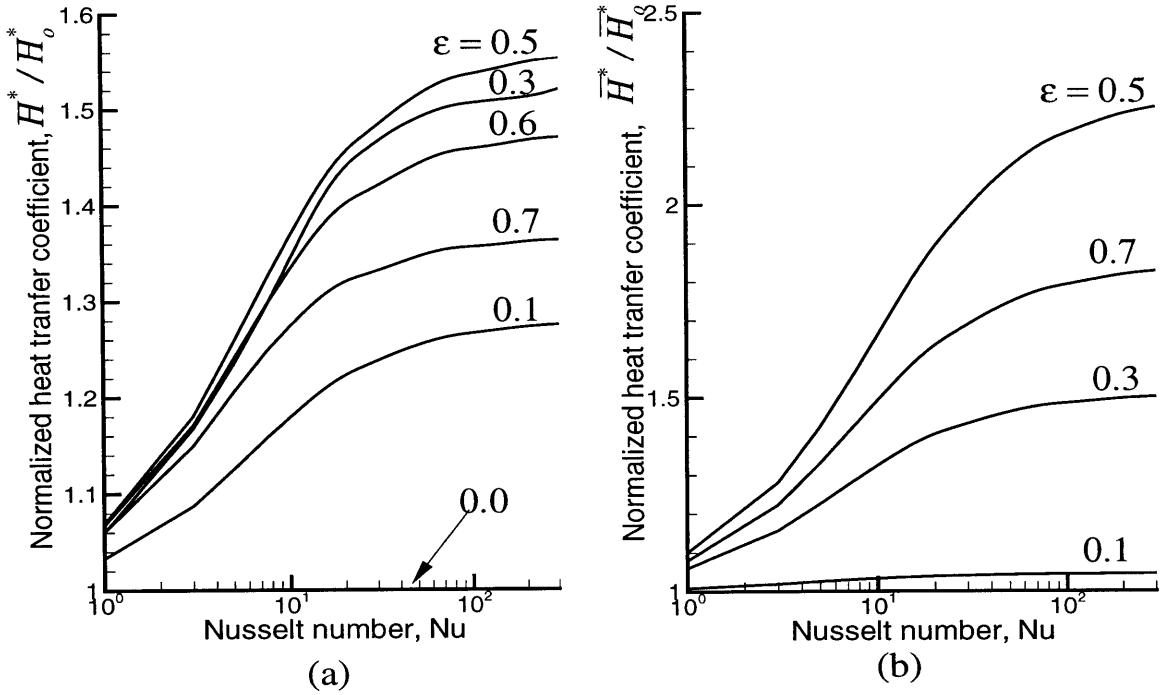

Figure 9-6: Dependence of the normalized heat transfer coefficient on the eccentricity: $\mathrm{Pe}_q = 5,000$, $R_i/R_o = 0.3$, $\Omega_i/\Omega_o = 6$. (a) Steady-flow case; (b) Time-periodic case. Note the different scales used for (a) and (b).

9.5.2 Convective Dispersivity

Taylor dispersion arises from the interaction of two separate transverse 'mixing' mechanisms: (i) Convection acting on the transverse length scale of the apparatus in which

the experiment is conducted; (ii) Diffusion acting on a molecular length scale. The phenomenon of chaotic advection, an offshoot of Hamiltonian chaos, was pathbreaking in that it shattered the myth that molecular diffusion was necessary to achieve 'mixing' in laminar flow systems.

As in eq. (9.17) the thermal Taylor dispersivity includes contributions from two distinct sources: molecular conductivity and convective dispersivity. The magnitude of the latter is enhanced by the following factors : (i) A larger probability of thermions preferentially sampling those axial streamlines across which larger transverse axial velocity gradients exist (viz. the slower-moving streamlines); (ii) A decrease in the size of the well-mixed region.

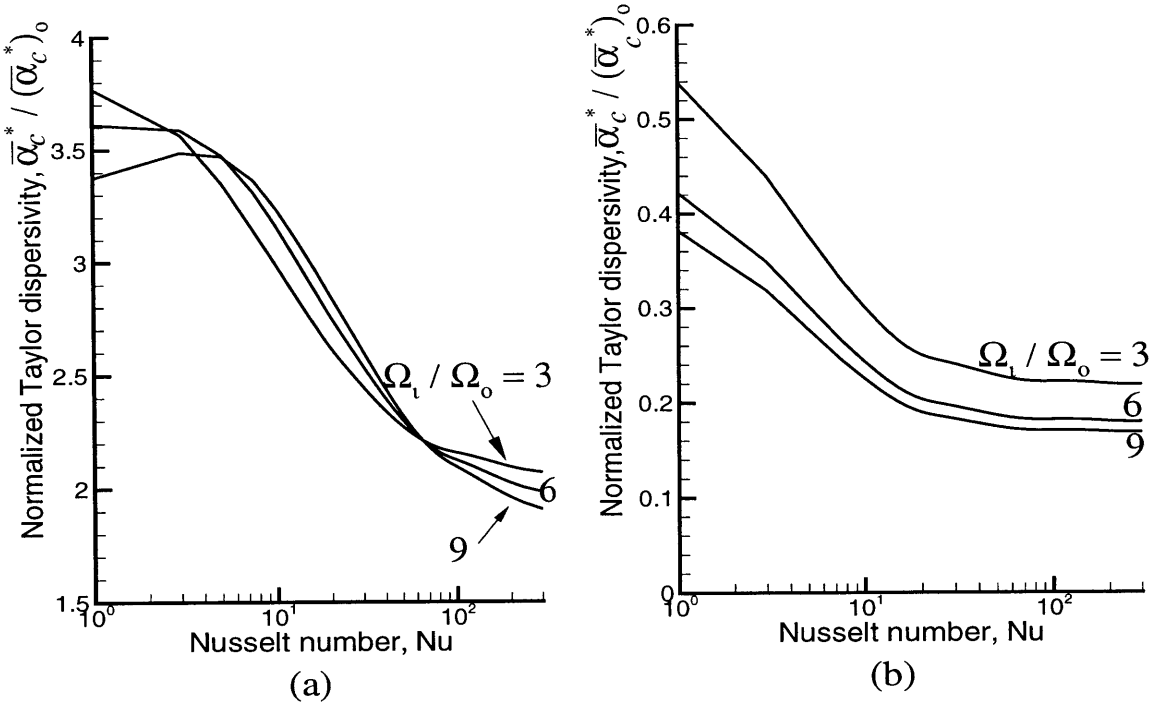

Figure 9-7: Effect of transverse Peclet number on the normalized Taylor convective dispersivity: $R_i/R_o = 0.3$, $\varepsilon = 0.5$, $\Omega_i/\Omega_o = 6$. (a) Steady-flow case; (b) Time-periodic case. Note the different scales used for (a) and (b).

Figure (9-7a) displays the variation with transverse Péclet number of the (normalized) convective Taylor dispersivity contribution for the steady-flow case [see section

(9.4.1) for the definition of $(\bar{\alpha}_c^*)_o$]. The streamline patterns for the case of steady flow reveal the existence of a recirculation region near the center of the annulus, surrounded by regions where the streamlines appear almost circular, so that transport through these latter outer regions towards the wall is purely through conduction [10]. Net transport of heat to the environment can be imagined as being equivalent to the consumption of the thermions at the outer wall, where the slower-moving axial streamlines are located. At small Pe_q values, consumption of these thermions at the wall leads to larger transverse thermal gradients in the conduction zones, resulting in a larger heat flux across the axial streamlines. This may formally be regarded as being equivalent to a lower molecular conductivity in a Fourier's law sense. As such, convective dispersivity, which is inversely proportional to the molecular conductivity, increases slightly. At these small Pe_q values, the large values of the convective dispersivity together with their insensitivity to Nusselt number variations indicate the inefficacy of the transverse mixing process. At larger transverse Péclet numbers the transverse *convective* transport becomes the more effective of the two mechanisms, whence the transverse gradients in the conduction zones become of lesser significance. In such circumstances the consumption of thermions at the wall reduces the probability of their being found in the slower-moving axial streamlines near the outer-cylinder wall, thereby leading to a decrease in dispersivity with increase in Nu.

Figure (9-7b) shows the comparable results for time-periodic flow. At very small Pe_q values the normalized dispersivity decreases with increasing Nu, although the trend is much less pronounced at larger Péclet numbers (where the dispersivity is practically a constant). This behavior can be rationalized in the following manner: At small Pe_q the transverse convection is ineffective, whence effects stemming from the consumption of thermions at the wall (a result of the increasing Nu) reduces the dispersivity. At larger Nu, transport to the wall becomes the rate-limiting step, whence the effects of consumption becomes less significant. The latter observation is consistent with the observed existence of asymptotes. The initial dispersivity increase ($\mathrm{Pe}_q = 25$ vs $\mathrm{Pe}_q = 10$) results from the increased probability for finding thermions in the slower-moving axial streamlines, owing to the existence of the recirculation

region. At still larger Péclet numbers the transverse transport rate increases, allowing thermions to more rapidly sample the axial streamlines, thereby eliminating the distinction between those sampling the faster- and those sampling the slower-moving streamlines. This is equivalent to a 'well-mixed' condition, leading to a smaller dispersivity. In this case the transverse transport rate becomes the significant factor, rationalizing the almost constant values obtained for the normalized dispersivity.

The Pe_q dependence of the thermal Taylor dispersivity provides further evidence of the effect of chaotic advection on transport. The time-periodic values achieved at large Péclet numbers are seen to be only about 10% of the comparable steady-flow values. This illustrates the better degree of mixing achieved in the time-periodic case as a consequence of the chaotic advection. Moreover, one can observe a transition to a transport-limited regime (at large Nu) in the steady-flow case, even at high Pe_q values, whereas no such regime is observed for the time-periodic case (almost constant dispersivities indicating the transport effectiveness).

Figures (9-8a) and (9-8b) serve to illustrate the functional dependence of the normalized axial dispersivity on the complex factors governing the transverse transport. In the case of steady rotation a recirculation region (the 'well-mixed' region) exists near the center of the annulus, whose size increases with relative rotation rate, Ω_i/Ω_o. At small Nu the wall heat transfer rate has little effect on the dispersivity, whence the dispersivity decreases with increasing relative rotation rates. At intermediate values of Nu a larger relative rotation rate is seen to yield a larger dispersivity. This is likely a result of the greater efficiency of those flows characterized by higher relative rotation rates to replenish the consumed thermions (consumption of which has now become more significant at these Nu values), resulting from the increased size of the recirculation regions. At the larger Nu values none of these rotary flows is able to replenish the consumed thermions, whence those flows characterized by better mixing (i.e. higher relative rotation rates) yield lower dispersivities. Simultaneously, this regime is characterized by very small values of the dispersivity. In the time-periodic flow case the dispersivity decreases with increasing relative rotation rate Ω_i/Ω_o due to the more efficient sampling of all of the axial streamlines at the larger Ω_i values.

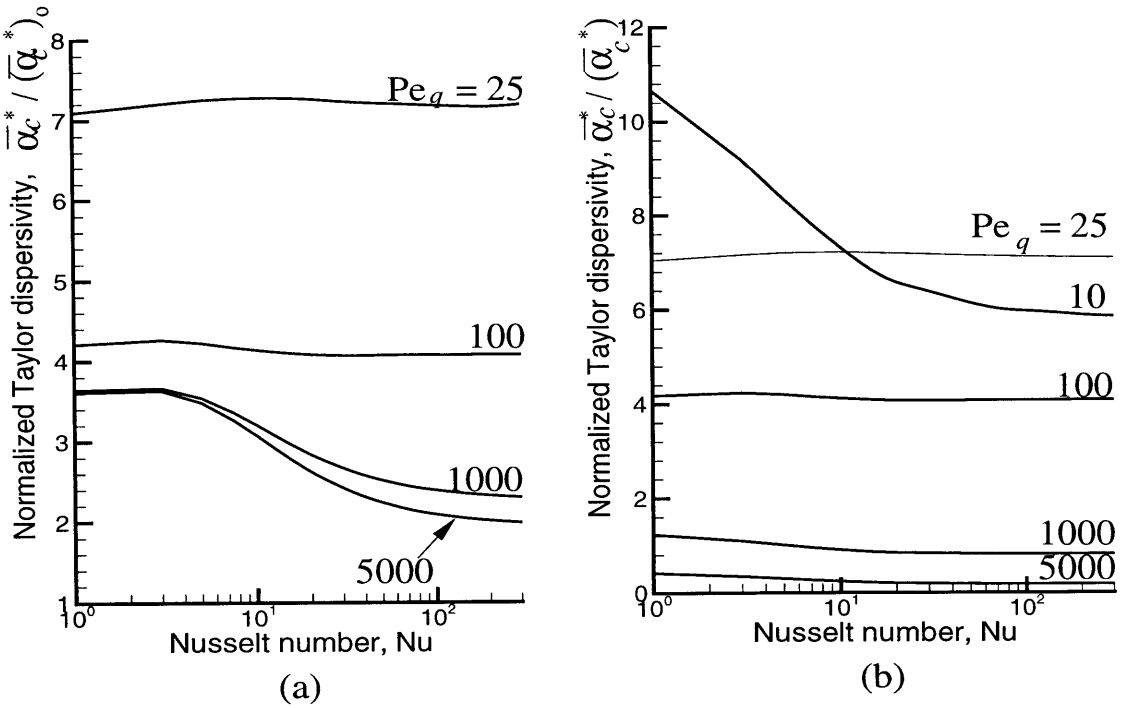

Figure 9-8: Dependence of the normalized Taylor convective dispersivity on the angular velocity ratio: $\mathrm{Pe}_q = 5,000$, $R_i/R_o = 0.3$, $\varepsilon = 0.5$. (a) Steady-flow case; (b) Time-periodic case. Note the different scales used for (a) and (b).

Here again we note how the presence of chaos leads to an enhanced degree of mixing, yielding dispersivities which are an order-of-magnitude less in the time-periodic case than in the steady-flow case.

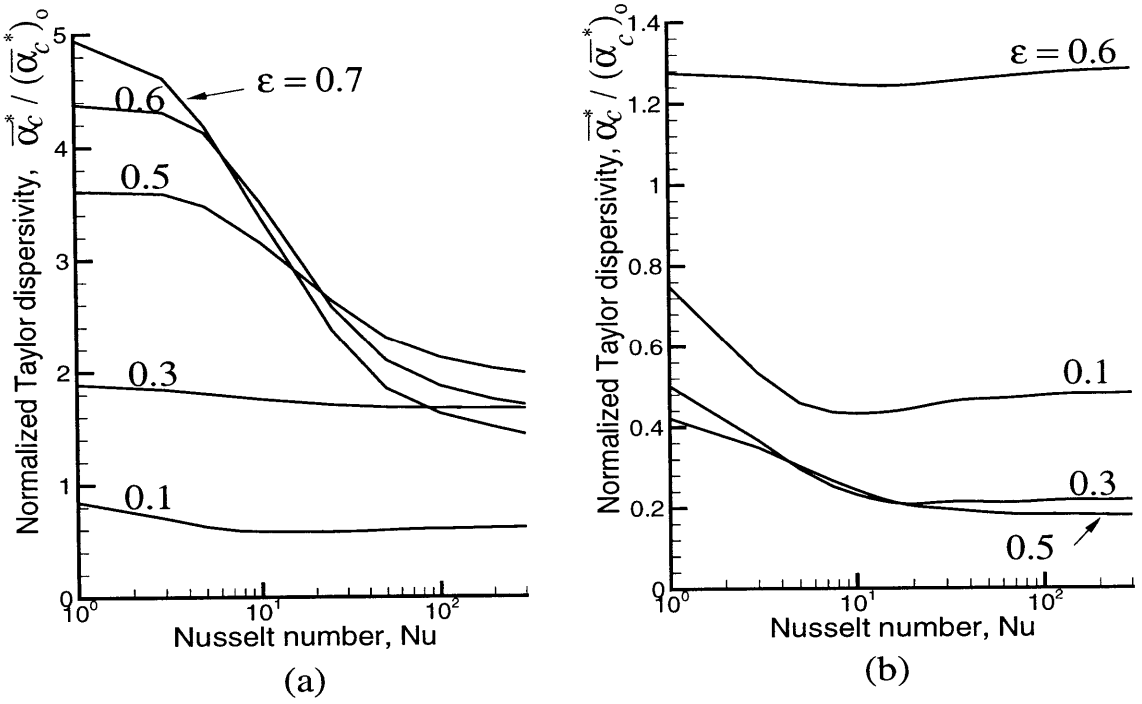

Figure 9-9: Dependence of the normalized Taylor convective dispersivity on the eccentricity: $\mathrm{Pe}_q = 5,000$, $R_i/R_o = 0.3$, $\Omega_i/\Omega_o = 6$. (a) Steady-flow case; (b) Time-periodic case. Note the different scales used for (a) and (b).

Figures (9-9a) and (9-9b) portray the variation of the normalized convective dispersivity with eccentricity. In the case of steady rotation occurring at small values of Nu, where the rate of thermion consumption at the wall is relatively low, the larger eccentricities are seen to result in larger dispersivities. This behavior results from the increased transverse axial velocity gradients arising at the larger eccentricities, and is consistent with the results of Shankarsubramaniam and Gill [23] who analyzed material Taylor dispersion in the absence of both wall mass transfer and transverse flow. At the larger eccentricities the observed decrease in dispersivity with increasing Nu is easily explained, as in the prior cases, as being a direct result of the increased

consumption of thermions brought near to the wall by the recirculation region. For the case of time-periodic flows the dispersivity is seen to initially decrease with an increase in eccentricity (despite increased transverse axial velocity gradients), subsequently displaying a relatively large dispersivity at $\varepsilon = 0.6$. This observation is easily explained from a kinematic viewpoint. The Poincaré plots show [9] increasingly chaotic behavior with increasing eccentricity in the range $\varepsilon = 0.1$ to 0.5. Thus, the improved mixing overcomes the increasing velocity gradients, leading to a decrease in dispersivity. The Poincaré plots for the larger eccentricities are seen [9] to possess extensive regular (hyperbolic) regions in the center of the annulus. This fact, in combination with the steep transverse axial velocity gradients, is responsible for the larger values of dispersivity observed for this case.

The preceding axial Taylor dispersivity calculations, wherein the steady- and time-periodic-flows display widely differing behaviors, serves as additional proof of the role of chaotic advection in enhancing the overall heat transfer rate. In particular, the axial dispersivity values, when extrapolated to zero Nusselt number, constitute a measure of mixing which is independent of the heat transfer kinetics at the wall. The trends displayed in this limiting case validate our discussion of the role of chaotic advection in mixing.

9.5.3 Counter-rotation vs Co-rotation

The results cited above apply for counter-rotation of the cylinders. Comparable co-rotation calculations of the global heat transfer coefficient for time-periodic flows in the same parametric ranges yielded values that were almost always slightly less (a phenomenon overlooked by Bryden & Brenner [8] due to minor numerical discrepancies). However, in contrast with our quantitative heat transfer rate comparison of the two cases, a qualitative comparison of the comparable Poincaré plots [9] as in the example of Fig. (9-10) would incorrectly suggest that the co-rotation case, appearing to be the more significantly chaotic of the two, should result in a larger rate of heat transfer. The virtually identical heat transfer values obtained for the two cases despite the vastly different appearance of respective Poincaré plots exemplifies the

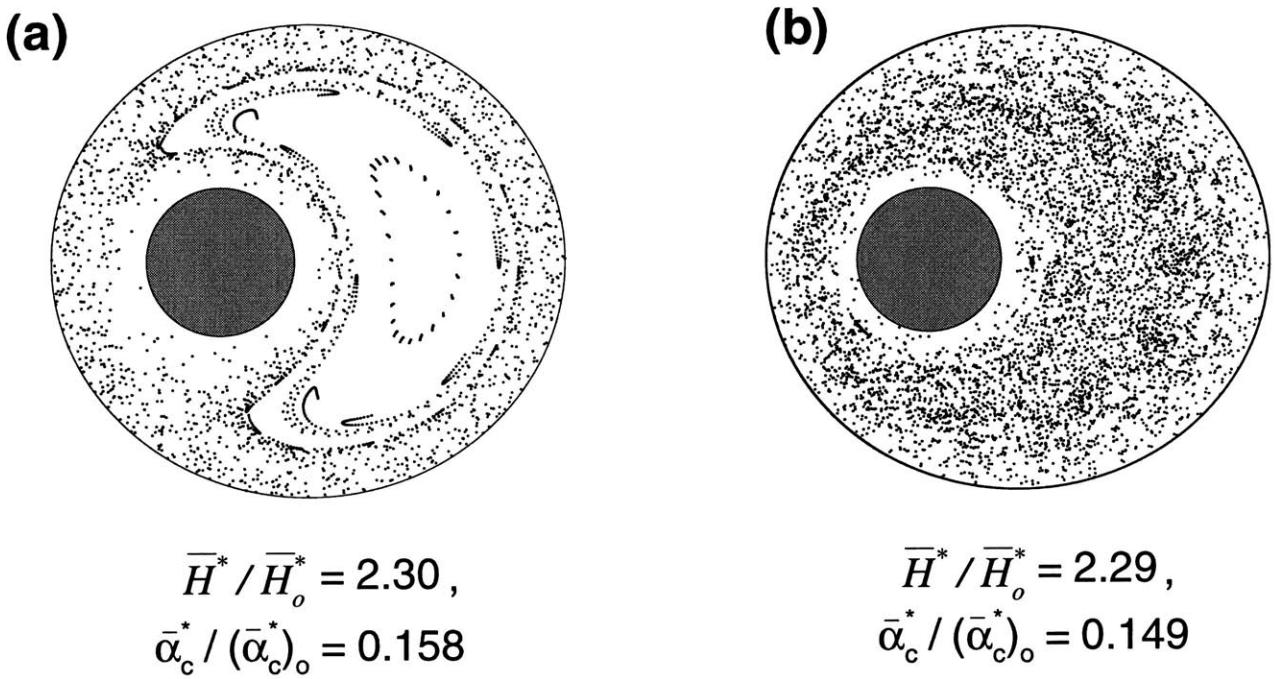

Figure 9-10: Comparison of Poincare plots for (a) counter- and (b) co-rotation protocols for time-periodic flow: $\mathrm{Pe}_q = 5,000$, $R_i/R_o = 0.3$, $\varepsilon = 0.5$, $\Omega_i/\Omega_o = 6$, $\mathcal{J} = 0.01$. Calculated values at $\mathrm{Nu} = \infty$ of the normalized heat transfer coefficient and normalized convective dispersivity are shown.

non-existence of a strict correlation between purely visual quantifications of chaotic intensities and global transport rates. Additional evidence is provided by the comparable values of the convective dispersivity noted in Fig. (9-10), which in contrast to what might otherwise be expected upon comparing their respective Poincaré plots, are very nearly equal. This disparity illustrates and underscores the point that graphical representations like Poincaré maps suffice only to provide a qualitative picture of the kinematics of fluid particles. Qualitatively, however, such purely kinematical transport measures may lead to erroneous conclusions when it comes to predicting actual trends, like heat- and mass-transfer rates in dynamical phenomena, where the relative time scales of transport via different mechanisms — namely, convection and conduction, as embodied in the dimensionless transverse Péclet number — play a critical role.

9.6 Conclusions

Time-periodic thermal Taylor dispersion theory [4] was used to calculate the three thermal macrotransport coefficients, namely $\bar{H}^*, \bar{U}^*$ and $\bar{\alpha}_T^*$, for the case of alternately-rotating, nonconcentric cylinders within which an axial annular flow occurs, and with heat transfer to the ambient environment taking place at the outer-cylinder wall. Calculation, *inter alia*, of the overall rate of heat transfer from the system as embodied in the coefficient $\bar{H}^*$, which was previously shown [8] to provide an excellent global measure of the chaotically-enhanced transport process, constitutes one of the main achievements of the present work. The functional dependence of this heat transfer coefficient upon a wide variety of system parameters was illustrated, and the qualitative aspects of this dependence explained in terms of the physical processes occurring. Parameters studied included Nusselt number, transverse Péclet number, eccentricity, modulation period, and co- vs counter-rotation protocols. Concomitant axial dispersion calculations furnished independent quantitative evidence of the existence of chaotically-enhanced heat transfer rates, consistent with the previous observations of related physical situations by several authors. In the interests of brevity,

the calculated values of the axial thermal velocities $\bar{U}^*$ were not displayed owing to their qualitatively similar behavior to that of the axial dispersivity. Finally, we have pointed out that qualitative kinematical measures of mixing, such as Poincaré maps, may suggest incorrect parametric trends as regards the global effectiveness of chaotic mixing in dynamical phenomena. Our Taylor dispersion methods for globally quantifying chaotic thermal transport rates permits the exploration of parameter ranges lying significantly beyond those previously investigated. It is hoped that our contribution will accelerate translation of the growing body of theoretical work on the novel subject of chaotic advection towards the solution of practical industrial design problems.

References

[1] H. Aref and S. Balachandar, "Chaotic advection in Stokes flow," *Phys. Fluids*, **29**, 3515 (1986).

[2] T. Atobe and M. Funakoshi, "Chaotic Motion of fluid particles due to the alternate rotations of two eccentric cylinders," *J. Phys. Soc. Japan.*, **63**, 1738 (1994).

[3] B.Y. Ballal and R.S. Rivlin, "Flow of a Newtonian fluid between eccentric rotating cylinders: inertial effects," *Arch. Rat. Mech. Anal.*, **62**, 237 (1976).

[4] R.P. Batycky, D.A. Edwards and H. Brenner, "Internal energy transport in adiabatic systems. Thermal Taylor dispersion phenomena," *Int. J. Non-Linear Mech.*, **29**, 639 (1994).

[5] R.P. Batycky, D.A. Edwards and H. Brenner, "Thermal Taylor dispersion in non-adiabatic systems," *Chem. Eng. Commun.*, **130**, 53 (1994).

[6] R.B. Bird, W.E. Stewart and E.N. Lightfoot, *Transport Phenomena*, Wiley, New York (1960).

[7] H. Brenner and D.A. Edwards, *Macrotransport Processes*, Butterworth-Heinemann, Boston (1993).

[8] M. Bryden and H. Brenner, "Effect of laminar chaos on reaction and dispersion in eccentric annular flow," *J. Fluid Mech.*, **325**, 219 (1996).

[9] J. Chaiken, C.K. Chu, M. Tabor and Q.M. Tan, "Lagrangian turbulence and spatial complexity in Stokes flow," *Phys. Fluids*, **30**, 687 (1987).

[10] S. Ghosh, H.C. Chang and M. Sen, "Heat transfer enhancement due to slender recirculation and chaotic transport between counter rotating eccentric cylinders," *J. Fluid Mech.*, **238**, 119 (1992).

[11] J. Guckenheimer and P. Holmes, *Nonlinear Oscillations, Dynamical Systems and Bifurcations of Vector Fields*, Springer-Verlag, New York (1983).

[12] J. Happel and H. Brenner, *Low Reynolds Number Hydrodynamics*, Kluwer, Dordrecht, The Netherlands (1983)

[13] G. Iosilevski, H. Brenner, C. M. V. Moore and C.L. Cooney, "Mass transport and chemical reaction in Taylor-vortex flows with entrained catalytic particles: applications to a novel class of immobilized enzyme biochemical reactors," *Phil. Trans. Roy. Soc. Lond. A*, **345**, 259 (1993).

[14] S.C. Jana and J.M. Ottino, "Chaos enhanced transport in cellular flows," *Phil. Trans. R. Soc. Lond. A*, **338**, 519 (1992).

[15] G.B. Jeffery, "The rotation of two cylinders in a viscous fluid," *Phil. Trans. R. Soc. Lond. A*, **101**, 169 (1922).

[16] T.J. Kaper and S. Wiggins, "An analytical study of transport in Stokes flows exhibiting large-scale chaos in the eccentric journal bearing," *J. Fluid Mech.*, **253**, 211 (1993).

[17] H.A. Kusch and J.M. Ottino, "Experiments on mixing in continuous chaotic flows," *J. Fluid Mech.*, **236**, 319 (1992).

[18] P.M. Morse and H. Fesbach, *Methods of Theoretical Physics, Part 1*, McGraw-Hill, New York)1953).

[19] J.M. Ottino, *The Kinematics of Mixing: Stretching, Chaos and Transport*, Cambridge University Press, Cambridge (1989).

[20] J.M. Ottino, "Mixing, chaotic advection and turbulence," *Ann. Rev. Fluid Mech.* **22**, 207 (1990).

[21] N.A.V. Piercy, M.S. Hooper and H.F. Winney, "Viscous flow through pipes with cores," *Phil. Mag.*, **15**, 647 (1933).

[22] A. San Andres and A.Z.Szeri, "Flow between eccentric rotating cylinders," *J. Appl. Mech.*, **51**, 869 (1984).

[23] R. Shankarsubramaniam and W.N. Gill, "Taylor dispersion in laminar flow in an eccentric annulus," *Intl. J. Heat Mass Trans.*, **14**, 905 (1971).

[24] W.T. Snyder and G.A. Goldstein, "An analysis of fully developed laminar flow in an eccentric annulus," *AIChE J.*, **11**, 462 (1965).

[25] P.D. Swanson and J.M. Ottino, "A comparative computational and experimental study of chaotic mixing of viscous fluids," *J. Fluid Mech.*, **213**, 227 (1990).

[26] S. Wiggins, *Introduction to Applied Nonlinear Dynamical Systems and Chaos*, Springer-Verlag, New York (1990).

Chapter 10

Long-time Non-preaveraged Diffusivity and Sedimentation Velocity of Clusters: Applications to Micellar Solutions

Reference: Venkat Ganesan and Howard Brenner,"Long-time Non-preaveraged Diffusivity and Sedimentation Velocity of Clusters: Applications to Micellar Solutions," *Phys. Rev. E*, **59**, 212 (1999).

The present chapter utilizes macrotransport theory to study the diffusion and sedimentation of size-fluctuating Brownian 'clusters' through otherwise quiescent, unbounded fluid continua. These Brownian solutions are assumed to be sufficiently dilute with regard to cluster concentration such that individual clusters do not interact hydrodynamically or physicochemically with one another. Clusters are envisioned as being composed of aggregates of solute molecules, i. e. 'monomers' (cf. [18] for a general discussion of systems comprising examples of this category). Each cluster is assumed to undergo a reversible association-dissociation (A - D) process, leading to a continuous temporal variation in the number of monomer molecules instantaneously constituting the aggregate. (In the following, the terms 'size' and 'aggregation num-

ber' are used interchangeably except where a need arises to distinguish between them.) A situation of dynamical equilibrium as regards the cluster-size distribution is ultimately expected to arise locally at each point of the fluid as a consequence of the inherently reversible nature of these A - D processes coupled with the relative rapidity of their kinetics compared with physical-space cluster transport rates. Because of this, it suffices to focus attention on the transport of a single representative cluster, hereafter termed a 'tracer.' The focus of our analysis is to quantify during such a scenario the transport of such a tracer cluster through the fluid continuum. The cluster is assumed to undergo both physical-space diffusion (due to thermal fluctuations) and sedimentation (due to external forces, if any), simultaneously accompanied by a continuous variation in its size due to the A - D processes. Of course, sedimentation will be absent in the case of force-free solute molecules, in which circumstances only molecular diffusion of the cluster occurs.

The novel feature of this problem, which has not previously been addressed in a systematic and rigorous manner, is the effect of the short-time cluster-size variation (due to the A - D processes) on the long-time physical-space transport processes. This temporal variation in cluster size manifests itself via an instantaneous size-specific translational diffusion coefficient and sedimentation velocity, each of which varies continuously during the movement of the cluster through the solution owing to changes in its size arising from the A - D processes. This temporal variation in size has a nontrivial effect on the physical-space transport properties of such dispersions. Most prior studies of cluster transport processes have been limited to evaluating the cluster mobility for the *pre-averaged* case, where the cluster size is assumed to remain fixed at its equilibrium mean value during its entire motion through the solvent (see, for example, [22]). In contrast, we treat here the non-preaveraged case, where the cluster is allowed to undergo relatively rapid fluctuations in its size due to the A - D processes as it wends its way through the solution.

Practical motivations for studying cluster transport processes are manifold. Association colloids are ubiquitous in nature, micellar dispersions and microemulsions [15, 20] representing common examples. Equilibrium aspects of these solutions have

been widely studied, including elucidating the many size and shape distributions thermodynamically possible in such systems. In contrast, the transport or nonequilibrium properties of these entities have received only sparse attention. In this context it is pertinent to note the emergence of recent interest in quantifying the rheology of clustering systems, exemplifying the more general class of so-called soft glassy systems [17, 24]. The same features that lead to intriguing thermodynamics [15] (namely, equilibrium size and shape distribution features) make the analysis of transport properties equally interesting, albeit more complex. In this initial foray into the field we do not address larger issues relating to the rheology of these systems when they undergo shear. Rather, we study only those more limited features accompanying the transport of clusters through otherwise quiescent systems in which shear is absent.

Owing to the polydispersivity of cluster sizes, transport processes occurring in these systems exhibit interesting attributes not present in monodisperse systems. Explicitly, we will quantify both the diffusivity and sedimentation (i.e. mobility) coefficient in dilute clustering systems. The diffusion coefficient is shown to involve an additional contribution (termed the 'convective' or 'Taylor' dispersivity) above and beyond the ordinary molecular contribution, which arises from the distribution of settling velocities among the differently-sized clusters. Furthermore, our analysis indicates that the size-fluctuation processes accompanying the *microscale* physical-space cluster transport processes may have a significant effect upon the *macroscale* physical-space transport coefficients. On the practical side we note that self-diffusion coefficients are widely used to characterize such features as size, shape, and cluster-cluster interactions in these systems [7, 8, 25]. As such, our analysis points up a scheme whereby key phenomena arising in these polydisperse systems can be accounted for when interpreting experimental self-diffusion and electrophoretic measurements in such clustering systems.

A modest prior literature examines several elements closely related to our study. Notably, Cussler [9] considered cluster diffusion in solutions near the consolute point, where very large sizes of the diffusing units ('clusters') — certainly bigger than the underlying monomeric molecular units — are to be expected. Frankel *et al.* [14]

investigated a system similar in spirit to ours, relating to diffusion and sedimentation coefficients in solutions of coiled linear polymer molecules, and arising from Brownian size fluctuations stemming from the inherently flexible nature of such entities. Our goal here is the development of a generic conceptual framework for quantifying the transport of dispersions of association colloids, with the accompanying association-dissociation process viewed as diffusional processes in 'size' - or 'aggregation number'-space (cf. also Ziabicki [29]).

The scheme ultimately developed will be illustrated by applications to two distinct, but interrelated examples of micellar cluster geometries. The first involves a micellar solution composed of spherical micelles, for which the size distribution encountered in practice is typically confined to a relatively narrow range centered about the mean aggregation number [20]. In the second case we consider similar phenomena for cylindrical micelles, frequently termed 'living polymers.' The latter exhibit a wide range of cluster sizes, ranging from monomeric to polymeric, the latter involving very large aggregation numbers. Pioneering studies of these systems appear in the works of Cates [5, 6], Bouchaud [3, 23], and others, who investigated the dynamics of these systems in the entangled-regime domain. Our analysis will focus on the diffusive and sedimentary aspects of these systems, albeit in the dilute regime.

In the dilute cluster solution limit it suffices to focus attention on the transport of a single cluster. In the subsequent analysis, hydrodynamic as well as physicochemical intercluster interactions are neglected, permitting attention to be focused exclusively on the effect of the internal A - D processes. Furthermore, owing to the dilute nature of the dispersion, only pairwise A - D reactions need to be considered. These assumptions, which hold in the dilute solution limit, ensure that the effective transport properties of the solution can be discerned by employing a tracer cluster to sample the configurational space (size- plus physical-space coordinates) of the clusters present in the solution. An exact microscale description of the transport process would require calculating the multivariate probability density function $P(\mathbf{R}, n, t)$ of the tracer cluster, defined in the four-dimensional configurational space described at time t by the three scalar physical coordinates parameterizing the instantaneous position vector $\mathbf{R}$

(of say, the center of mass) of the cluster in physical space, and the cluster aggregation number n. In most cases, however, physical interest does not center on the detailed microscale description provided by $P(\mathbf{R}, n, t)$ but rather on a coarse-grained macroscale probability density $\bar{P}(\mathbf{R}, t)$ characterizing the totality of the molecular solute species being transported, irrespective of the size of the cluster in which the monomer molecule characterizing the chemical species being transported finds itself at any given instant of time. The less detailed density distribution $\bar{P}(\mathbf{R}, t)$ quantifies the solute species transport process through three-dimensional physical space (i.e. through the solution), accounting for variations occurring in cluster size in an appropriately averaged manner which eschews pre-averaging.

This coarse-grained density is expected to evolve asymptotically according to the macroscale i.e. physical-space convective-diffusive conservation equation [4]

$$\frac{\partial \bar{P}}{\partial t} + \bar{\mathbf{U}} \cdot \nabla \bar{P} = \bar{\mathbf{D}} : \nabla \nabla \bar{P}, \tag{10.1}$$

wherein the time- and position-independent sedimentation vector velocity $\bar{\mathbf{U}}$ and dispersion dyadic $\bar{\mathbf{D}}$ respectively quantify the coarse-grained convective and diffusive solute transport mechanisms in the fluid continuum. The above equation is analogous to the macrotransport equation (8.16), wherein the global space $\mathbf{Q}$ is represented by the physical space $\mathbf{R}$. Implicitly embedded within these coefficients are the overall effects of the comparable microscale transport processes arising from the continuous variations in cluster size. For a monodisperse system (of aggregation number $\bar{n}$) these coefficients are respectively identical to the Stokes settling velocity $\mathbf{U} \equiv \mathbf{U}(\bar{n})$ and molecular diffusivity $\mathbf{D} \equiv \mathbf{D}(\bar{n})$ appropriate to clusters of size $\bar{n}$. Our objective is, starting from the specified microscale transport data, to calculate the coefficients $\bar{\mathbf{U}}$ and $\bar{\mathbf{D}}$ governing the macroscale transport processes for circumstances where a distribution of cluster sizes exists owing to the A - D processes.

10.1 Formulation

As indicated in the Introduction, attention is directed towards the transport of a single cluster undergoing fluctuations in size due to the reversible A - D processes. Conformational changes in *shape*, though potentially interesting, are not considered in this work. A variety of schemes can be imagined for the A - D processes accompanying the physical-space transport. However, many such processes lead to reaction schemes that can be represented physically as size-space diffusional processes, with an internal force-derived potential energy function restricting the cluster size range. Our analysis will, in general, focus only upon those reaction schemes for which such a *diffusion equation* representation is consistent with the underlying physics [29].

The starting point for our analysis is the four-dimensional microscale conservation equation governing both size-specific spatial ($\mathbf{R}$) and position-specific aggregational (n) transport of the tracer cluster through the unbounded fluid:

$$\frac{\partial P}{\partial t} + \nabla \cdot \mathbf{J} = j_n - j_{n-1}, \tag{10.2}$$

where $P \equiv P(\mathbf{R}, n, t|\mathbf{R}', n_o) \equiv P(\mathbf{R} - \mathbf{R}', n, t|n_o)$ represents the complete microscale conditional probability density (Green's function) signifying the probability that at a time t the tracer cluster is of aggregation number n and is located at position $\mathbf{R}$, given that at time $t = 0$ the cluster was centered at position $\mathbf{R}'$ and was of size n_o.[1] The operator $\nabla \equiv (\partial/\partial\mathbf{R})_{n,t}$ denotes the size-specific physical-space gradient operator. The physical- and size-space fluxes of the probability density P, are denoted respectively by $\mathbf{J}$ and j. In situations wherein a large range of aggregation numbers are possible (such as will be assumed of all the examples considered in this paper), it is permissible to replace the above discrete 'diffusion equation' (10.2) by a version involving a continuously varying index n:

$$\frac{\partial P}{\partial t} + \nabla \cdot \mathbf{J} + \frac{\partial j}{\partial n} = 0, \tag{10.3}$$

[1]Because the physical space is assumed infinite and homogeneous throughout, only the difference $\mathbf{R} - \mathbf{R}'$ appears, rather than $\mathbf{R}$ and $\mathbf{R}'$ separately.

wherein $j \equiv j(\mathbf{R}, n, t|n_o)$ now represents the size-space flux, a continuous function of n, and $\partial/\partial n \equiv (\partial/\partial n)_{\mathbf{R},t}$ denotes the position-specific size-space gradient operator..

The fluxes $\mathbf{J}$ and j, can be expected constitutively [4] to possess conventional convective and diffusive contributions as follows:

$$\mathbf{J} = M(n)\mathbf{F}(n)P - D(n)\nabla P, \tag{10.4}$$

$$j = m(n)f(n)P - d(n)\frac{\partial P}{\partial n}, \tag{10.5}$$

wherein $M(n)$ denotes the physical-space cluster mobility coefficient, and $\mathbf{F}(n)$ the external vector force exerted on the cluster as a whole. Their respective counterparts in size space are denoted by $m(n)$ and $f(n)$. Diffusivities in physical and size space, respectively denoted by $D(n)$ and $d(n)$, are related to the respective hydrodynamic mobility coefficients through configuration-specific Stokes-Einstein relations [11]:

$$D(n) = k_B T\, M(n); \quad d(n) = k_B T\, m(n), \tag{10.6}$$

with k_B the Boltzmann constant. For the reversible reaction schemes subsequently considered, the scalar force $f(n)$ can always be written as the negative size-space gradient of a potential energy function $V(n)$ [see sections 10.2 and 10.4]. Use of this information together with eq. (10.6) permits (10.5) to be rewritten as

$$j = -d(n)\exp\left[-V(n)/k_B T\right]\frac{\partial}{\partial n}\left\{P\exp\left[V(n)/k_B T)\right]\right\}. \tag{10.7}$$

The above microscale data are to be supplemented by respective physical- and size-space boundary conditions. The former is embodied in the generic requirement that all the algebraic moments of the distribution function P converge, namely [13] [also cf. eq. (8.9)]

$$|\mathbf{R} - \mathbf{R}'|^m P \to 0 \quad (m = 0, 1, 2, \dots) \text{ as } \quad |\mathbf{R} - \mathbf{R}'| \to \infty, \tag{10.8}$$

and the latter as

$$j = 0 \quad \text{for} \quad n = 1, \infty. \tag{10.9}$$

In addition, we have for the initial condition that

$$P = \begin{cases} \delta(\mathbf{R} - \mathbf{R}')\delta(n - n_o) & (t = 0), \\ 0 & (t < 0), \end{cases} \tag{10.10}$$

with δ the Dirac delta function, and n_o the initial size of the cluster at time $t = 0$. Satisfaction of (10.8) assures the convergence of the various momental integrals arising in the general theory [4]. It is also readily verified from the above system of equations that the solution P satisfies the normalization condition

$$\int_{\mathbf{R}_\infty} \int_1^\infty P(\mathbf{R} - \mathbf{R}', n, t|n_o)\, dn\, d^3\mathbf{R} = 1 \quad (t > 0) \quad \forall (n_o, \mathbf{R}'). \tag{10.11}$$

In the above, $d^3\mathbf{R}$ denotes a volume element in three-dimensional physical space and dn the comparable-size space incremental element. Size space is assumed to extend from the basic monomer unit ($n = 1$) to clusters of size $n = \infty$. Note that we have used the Euler-Maclaurin sum formula to replace the sum over the discrete index n by a comparable integration over the continuous index n. Equation (10.11) shows that the total probability of finding the tracer somewhere in physical space, $\mathbf{R}_\infty : \{-\infty < x_i < \infty; i = 1, 2, 3\}$, and contained within a cluster of some size $n : \{1 \leq n < \infty\}$ is conserved at each instant.

As stated in the Introduction, physical interest generally centers not on the four-dimensional microscale distribution P, but rather only on the coarse-scale macroscopic descriptor $\bar{P}$ of the transport processes occurring in three-dimensional physical space, as embodied in the macroscale conditional density:

$$\bar{P}(\mathbf{R} - \mathbf{R}', t|n_o) \stackrel{\text{def.}}{=} \int_1^\infty P(\mathbf{R} - \mathbf{R}', n, t|n_o)\, dn. \tag{10.12}$$

It is an immediate consequence of (10.11) and (10.12) that this coarse-grained probability is conserved in physical space:

$$\int_{\mathbf{R}_\infty} \bar{P}(\mathbf{R}-\mathbf{R}',t|n_o)d^3\mathbf{R} = 1 \ (t>0) \quad \forall(n_o,\mathbf{R}'). \tag{10.13}$$

Asymptotically, for sufficiently long times (see below), $\bar{P}$ is independent of the initial cluster size n_o [4], and hence is functionally of the form $\bar{P}(\mathbf{R}-\mathbf{R}',t)$.

The initial- and boundary-value problem posed by the system of microscale equations (10.3) - (10.11) possesses the same physico-mathematical structure as that of the generic problem of macrotransport theory outlined in the previous chapters. This equivalence is established when one identifies the size (n) and physical-space position ($\mathbf{R}$) with the respective 'local' ($\mathbf{q}$) and 'global' ($\mathbf{Q}$) coordinates of the latter theory. In this case, macrotransport theory shows that, for long times, namely $||d(n)||t/\bar{n}^2 \gg 1$ (with $||d(n)||$ denoting some norm of the size-space diffusivity, and $\bar{n}$ denoting the mean aggregation number), the asymptotic solution P of eq. (10.3) satisfying (10.4) - (10.11) matches momentwise the comparable dominant long-time asymptotic solution of $\bar{P}$, whose transport through physical space is governed by eq. (10.1) together with the respective boundary and initial conditions

$$|\mathbf{R}-\mathbf{R}'|^m\bar{P} \to 0 \quad (m=0,1,2,\dots) \ \text{ as } \quad |\mathbf{R}-\mathbf{R}'| \to \infty \tag{10.14}$$

and

$$\bar{P} = \begin{cases} \delta(\mathbf{R}-\mathbf{R}') & (t=0), \\ 0 & (t<0). \end{cases} \tag{10.15}$$

Furthermore, by virtue of having matched the respective moments of $\bar{P}$ and P, the theory also provides an explicit scheme for determining the macrotransport coefficients $\bar{\mathbf{U}}$ and $\bar{\mathbf{D}}$ via appropriate quadratures of the specified microscale phenomenological data [data explicitly embodied in the microscale transport coefficients, and

implicitly appearing in eqs. (10.3) - (10.5)] over the cluster-size domain.

Implementation of the theory [4] requires, *inter alia*, knowledge of the solution of a steady-state scalar field $P_0^\infty(n)$, the latter corresponding to the steady, long-time limit of the unsteady-state conditional probability density,

$$P_0(n,t|n_o) \stackrel{\text{def.}}{=} \int_{\mathbf{R}_\infty} P(\mathbf{R}-\mathbf{R}',n,t|n_o)\, d^3\mathbf{R},$$

that the cluster possesses a size n at time t irrespective of its physical-space location $\mathbf{R}$. The equations and the boundary conditions satisfied by the field $P_0^\infty(n)$ was outlined in a chapter 8 [refer eqs. (8.21) - (8.24)]. However, to maintain continuity within the text, in what follows we list the comparable equations and the boundary conditions satisfied by $P_0^\infty(n)$ for the specific case wherein the 'size' coordinate constitutes the local space of transport. Thereby, the field $P_0^\infty(n)$ satisfies the steady-state differential equation

$$\frac{dj_0^\infty}{dn} = 0, \tag{10.16}$$

with

$$j_0^\infty(n) \stackrel{\text{def.}}{=} -d\exp(-V/k_BT)\frac{d}{dn}[P_0^\infty \exp(V/k_BT)], \tag{10.17}$$

in which the latter flux density satisfies the boundary conditions

$$j_0^\infty = 0 \quad \text{at} \quad n = 1,\infty \tag{10.18}$$

together with the normalization condition

$$\int_1^\infty P_0^\infty\, dn = 1. \tag{10.19}$$

The solution of eqs. (10.16) to (10.19) is

$$P_0^{\infty}(n) = \left\{ \int_1^{\infty} \exp\left[-V(n)/k_BT\right] dn \right\}^{-1} \exp\left[-V(n)/k_BT\right]. \tag{10.20}$$

The macrotransport coefficients $\bar{\mathbf{U}}$ and $\bar{\mathbf{D}}$ appearing in eq. (10.1) are expressed in terms of respective quadratures of $P_0^{\infty}(n)$ [cf. eq. (8.16)]. In this manner, the average settling velocity $\bar{\mathbf{U}}$ of the cluster is given by

$$\bar{\mathbf{U}} = \bar{U}\hat{\mathbf{F}}, \tag{10.21}$$

where

$$\bar{U} \equiv \langle U(n) \rangle \stackrel{\text{def.}}{=} \int_1^{\infty} dn\, P_0^{\infty}(n)\, U(n), \tag{10.22}$$

in which

$$U(n) = M(n)F(n) \tag{10.23}$$

is the settling velocity of an aggregate of size n, and $\hat{\mathbf{F}} = \mathbf{F}/F(n)$ represents a unit vector in the spatial direction parallel to the applied force $\mathbf{F}$, in which $F(n) = |\mathbf{F}(n)|$.

The dispersivity dyadic is represented by the sum [4]

$$\bar{\mathbf{D}} = \bar{D}^M \mathbf{I} + \bar{D}^C \hat{\mathbf{F}}\,\hat{\mathbf{F}}, \tag{10.24}$$

wherein

$$\bar{D}^M \equiv \langle D^M(n) \rangle \stackrel{\text{def.}}{=} \int_1^{\infty} dn\, P_0^{\infty}(n)\, D(n) \equiv k_BT \int_1^{\infty} dn\, P_0^{\infty}(n) M(n) \tag{10.25}$$

is the average physical-space molecular diffusivity of the cluster, and

$$\bar{D}^C = \int_1^\infty dn P_0^\infty(n) B(n)[U(n) - \bar{U}] \tag{10.26}$$

represents the Taylor or convective contribution to the dispersivity. The latter contribution stems from the continuous variation in settling velocity arising from the size-space transport processes (i.e. due to continuous changes in the size of the cluster as it traverses the fluid).

Appearing in the latter integral is the other scalar field, $B(n)$ which represents the solution of the differential equation [4]

$$j_0^\infty(n)\frac{dB}{dn} - \frac{d}{dn}\left[P_0^\infty d(n)\frac{dB}{dn}\right] = P_0^\infty(n)[U(n) - \bar{U}], \tag{10.27}$$

subject to the boundary conditions:

$$\frac{dB}{dn} = 0 \quad \text{at} \quad n = 1, \infty. \tag{10.28}$$

The solution of eqs. (10.27) - (10.28) can easily be obtained from the knowledge of the field P_0^∞ given by (10.20), yielding

$$B(n) = b_o - \int_1^n dn' \frac{\exp[V(n')/k_BT]}{d(n')} \int_1^{n'} d\tilde{n}[U(\tilde{n}) - \bar{U}] \exp[-V(\tilde{n})/k_BT], \tag{10.29}$$

where b_o is an integration constant whose numerical value is irrelevant in establishing $\bar{D}^C$ via (10.26). Substitution of (10.29) into (10.26) yields the following expression for $\bar{D}^C$:

$$\begin{aligned}\bar{D}^C = &\left\{\int_1^\infty dn \exp[-V(n)/k_BT]\right\}^{-1} \int_1^\infty dn'' \frac{\exp[V(n'')/k_BT]}{d(n'')} \\ &\left\{\int_1^{n''} dn'[U(n') - \bar{U}] \exp[-V(n')/k_BT]\right\}^2.\end{aligned} \tag{10.30}$$

Explicit calculation of $\bar{U}$, $\bar{D}^M$ and $\bar{D}^C$ from the preceding formulas requires speci-

fying constitutive equations for both the size- and physical-space mobility coefficients, $m(n)$ and $M(n)$, respectively, as well as the size-space potential $V(n)$. As already indicated, a variety of schemes can be imagined for constitutively quantifying the A - D size-space transport processes. However, the above formulation is sufficiently general to provide robust generic prescriptions for determining the three macrotransport coefficients pending explicit specification of the requisite constitutive relationships.

An outline of the rest of the paper is as follows: To place the preceding concepts on a firmer basis while also illustrating the significance of size variation effects, two distinct A - D schemes will be considered. Sections 10.2 and 10.4 each outline respective schemes whereby the the master equation for the size-space transport processes can be recast into a diffusion equation format, thereby identifying both $d(n)$ and $V(n)$. In sections 10.3 and 10.5 we revert to the generic quadrature formula developed in section 10.1, using appropriate models for the physical-space transport coefficients $M(n)$[and hence $D(n)$] to obtain the macrotransport coefficients $\bar{\mathbf{U}}$ and $\bar{\mathbf{D}}$. Section 10.6 concludes with an outlook for future research directions.

10.2 Size-space Diffusion Equation Describing Step-wise Association

10.2.1 Basic Reaction

Step-wise association schemes serve as models of the association - dissociation (A - D) processes governing the growth of spherical micelles [1]. Herein, the basic unit is taken to be a monomer, denoted by A_1. The A - D scheme can then be portrayed as a reversible reaction of the following general form

$$A_{n-1} + A_1 \underset{k^-_{n-1}}{\overset{k^+_{n-1}}{\rightleftharpoons}} A_n, \tag{10.31}$$

wherein A_n denotes a cluster containing n monomers. The micellar solution is assumed to be at equilibrium (size-wise) at the start of the observation process. We

then select a monomer molecule bound to a cluster as our tracer and subsequently follow its evolution as it moves through the solvent. This monomer tracer can undergo the following transport processes: (i) diffusion and sedimentation bound to a cluster of the same size; (ii) transport bound to a cluster of a different size resulting from A - D processes of monomers to and from the original cluster; (iii) dissociation of the tracer monomer from the cluster to recombine with another cluster. During each of these processes the tracer undergoes physical-space transport representative of a cluster whose dimensions are identical to that of the cluster to which the monomer is instantaneously attached. As such, the monomer tracer undergoing these transport processes may be equivalently represented by a tracer cluster undergoing continuous changes in size, simultaneous with the cluster undergoing movement through the fluid continuum. In the following, a tracer cluster will be taken to denote a cluster with $n > 2$. As elucidated later, transport by mechanism (iii), which occurs when the tracer is present as a monomer, is accounted for in an indirect manner.

The procedure employed to derive the size-space diffusion equation is outlined below. This scheme is identical to that employed in the next section to derive the comparable equation for the case of a worm-like micelle. In either case we consider a solution initially at equilibrium with respect to transport in size space (i.e. one wherein the equilibrium size distribution prevails). Into this solution we imagine a tracer cluster to be added, which then undergoes physical-space transport as well as the reversible A - D processes described by eq. (10.31). As is rigorously proved within the framework of generalized Taylor dispersion theory, the initial size of such a cluster proves irrelevant in the calculation of macrotransport coefficients. In addition to the original assumption of an equilibrium solution (requiring that the concentration of 'non-tracer' clusters satisfy the law of mass action[2]) we subsequently we employ a master equation approach to quantify the rate of change of the cluster probability dis-

[2]Note that the assumption of an initially equilibrium solution is not equivalent to the (incorrect) requirement that the size-space probability distribution of the tracer cluster possesses its equilibrium value. The introduction of a tracer cluster into a bath of clusters which are at equilibrium disturbs the bath only mildly; nevertheless it has a non-trivial effect on the unsteady-state development of the cluster size-space probability distribution.

tribution, thereby obtaining an appropriate continuous size-space transport equation governing movement of the tracer cluster.

10.2.2 Master Equation for the Tracer

Based on the above reaction scheme for representing the A - D processes one can write a master equation for $P(n)$ (whose explicit time dependence is notationally suppressed), namely the probability that the tracer is present in a cluster containing n monomers, including itself, irrespective of its position in the physical space. Such an equation is derived by considering the possible A-D reactions undergone by the *tracer* cluster containing n monomers (denoted as A_n^*):

$$A_{n-1}^* + A_1 \underset{k_{n-1}^-}{\overset{k_{n-1}^+}{\rightleftharpoons}} A_n^*, \tag{10.32}$$

$$A_n^* + A_1 \underset{k_n^-}{\overset{k_n^+}{\rightleftharpoons}} A_{n+1}^*. \tag{10.33}$$

Accordingly, the master equation governing the probability $P(n)$ satisfies the equation

$$\frac{dP(n)}{dt} = k_{n-1}^+ \, P(n-1)X_1 - k_{n-1}^- \, P(n) + k_n^- \, P(n+1) - k_n^+ \, P(n)X_1, \tag{10.34}$$

in which X_1 denotes the concentration of the free monomeric species. As a simplification we assume that k^- is independent of n. This will subsequently be shown to be equivalent to the assumption that $d(n)$ in (10.5) is independent of n. While the prescription in section 2 is general enough to treat other cases, we nevertheless invoke this assumption so as to focus exclusively upon the effect of the A - D processes on the physical-space macrotransport coefficients. Based on the above assumption we

obtain that

$$\frac{dP(n)}{dt} = k^{-}\left[\frac{k_{n-1}^{+}}{k^{-}}\,P(n-1)X_1 - P(n) + P(n+1) - \frac{k_n^{+}}{k^{-}}\,P(n)X_1\right]. \tag{10.35}$$

Equilibrium considerations for reactions (10.32) and (10.33) on the other hand require that

$$\frac{k_{n-1}^{+}}{k^{-}} = \exp\left[-\frac{(\mu_n^{*} - \mu_{n-1}^{*} - \mu_1^{o})}{k_B T}\right]; \quad \frac{k_n^{+}}{k^{-}} = \exp\left[-\frac{(\mu_{n+1}^{*} - \mu_n^{*} - \mu_1^{o})}{k_B T}\right], \tag{10.36}$$

in which μ_n^{*} denotes the standard-state chemical potential of the cluster of size n. The latter is equal to the free energy change occurring when a cluster of size n is introduced into the pure solvent; μ_1^{o} represents the comparable standard-state chemical potential of the monomer [19]. For the dilute solutions assumed, the chemical potential μ_1 of the monomer can be expected to obey the ideal solution relation

$$\mu_1 = \mu_1^{o} + k_B T \ln X_1. \tag{10.37}$$

Upon using eq. (10.37) and writing $\mu_1^{o} = n\mu_1^{o} - (n-1)\mu_1^{o}$ we obtain

$$\frac{k_{n-1}^{+}X_1}{k^{-}} = \exp\left\{-\frac{[\mu(n) - \mu(n-1)]}{k_B T}\right\}; \quad \frac{k_n^{+}X_1}{k^{-}} = \exp\left\{-\frac{[\mu(n+1) - \mu(n)]}{k_B T}\right\}. \tag{10.38}$$

In the above, $\mu(n) \equiv \mu_n^{*} - n\mu_1$. Insertion of the above identification into eq. (10.35) yields

$$\frac{dP(n)}{dt} = k^{-}\left\{P(n-1)\,\exp\left[-\frac{[\mu(n) - \mu(n-1)]}{k_B T}\right] - P(n) + P(n+1) - P(n)\exp\left[-\frac{[\mu(n+1) - \mu(n)]}{k_B T}\right]\right\}. \tag{10.39}$$

van Kampen's [26] expansion method may be utilized in the above discrete master equation to derive the aggregation-space diffusion equation corresponding to the limit

of a continuous variation of sizes. This continuum limit is obtained by introducing a parameter Ω denoting the density of the discrete variable n, followed by an expansion in $1/\Omega$. Upon setting $x = n/\Omega$, $P(x\Omega) = p(x)$ and $\mu(x\Omega)/k_BT = v(x)$, eq. (10.39) becomes

$$\frac{dp(x)}{dt} = k^- \Big[p(x - \frac{1}{\Omega}) \ \exp\{-[v(x) - v(x - 1/\Omega)]\} - p(x) + p(x + \frac{1}{\Omega}) \\ - p(x) \exp\{-[v(x + 1/\Omega) - v(x)]\} \Big]. \tag{10.40}$$

The right-hand side of the above equation can be expanded in a Taylor series around x and the resultant expression simplified. For the sake of brevity the details of such an exercise are omitted here, ultimate result being

$$\frac{\partial p(x)}{\partial t} = \frac{k^-}{\Omega^2} \frac{\partial}{\partial x} \left[\frac{\partial p}{\partial x} + p(x) \frac{\partial v}{\partial x} \right] + O(\frac{1}{\Omega^4}). \tag{10.41}$$

To terms of leading order the above equation resembles a diffusion equation in the presence of a field of force, which can be recast in terms of our original variables as

$$\frac{\partial P(n)}{\partial t} = k^- \frac{\partial}{\partial n} \left\{ \frac{\partial P}{\partial n} + P(n) \frac{\partial [\mu(n)/k_BT]}{\partial n} \right\}. \tag{10.42}$$

The latter is equivalent to the diffusion equation

$$\frac{\partial P(n)}{\partial t} + \frac{\partial j}{\partial n} = 0, \tag{10.43}$$

[cf. eqs. (10.3) and (10.7)], wherein the following identifications hold [in (10.5)]:

$$m(n) = k^-; \quad V(n) = \mu(n); \quad d(n) = k^-. \tag{10.44}$$

The relationship between eqs. (10.43) and (10.3) is such that the former may be regarded as a transport equation in size-space for circumstances where the 'source-term' $\nabla \cdot \mathbf{J} = 0$, such as would be the case when the probability density P appearing in eqs. (10.3) - (10.7) was independent of $\mathbf{R}$.

10.2.3 Model for μ_n^o

This section deals with the identification of the potential $V(n) \equiv \mu(n)$. Experimental observations [19] in spherical micellar solutions indicate the existence of an equilibrium size distribution characterized by a slight degree of polydispersivity centered around a mean aggregation number. Based on these observations we propose the following simple quadratic model for the potential:

$$\frac{V(n)}{k_B T} = \hat{V}_o + \frac{(n-\bar{n})^2}{2\sigma^2}, \tag{10.45}$$

where $\bar{n}$ represents the mean aggregation number and σ quantifies the degree of polydispersivity. The numerical value of constant $\hat{V}_o \equiv V(\bar{n})/k_B T$ proves to be irrelevant under subsequent normalization. Furthermore, in the ensuing analysis k^- will be set to unity without any loss of generality. This completes the size-space identifications prerequisite to performing explicit calculations of the macrotransport coefficients.

10.2.4 Time Scales

Our coarse-grained quantification of the overall transport process can be justified only in circumstances for which the time scales T characterizing the A - D processes are much less than those characterizing the physical-space transport processes, thereby enabling us to assume an instantaneous size-space equilibrium distribution despite a comparable lack of equilibrium in physical space. Typical values describing the kinetics of the aggregation process involve time scales of micro- to milli-seconds [18, 1]. On the other hand, transport in physical space typically involves a diffusion coefficient of $O(10^{-5}\text{cm}^2/\text{s})$ [8]. For a dilute solution (wherein the mean interparticle separation is quite large) one can easily corroborate the assertion that T(physical-space diffusion) $\gg T$(kinetics).

10.2.5 Transport by Mechanism (iii)

In the above analysis the cluster has been consistently assumed to be of a size such that $n > 2$, with the possibility of transport as a monomer ignored. The reason for such an approach resides in the fact that a monomer does not satisfy the general form of the master equation (10.34). Under the long-time limit considered in section 3, the tracer can be expected to possess a probability $X_1/X_s \equiv p$ of evolving as a monomer, where X_s is the total solute concentration in the solution. Thereby, the normalization condition (10.19) needs to be modified to the form

$$\int_1^\infty dn\, P_0^\infty = 1 - p. \tag{10.46}$$

However, we ignore the above constraint with the understanding that the macrotransport coefficients $\bar{U}, \bar{D}$, etc., as calculated in section 3, need to be corrected for the presence of monomer transport by appropriate renormalization, e.g.,

$$\bar{M}(\text{Section 4}) = \frac{\bar{M}(\text{actual})}{1-p} - \frac{p\,M(\text{monomer})}{1-p}, \quad \text{etc.} \tag{10.47}$$

10.3 Macrotransport Coefficients for Spherical Micellar Solutions

Identification of the size-space mobility coefficient $m(n)$ and the potential energy driving force $V(n)$ for the spherical micelle case was effected in section 10.2. The latter identified the potential in terms of the mean aggregation number $\bar{n}$ and spread σ in the chemical potential distribution. Calculation of the macrotransport coefficients requires specification of the physical-space mobility coefficient $M(n)$ and force $F(n)$. For the present spherical micellar case the physical-space mobility coefficient can be obtained from Stokes law by modeling the cluster as an impermeable sphere of radius r. The corresponding mobility then scales inversely with the radius of the sphere.

The radius of the spherical micelle can itself be related to the aggregation number as

$$r(n) \propto n^{1/3}, \tag{10.48}$$

whence the mobility obeys the relationship

$$\frac{M(n)}{M(\bar{n})} = \frac{n^{-1/3}}{\bar{n}^{-1/3}}. \tag{10.49}$$

Furthermore, using the fact that the force $F(n)$ on a cluster scales with n, we have that

$$\frac{U(n)}{U(\bar{n})} = \frac{n^{2/3}}{\bar{n}^{2/3}}. \tag{10.50}$$

This serves to identify the physical-space coefficients prerequisite to calculating the macrotransport coefficients $\bar{\mathbf{U}}, \bar{\mathbf{D}}$ via eqs. (10.21) - (10.25) and (10.30). The remaining size-space coefficients are identified in section 10.2 [cf. eqs. (10.44), (10.45)].

Use of the preceding identifications in eq. (10.20) yields

$$P_0^{\infty}(n) = \left\{ \int_1^{\infty} dn \exp\left[-\frac{(n-\bar{n})^2}{2\sigma^2} \right] \right\}^{-1} \exp\left[-\frac{(n-\bar{n})^2}{2\sigma^2} \right]. \tag{10.51}$$

The fact that the lower limit of integration in the normalizing weight function is cut off at $n = 1$ rather than $n = 0$ results in analytic expressions that are quite cumbersome. However, the computed values do not depend crucially on the lower limit used in evaluating the above integrals so long as the mean aggregation number is sufficiently large and the distributional spread small compared with the mean aggregation number. This represents the situation typically encountered for spherical micellar solutions [20]. In such circumstances it is possible to replace the lower integration limit by $n = 0$ without significant error. The resulting expressions for the macrotransport coefficients obtained from eqs. (10.21) - (10.25) and (10.30) can then

be generically expressed in terms of a scaling function as

$$\psi = \bar{n}^{\nu} f(\tilde{\sigma}), \tag{10.52}$$

wherein ψ represents a generic macrotransport coefficient and f denotes a scaling function that exhibits the following behavior:

$$f(x) \longrightarrow \begin{cases} 1 & (x \to 0), \\ x^{\alpha} & (x \gg 1), \end{cases}$$

in which the exponents α and ν depend[3] upon the specific transport coefficient being considered. Also appearing in (10.52) is the weighted distributional spread:

$$\tilde{\sigma} \stackrel{\text{def.}}{=} \frac{\sigma}{\bar{n}^{1/2}}. \tag{10.53}$$

When the lower limit in eq. (10.51) cannot be replaced by zero, such as occurs when the spread satisfies the inequality $\tilde{\sigma} > 1$, the above scaling arguments do not hold and the resulting transport coefficients depend nontrivially on the mean aggregation number $\bar{n}$. Despite the fact that some of the assumptions underlying the analysis do not remain rigorously valid in such circumstances [cf. the discussion preceding eq. (10.45)] we have nevertheless also studied such cases.

The analytic quadratures obtained by substituting eqs. (10.49) - (10.51) into (10.21) - (10.25) for the $n = 0$ case can be expressed in terms of parabolic cylinder functions, whose asymptotic expansions are well documented [16]. In the following discussion, however, owing to their algebraic complexity we do not present explicit analytic expressions for the resulting macrotransport coefficients, as such formulae are not very illuminating in and of themselves. Instead, we indicate qualitative features (obtained numerically) describing the functional dependence of the macrotransport coefficients upon the spread in cluster sizes. All of the resulting features are

[3]The exponent ν can be obtained from the knowledge of the variation of ψ with $\bar{n}$ for a monodisperse solution.

graphically indicated in terms of the scaling variable $\tilde{\sigma}$. Even in those cases wherein replacement of the lower integration limit by zero does not strictly hold, we found that the qualitative features displayed in the subsequent plots are not significantly altered. Accordingly, we have restricted ourselves in what follows primarily to studying the effect of the scaled variable $\tilde{\sigma}$ upon the three macrotransport coefficients.

Mean Velocity of Settling: Figure (10-1) depicts the effect of the size-distribution spread upon the ratio of the mean cluster settling velocity $\bar{U}$ to that of the settling velocity $U(\bar{n}) \equiv M(\bar{n})F(\bar{n})$ at the mean aggregation number. Initially, for small departures from monodispersivity, this ratio decreases below unity, followed by a steep rise thereafter. The physical explanation of this behavior is straightforward: As already noted, the settling velocity scales as $n^{2/3}$. For small values of the spread $\tilde{\sigma}$, the smaller values of n are sampled more frequently than are the larger values.[4] This leads to a reduction in the mean settling velocity below that which would have occurred had the tracer size simply coincided with the mean aggregation number. However, at the larger values of $\tilde{\sigma}$ the lower limit is cutoff at $n = 1$, whereas no such constraint exists for the upper limit. Thus, when the chemical potentials are such that a large spread in the distribution occurs, the mean settling velocity will generally far exceed the settling velocity occurring at the mean aggregation number. Furthermore, from the computed values it can be discerned that the scaling function in the above exhibits exponents $\nu = 1/3$ and $\alpha \sim 2/3$.[5]

Mean Diffusivity: Polydispersivity effects on the normalized mean molecular diffusivity, $\bar{D}^M/D^M(\bar{n})$ are portrayed in Fig. (10-2). Since the microscale diffusivity $D(n)$ scales as $n^{-1/3}$ the observed variation is consistent with the expected initial rise deriving from the preferential sampling of the smaller aggregation numbers, followed by a manifestation of the effect of the cut off at the lower aggregation number limit. Scaling exponents for this case were determined from the plots to be $\nu = -1/3$ and $\alpha = -0.4$.

---

[4]Denote $n/\bar{n} = x$. Then the average of weights of two sizes $n - \bar{n}$ and $n + \bar{n}$ on either side of the mean aggregation number is $\propto \frac{1}{2}[(1-x)^{2/3} + (1+x)^{2/3}] \propto (1 - \frac{1}{9}x^2) < 1$.

[5]Since $n^{2/3} \to 0$ as $n \to 0$, for large $\tilde{\sigma}$ the expression for the mean velocity can be written approximately in this limit as $\int_0^\infty dn\, n^{2/3} \exp(-n^2/2\tilde{\sigma}^2) / \int_0^\infty dn \exp(-n^2/2\tilde{\sigma}^2) \sim \tilde{\sigma}^{2/3}$ by simple scaling arguments.

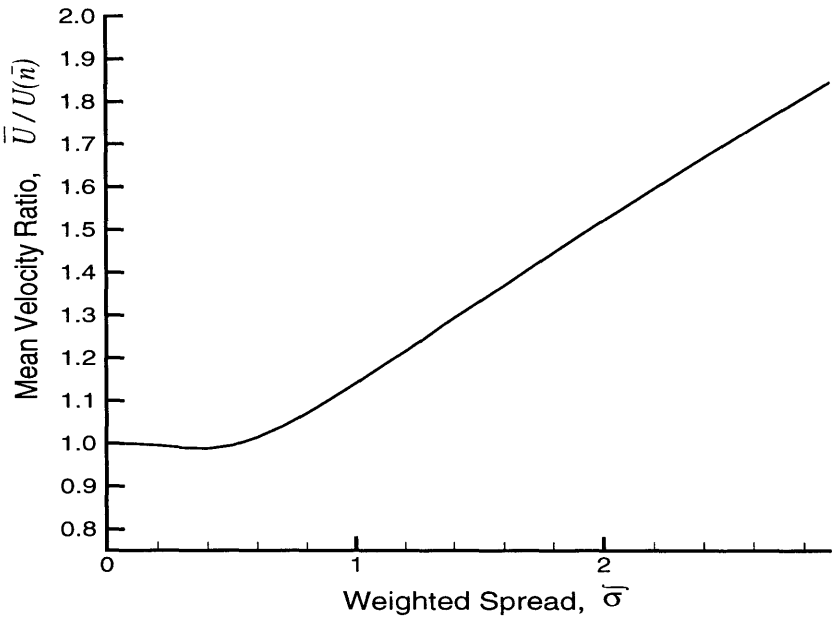

Figure 10-1: Effect of polydispersivity $\tilde{\sigma}$ on the mean settling velocity ratio $\bar{U}/U(\bar{n})$ for spherical micellar solutions.

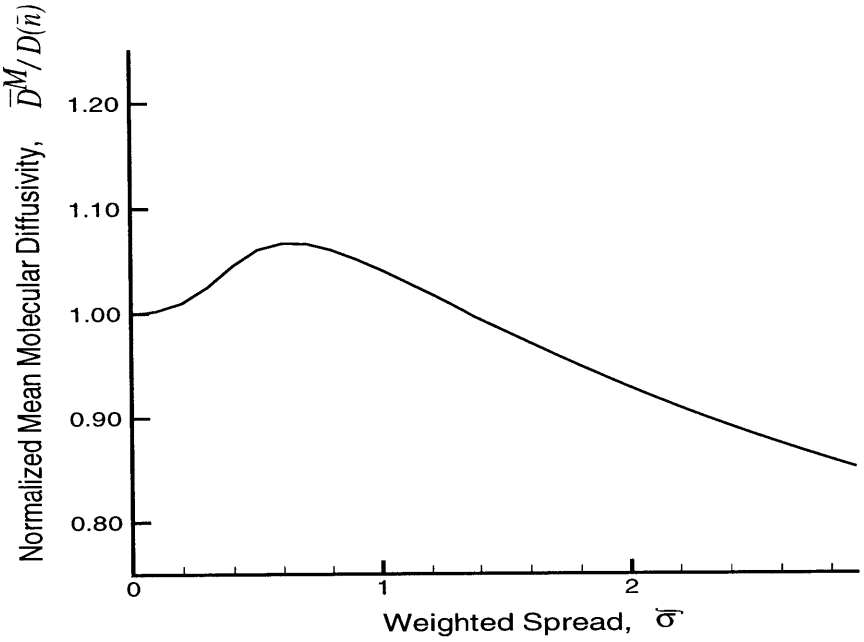

Figure 10-2: Effect of the polydispersivity $\tilde{\sigma}$ on the normalized mean molecular diffusivity $\bar{D}^M/D(\bar{n})$ for spherical micellar solutions.

Convective Dispersivity: Figure (10-3) depicts the effect of varying the size distribution on the convective dispersivity, indicating a monotonic increase with increasing departure from monodispersivity. No counterpart of this Taylor dispersion phenomenon arises during either the diffusion or sedimentation of *monodisperse* clusters. The qualitative trends depicted in Fig. (10-3) are completely consistent with the fluctuational origins of $\bar{D}^C$.

Significance of results: The above plots display the respective variations in the three macrotransport coefficients caused by the size-induced spread in chemical potential. Each manifests polydispersivity effects resulting from the reversible A - D processes, wherein the cluster-size growth mechanism occurs by stepwise association processes. In practical situations involving spherical micellar solutions the above effects are unlikely to prove very significant owing to the relatively low polydispersivity

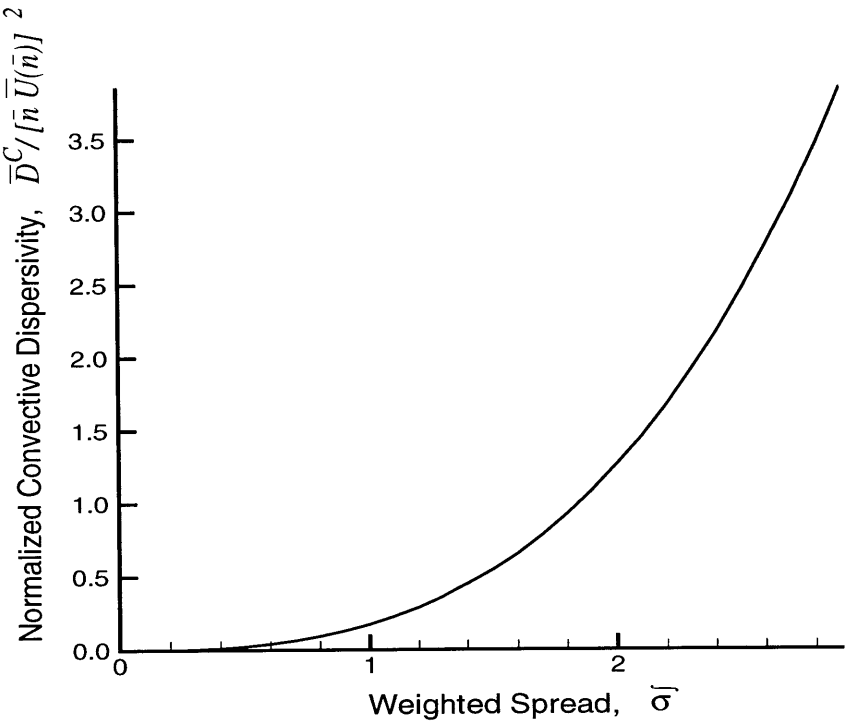

Figure 10-3: Dependence of the normalized convective dispersivity $\bar{D}^C/[\bar{n}U(\bar{n})]^2$ on the degree of polydispersivity $\tilde{\sigma}$ for spherical micellar solutions.

indices typically encountered in such systems. Nevertheless, our analysis provides rigorous estimates of the magnitudes of such effects. A perhaps unexpected feature of this example is the existence of a convective or Taylor contribution to the diffusional process, a phenomenon which has no counterpart in monodisperse micellar solutions.

It might appear that the above features with respect to both the mean molecular diffusivity and mean settling velocity could be subsumed under the choice of an appropriately defined mean aggregation number. For instance, one might propose to define a mean aggregation number, $\tilde{n}$, say, based upon the observed settling velocity:

$$\frac{\bar{U}}{U(\bar{n})} = \frac{\tilde{n}^{2/3}}{\bar{n}^{2/3}}. \tag{10.54}$$

This choice would, however, imply that

$$\frac{\bar{D}^M}{D(\bar{n})} \neq \frac{\tilde{n}^{-1/3}}{\bar{n}^{-1/3}}, \tag{10.55}$$

an apparent violation of the Stokes-Einstein equation owing to the fact that

$$\bar{U} = \langle M(n)F(n)\rangle \neq \langle M(n)\rangle\langle F(n)\rangle. \tag{10.56}$$

If, alternatively, one chose to define a mean mobility coefficient such that

$$\langle \tilde{M}(n)\rangle \stackrel{\text{def.}}{=} \frac{\bar{U}}{\langle F(n)\rangle}, \tag{10.57}$$

then

$$\bar{D}^M = k_B T\langle M(n)\rangle \neq k_B T\langle \tilde{M}(n)\rangle. \tag{10.58}$$

The latter serves to quantify the apparent violation of the Stokes-Einstein relationship. Figure (10-4) displays the ratio $\langle \tilde{M}(n)\rangle/\langle M(n)\rangle$ obtained for different $\tilde{\sigma}$.

Illustrated in this section were several effects arising from the spread in cluster sizes about a mean aggregation number. Specifically, the spherical micellar solution case was motivated by the availability of the constitutive equations for the microscale

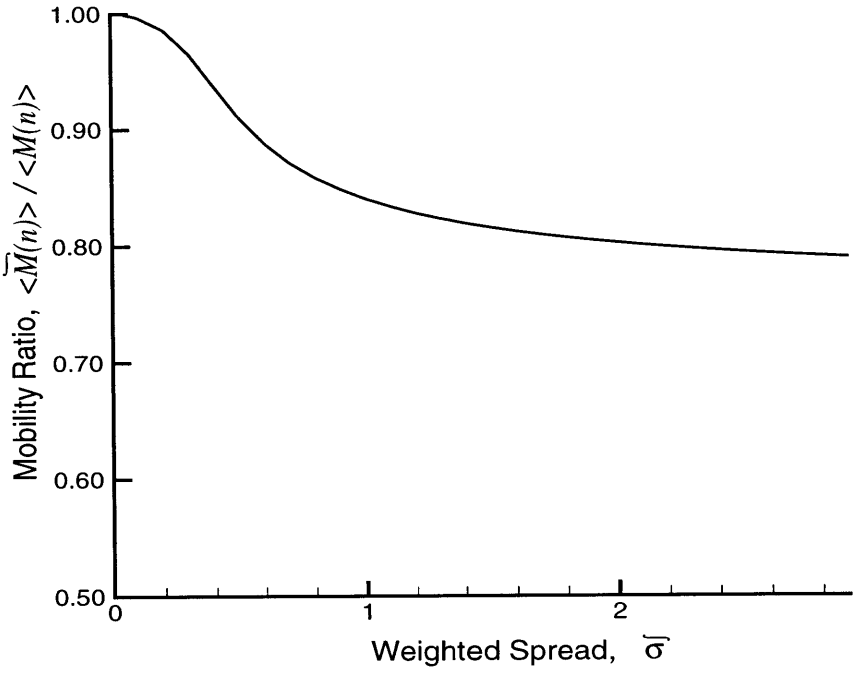

Figure 10-4: Dependence of the mobility ratio $\langle \tilde{M}(n) \rangle / \langle M(n) \rangle$ on the polydispersivity parameter $\tilde{\sigma}$ for spherical micellar solutions.

size- and physical-space transport coefficients. The next section quantifies similar behavior for another important case, wherein the cluster size distribution exhibits novel features not present in the spherical micellar case.

10.4 Size-space Diffusion Equation for a Worm-like Micelle (Living Polymer)

Worm-like micelles provide an interesting class of micellar entities, distinct from the spherical micelles considered in the previous section. Studies of these systems were pioneered by Cates [5, 6]. Unlike spherical micellar solutions, which display an equilibrium size-distribution peaked around a mean aggregation number $\bar{n}$, worm-like micelles manifest a range of sizes extending over a significant interval. The latter scenario provides a natural background to illustrate extremal size-distribution effects. Explicitly, this section is concerned with the derivation of the size-space diffusion equation for a tracer cluster (the labeling of which is carried out in a manner similar to that of the previous section). Since a number of details are similar to those of the preceding section, only essential distinguishing features are outlined here.

10.4.1 Basic Reaction

In contrast to the stepwise association scheme of the preceding case, we here assume scission, recombination, and growth from micelles of arbitrary sizes. The reaction step is represented by the equation

$$\mathrm{A}_n + \mathrm{A}_{n'} \underset{k^-(n+n')}{\overset{k^+(n;n')}{\rightleftharpoons}} \mathrm{A}_{n+n'}. \tag{10.59}$$

As in the previous section we consider a solution which is originally at equilibrium (in size space) wherein we effect the tracer observation. Furthermore, as in the preceding example, $k^-(n)$ is assumed to be independent of n.

10.4.2 Master Equation for the Tracer

The above reaction scheme for characterizing the A - D process enables us to write a master equation for $P(n)$, the probability that the tracer is present in a cluster containing n monomers (including itself). The reaction pathways undergone by the tracer cluster are represented by the scheme

$$\mathrm{A}_n^* + \mathrm{A}_{n'} \underset{k^-}{\overset{k^+(n;n')}{\rightleftharpoons}} \mathrm{A}_{n+n'}^*, \tag{10.60}$$

$$\mathrm{A}_{n-n'}^* + \mathrm{A}_{n'} \underset{k^-}{\overset{k^+(n-n';n')}{\rightleftharpoons}} \mathrm{A}_n^*. \tag{10.61}$$

The above reaction sequence yields

$$\frac{dP(n)}{dt} = \int dn' \, [k^- P(n+n') - k^+(n;n')P(n)C(n') + k^+(n-n';n')P(n-n')C(n') - k^- P(n)], \tag{10.62}$$

wherein $C(n)$ represents the concentration of clusters of size n in the solution. Equilibrium considerations, however, require that

$$\frac{k^+(n;n')}{k^-} = \exp\left[-\frac{(\mu_{n+n'}^* - \mu_n^* - \mu_{n'}^o)}{k_B T}\right]; \quad \frac{k^+(n-n';n')}{k^-} = \exp\left[-\frac{(\mu_n^* - \mu_{n-n'}^* - \mu_{n'}^o)}{k_B T}\right], \tag{10.63}$$

where the symbols μ_n^*, etc. possess the same meanings as encountered in section 10.2. Furthermore, since the original solution was assumed to be at equilibrium in size space, the chemical potentials of clusters of sizes n, n' and $n+n'$ (denoted respectively as $\mu_n, \mu_{n'}$ and $\mu_{n+n'}$) satisfy the equilibrium condition corresponding to the reaction (10.59), viz.,

$$\mu_{n'} + \mu_n = \mu_{n+n'}, \tag{10.64}$$

where the μ_n's are assumed to obey an ideal solution law of the form

$$\mu_n = \mu_n^o + k_B T \ln C(n). \tag{10.65}$$

Based upon the above considerations it is straightforward to implement an expansion of the above master equation, as was done in the preceding section. The resulting equation is of the same form as follows from eq. (10.34) [cf. remarks following (10.44) for the correspondence to eq. (10.3)], wherein the following identifications hold:

$$m(n) = k^-; \quad V(n) = \mu(n) \equiv \mu_n^* - \mu_n^o \equiv k_B T \ln C(n); \quad d(n) = k^-. \tag{10.66}$$

In addition to a different size distribution from the spherical micellar case we observe another interesting feature of this model, namely the dependence of $V(n)$ upon the micellar concentration of the solution through $C(n)$. It is pertinent to observe that the solution is nevertheless still considered to be a dilute, ideal solution, in which hydrodynamic and inter-cluster physicochemical interactions are both completely neglected. The manifestation of the A - D processes through the concentration dependence of the macrotransport coefficients provides an interesting, unconventional source of nonideality.

10.4.3 Equilibrium

Calculation of the transport coefficients necessitates obtaining the equilibrium concentration distribution in the micellar solution. Upon invoking the equilibrium condition for eq. (10.59) we find that

$$\frac{k^+(n;n')}{k^-} = \frac{C(n+n')}{C(n)\,C(n')} = \exp\left\{ - \frac{[\mu_{n+n'}^o - \mu_n^o - \mu_{n'}^o]}{k_B T} \right\}. \tag{10.67}$$

Based on the latter we make the following *ansatz* for the equilibrium concentration (cf. also Cates [5]):

$$C(n) = \exp(-\mu_n^o - \alpha n), \tag{10.68}$$

where α is a constant to be determined via the normalization condition imposed upon the concentration. Additionally, μ_n^o represents the standard chemical potential of a cluster consisting of n monomers.

For worm-like micelles, which are inherently two dimensional, it is conventional to assume a standard chemical potential of the form [19]

$$\frac{\mu_n^o}{n} = \hat{\mu}_\infty^o + \frac{A}{n}, \tag{10.69}$$

where A is a constant reflecting the energetic interactions occurring within the cluster, and

$$\hat{\mu}_\infty^o \stackrel{\text{def.}}{=} \lim_{n\to\infty} \frac{\mu_n^o}{n}.$$

This prescription for the standard chemical potential μ_n^o retains the form of the *ansatz* proposed for the equilibrium concentration $C(n)$, wherein the constant α is replaced by another constant, namely, $\alpha' \equiv \alpha + \hat{\mu}_\infty^o$. Consequently,

$$C(n) = \beta \exp(-\alpha' n), \tag{10.70}$$

with β a constant that can be determined from the specified microscale parameters. Use of the normalization condition for the total solute concentration C, namely

$$\int_0^\infty dn\, n\, C(n) = C, \tag{10.71}$$

yields

$$\frac{\beta}{(\alpha')^2} = C. \tag{10.72}$$

If we define a mean aggregation number $\bar{n}$ as

$$\frac{\int_0^\infty dn\, n\, C(n)}{\int_0^\infty dn\, C(n)} = \bar{n}, \tag{10.73}$$

then, using eqs. (10.66), (10.68) - (10.73), we obtain

$$V(n) = -\frac{n}{\bar{n}} + V_o, \tag{10.74}$$

with $V_o \equiv V(0)$ an arbitrary constant which will prove irrelevant under normalization of the probability.

This completes our identification of the potential $V(n)$ in terms of the aggregation number n. This potential is dependent upon the single parameter $\bar{n}$, the latter representing the mean aggregation number. In contrast with the spherical micellar solution case, this mean aggregation number can be shown [19] to be proportional to $\sqrt{C}$ [using eqs. (10.72), (10.73)]. As such, investigating the effect of the parameter $\bar{n}$ on the transport coefficients is equivalent to investigating the comparable effect of micellar concentration. As already noted, this concentration effect on the transport coefficients, even in the dilute limit considered, constitutes an interesting phenomena with origins in the clustering phenomena taking place within these systems.

10.4.4 Time scales

As in the preceding section we need to justify *a posteriori* the legitimacy of the coarse-graining process in terms of the time scales involved. Typical values of the kinetic time scales arising in these systems are quoted by Bouchaud *et al.* [23], wherein the time scale of recombination and scission was estimated to be of the order of 100 milliseconds. In contrast, the time scales characterizing physical-space diffusion of these especially large molecules through dilute systems, such as here envisioned, can be expected to be of the order of hours. This justifies our assumption that the size-space diffusional process can be 'projected out,' resulting in a coarse-grained three-dimensional diffusion process that accurately portrays the overall transport phe-

nomena in physical space without invoking the classical pre-averaging assumption.

10.5 Macrotransport Coefficients for Worm-like Micellar Solutions

Results are presented in this section for the macrotransport coefficients arising in situations for which the aggregation processes are represented by eq. (10.59). Derivation of the required size-space diffusion equation was effected in section (10.4, wherein we identified the size-space transport coefficients in eqs. (10.66) and (10.74). Interesting features of this example, which contrast with the preceding spherical micellar case are: (i) dependence of the mean aggregation number on micellar concentration; and (ii) the unique form of the potential energy function governing the size distribution. As in the spherical micellar example, the force $F(n)$ scales with n. The mobility coefficient $M(n)$, however, requires a bit more explanation. This example is analyzed in the spirit of extreme simplicity, omitting complications that necessarily accompany more realistic descriptions of polymer solution behavior, especially with regard to excluded-volume issues and the like [28]. Complications accompanying a more rigorous analysis can easily be accommodated within the general framework outlined in section 2.

Since our primary aim is to illustrate macroscopic effects resulting from fluctuations in the cluster aggregation number, rather than concentrating on detailed theories of polymer behavior in solutions we instead consider a simplistic model for the mobility of a polymer cluster, namely the classical Debye-Bueche porous sphere model [10]. Research on the dynamics of polymer solutions is often based upon the geometric representation of polymers as macromolecular chains possessing an enormous number of degrees of freedom, and subsequently employing simplified kinetic models such as 'bead-spring' or 'bead-rod' models as well as extensions thereof (cf. Bird *et al.* [2]). In these models, hydrodynamic interactions among beads are either completely neglected or simplistically accounted for via use of the equilibrium pre-averaged Oseen-Burgers

tensor. In contrast, the porous sphere model proposed by Debye-Bueche accounts for hydrodynamic interactions by considering the hindered flow of the solvent through a permeable sphere composed of a cluster of resisting beads. Felderhof and Deutch [12] studied the relationship between the Kirkwood-Risemann [21] and Debye-Bueche theories. They concluded that both theories possessed an equivalent microscopic status, differing only in the statistical assumptions underlying their derivation. Further details regarding both motivation for and use of the porous sphere model can be found in Frankel *et al.* [14], wherein a related example involving size fluctuations of a porous-sphere, polymer model was studied. The essential scenario studied therein is similar in spirit to the case analyzed here, except that there the size fluctuations resulted from the inherently flexible nature of the polymer molecule undergoing thermal fluctuations, rather than from the A - D mechanism as outlined here.

According to the Debye-Bueche theory, the mobility coefficient of a uniformly homogeneous porous sphere of radius r and permeablilty K' moving through a solvent of viscosity μ is

$$M(r) = \frac{1}{6\pi\mu r}\left[\frac{1+(3/2)K(1-K^{1/2}\tanh K^{-1/2})}{1-K^{1/2}\tanh K^{-1/2}}\right], \tag{10.75}$$

where $K = K'/r^2$ is the dimensionless Darcy permeability. The dimensional permeability is known [27] to scale inversely with the volume fraction of the chains (i. e. beads) comprising the porous sphere. In conjunction with the fact that the radius of the sphere scales with $n^{1/2}$, for an ideal random walk we obtain

$$K = \lambda n^{-1/2}, \tag{10.76}$$

where λ is a nondimensional proportionality constant. Using representative parametric values provided in Debye-Bueche's article the constant λ was estimated to be $O(1)$, whereupon we adopt the value $\lambda = 5$ in this analysis. Substitution of (10.76) into (10.75) yields the requisite expression for $M(n)$.

The essential framework of the subsequent theory is similar to that illustrated in the preceding section. Accordingly, we restrict ourselves in what follows only to

the unique features of the worm-like micelle case, followed by a brief discussion of the results obtained. One of the features distinguishing the present case from the previous one is the concentration dependence of the mean micelle length. While this feature makes the present case more interesting, it simultaneously imposes certain constraints upon the mean aggregation number owing to our prior assumption of diluteness. Large mean aggregation numbers would necessarily imply high concentrations, nullifying the assumption of a dilute system. And at these high concentrations one encounters regimes wherein concentration effects arising from entanglement and reptation of polymer chains acquire heightened significance. Bouchaud and coworkers [3, 23] have observed several interesting features accompanying diffusion in these regimes, including evidence for Levy flights (in contrast to the normal Brownian random walk). These effects, though interesting, are beyond the scope of the present work. We thus proceed with this caveat of limitations imposed by the diluteness criterion.

Using (10.74), $P_0^\infty(n)$ can be obtained from eq. (10.20) as

$$P_0^\infty(n) = \left[\int_1^\infty dn\, \exp(-n/\bar{n})\right]^{-1} \exp(-n/\bar{n}). \tag{10.77}$$

This expression indicates that at a given value of n, $P_0^\infty(n)$ is functionally dependent only upon the mean aggregation number $\bar{n}$. In a manner similar to the scaling *ansatz* made in the previous section, all the macrotransport coefficients can be expected to scale as $f(\bar{n})$, with $f(x) \to x^\alpha$ for $x \gg 1$. Results obtained for the mean settling velocity, mean molecular diffusivity, and convective dispersivity are discussed below.

Mean Velocity of Settling: Figure (10-5) indicates the effect of cluster polydispersivity on the mean settling velocity $\bar{U}$. This mean settling velocity is almost identical to the settling velocity $U(\bar{n})$ at the mean aggregation number. The source of this behavior can be comprehended by analyzing the variation of the size-specific settling velocity $U(n)$ with aggregation number n. Figure (10-6) qualitatively depicts the settling velocity for different aggregation numbers. Due to a combination of effects resulting from the dependence of the force and mobility upon the aggregation

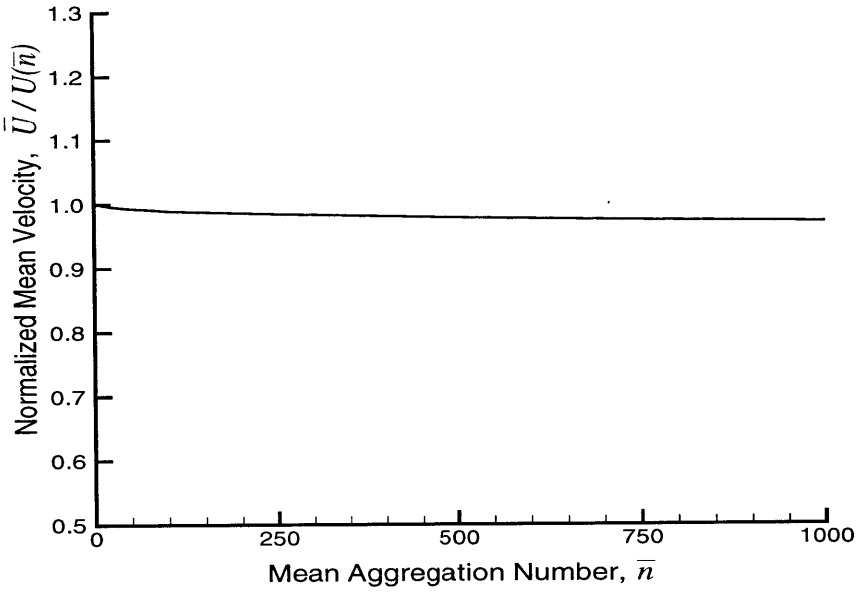

Figure 10-5: Effect of the mean aggregation number $\bar{n}$ on the mean velocity ratio $\bar{U}/U(\bar{n})$ for worm-like micellar solutions.

number, this velocity increases with increasing aggregation number. On the other hand the probability distribution (10.77) for the cluster size indicates an exponential decrease with aggregation number. Thus, larger velocities are sampled only infrequently and vice versa. Together, these factors nullify one another, resulting in an almost imperceptible effect of size distribution upon mean settling velocity.

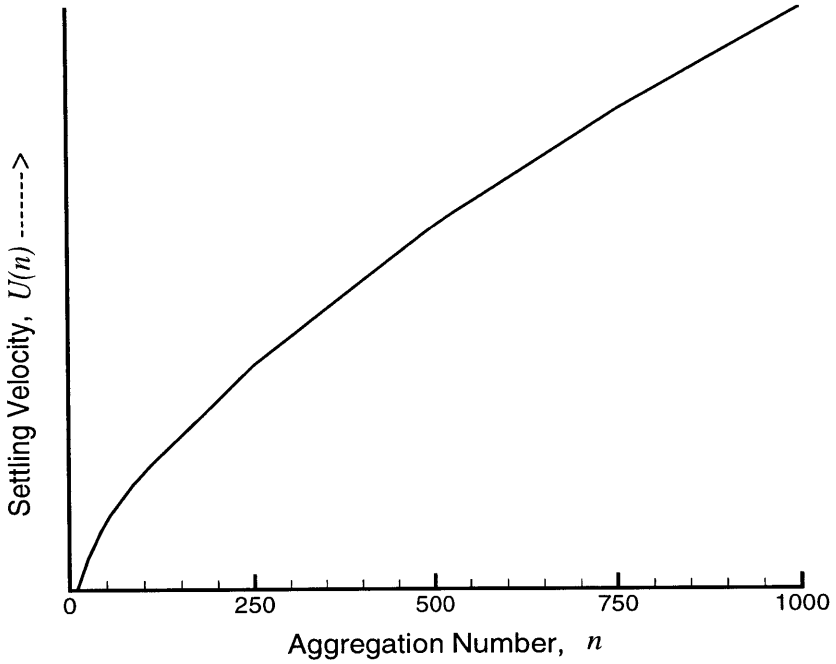

Figure 10-6: Variation of the settling velocity $U(n)$ with cluster size n for monodisperse wormlike micellar solutions. Since only the qualitative features of this behavior are of interest we do not explicitly display values for $U(n)$ (a dimensional quantity).

Mean diffusivity of Settling: Figure (10-7) depicts the effect of aggregation number on the mean molecular diffusivity. In contrast to the comparable settling velocity case, size effects here are quite significant. Mean diffusivity values at different aggregation numbers (in regimes which are expected to be classified as dilute) are seen to be greater by a factor of almost 2 to 3 than those arising at the mean aggregation number. The underlying reason for such behavior resides in the preferential sampling of the low aggregation number clusters, which in turn possess larger mobilities [Fig. (10-8)].

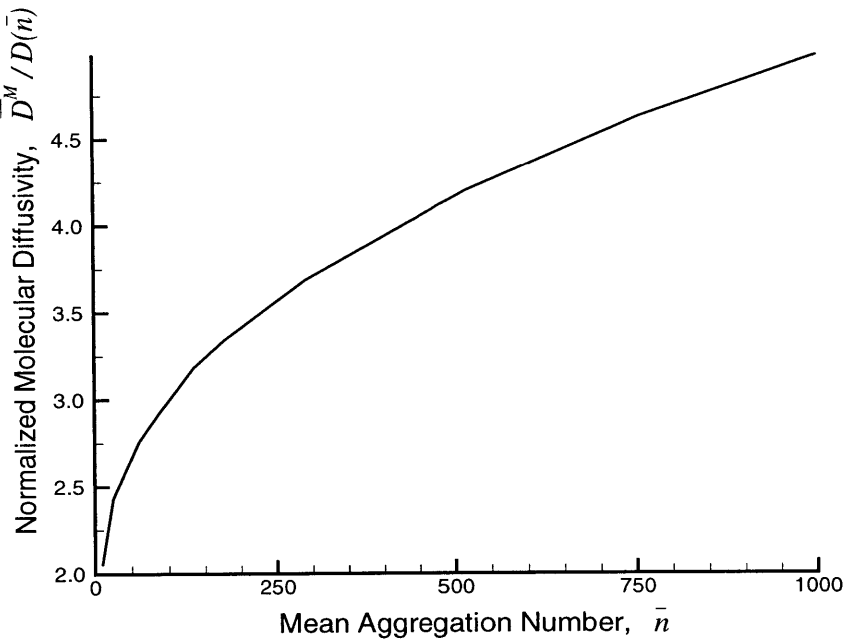

Figure 10-7: Effect of mean aggregation number $\bar{n}$ on the normalized molecular diffusivity $\bar{D}^M/D(\bar{n})$ for worm-like micellar solutions.

At high aggregation numbers the mean diffusivity appears to reach an asymptotic limit characteristic of the fact that the mobility and probability distribution both fall to zero at large n. However, at such large aggregation numbers the transport coefficients will depend primarily upon entanglement effects, in which circumstances the assumption of a dilute solution would clearly be invalid.

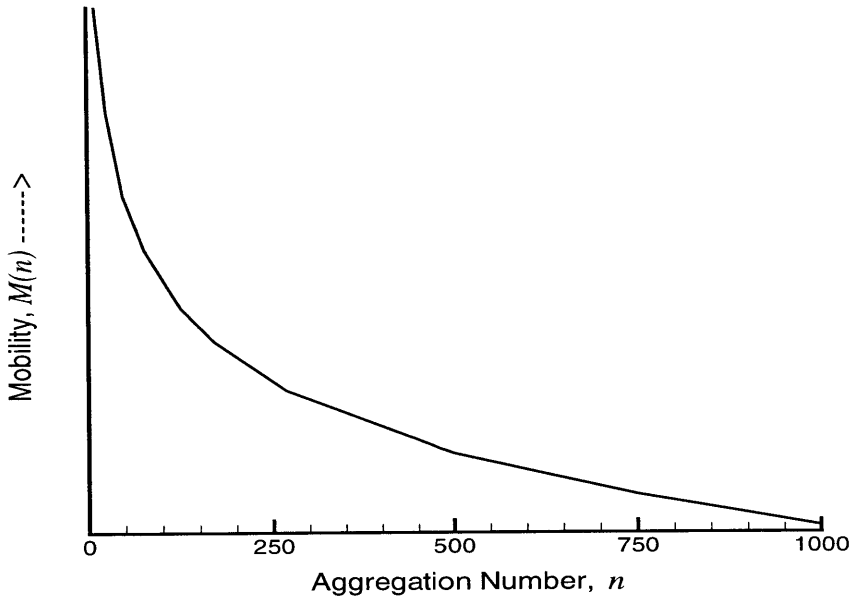

Figure 10-8: Variation of the mobility $M(n)$ with size n for monodisperse wormlike micellar solutions. Since only qualitative features of this behavior are of interest we do not explicitly display values for $M(n)$ (a dimensional quantity).

Convective Dispersivity: Figure (10-9) displays the functional dependence of the convective dispersivity upon the mean aggregation number. Such size effects can be expected to be much more dramatic for the convective dispersivity case than for the other two macrotransport coefficients. As already noted, the convective dispersivity arises solely in response to the distribution of micelle sizes. An increase in mean aggregation number leads to a wider spread in the size distribution, exemplifying the exponential distribution (10.77) of sizes. Such behavior is consistent with the

observed increase in convective dispersivity with increasing mean aggregation number. Based upon the dispersivity values observed at large aggregation numbers the scaling exponent α for $\bar{D}^C/[\bar{n}U(\bar{n})]^2$ is empirically established to be about $\alpha \approx 0.7$.

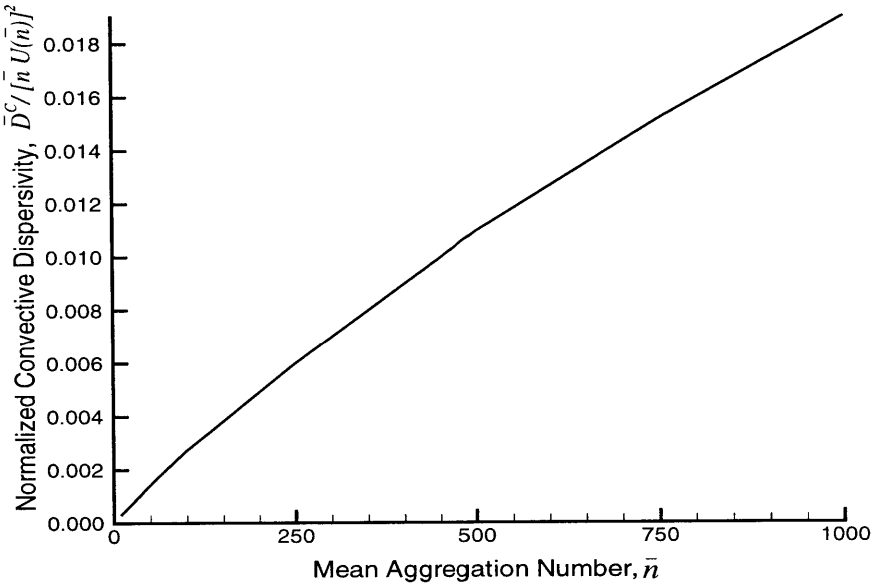

Figure 10-9: Dependence of the normalized convective dispersivity $\bar{D}^C/[\bar{n}U(\bar{n})]^2$ on mean aggregation number $\bar{n}$ for worm-like micellar solutions.

Mean Mobility: As in the spherical micelle case a mean mobility based on mean settling velocity can be defined [cf. eq. (10.57)]. The variation in the resulting ratio of apparent-to-actual mean mobility is indicated in Fig. (10-10), again quantifying the apparent violation of the Stokes-Einstein relation.

Significance of results: The preceding discussion deals with size distribution effects on the macrotransport coefficients $\bar{U}, \bar{D}^M$ and $\bar{D}^C$ characterizing the transport of polydisperse worm-like micelles through the solution. Such polydispersivity effects appear to be specially pronounced for the mean molecular diffusivity case. Moreover, the presence of a Taylor dispersion contribution stems entirely from the polydispersivity of the micellar system. An order-of-magnitude estimate for this additional diffusiv-

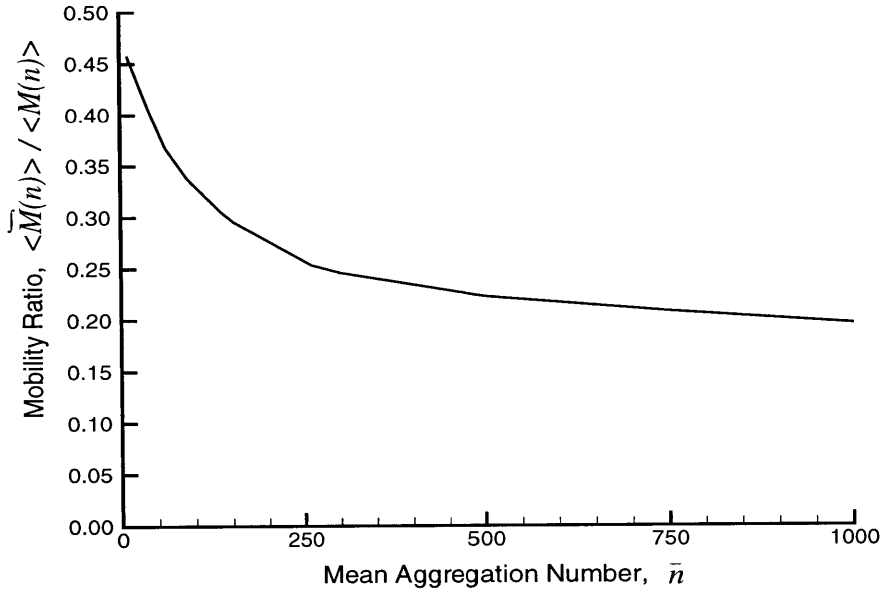

Figure 10-10: Dependence of the mobility ratio $\langle\tilde{M}(n)\rangle/\langle M(n)\rangle$ on mean aggregation number $\bar{n}$ for worm-like micellar solutions.

ity contribution serves to quantify its significance in relation to the mean molecular diffusivity. From Fig. (10-9) we extract a 'typical' value of $\bar{D}^C/[\bar{n}U(\bar{n})]^2 = 1000$. Consequently,

$$\frac{\bar{D}^C}{\bar{D}^M} \sim 10^{-3}\bar{n}^3 \frac{U(\bar{n})^2}{k_B T M(\bar{n})}. \tag{10.78}$$

Using approximate scaling relationships, namely $U(\bar{n}) \sim n^{1/2}$ and $M(\bar{n}) \sim n^{-1/2}$ (not rigorously true for the porous sphere model) together with characteristic values of $M(\bar{n})$ to obtain the prefactor, we find that

$$\frac{\bar{D}^C}{\bar{D}^M} \sim 10^{-28}\bar{n}^{4.5} g^2, \tag{10.79}$$

with g denoting the dimensionless force. This suggests that the extra contribution to the diffusivity becomes significant only for very long macromolecules subject to large accelerations (such as would arise during ultracentrifugation). Despite the relatively small value predicted for the convective dispersivity under normal sedimentation conditions, we have shown that the effect of polydispersivity on the molecular diffusivity is a nontrivial one, leading to an increase in cluster mobility by a factor of almost 3. Furthermore, we have evaluated the functional dependence of the macrotransport coefficients on the mean aggregation number $\bar{n}$. In view of the relationship that exists between $\bar{n}$ and micellar concentration the above result can, *inter alia*, be considered as representing the effect of concentration on the transport coefficients. It is interesting to note that such an effect arises even in the dilute solution regime.

10.6 Conclusions

The preceding analysis furnishes a general framework for analyzing diffusion and sedimentation phenomena in systems exhibiting a distribution of cluster sizes stemming from the existence of reversible association-dissociation processes. Examples of such systems include micellar solutions and microemulsions. The generic scheme developed describes the transport of dilute dispersions of clusters through an other-

wise quiescent solvent via the use of coarse-grained, size-independent, physical-space transport coefficients appearing in a convective-diffusion equation governing the local spatial cluster concentration (probability density). This was achieved through use of generalized Taylor dispersion theory.

Our scheme was illustrated by analyzing two practically-motivated examples encountered in dealing with micellar solutions. In the first case we studied the aforementioned effects for a solution composed of spherical micelles. In such a scenario the cluster size is characterized by a Gaussian distribution about a mean aggregation number. Using known information about such solutions we quantified the mean transport coefficients in terms of typical micellar data available in literature. In the second case, similar effects were studied for cylindrical or worm-like micelles. Due to the reversible scission processes present in these latter systems they are widely regarded as models of 'living polymers.' Interesting features arising for this case include an exponential attenuation of the size distribution with mean aggregation length. Furthermore, in such systems the mean aggregation length depends upon the micellar concentration. Thus, for this class of systems the macrotransport coefficients obtained in our work serve to quantify the variation of the transport coefficients with micelle concentration, at least in dilute systems.

A number of potential applications arise from the above results. Self-diffusion coefficients are often employed to provide a measure of mean aggregation numbers in spherical micellar solutions, at least in circumstances where such solutions may be regarded as being approximately monodisperse. Our analysis provides a scheme whereby polydispersivity effects can be incorporated into the interpretation of experimental results so as to furnish estimates of the errors arising from a lack of true monodispersivity. Moreover, our analysis is sufficiently general to also embrace the effects of micellar shape (such differences being embodied in the constitutive forms assumed for the microscale potential and the mobility coefficients) on the macroscale transport coefficients. This constitutes a possible future application for determining the mean properties of such micelles in solution from measurements of their settling (or electrophoretic) velocities and mean self-diffusivities [7]. Furthermore, the fact

that our generic analysis is not restricted exclusively to micellar applications permits possible extensions towards studying the effects of 'mixing' on the kinetics of aggregation processes. Such an investigation would involve the opposite extreme of time scales, whereby the A - D kinetic time scale is more sluggish than the physical-space transport time scales. Our analysis points up a scheme whereby a systematic study of these effects could be pursued.

References

[1] E. A. G. Aniansson and S. N. Wall, "Kinetics of step-wise association," *J. Phys. Chem.*, **78**, 1024 (1974).

[2] R. B. Bird, C. F. Curtiss, R. C. Armstrong and O. Hassager, *Dynamics of Polymeric Liquids*, Wiley-Interscience, New York (1987).

[3] J. P. Bouchaud, A. Ott, D. Langevin and W. Urbach, "Anomalous diffusion in elongated micelles and its Levy flight interpretation," *J. Phys. II (France)*, **1**, 1465 (1991).

[4] H. Brenner and D. A. Edwards, *Macrotransport Processes*, Butterworth-Heinemann, Newton MA (1993).

[5] M. E. Cates, "Reptation of living polymers — Dynamics of entangled polymers in the presence of reversible chain-scission reactions," *Macromolecules*, **20**, 2289 (1987).

[6] M. E. Cates, "Dynamics of living polymers and flexible surfactant micelles - Scaling laws for dilution," *J. Phys. (France)*, **49**, 1593 (1988).

[7] D. Chatenay, W. Urbach, M. Cazabat and D. Langevin, "Onset of droplet aggregation from self-diffusion measurements in microemulsions," *Phys. Rev. Lett.*, **54**, 2253 (1985).

[8] D. Chatenay, W. Urbach, R. Messager and D. Langevin, "Self-diffusion of interacting micelles — FRAPP study of micelles self-diffusion," *J. Chem. Phys.*, **86**, 2343 (1987).

[9] E. L. Cussler, "Cluster diffusion in liquids," *AIChE J.*, **26**, 43 (1980).

[10] P. Debye and A. M. Bueche, "Intrinsic viscosity, diffusion and sedimenation rate of polymers in solution," *J. Chem. Phys.*, **16**, 573 (1948).

[11] A. Einstein, *Theory of Brownian Motion*, Dover reprint New York (1956).

[12] B. U. Felderhof and J. M. Deutch, "Frictional Properties of Dilute Polymer Solutions II. The Effect of Preaveraging," *J. Chem. Phys.*, **62**, 2398 (1975).

[13] I. Frankel and H. Brenner, "On the foundations of generalized Taylor dispersion theory," J. Fluid Mech., **204**, 97 (1989).

[14] I. Frankel, F. Mancini and H. Brenner, "Sedimentation, diffusion and Taylor dispersion of a flexible fluctuating macromolecule. The Debye-Beuche equation revisited," J. Chem. Phys., **95**, 8636 (1991).

[15] W. M. Gelbart, A. Ben-Shaoul and D. Roux (eds.), *Micelles, Membranes, Microemulsions and Monolayers*, Springer-Verlag, Berlin (1994).

[16] I. S. Gradshteyn and I. M. Ryzhik, *Table of Integrals, Series and Products*, Academic Press, New York (1980).

[17] P. Hebraud and F. Lequeux, "Mode-coupling theory for the pasty rheology of soft glassy materials," *Phys. Rev. Lett.*, **81**, 2934 (1998).

[18] R. J. Hunter, *Foundations of Colloid Science*, Oxford University Press, New York (1987).

[19] J. Israelachavili, D. J. Mitchell and B. W. Ninham, *J. Chem. Soc. Faraday Trans.*, **72**, 1525 (1976).

[20] J. Israelachvili *Intermolecular & Surface Forces*, Academic Press, San Diego (1991).

[21] J. G. Kirkwood and J. Riseman, *J. Chem. Phys.*, **16**, 565 (1948).

[22] B. Lindman and P. Stilbs, *Molecular Diffusion in Microemulsions*, in "Microemulsions: Structure and Dynamics," S. E. Friberg and P. Bothorel (eds.), CRC press, Boca Raton (1987).

[23] A. Ott, J. P. Bouchaud, W. Urbach and D. Langevin, "Collective diffusion of living polymers," *J. Phys. II (France)* **7**, 1099 (1997).

[24] P. Sollich, F. Lequeux, P. Hebraud and M. E. Cates, "Rheology of soft glassy materials," *Phys. Rev. Lett.*, **78**, 2020 (1996).

[25] W. Urbach, H. Hervet and F. Rondelez, "On the application of forced Rayleirigh light scattering to mass diffusion measurements," *J. Chem. Phys.*, **83**, 1877 (1985).

[26] N. G. van Kampen, *Stochastic Processes in Physics and Chemistry*, North-Holland, Amsterdam (1992).

[27] F. W. Wiegel, *Fluid Flow Through Porous Macromolecular Systems*, Springer, New York (1980).

[28] H. Yamakawa, *Modern Theory of Polymer Solutions*, Harper & Row, New York (1971).

[29] A. Ziabicki, "Generalized theory of nucleation kinetics. 4. Nucleation as diffusion in the sapce of cluster dimesnions, postiions, orientations, and internal structure," *J. Chem. Phys.*, **85**, 3042 (1986).

Chapter 11

Summary

This portion of the thesis was explicitly concerned with applications employing macrotransport theory (or generalized Taylor dispersion theory) to effect the coarse-graining of multiscale systems. Chapter 8 elucidated the basic concepts of this generalized solute dispersion theory, along with the prerequisites demanded of the physical parameters in order to enable a "macrotransport" description. Our exposition underlined the need for two distinct subspaces within which the transport of the solutes occur. These two subspaces were respectively termed the "local" and "global" spaces. While we outlined a sufficiency criterion based on geometric compactness (or boundedness) to distinguish between the subspaces, a more rigorous condition for the delineation of the two subspaces based on the time scales of transport within each of the subspaces was subsequently proposed, permitting a quantitative delineation of the respective subspaces. Explicitly, we required the timescales for transport in the local space to be significantly smaller than for global space values. Fulfillment of such a condition requires that the transport processes occurring in the local space attain a state of equilibrium within time scales significantly smaller than that embodying the comparable global space transport processes. This enabled us to propose a "macrotransport" description of the transport processes, one governing the global space transport of the average solute concentration. Furthermore, the macrotransport "paradigm" furnishes an explicit procedure whereby the phenomenological coefficients present in the macrotransport description can be determined. These phenomenological coefficients

quantitatively embody, in an averaged manner, the transport processes occurring in the local space. Physical interpretations were also furnished for these "macrotransport coefficients," thereby providing significant insights into the transport processes occurring within the system.

The first application of macrotransport theory was considered in chapter 9 wherein thermal Taylor dispersion theory for time-periodic systems was used to study the extent of chaotic enhancement of laminar heat transfer and axial thermal dispersion occurring during combined transverse and axial annular flow between two nonconcentric circular cylinders undergoing alternate rotations. A local Newton's 'law of cooling' heat transfer boundary condition was used on the outer cylinder, whereas the inner cylinder was supposed insulated. The effective heat transfer coefficient $\bar{H}^*$ describing the global rate of heat loss from the system (differing in general from the true microscale Newton's law heat transfer coefficient h on the outer cylinder) was calculated as a function of the system parameters, thereby serving to quantify the extent of chaotic heat transfer enhancement. The axial thermal Taylor dispersivity provided an independent measure of the effects of chaotic mixing, as too did the axial thermal velocity. Calculations were performed for three different cases: (i) Concentric cylinder rotation (for which case the resulting circular transverse flow has no effect upon the effective transport properties); (ii) Nonconcentric counter-rotating circular cylinders, each undergoing a steady rotation, thereby creating a time-independent transverse flow field; (iii) Nonconcentric counter- and co-rotating circular cylinders, each undergoing time-periodic alternate rotation while the other remains at rest. A 'regular', nonchaotic enhancement of the heat transfer rate over the concentric cylinder case was observed in case (ii), arising from the presence of a secondary-flow recirculation region. Enhancement due to chaotic advection was observed in case (iii) [about 50% more than that of case (ii) and more than double that of case (i), all other things being equal]. Concomitant values of the axial thermal Taylor dispersivity and axial thermal velocity confirmed the existence of enhanced transverse transport due to chaotic advection. It was observed that the functional dependence of the enhanced heat transfer rate upon the system parameters does not consistently display the same

trends as were qualitatively suggested by the 'degree of chaoticity' of the comparable Poincaré plots. This observation signals the need for caution in simply assuming that the greater the degree of chaotic 'mixing' implicit in the Poincaré plot the greater will be the corresponding global transport rate. By simple redefinition of the symbols used, our energy transport results may be re-interpreted so as to apply to the case of reactive-species transport involving a first-order irreversible chemical reaction occurring on the outer-cylinder surface; explicitly, the Nusselt number quantifying the local heat transfer coefficient rate is simply replaced by a comparable Damköhler number quantifying the local kinetics of the surface reaction.

In chapter 10 we considered another application of macrotransport theory. Calculations were presented for the long-time diffusivity and sedimentation velocity of *associating colloids.* Examples of the latter are micellar solutions and microemulsions. The analysis incorporated the role of reversible association-dissociation processes accompanying the physical-space transport of these clusters through the solution. This was accomplished without the need for pre-averaging by transforming the association-dissociation processes into equivalent 'size-space' diffusional processes, which were then embedded into the simultaneous physical-space transport processes occurring in three-dimensional space so as to obtain a four-dimensional 'microtransport' convective-diffusion equation governing transport of the clusters in both the physical and size spaces. A generic 'projection' scheme framework based on generalized Taylor dispersion theory was then applied to the problem, thereby reducing the four-dimensional microtransport equation to a coarse-grained three-dimensional *physical-space* macrotransport convective-diffusion equation. Effects arising from the existence of a distribution of cluster sizes were are accounted for in the latter formulation governing the *mean* transport process by the appearance of three coarse-grained phenomenological coefficients whose values depended *inter alia* upon the cluster-size distribution. These macrotransport coefficients included a mean sedimentation velocity vector arising from the action of external forces (if any), a mean molecular diffusivity, and an additional diffusive-type contribution to the diffusivity dyadic, corresponding to a convective ('Taylor') dispersivity. The latter contribution arose as

a consequence of the spread in settling velocities of the differently-sized clusters. The generic framework developed was illustrated by applications to two classes of micellar solutions: (*i*) solutions comprised of spherical micelles; (*ii*) solutions comprised of cylindrical or worm-like micelles (so-called 'living polymers'). Each spherical micelle was modeled as an impenetrable rigid sphere whose radius is determined by its aggregation number. The living polymers were modeled by the Debye-Bueche theory, wherein a coiled macromolecular chain was regarded as a Brownian 'sponge-like' porous sphere through whose interior solvent percolates. Calculations of the resulting macrotransport coefficients, including their scaling relationships, were presented for both cases, and their physical significance discussed in terms of the underlying microscale physics. Possible applications and potential extensions of the generic framework were outlined.

In conclusion, the preceding chapters expound the versatility and use of macrotransport theory for coarse-graining multiscale systems. Despite the limitations imposed, requiring the presence of two distinct subspaces, significant applications could nevertheless still be envisioned. Within the generic context of coarse-graining theories, macrotransport theory falls under the general category of projection operator theories (Pagitsas *et al.* [1]). However, the physico-mathematical framework which accompanies the development of the macrotransport theory enables significant physical conclusions to be drawn based upon implementation of the scheme. Such a physical link is typically lacking within more formal, albeit general, theories of projection operator coarse-graining schemes. The achievement of this physical link was, however, not accomplished without severely restricting the class of problems which are amenable to a "macrotransport description." Efforts are underway, aimed at extending macrotransport theory to broader classes of problems (so as to include, for example, momentum dispersion processes, "almost" time-periodic systems, etc.). If the physical, Lagrangian link could be sustained within such extensions (in contrast to more formal techniques, such as multiple time scale analyses), potential applications of macrotransport theory would be increased manifold.

References

[1] M. Pagitsas, A. Nadim and H. Brenner, "Projection operator analysis of macro-transport processes," *J. Chem. Phys.*, **84**, 2801 (1986).

Part 3: Dynamics of Two-Phase Fluid Interfaces in Random Porous Media

Chapter 12

Scaling Concepts for Interfaces

The vast diversity of shapes that surround us has had a profound impact on the quality of our lives. A quantitative characterization of natural forms would constitute an important step towards understanding their origins and behavior. Unfortunately, until recently, there have been very few general approaches towards the quantitative description complex disorderly patterns that characterize most of the natural phenomena. To a certain extent, the inherently nonequilibrium nature of pattern formation processes have contributed to the slow development of the requisite tools pertaining to their characterization.

However, the outlook has improved substantially in the past two decades. The pioneering interdisciplinary work of Mandelbrot [16] has demonstrated that mathematical concepts, once believed to be of little relevance to the real world phenomena, can provide us with creative ways of describing and thinking about an amazingly broad range of structures and phenomena [7]. In addition, scaling concepts that were originally applied to describe a relatively narrow range of physical problems, such as critical phenomena, structure of macromolecules, etc., have been successfully extended and applied to much broader ranges of problems [4, 9]. In fact, fractal concepts are now utilized to provide a theoretical basis for the description of objects of diverse shapes and sizes, ranging for instance from small polymer molecules [9] on

the one hand to the coastlines of continents [16] on the other.[1] Fractal phenomena and the accompanying characterization methodologies are however too numerous to be completely enumerated in this thesis. Barabasi and Stanley [1], and Meakin [18] constitute useful pedagogical references oriented towards fundamental concepts and applications to a number of practical problems.

In the following section we give a brief description of 'scaling' concepts which possess special relevance in the context of 'self-affine fractals.' Subsequently, we specialize these general mathematical concepts to characterizing the morphology of interfaces.

12.1 Self-Affinity and Power Laws

Within a mathematical framework, self-similarity constitutes an example of a symmetry group. A symmetry group embodies a transformation law, requiring that the object which exhibits the symmetry be invariant under the specified transformation [11]. For example, a function $y(x)$ possessing translational symmetry is unchanged under a transformation $T : x \rightarrow x + d$. In an analogous manner, the property of self-similarity requires that the system be invariant to a transformation embodying an *isotropic dilation*. For instance, if O denotes an object which is self-similar, then invariance under an isotropic dilation requires that, if X denotes the set of points $\{x_1, x_2, \cdots, x_n\}$ contained within O, and if the dilation operation corresponds to stretching (or compressing) the coordinates of each and every point by a factor b, then the new set of points X' (represented by $\{x'_1, x'_2, \cdots, x'_n\}$, where $x'_i = bx_i$, $\forall\, i = 1, n$) satisfy $X' \subseteq X$ [1]. Figure 12-1 shows one such example of a self-similar fractal object known as the Sierpenski Gasket. (The figure explicitly demonstrates the procedure for the construction of a Sierpenski Gasket. The object so obtained by continuing the procedure *ad infinitum* constitutes a self-similar fractal.) In this part of the thesis, we are however concerned with an extended concept of self-similarity termed as *self-*

[1]Even one of the major contenders for *the* theoretical description of the cosmological genesis of the Universe, viz., the 'inflationary model,' possesses an underlying fractal basis [12].

affinity. An object is self-affine if it exhibits invariance under an *anisotropic scaling,* i.e. dilation by disparate factors in different spatial (and possibly temporal) directions [17].

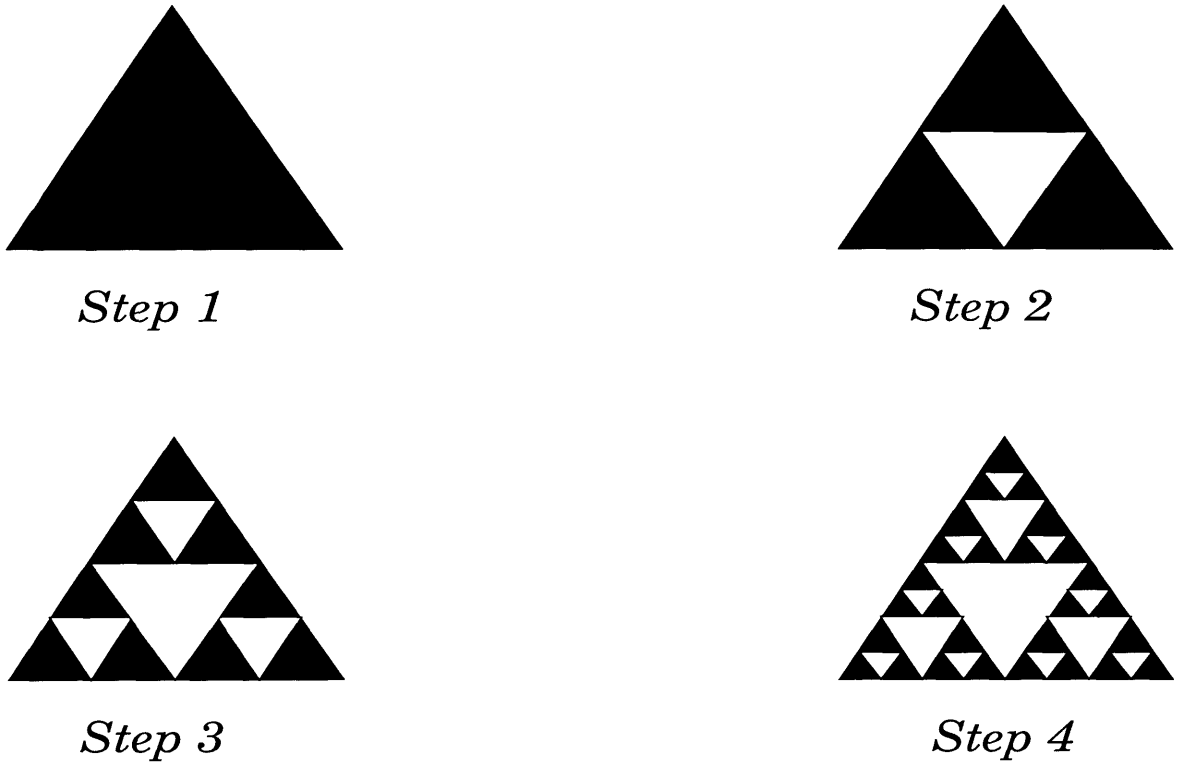

Figure 12-1: The Sierpenski gasket: An example of a deterministic fractal

Power laws play a central role in the description of self-affine fractals and their scaling [14]. A function $f(x)$ is said to be a power law function of x if it is of the form

$$f(x) = cx^m, \tag{12.1}$$

where c is a constant independent of x. A special symmetry property exhibited by the above function enables clarifying the explicit nature of our interest in such power laws. In the above equation we consider implementing a dilation operation, quantified by a rescaling of the length scale x by a factor λ, thereby yielding

$$\begin{aligned} f(\lambda x) &= c(\lambda x)^m \\ &= c\lambda^m x^m. \end{aligned} \tag{12.2}$$

The latter result implies that

$$f(\lambda x) = \lambda^m f(x). \tag{12.3}$$

The above property quantifies the invariance of the set $\{f(x), x\}$ under a *dual, anisotropic scaling*[2] generated by the transformation $x \to \lambda x$, $f \to \lambda^m f$.[3] Furthermore, a direct and important consequence of this scale invariance posits that the exponent m is independent of the units which are employed to measure x or f.

The above demonstration elucidates the role of power-laws in the context of characterizing self-affine functions. As such, the above illustration proves that a self-affine function necessarily needs to be a power law function of its dependent variables. Furthermore, the magnitude of the scale invariant exponent 'm' embodies a quantitative characterization of the function f. This philosophy embodies the entirety of the analysis accomplished in this part of the thesis.

Note: In subsequent sections the symbol "$\sim$" will be employed to denote the phrase 'scales as,' i.e., $f(x) \sim x^m$ implying, $f(x) = cx^m$, where c is constant, typically, but not necessarily, of magnitude $O(1)$.

It is pertinent to elucidate the typical physical scenarios accompanying a power law or self-affine behavior. Empirical experimental observations have suggested that power laws can possibly arise in two distinct contexts: (a) As a consequence of a single process that possesses no inherent length scale apart from an inner and outer cutoff lengthscale (serving to impose geometrical compactness) that implicitly determine the range of validity of the power law behavior. In such a scenario, a homogeneous

[2]Note the connection to self-affinity.

[3]In fact, it can be proved that the only function which exhibits this 'self-affine' property is the power law function. The proof is as follows:

$$\begin{aligned} & f(\lambda x) = \lambda^m f(x), \\ \Longrightarrow \quad & \frac{d[f(\lambda x)]}{d\lambda} = m\lambda^{m-1} f(x) \\ \text{or,} \quad & x\frac{d[f(\lambda x)]}{d(\lambda x)} = m\lambda^{m-1} f(x). \end{aligned} \tag{12.4}$$

Setting $\lambda = 1$ in the final equation and then integrating yields $f(x) = cx^m$.

power law description characterizing the self-affine function can be constructed, which possesses validity over the entire range of length scales. An example wherein such behavior is evinced includes the power law divergences observed in the functional form of thermodynamic properties near second-order critical points [8, 14]; (b) Alternatively, power law behavior may arise as a consequence of a number of small-scale processes, each possessing its own length scale. In these situations, the functional form of the power law *is typically inhomogeneous*, being modified upon spatial modulation. In such cases, interest is typically centered upon the behavior exhibited by the self-affine function at large length scales (termed "hydrodynamic" behavior) — though situations might arise requiring one to consider the intervening length scales. (The following chapter constitutes an example wherein such an analysis is effected.)

In this section we briefly reviewed the concepts of scale invariance and self-affinity. The remainder of the chapter concentrates on phenomenological models of interfacial dynamics, enabling similar conclusions to be drawn regarding the statistics of interfacial fluctuations. Interfacial fluctuations are characterized by fluctuations in the magnitude of the interfacial height, which is a statistical quantity animated by thermal fluctuations and other sources of stochasticity. Characterization of the morphology of interfaces therefore requires extension of the concept of self-affinity to embody statistical quantities. In this context, a statistical quantity is termed self-affine if the parameters characterizing its distribution (like for instance, the mean, variance, skewness, curtosis, etc.) remain invariant under an anisotropic scaling. This property is employed in subsequent sections as well as in the next chapter to glean quantitative insights into the characterization of interfacial fluctuations. Preliminary to the discussion we clarify the concepts of dynamic scaling in the context of interfaces, thereby laying the foundations for the subsequent analyses in this and the following chapter. This also enables us to clarify the notation which we have used in describing the interfacial dynamics. Following this, we consider some well-known phenomenological equations postulated for describing evolution of the interfaces, including illustrating the basic concepts of underlying Flory scaling analysis. The motivation in this section is intended to provide an illustration of some concepts used in the next chapter.

Accordingly, we herein eschew an elaborate review of literature pertinent to the vast field of interfacial growth models (cf. [1, 18] for more details).

12.2 Dynamic Scaling

In the ensuing discussion in this chapter, and in the subsequent chapter, we restrict our discussion to continuum models of interfacial growth. While discrete models for interfacial growth have played a very important role in explaining observed phenomena (even in situations where continuum models have sometimes failed), the discrete models typically involve a computational simulation of the growth rules to draw conclusions based on the results obtained by such schemes [23]. As such, our motivation is to seek models wherein analytical techniques are implementable, thereby enabling us to glean physical insights into the issues of interest.

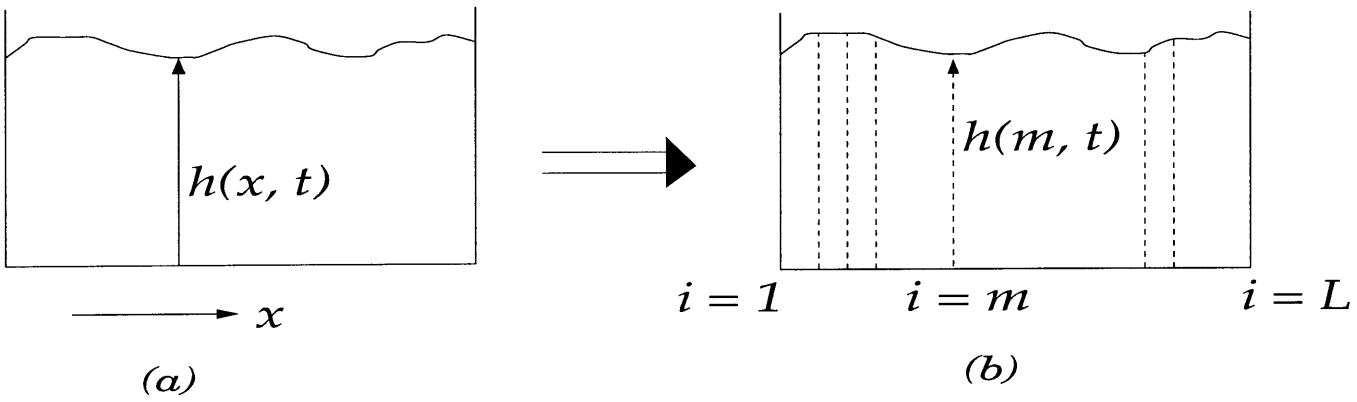

Figure 12-2: Interfacial representation in: (a) continuous; and (b) discrete formulations.

Figure (12-2) describes the notation used in this part of the thesis. The interfacial height $h \equiv h(x,t)$, and is a function of the transverse spatial coordinate x and time t. Due to the fluctuating nature of the interface (possible origins of which are clarified in subsequent sections), we confine our interest to the *statistical features* of the interfacial height $h(x,t)$ rather than attempt an exact description of the interfacial configuration. In this context, one of the most commonly studied statistical features

in problems relating to interfacial growth corresponds to the mean-squared displacement of the interface measured from its mean position. To facilitate the definition of the appropriate quantities, we consider the simple case wherein the transverse space is restricted to one dimension. It is quite straightforward to generalize the following definitions to cases wherein the interface possesses higher dimensionality. In the one-dimensional case, let us further assume that the transverse space is discretized and enumerated by a discrete variable i running from 1 to L. Then, we define [1] the mean height of the interface as

$$\bar{h}(t) = \frac{1}{L}\sum_{i=1}^{L} h(i,t). \tag{12.5}$$

The corresponding interfacial width (which characterizes the *roughness* of the interface) is defined as

$$w(L,t) = \sqrt{\frac{1}{L}\sum_{i=1}^{L}[h(i,t) - \bar{h}(t)]^2}. \tag{12.6}$$

A typical experimental observation monitoring the time evolution of the interfacial width resembles the morphology illustrated in Fig. (12-3). From the figure we discern that the time evolution of the surface width displays two distinct, characteristic scaling regions with the crossover between them occurring at time $t \simeq t_X$.

1. In the first scaling regime, the width grows algebraically as a function of time, i.e.,

$$w(L,t) \sim t^{\beta} \quad t < t_X. \tag{12.7}$$

The exponent β, termed the dynamical exponent, characterizes the temporal evolution of the roughening process.

2. The power-law increase in the width saturates at $t \simeq t_X$, beyond which the width maintains a constant value, w_{sat}. It has further been determined from experimental observations (and numerical simulations based on interfacial growth models)

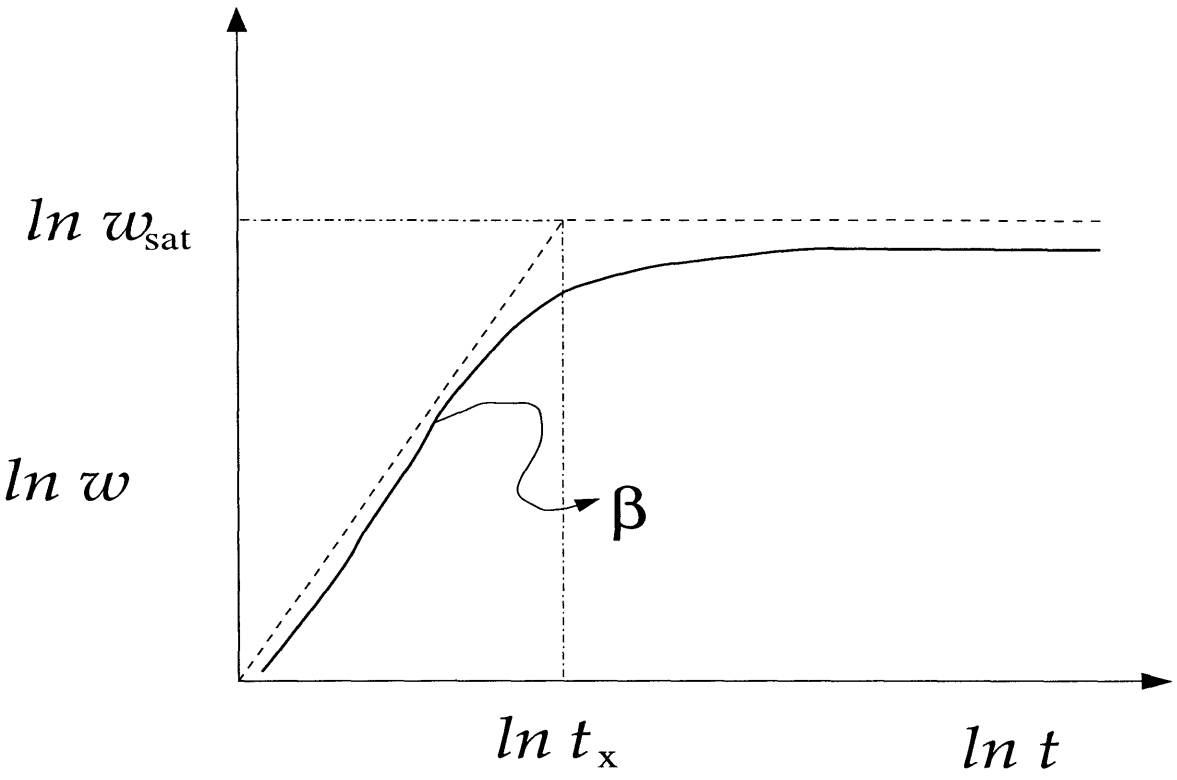

Figure 12-3: Evolution of the interfacial width

that w_{sat} obeys the following scaling relationship as a function of the length of the apparatus L:

$$w_{\text{sat}} \sim L^{\alpha}. \tag{12.8}$$

The exponent α which quantifies the fluctuations of the interface (as deviations from its mean value) is appropriately known as the *roughness exponent* of the interface. The requirement of a smooth matching at the crossover point furnishes one further scaling relationship relating the crossover time t_X to the length of the apparatus L:

$$t_X \sim L^{z}, \tag{12.9}$$

where $z = \alpha/\beta$.

Based on the above two observations, it has been proposed on an empirical basis [6] (and confirmed experimentally) that the width of the interface, $w(L,t)$, normalized

by the saturation width w_{sat} obeys the scaling relationship

$$\frac{w}{w_{\text{sat}}} \sim L^{\alpha} f(\frac{t}{t_X}), \tag{12.10}$$

where the scaling function f possesses the following properties:

$$f(u) \longrightarrow \begin{cases} u^{\beta}, & u \ll 1, \\ 1, & u \gg 1. \end{cases} \tag{12.11}$$

The above scaling hypothesis for the width of the interface is known as the *Family-Viscek* scaling hypothesis, it forms the basis for most studies involving the statistics of interfacial growth.

To determine the dynamical and the roughness exponents through a scaling procedure one needs to utilize the general properties of self-affine functions outlined in the preceding section. The interface is assumed to be statistically self-affine and single-valued.[4] Further, the roughness exponent α is assumed to be less than or equal to 1. The latter assumption is requisite to the formulation of a gradient theory of the fluctuations of the interface. If $\alpha < 1$ then $\nabla h \sim L^{\alpha-1}$ which becomes negligible for $L \gg 1$. This permits one to formulate a gradient theory of interfacial fluctuations by retaining the dominant terms of a gradient expansion. This simplification facilitates construction of phenomenological equations and enables scaling analysis based conclusions to be drawn.

The properties of self-affine functions outlined in the previous section lead us to expect statistical self-similarity of the interface upon rescaling the spatial and temporal variables. Suppose that the spatial variable x is rescaled in the following manner:

$$x' \rightarrow bx. \tag{12.12}$$

[4]There are a number of cases of practical interest wherein the assumption that our interfacial coordinate system yields a single-valued representation of the interfacial height is inapplicable; some examples in this category are the morphology of the interfaces formed during fingering instabilities in porous media [22], patterns encountered during diffusion-limited aggregation processes [25], etc.

This requires that the temporal variable t be rescaled as

$$t' \rightarrow b^z t \tag{12.13}$$

to ensure that the ratio t/t_X remains unchanged. The transformation (12.12), used in conjunction with the *Family-Viscek* scaling hypothesis requires that the interfacial height $h(x,t)$ simultaneously be transformed as

$$h' \rightarrow b^\alpha h. \tag{12.14}$$

Under the triplet of transformations (12.12) - (12.14), the statistical properties of the interface described by $h'(x',t')$ are expected to be identical to those of the original interface, namely $h(x,t)$. Therefore, $h'(x',t')$ would also be expected to satisfy an equation identical to that for $h(x,t)$. This conclusion enables explicit determination of the dynamical and roughness exponents of the interface.

It is pertinent to recall here the assumptions that were effected in the preceding analysis, so as to delineate the conditions under which the above-outlined procedure retains accuracy. This would also thereby clarify the shortcomings of the approach, enabling us to highlight other important as well as more rigorous techniques for effecting similar conclusions. Scaling analysis is inherently a 'mean-field' type of analysis. In most instances α and β acquire only rational values — in contrast to numerical simulations and more rigorous analytical calculations where irrational values are possible. For instance, a scaling analysis that establishes a roughness exponent α greater than one suggests a need for more rigorous analysis incorporating the fluctuations from the mean-field results. Furthermore, scaling analysis is performed on a specific model, the choice of which is decided at the outset during the problem formulation. Scaling concepts cannot provide any indication of the terms that might, in fact, be present within the model, or be subsequently generated in the analysis.

Renormalization group techniques constitute a more rigorous approach towards describing the statistical properties of the interfacial dynamics [1, 19]. These techniques incorporate the effect of fluctuations rigorously, thereby furnishing an accurate

determination of the exponents, albeit in most cases as an asymptotic series. Renormalization group techniques are also powerful enough to treat cases of generalized stochasticity (see the next section), enabling conclusions to be drawn even when the scaling analysis either fails or yields incorrect results.[5] However, this method is quite involved as regards technical details, and its use for complicated scenarios tends to require further development as the situation demands [24]. In such cases, scaling analysis usually provides a good estimate of the exponents, values which would possibly be obtained from more sophisticated renormalization group arguments [13].

The formulation of a model for the interfacial dynamics is a broad subject, one which lies is beyond the scope of this thesis [15]. In general, symmetry principles akin to Landau's original conception [10] are typically utilized to determine the terms that are present. Other approaches employed to derive and/or propose interfacial dynamical equations include considerations of microscopically occurring processes for the description of the macroscopic interfacial dynamics. (A specific context will be illustrated in the next chapter via our formulation of the problem.)

In this section we discussed the general characteristics of interfacial fluctuations arising from its self-affine nature, and the consequences thereof in terms of scaling laws. In the next section we discuss the origins of the stochastic fluctuations present in the dynamics of these interfaces together with some common representations employed to model these features.

12.3 Stochasticity

Physically, stochasticity can arise from a number of different sources, the most common of which includes: thermal fluctuations, random driving forces, disorder in the environment, or even as a manifestation of the microscopic degrees of motion. The statistical nature of the interface derives from this stochastic component, which influences the dynamical evolution of the interface. Within a mathematical framework, the

[5]The accuracy of the results can be determined by a direct numerical simulation of the continuum equation.

stochastic noise usually provides the random component appearing in the evolution equation for the interfacial dynamics. As such, i.e. thereby plays an important role in determining the statistical properties of the self-affine interface. The noise function (denoted by η in our text) is mathematically represented by a random function which is specified by the functional form of its correlations. Therefore, one would expect different functional forms for the correlations to lead to different statistical behaviors for interfaces, which might in fact be governed by identical deterministic components. Below, we give a brief introduction to some of the commonly employed models for noise, while simultaneously highlighting the features that the model represents. This list is by no means exhaustive. For more details refer to [1].

12.3.1 Annealed Noise

The most common model for noise, namely "annealed noise," is a random function of both spatial and temporal coordinates. The origin of such a noise term may result from thermal fluctuations present in the system, or as from an external forcing which is random in both space and time. In most cases the noise is assumed to be delta-correlated in space and time (equivalent to extremely short-ranged correlations):

$$\langle \eta(\mathbf{x}, t)\eta(\tilde{\mathbf{x}}, \tilde{t})\rangle = 2\Delta\delta^d(\mathbf{x} - \tilde{\mathbf{x}})\delta(t - \tilde{t}), \tag{12.15}$$

where Δ measures the amplitude of the noise, δ denotes the Dirac delta function, and d is the dimensionality of the transverse space. The delta-correlated annealed noise is sometimes also termed thermal noise.

A generalized form of the above noise is one which exhibits long-range correlations in space and time of the form:

$$\langle \eta(\mathbf{x}, t)\eta(\tilde{\mathbf{x}}, t')\rangle \sim |\mathbf{x} - \tilde{\mathbf{x}}|^{2\rho-d}|t - \tilde{t}|^{2\theta-1}, \tag{12.16}$$

where ρ and θ are exponents characterizing the spatial and temporal correlations of the noise. While the physical origin of such correlations is unclear, mathematically

such correlations might arise via the mathematical elimination (projection) of those physical quantities that exhibit relaxation timescales much smaller than those possessed by the other quantities present (as will be illustrated in the next chapter).

12.3.2 Quenched Noise

Quenched noise [3] is usually used to model stochasticity arising from the disorder present within the medium wherein the interface evolves. The statistical nature of the medium is assumed to be unchanging in time (within the time scales of interest). As such, the functional forms chosen for the noise correlations are explicitly independent of time, i.e. $\eta \equiv \eta(\mathbf{x}, y)$, where y is the distance normal to the plane of the interface. The functional form for the correlations of the corresponding delta-correlated quenched noise is

$$\langle \eta(\mathbf{x}, y)\eta(\tilde{\mathbf{x}}, \tilde{y})\rangle \sim \delta^d(\mathbf{x} - \tilde{\mathbf{x}})\delta(y - \tilde{y}). \tag{12.17}$$

Figure (12-4) illustrates a physical scenario wherein the dynamics modulated by the random medium can be modeled by incorporating a quenched noise within the evolution equation.

12.3.3 Scaling of the Noise

In the previous section we discussed the triplet of scaling transformations [cf. (12.12) - (12.14)] which need to be effected to impose invariance of the statistics of the self-affine interface. However, as a result of the transformations undergone by the spatial and the temporal coordinates, the strength of the noise needs to be appropriately rescaled. In this section we consider the rescaling transformation which needs to be effected on the noise term to thereby account for the spatio-temporal transformations.

Consider the structure of the correlations of delta-correlated annealed noise. If we employ the transformations (12.12) and (12.13), by rescaling the spatial coordinate $\mathbf{x} \to \mathbf{x}'$ (with a similar transformation being applicable for $\tilde{\mathbf{x}}$) and $t \to t'$ (and similarly for $\tilde{t}$),

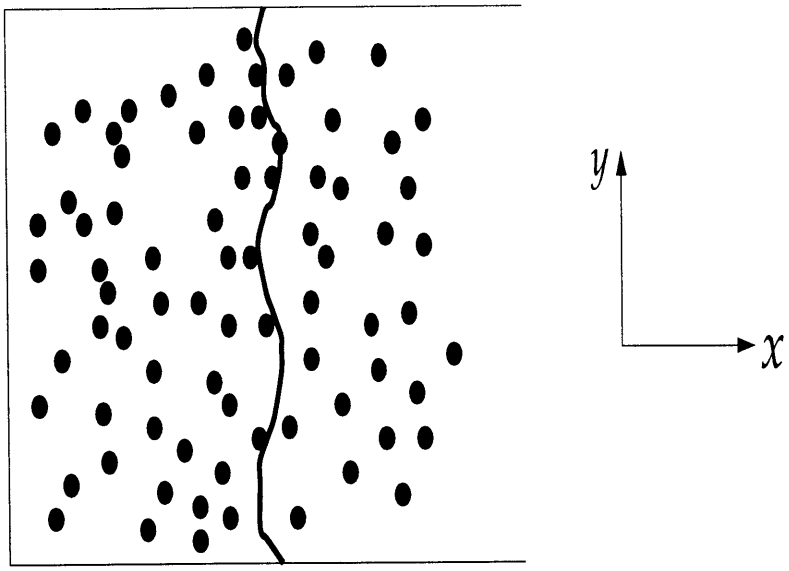

Figure 12-4: An example of quenched noise: The movement of an interface in a random medium. The random medium is manifested as a 'quenched' (assuming that the distribution is fixed in time) random force on the interface.

we obtain,[6]

$$\langle \eta(b\mathbf{x}, b^z t)\eta(b\tilde{\mathbf{x}}, b^z \tilde{t}')\rangle = 2\Delta b^{-(d+z)}\delta^d(\mathbf{x}-\tilde{\mathbf{x}})\delta(t-\tilde{t}). \tag{12.18}$$

Thus, the strength of the rescaled noise is modulated by a multiplicative factor $b^{-(d+z)/2}$. This suggests that the transformations (12.12) - (12.14) require transforming the noise simultaneously (for a delta-correlated annealed noise) as:

$$\eta' \to \eta b^{-(d+z)/2}. \tag{12.19}$$

For situations wherein quenched noise is present, one typically encounters a situation where the amplitude and the correlations of the noise at the interfacial position

[6]In the equation (12.18) we utilized the following identity pertaining to Dirac delta functions:

$$\delta^d(b\mathbf{x}) = \frac{1}{b^d}\delta^d(\mathbf{x}).$$

is the relevant quantity, in which case the noise term appears in the functional form $\eta(\mathbf{x}, h)$. In such cases, the appropriate transformation, which can be determined along the same lines as indicated above for the delta-correlated noise, is of the form

$$\eta' \to \eta b^{-(d+\alpha)/2}. \tag{12.20}$$

12.4 Simple Examples of Flory Scaling Analysis

In this section we illustrate the spirit of Flory scaling analysis by means of three simple examples. Each example represents a widely used model for interfacial growth. In all three cases we eschew details regarding the origin and the derivation of these equations, except for a brief description of the physical significance of the terms present in the model. Subsequently we focus on determining of the roughness and dynamical exponents, based on the simple scaling principles elucidated in the previous sections.

12.4.1 Edwards-Wilkinson Equation

One of the simplest models for interfacial growth processes is the Edwards-Wilkinson model [5]:

$$\frac{\partial h}{\partial t} = \sigma \nabla^2 h + \eta(x, t). \tag{12.21}$$

The above model was proposed to quantify the growth of interfaces during a random deposition process. The random deposition processes are modeled through the stochastic annealed noise term $\eta(x, t)$, which is assumed to be delta-correlated. The term $\sigma \nabla^2 h$ describes the surface-diffusional relaxation processes that accompany the interfacial evolution. The above equation can also be used to describe the dynamics of the thermal fluctuations of a fluid interface. In this context σ corresponds to the interfacial tension of the fluid, and $\eta(x, t)$ to the thermal fluctuations of the interface. In the latter case, the above equation can be derived as a Langevin equation from the

corresponding Hamiltonian that embodies the energy cost of interfacial fluctuations.

To perform a scaling analysis of the above equation we assume *a priory* that the interface and its statistics are self-affine. This allows us to assume that the rescaled equation [governing $h'(\mathbf{x}', t')$] also satisfies an equation identical in form to the above. Therefore,

$$\frac{\partial h'}{\partial t'} = \sigma \nabla'^2 h' + \eta'(x', t'). \tag{12.22}$$

Inserting the transformation laws described by eqs. (12.8) - (12.12) and eq. (12.19) into the above equation yields

$$b^{\alpha - z} \frac{\partial h}{\partial t} = b^{\alpha - 2} \sigma \nabla^2 h + b^{-(d+z)/2} \eta(x, t). \tag{12.23}$$

Further, since eq. (12.21) represents the dynamical equation for $h(x, t)$, we require that

$$b^{\alpha - z} = b^{\alpha - 2} = b^{-(d+z)/2}. \tag{12.24}$$

Equating exponents furnishes the following three equalities:

$$\alpha = \frac{2 - d}{2}; \quad z = 2; \quad \beta = \frac{2 - d}{4}. \tag{12.25}$$

The above analysis demonstrates the utility of scaling analysis in determining statistical exponents without explicitly invoking the exact solution of the complete dynamical model. However, it must be borne in mind that the above analysis needs to be confirmed by more rigorous methods, like that of the renormalization group. Within renormalization group theories the scaling forms arise naturally, in contrast to the above case where it was necessary to make an *a priori* assumption regarding the self-affinity of the interface. In this particular model the rigorous analyses yields precisely the same exponents as obtained through our scaling analysis. The reasons for this coincidence are embodied within the linear nature of the governing equations

[5].

In fact, one can speculate the possibility of σ being transformed during a scale transformation. In this case it can be proved (based on more rigorous methods) that such a renormalization is absent. This again underlines the utility of rigorous analysis in situations wherein such an analysis is indeed possible.

12.4.2 Interfaces in Random Field Ising Model

The Edward-Wilkinson model can be appropriately modified for the situation wherein the disorder is quenched rather than annealed, as assumed above. Such a modification is used to model interfaces between two spin phases (as in an Ising model), wherein a random force acts simultaneously on the spins [3]. Such systems are of interest in condensed matter theory, where they are encountered in the context of sliding charge-density waves, vortex lines in superconductors, etc. Upon effecting this modification, the Edwards-Wilkinson model for the dynamics of interfacial profile is then transformed to the form

$$\frac{\partial h}{\partial t} = \sigma \nabla^2 h + \eta(x, h). \tag{12.26}$$

In the next chapter, we indicate the Hamiltonian from which the above equation can be derived using a Langevin formulation. For the purpose of the present discussion we consider the scaling analysis of the above equation. Using the transformation principles outlined in the previous example, along with the corresponding transformation outlined for the quenched noise [cf. eq. (12.20)], we obtain:

$$b^{\alpha - z} \frac{\partial h}{\partial t} = b^{\alpha - 2} \sigma \nabla^2 h + b^{-(d+\alpha)/2} \eta(x, h). \tag{12.27}$$

Comparison with eq. (12.26) yields

$$b^{\alpha - z} = b^{\alpha - 2} = b^{-(d+\alpha)/2}, \tag{12.28}$$

which, upon equating the respective exponents yields,

$$\alpha = \frac{4-d}{3}; \quad z = 2; \quad \beta = \frac{4-d}{6}. \tag{12.29}$$

The above scaling analysis yields both the roughness and the dynamical exponent for the Random Field Ising Model. The presence of the quenched noise term acts as a nonlinear forcing mode in the dynamical evolution of the interface [since the noise term is also a function of $h(x,t)$]. In such a scenario the scaling analysis would be a bit suspect due to possible renormalizations under the transformations (for instance, the surface tension σ could possibly be renormalized). A rigorous analysis of the above example requires the use of an intricate form of functional renormalization group analysis. Such a procedure yields an identical value for the roughness exponent; however, the dynamical exponent is different from that obtained in the scaling analysis above. The physical origin of the breakdown in our scaling analysis arises from the fact that the *functional form* of the noise becomes transformed during the rescaling process. Details of the intricacies accompanying such a 'functional' renormalization can be found in [20, 21]. This example serves to underline the caution that needs to be exercised in interpreting the results of the scaling analysis.

Finally, the spirit of Flory scaling analysis is illustrated by the following simple example.

12.4.3 Growth During Molecular Beam Epitaxy (MBE)

In the section we consider one of the simplest models involving the presence of two distinct length scales. Thereby, this example thereby to illustrate the principles of Flory analysis as employed in the next chapter. The following model is proposed for the evolution of the interfacial profile during MBE processes [26], embodying within itself the surface diffusion and the desorption processes taking place in conjunction with the random deposition:

$$\frac{\partial h}{\partial t} = \sigma \nabla^2 h + K \nabla^4 h + \eta(x,t). \tag{12.30}$$

Here η is assumed to be an annealed noise having no long-range correlations, whereas K represents a phenomenological coefficient.

Rescaling the above equation, yields

$$b^{\alpha-z}\frac{\partial h}{\partial t} = b^{\alpha-2}\sigma\nabla^2 h + b^{\alpha-4}K\nabla^4 h + b^{-(d+z)/2}\eta(x,t). \tag{12.31}$$

If we proceed as in the previous examples by equating the exponents in the above a contradiction arises, since this would require that

$$b^{\alpha-z} = b^{\alpha-2} = b^{\alpha-4} = b^{-(d+z)/2}. \tag{12.32}$$

The contradiction is resolved by noting that the above model is characterized by the presence of more than one term governing the dynamics (in addition to the noise, which is essential to provide the stochasticity in the dynamics). As such it and therefore involves the presence of more than one length scale. In such situations we need to delineate the distinct length scales at the outset to determine the different scaling regimes.

In the above model, let us first assume that the second gradient term dominates over the fourth gradient term (which proves to be reasonable in the long wavelength limit being considered). This will be valid for length scales l such that

$$\sigma\frac{h}{l^2} \gg K\frac{h}{l^4}. \tag{12.33}$$

Equivalently,

$$l \gg l^* = \sqrt{\frac{K}{\sigma}}. \tag{12.34}$$

In this regime the $\nabla^4 h$ term can be neglected in the analysis, thereby yielding the same identical exponent values as the Edwards-Wilkinson model [cf. eq. (12.25)]. Thus, the characteristic fluctuations of the interface, as measured on lengthscales l such that $l \geq l^*$, exhibit self-affine characteristics with exponent values identical to those of the

Edwards-Wilkinson exponents. However, situations may arise wherein the physical dimensions of the apparatus do not allow l to satisfy the above inequality. In such cases, wherein $l \leq l^*$, the $\nabla^4 h$ term dominates over the $\nabla^2 h$ term. This identification would require us to match the corresponding exponents arising from these terms, requiring that

$$b^{\alpha - z} = b^{\alpha - 4} = b^{-(d+z)/2}, \tag{12.35}$$

thereby yielding

$$\alpha = \frac{4-d}{2}; \quad z = 4; \quad \beta = \frac{4-d}{8}. \tag{12.36}$$

Consequently, on scales such that $l \ll l^*$ the interface is self-affine with exponents given by eq. (12.36).[7]

Through the above simplistic example we clarified the nature of Flory analysis and its underlying basis in terms of the delineation of the appropriate length scales and thereby determining the scaling regimes by matching the corresponding exponents. This type of Flory analysis, and the general principles outlined in this chapter will be used extensively in the next chapter to derive and analyze the dynamical equation for the problem of interest.

[7]Note that the above scaling argument yields that $\alpha = 3/2$ for $d = 1$. This suggests that our continuum approximation which led to eq. (12.30) breaks down for $d = 1$.

References

[1] A.-L. Barabasi and H. E. Stanley, *Fractal Concepts in Surface Growth*, Cambridge University Press, Cambridge (1995).

[2] P. Bak, *How Nature Works: The Science of Self-organized Criticality*, Copernicus, New York (1996).

[3] R. Bruinsma and G. Aeppli, "Interface motion and nonequilibrium properties of the random-field Ising model," *Phys. Rev. Lett.*, **52**, 1547 (1984).

[4] J. des Cloizeaux and G. Jannink, *Polymers in Solution: Their Modeling and Structure*, Oxford University Press, New York (1990).

[5] S. F. Edwards and D. R. Wilkinson, "The surface statistics of a granular aggregate," *Proc. R. Soc. London A*, **381**, 17 (1982).

[6] F. Family and T. Viscek, *Dynamics of Fractal Surfaces*, World Scientific, Singapore (1991).

[7] J. Feder, *Fractals*, Plenum Press, New York (1988).

[8] M. E. Fisher, "Renormalization group theory: Its basis and formulation in statistical physics," *Reviews of Modern Physics*, **70**, 653 (1998).

[9] P. G. de Gennes, *Scaling Concepts in Polymer Physics*, Cornell University Press, Ithaca (1979).

[10] V. L. Ginzburg and L. D. Landau, "On the theory of superconductivity," *Zh. Eksp. Teor. Fiz.*, **20**, 1064 (1959).

[11] H. Goldstein, *Classical mechanics*, Addison-Wesley, Reading, Massachussetts (1980).

[12] A. H. Guth, *The Inflationary Universe: The Quest for a New Theory of Cosmic Origins*, Addison-Wesley, Reading, Massachussetts (1997).

[13] H. G. E. Hentschel and F. Family, "Scaling in open dissipative systems," *Phys. Rev. Lett.*, **66**, 1982 (1991).

[14] L. P. Kadanoff, "Static phenomena near critical points: Theory and Experiment," *Rev. Mod. Phys.*, **39**, 395 (1967).

[15] M. Kardar, "Nonequilibrium dynamics of interfaces and lines," *Phys. Rep.*, **301**, 85 (1998).

[16] B. B. Mandelbrot, *The Fractal Geometry of Nature*, W.H. Freeman, San Francisco (1982).

[17] B. B. Mandelbrot, "Self-affine fractals and fractal dimension," *Physica Scripta*, **32**, 257 (1985).

[18] P. Meakin, *Fractals, Scaling and Growth far from Equilibrium*, Cambridge University Press, New York (1998).

[19] E. Medina *et al.*, "Burgers equation with correlated noise: Renormalization group analysis and applications to directed polymers and interfacial growth," *Phys. Rev. A*, **39**, 3053 (1989).

[20] O. Narayan and D. S. Fisher, "Threshold critical dynamics of driven interfaces in random media," *Phys. Rev. B*, **48**, 7030 (1993).

[21] T. Nattermann, S. Stepanow, L.-H. Tang and H. Leschhorn, "Dynamics of interface depinning in a disordered medium," *J. Phys. II*, **2**, 1483 (1992).

[22] J. Nittmann, G. Daccord and H. E. Stanley, "Fractal growth of viscous fingers: A quantitative characterization of a fluid instability phenomenon," *Nature*, **314**, 141 (1985).

[23] A. Pimpinelli and J. Villain, *Physics of Crystal Growth*, Cambridge University Press, New York (1998).

[24] M. Schwartz and S. F. Edwards, "Nonlinear deposition: A new approach," *Europhys. Lett.*, **20**, 301 (1992).

[25] T. A. Witten and L. M. Sander, " Diffusion-limited aggregation," *Phys. Rev. Lett.*, **47**, 1400 (1981).

[26] D. E. Wolf and J. Villain, "Growth with surface diffusion," *Europhys. Lett.*, **13**, 389 (1990).

Chapter 13

Two-Phase Fluid Interfaces in Random Media

Reference: Venkat Ganesan and Howard Brenner, "Dynamics of Two-Phase Fluid Interfaces in Random Porous Media," *Phys. Rev. Lett.*, **81**, 578 (1998).

In the preceding chapter we expounded some of the salient features commonly employed in the description of the statistical properties of fluctuating interfaces. These interfaces are 'roughened' by stochastic inputs, which are either inherently present within the system (as in the case of thermal noise), or may arise from sources external to the system (like a random deposition or externally applied random forces). In this chapter we utilize some of those quantitative techniques to analyze the effect of disorder on the morphology of moving interfaces. Explicitly, this analysis is effected within the specific context of *two-phase fluid flow through porous media.* The interfacial morphologies displayed during the displacement of one fluid by another in a porous medium display a rich variety of behaviors depending upon the respective viscosities and wetting properties of the two fluids [32]. Some characteristic behavior, which have been observed during experiments (performed on lab-scale porous media) include:

1. The displacement of a viscous fluid by a less viscous fluid leads to the well-known phenomenon of fingering instability. In a generic sense, this instability is related to the Saffman-Taylor instability proposed based on theoretical and experi-

mental studies on Hele-Shaw cells [30]. The original study (cf. [28] for a collection of papers related to studies on viscous fingering instabilities) did not explicitly address the influence of the wetting properties of the respective fluids on the fingering patterns. Subsequent experimental studies [23, 32] probed the specific effects of wetting properties, and observing the presence of a rich variety of behavior wherein: (i) when the non-wetting fluid constituted the displacing fluid, the finger widths were found to be comparable to the pore size of the porous medium; (ii) however, when the wetting fluid was the displacing fluid, the finger sizes were found to scale with the capillary number Ca as $(\kappa/\mathrm{Ca})^{1/2}$, where κ denotes the permeability of the porous medium. The origin of this new length scale constitutes an hitherto unresolved issue in the modeling of interfacial fronts in porous media (cf. also Weitz *et al.* [35] for a deeper exposition of this issue).

2. In the opposite viscosity ratio limit, namely the case where the displacing fluid is of higher viscosity than the displaced fluid, the interfacial front is stable. Despite the fact that at the fine-scale[1] the interfacial front manifests singularities and discontinuities (due to the presence of boundaries arising from the porous structures), at the coarse-grained scale the interface can be viewed as a *continuous* entity, which has been nevertheless 'roughened' because of the existence of the porous structures [29]. [This viewpoint is explicitly displayed in Fig. (13-1).] Experiments probing the morphology of this roughened interfacial front (within the continuous representation) have concluded that the interfacial front possesses statistical self-affinity. This observation has subsequently led to a number of experiments performed with the objective of quantifying the roughness exponents of the self-affine interface. Even, within this relatively simpler 'stable-front' situation, these experiments nevertheless suggested the presence of a rich diversity of behaviors:

a. The random pinning forces (arising from the porous structures) compete with the applied driving pressure, resulting in a critical threshold force which needs to

[1] In the notation of the previous section of the thesis, the phrase 'fine scale' corresponds to the 'microscale,' and the corresponding 'coarse-grained scale' the 'macroscale.'

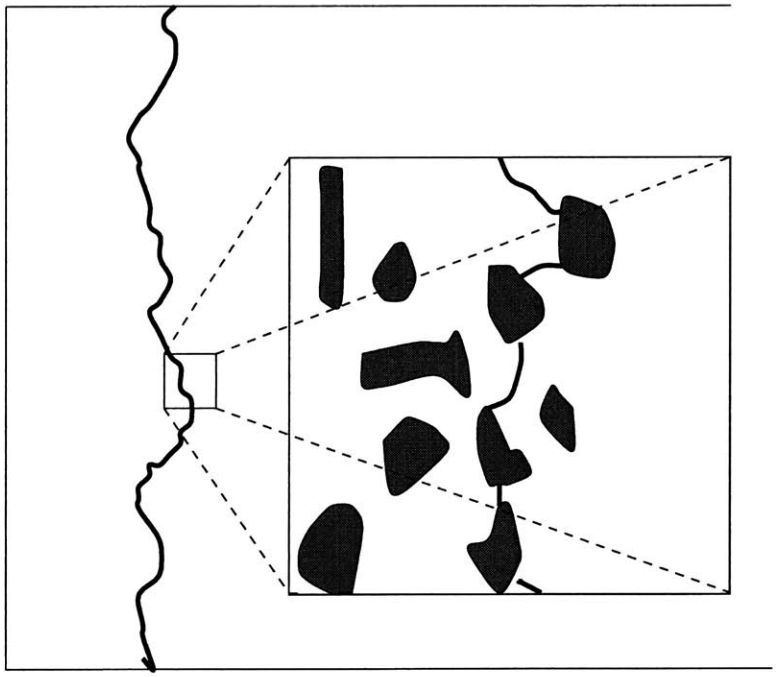

Figure 13-1: "Fine scale" and the "coarse-grained scale" representations of the interface.

be overcome before the interface starts moving. The transition from the trapped metastable state (i.e. pinned interface) to a (depinned) moving state is purported to be a *nonequilibrium phase-transition* [33, 35]. Considerable interest exists in studying the morphology of the fluid interfacial fronts in the regime near this phase transition, when the applied pressure just exceeds the critical pressure. This regime is qualitatively similar to the regime existing near an equilibrium critical point [17], and has been analogously found to exhibit characteristic universal behavior in laboratory scale experiments.[2] Some salient experimental observations in this regime include:

(i) In the case termed Forced Fluid Invasion (FFI), wherein a 'depinning transition' occurs at a critical value of the applied pressure gradient, experiments have unequivocally indicated that a range of interfacial scaling exponents is possible, depending upon the magnitude of the capillary number. At very low capillary numbers the roughness exponent α was found to be equal to 0.8 [13, 29]. An increase in the capillary numbers (achieved by increasing the invasion velocity) displayed a concomitant

[2]In this context, universality refers to identical interfacial scaling statistics for different systems.

gradual crossover to a roughness exponent of 0.5 [11].

(ii) In the case wherein the displacing fluid invaded the porous medium by virtue of its own capillary forces [termed as imbibition invasion (IMI)], the system exhibits a 'pinning transition' wherein the interface gets pinned because of its inability to overcome the random forces. This moving-pinned transition has also subsequently been claimed to be an example of a nonequilibrium phase transition, with the comparable experiments manifesting a roughness exponent of $\alpha = 0.63$ [1].

b. Finally, when a nonwetting fluid displaces a wetting fluid (still within the stable-front regime), a self-similar fractal structure of the interfacial front has been observed [24].

Due to the universal nature observed in the experiments, this regime has attracted a number of phenomenological modeling efforts (cf. Stepanow [31]) to accurately explain the physics of the phenomena at hand. Despite innumerous experimental and theoretical studies, a unifying feature of the entire gamut of observations is still fundamentally lacking. In this work we formulate and analyze a model based on a gradient expansion of the interfacial fluctuations to thereby providing some unifying aspects of the observed phenomena.

13.1 Philosophy of the Analysis

In the following analysis, we focus on those scenarios wherein experiments have revealed a self-affine interface. Further, we specifically concentrate on the regime near the 'depinning (and pinning) transition,' since a number of experiments have purported to observe universal values for the exponents in this regime. Our analysis performed will be purely at a macroscopic level — in contrast to the previous sections of the thesis — which dealt with the explicit transition from the microscale to the macroscale. The following remarks constitute the philosophy underlying the subsequent macroscopic phenomenological analysis: near a critical point (the depinning transition), the macroscopic details of the system become independent of most of the innumerable microscopic details of the systems studied [9], and instead depend upon

only on a few salient features of the system. These basic microscopic features can be captured by appropriate phenomenological parameters within a macroscopic model. Quantification of these parameters would require detailed analysis (along the lines of the preceding parts of thesis) to effect the transition from the microscale to the macroscale level. However, even in the absence of such an explicit identification of the macroscopic parameters, we can deduce certain universal macroscale properties of the system (near its critical point) based on quantitative analysis of the phenomenological model. It will be shown in the following analysis that the roughness exponent is one such result which can be deduced based upon considerations of the phenomenological model [19].[3]

Based on such a philosophy, we eschew consideration of details of the porous medium, and instead content ourselves to represent the latter as a 'quenched random force' acting on the fluid. The origin of this force can be heuristically justified in terms of the respective wetting properties of the fluids and the accompanying gain in chemical potential due to invasion [4]. Furthermore, we represent the interfacial structure by a coarse-grained parameter h, which is assumed to be a continuous function of the transverse spatial coordinate (denoted by x in our analysis). Despite the innumerous discontinuities which occur at the microscale level, construction of a coarse-grained interfacial representation is justified in the self-affine case where the interface is smooth, i.e. $\nabla h \sim L^{\alpha-1} \to 0$, as $L \to \infty$. Further, we concentrate on capturing the physics accompanying fluid flow phenomena (thereby distinguishing it from magnetic systems), which features where overlooked in the previous theoretical researches on this issue. These researches are briefly summarized in the next section along with their predictions, most of which we believe are either incorrect or incomplete.

Subsequent to the derivation of a new model representing the phenomena, we resort to a simplistic scaling analysis of our model so as to elucidate the possible

[3]The burden of the entire analysis is to formulate a reasonable phenomenological model to quantify the situation. The test of the model lies in a comparison of its predictions with experimental observations.

roughness exponents predicted by the model. As cautioned in the preceding chapter, scaling analysis is a bit suspect when nonlinearities arising from quenched roughness are present. However, in most of the previous researches which dealt with the rigorous renormalization group analysis of quenched random systems, Flory analysis has predicted the roughness exponent quite accurately [25]. Therefore, in this work we utilize scaling analysis to predict the roughness exponent in our model. Moreover, experiments measuring the dynamical exponents are too few and contradictory (see for instance [15]) to draw meaningful conclusions sufficient to enable comparison of predictions derived from theoretical models.

13.2 Review of Previous Studies

Analogies between the behavior exemplified by two-phase fluid interfaces and interfaces occurring in condensed matter systems (for example, between the two phases of magnets) have led to the claims that same phenomenological model might be used to characterize the interfacial dynamics in both cases. The model most widely proffered for the depinning transition case is the dynamical version of RFIM [5], namely

$$\frac{\partial h}{\partial t} = F + \sigma \frac{\partial^2 h}{\partial x^2} + \eta(x,h), \tag{13.1}$$

wherein h denotes the interfacial position of the front in the longitudinal y direction and x the transverse coordinate (we are concerned exclusively with the experimental case where x is one-dimensional). σ denotes the so-called macroscopic interfacial tension and F the applied force. $\eta(x,h)$ constitutes the quenched random noise, representing the affinity of the disordered medium for one of the two phases. For random field disorder the noise term is assumed to be delta-correlated in both the x and y directions with a zero mean value, i.e.

$$\begin{aligned} \langle \eta(x,h) \rangle &= 0. \\ \langle \eta(x,h)\eta(x',h') \rangle &= \Delta_o \delta(x-x')\delta(h-h'). \end{aligned} \tag{13.2}$$

In the above equation Δ_o quantifies the strength of the noise.

Studies of eq. (13.1) have hitherto yielded inconclusive results regarding the scaling exponents α and z observed in the fluid-flow experiments. As expounded earlier, two distinct universality classes are believed to exist for the scenario accompanying fluid-flow experiments:

(a) Forced fluid invasion (FFI): Experiments corresponding to this situations involves the displacement of one fluid by another due to an applied pressure gradient. In such cases renormalization group arguments based on eq. (13.1) predict $\alpha = 1$ [25, 26], whereas numerical algorithms based on the above model yield $\alpha = 1.25$ [22] (also cf. Kessler *et al.* [20]). In contrast, experiments performed for such a scenario result in a range of exponents, $\alpha = 0.5 - 0.8$ (cf. [11, 13, 29]), depending upon the magnitude of the capillary number. Zhang [36] proposed (subsequently corroborated by experiments of Horvath *et al.* [14]) that an uncorrelated annealed noise with a power law distribution of noise amplitudes could possibly rationalize the roughness exponents observed in experiments. In a seminal computer simulation investigation of the fluid invasion phenomena, Nolle *et al.* [27] obtained $\alpha = 0.8$, further showing that for a medium with *quenched disorder* the definition of the noise as proposed in [14] would yield the noise statistics proposed by Zhang. Since power law statistics manifest difficulties in interpreting the exponent [36] we content ourselves here with representing the porous medium as a quenched random field disorder.

(b) The second universality class corresponds to the imbibition invasion (IMI) of one fluid into another by capillary forces. In this case, the experimentally observed depinning exponent of $\alpha = 0.63$ is justified by a phenomenological mapping onto Directed Percolation Depinning (DPD) [2, 34]. The continuum model believed to be appropriate for this scenario is obtained by incorporating a nonlinear term into eq. (13.1) [1]:

$$\frac{\partial h}{\partial t} = F + \sigma \frac{\partial^2 h}{\partial x^2} + \lambda \left(\frac{\partial h}{\partial x} \right)^2 + \eta(x, h). \tag{13.3}$$

The basis for the difference in universality classes of FFI and IMI phenomena, as

well as the observed discrepancies between theoretical and experimental values of α in FFI, remain unresolved. Some of the salient features which distinguish the FFI and IMI cases are: (a) the absence of an external driving force in IMI; (b) weak strength of the disorder in FFI, contrasted with the strong disorder characterizing IMI. However, based on these two features it has not yet been possible to justify the applicability of continuum equation (13.1) for FFI and (13.3) for IMI.

In the following sections we use a more microscopic-based derivation of a model for describing the two-phase fluid interfaces in random media. Subsequently, this model will be shown to reduce to the above two models under appropriate limiting scenarios. Thereby our model yields a unified representation of the phenomena occurring during fluid flows in porous media.

13.3 Derivation of Dynamical Equation

Our analysis examines an oft-neglected issue (although, see He *et al.* [11] and Krug & Meakin [21]), one which distinguishes two-phase fluid flows from random magnets. This relates to the *nonlocal* nature of the flow field characterizing two-phase flows. While models involving local dynamics can be obtained from symmetry considerations, nonlocal models necessitate a more detailed microscale analysis. In our case, such a description of the dynamics is obtained from Darcy's law, which is assumed to govern the fluid motion at the macroscale. The latter relates the velocity field to the pressure *gradient*[4] rather than to the driving pressure itself. This feature which distinguishes the dynamics of magnets and fluid-flows turns out to be a crucial aspect, and enables the rationalization of experimental observations.

We consider an experimental scenario in which water constitutes the displacing fluid, and air the displaced fluid (allowing us to set the viscosity ratio to 0, thereby simplifying the analysis considerably). Furthermore, we assume a quasistatic response of the pressure field to the instantaneous interfacial configuration. We believe that such an approximation is reasonable near the depinning transition, where the mean

[4]The dependence on the gradient of the pressure constitutes the 'non-locality' in the phenomena.

velocity V of the interface approaches zero. For simplicity, in the following analysis we confine ourselves to the experimentally relevant case of one-dimensional interfaces. A new model of interfacial dynamics is thereby derived by adapting the RFIM. Based on this equation derived from microscopic considerations, we outline the expected form of the general equations for FFI and IMI regimes. For the FFI regime a dynamical Flory-type scaling analysis is carried out on the model, carefully delineating the length scales of its validity, thereby enabling us to speculate on the magnitude of the roughness exponent α. This yields $\alpha = 3/4$ which accords well with experimental results. We are also able to justify the observed cross-overs in the roughness exponents observed at higher capillary numbers. Furthermore, we also heuristically justify the difference in universality classes between FFI and IMI based on the absence of an applied pressure gradient and the strength of the disorder. The notation used in the following analysis is clarified in Fig. (13-2).

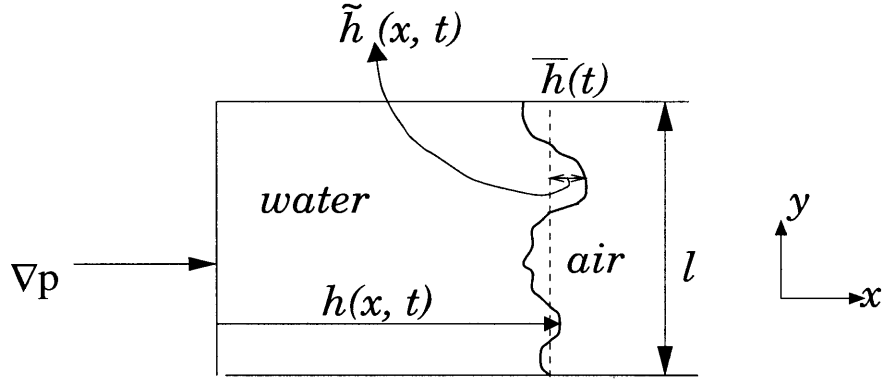

Figure 13-2: The notation used in the analysis of the problem. $h(x,t)$ denotes the instantaneous configuration of the interface. $\bar{h}(t)$ denotes spatially averaged mean position of the interface, and $\tilde{h}(x,t)$ the deviation of the interface from its mean position. l denotes the macroscopic length scale of the porous medium and represents the length scale at which the exponents are measured.

Two-phase flows in porous media are governed by Darcy's law,

$$\mathbf{v} = -\kappa \nabla p, \tag{13.4}$$

relating the pressure gradient ∇p to the velocity field $\mathbf{v}$. κ represents the permeablilty

of the porous medium, which in our work will be taken to be a spatially uniform scalar quantity.[5] The assumption of fluid incompressibility requires that

$$\nabla \cdot \mathbf{v} = 0. \tag{13.5}$$

This volume conservation feature which contrasts two-phase fluid flows from random magnets has also been indicated in the work of Delker *et al.* [7]. Utilizing eqs. (13.4) and (13.5) we obtain

$$\nabla^2 p = 0. \tag{13.6}$$

Equation (13.6) possesses the general solution

$$p = -p_1 y + \frac{1}{2\pi} \int dk\, e^{|k|\tilde{y}} e^{ikx}\, \phi(k), \tag{13.7}$$

where p_1 represents the applied average pressure gradient, and $\tilde{y}$ the deviation from a flat interface situated at the mean position [see Fig. (13-2)]. The Fourier components $\phi(k)$ of the pressure field are unknown as yet, and are to be determined from the boundary condition imposed at the interface.

For fluid-fluid interfaces the Laplace condition relating the difference in the local pressures on the two sides of the interface to the local curvature of the interface constitutes the appropriate boundary condition.[6] However, for fluid interfaces in random media, this boundary condition needs to be modified to account for the random forces which act on the interface. The appropriate boundary condition is thereby derived starting from the Grinstein - Ma expression for the energy $\mathcal{H}$ of an

[5] In the spirit of simplicity, we ignore the possible tensorial nature of the permeability.

[6] This boundary condition is an equilibrium boundary condition, and needs to be supplemented by the deviatoric stress terms to account for any nonequilibrium phenomena that might be present. However, the assumption of a quasistatic response of the pressure field enables us to utilize an identical boundary condition for the situation at hand despite the presence of nonequilibrium phenomena.

interface in a random medium [10]:

$$\mathcal{H} = \int dx \left\{ \frac{\sigma}{2} \left(\frac{\partial h}{\partial x} \right)^2 - \int_{-\infty}^{h} dy \, [p(x,y) - \eta(x,h)] \right\}. \tag{13.8}$$

The appropriate boundary condition is obtained by then assuming quasistatic dynamics, thereby requiring that

$$\frac{\delta \mathcal{H}}{\delta h} = 0 \implies p(x,h) = -\sigma \frac{\partial^2 h}{\partial x^2} + \eta(x,h). \tag{13.9}$$

In the absence of the the random noise term the above boundary condition reduces to the classical Laplace boundary condition.

The field $\phi(k)$ is now obtained by first Fourier transforming eq. (13.9) and subsequently invoking eq. (13.7). For small deviations from a flat interface ($|k|h \ll 1$), the leading-order term in the expansion adopts the form

$$\phi(k) = p_1 h(k) + \sigma k^2 h(k) + \eta(k), \tag{13.10}$$

where

$$h(k) = \int dx \, e^{-ikx} h(x) \tag{13.11}$$

and

$$\eta(k) = \int dx \, e^{-ikx} \eta[x, h(x)] \tag{13.12}$$

denote the respective Fourier transforms of $h(x)$ and $\eta[x, h(x)]$. (In the interests of notational conciseness, the explicit time-dependence of h has been suppressed.)

The dynamical evolution of the interface is described by the normal component of Darcy's law:

$$\frac{\partial h}{\partial t} = -\kappa \mathbf{n} \cdot \nabla p, \tag{13.13}$$

where $\mathbf{n}$ represent the local unit normal to the interface. For a surface described parametrically by

$$y = h(x,t), \tag{13.14}$$

the unit normal is given by,

$$\mathbf{n} = \frac{\hat{\mathbf{y}} - \nabla_x h \hat{\mathbf{x}}}{\sqrt{1 + (\nabla_x h)^2}}. \tag{13.15}$$

In the above expression $\hat{\mathbf{x}}$ and $\hat{\mathbf{y}}$ denote the unit vectors in x and y directions respectively. Utilizing the above equation in eq. (13.13) we obtain

$$\frac{\partial h}{\partial t} = -\kappa \left[\frac{\partial p}{\partial y} - \frac{\partial h}{\partial x} \frac{\partial p}{\partial x} \right]_{y=h}. \tag{13.16}$$

(In the above equation, based on considerations of power counting we have neglected terms involving the products of time derivatives and spatial derivatives. This simplification is subject to *a posteriori* verification.) Substitution of (13.10) into (13.16), with p given by (13.7), leads to the Fourier representation of the dynamical equation of motion:

$$\begin{aligned} \frac{\partial \tilde{h}(k)}{\partial t} &= [\kappa p_1 - V]\delta(k) - \kappa p_1 |k| \tilde{h}(k) - \kappa \sigma k^2 |k| \tilde{h}(k) + \nu(k) \\ &\quad - \kappa p_1 \int dk' \, [k - k'][k'] \tilde{h}(k - k') \tilde{h}(k') - \kappa \sigma \int dk' \, [k - k'][k']^3 \tilde{h}(k - k') \tilde{h}(k'), \end{aligned} \tag{13.17}$$

with $\tilde{h}(k)$ the Fourier transform of $\tilde{h}(x)$, which in turn denotes the deviation from a flat interface moving at a velocity V. The $\nu(k)$ term represents the noise obtained from effecting the substitutions above.

Before discussing the individual cases of FFI and IMI in the context of eq. (13.17), we consider the noise $\nu(k)$. The expression for p obtained by substituting (13.10) into (13.7) contains the term

$$\zeta(x,y) = \frac{1}{2\pi} \int dk \, e^{ikx} \, e^{|k|y} \int dx' \, e^{-ikx'} \, \eta[x', h(x')], \tag{13.18}$$

representing the manifestation of the noise term η. From (13.18), the resulting two-point correlation of ζ thereby obtained is

$$\langle \zeta(x,y)\zeta(x',y') \rangle \sim \frac{y+y'}{(x-x')^2+(y+y')^2}. \tag{13.19}$$

As is intuitive, translational symmetry in the y direction is lost. We observe that the noise term $\zeta(x,y)$ exhibits long-range correlations in both x and y space. This results from the quasistatic assumption used to project out the fast relaxing variables, together with the special form of the driving field p, which necessarily needs to satisfy the Laplace equation (13.6) — features not accounted for in past works. Noise terms with long-range correlations have been studied in the past, albeit in a different context [18]. In a recent work, Chow [6] has proposed that $\alpha > 1/2$ would require the presence of long-range correlations in the noise. Our analysis appears to be the first to postulate the existence of such noise accompanying fluid flow through porous media. As is easily verified, long-range correlated noise of the type (13.19) modifies the scaling of the noise, whence ζ scales as $l^{-1/2}$. The inverse Fourier transform of $\nu(k)$, viz. $\nu(x)$, involves a dominant term of the form $\partial\zeta(x,h)/\partial h$, which can be expected to scale as $h^{-1}l^{-1/2}$. This behavior contrasts with random field noise, which scales as $h^{-1/2}l^{-1/2}$.

In contrasting eqs. (13.1) and (13.17), note that the last two terms of (13.17) are nonlinear in h. One might expect, and indeed confirm, that similar nonlinear terms arise from the next-order term in the expansion of $\phi(k)$. For example, a nonlinear term of the form $h\nabla^2 h$ (in physical space) is generated by such a procedure. However, for the eventual scaling analysis we have performed, the results are not modified by the presence of these additional terms (i.e. the leading nonlinear term scales as h^2l^{-2}). Accordingly, we do not dwell upon them here. More importantly, one should note the structure of the terms appearing in eq. (13.17). Explicitly, the first two terms exemplify the nonlocal nature of the dynamics in the normal driving force. The $|k|$ term has been predicted in the context of capillary line depinning, which also involves nonlocal dynamics [16]. Thus, from our microscale analysis of the equations of motion, we discern at least two main features distinguishing two-phase flows from

RFIM dynamics: (a) the structure of the noise term; and (b) the nonlocal nature of the terms present in the dynamical equations.

13.4 FFI – Depinning

In this section we consider the features specific to the experiments accompanying FFI depinning. In this case, p_1 is finite even though the mean velocity V may approach zero. Hence, the third term in (13.17), representing a nonlinear term is nonzero despite the proximity of the system to the depinning transition. Several mechanisms have been proposed to justify the presence of such a nonlinear term in the dynamics [34]. Through our analysis we propose one further possible source namely, the anisotropy of the driving force, coupled with the fact that the driving force at every interfacial point acts normal to the interface at that point. However, as we subsequently find, such a nonlinear term is irrelevant in the dynamical description of FFI depinning.

What is the nature of the roughness exponent that would be expected to arise from eq. (13.17) ? Two important features arise in this context :

(i) In addition to those terms explicitly indicated in the equations, the capillary term $\kappa\sigma k^2|k|\,\tilde{h}$ might, in the presence of a nonlinear term ν, generate a Darcy-scale 'surface tension'-like term (we eschew the details of this claim, which can be proved by a rigorous field-theoretic perturbation analysis). In such circumstances, we expect a general equation of the form,

$$\begin{aligned}\frac{\partial h(k)}{\partial t} = \quad & P_1\,|k|\,h(k) + P_2 k^2 h(k) + \nu(k) + \\ & P_1 \int dk'\,[k-k']\,[k']\,h(k-k')h(k'),\end{aligned} \tag{13.20}$$

wherein the other terms in eq. (13.17) have been discarded on the basis of power counting arguments.[7] Algebraic sign issues for the above coefficients necessarily play

[7]In the long length scale limit we can neglect terms based on the powers of the lengths which appear in the equation. Such a quantification is enabled by the utilization of the dynamical scaling $h \sim l^{\alpha}$.

a crucial role in interfacial stability, requiring a more sophisticated treatment than that attempted here.

(ii) The $|k|h(k)$ term dominates in the hydrodynamic (large wavelength) limit. However, flow experiments in porous media have persistently shown that the observed roughness exponents constitute an intermediate length scale phenomenon, rather than being a manifestation of asymptotic behavior [11]. Thus, we employ a dynamical Flory-type scaling [12] to analyze the intermediate length scales representative of experimental conditions. For instance, the small capillary number regime suggests a scenario wherein P_1 is small compared with the capillary terms (represented by P_2).

Respective scalings of various terms on the RHS of eq. (13.20) are as follows:[8]

$$|k|\, h(k) \sim h/l;\ k^2 h(k) \sim h/l^2;\ \int dk'\,(k-k')\,k'\,h(k-k')h(k') \sim h^2/l^2;\ \nu(k) \sim \Delta_o^{1/2}/hl^{1/2}$$

(wherein Δ_o represents the strength of the disorder). These scaling relations permit us to calculate the roughness exponents by matching the scalings of the individual terms with those of the noise. At long length scales the noise can be expected to occur as an delta-correlated annealed noise (cf. Narayan & Fisher [25] and Horvath *et al.* [13]). However, here we consider only the regime wherein the noise manifests as a quenched noise.

The results of such a Flory analysis are:

(a) Matching the second term with the noise yields

$$h \sim l^{3/4} \text{ for } l \ll \text{Min}(P_2^2/\Delta_o^{1/3}P_1^{4/3}, P_2/P_1).$$

The scaling exponent obtained in this regime ($\alpha = 3/4$) agrees well with the experimentally observed value of $\alpha = 0.8$. The length scales also appear to correspond to the experimental conditions as a consequence of the small capillary numbers characterizing such experiments.

[8] In contrast to the previous chapter, wherein the concepts of scaling where illustrated by rescaling the equation and then subsequently using the original equation, we use a more direct but completely equivalent approach here. In this approach, we equate the scalings of the different terms and allow the roughness exponent to be obtained as a direct result of the analysis.

(*b*) A similar exercise in matching the nonlinearity with the noise yields

$$h \sim l^{1/2} \text{ for } P_2^2/\Delta_o^{1/3}P_1^{4/3} \ll l \ll \Delta_o^{1/3}/P_1^{2/3}.$$

The self-consistency condition for the existence of such a regime (the nonlinear term dominates the linear term) requires that

$$\Delta_o^{2/3}P_1^{2/3}/P_2^2 \gg 1,$$

whence suggesting that this regime probably does not exist in the FFI case at low capillary numbers due to the weak strength of the disorder. However, manifestations of this regime are likely to appear at higher capillary numbers.

Thus, we propose that *the long-range correlated nature of the noise, unique to two-phase fluid flows, is responsible for the anomalous exponents observed in experiments. The observed range of exponents is a manifestation of cross-over behavior at higher capillary numbers. Furthermore, the nonlinear terms which are generated prove to be irrelevant at low capillary numbers due to the weak nature of the disorder and the presence of long length scale viscous smoothing effects.*

13.5 IMI - Depinning

In this section we propose an explanation for the different behaviors exemplified by the FFI and IMI regimes, hitherto unresolved. In the case of IMI, due to the strong disorder forces, the motion of the interface at any point depends only on the local disorder forces. In two dimensions, the pinning transition was argued by previous researchers [2] to be of the same universality class as the transitions occurring in directed percolation depinning (DPD), wherein the interface becomes pinned when strong impurities that stop its motion span the system. The main feature of IMI is the lack of an external driving force, in lieu of which capillary forces drive the flow. Consequently, we set $P_1 = 0$ in our equations. In such circumstances we expect a

general equation of the form

$$\frac{\partial h(k)}{\partial t} = P_2 k^2 h(k) + P_3 |k| k^2 h(k) + \nu(k) + P_5 \int dk' [k - k'][k']^3 h(k - k') h(k'). \quad (13.21)$$

The latter equation reveals that rotational symmetry about the surface normal is broken due to the presence of the nonlinear term $\nabla h \cdot \nabla(\nabla^2 h)$.[9] Thus, even in a geometrically isotropic porous media, anisotropy can be generated by the dynamics. Reasons for the presence of such a term can be attributed to a combination of two factors: (*a*) The driving force for the dynamics is the gradient of the pressure field, rather than the pressure itself; (*b*) The fact that the pressure field p satisfies the Laplace equation leads to an exponential decay of the pressure field in the direction normal to the interface. As postulated by Tang *et al.* [34], the presence of anisotropy in the dynamics can lead to the generation of a nonlinear term of the form $(\nabla h)^2$. Such terms, which were shown to be irrelevant in the FFI case, can be shown (by rigorous arguments, which are omitted here for the sake of brevity) to be relevant in this case, the reasons for which can be attributed to the strength of the disorder and the absence of the $|k|$ term. The presence of anisotropy places this model in the same universality class as DPD, which also constitutes an example of anisotropic depinning, thereby explaining the observed roughness exponent of $\alpha = 0.63$.

Thus, we propose that *the anisotropy generated in the description of dynamics is responsible for the universality class of imbibition, corresponding to* $\alpha = 0.63$. We believe that our arguments provide the first theoretical rationale for the experimentally observed distinction between FFI and IMI.

13.6 Summary

In summary, we have derived a new model for two-phase frontal displacement flows in random porous media. The underlying analysis utilizes a quasistatic approximation

[9] We are grateful to Prof. M. Kardar for this remark.

for the pressure field, along with Darcy's law governing the dynamical evolution of the interface. The resulting evolution equation contains nonlocal terms as well as a noise term, the latter exhibiting long-range correlations.

For FFI, a Flory-type scaling analysis was performed and the possible scaling regimes carefully delineated. Such an analysis yielded results in good agreement with experimental observations. Despite the success of our scaling analysis it is to be cautioned here that dynamical Flory-type analysis does not enjoy the same success as equilibrium Flory scaling [18]. It does, however, provide a lower bound for RG calculations.

We also studied the IMI regime, pointing out the distinctions between FFI and IMI, and justifying anisotropic depinning in the IMI case. Our analysis points up the marked contrast between two-phase fluid dynamics in random media and random magnets, thereby rationalizing existing discrepancies between experimental measurements of two-phase flows and analytical calculations thereof based on RFIM.

References

[1] L. A. N. Amaral, A.-L. Barabasi and H. E. Stanley, "Universality classes for interface growth with quenched disorder," *Phys. Rev. Lett.*, **73**, 62, (1994).

[2] L. A. N. Amaral, A.-L. Barabasi, H. A. Makse and H. E. Stanley, "Scaling properties of driven interfaces in disordered media," *Phys. Rev. E*, **52**, 4087 (1995).

[3] A.-L. Barabasi and H. E. Stanley, *Fractal Concepts in Surface Growth*, Cambridge University Press, Cambridge (1995).

[4] F. Brochard and P. G. de Gennes, "Phase transitions of binary mixtures in random media," *J. Phys. Lett. (Paris)*, **44**, L758 (1983).

[5] R. Bruinsma and G. Aeppli, "Interface motion and nonequilibrium properties of the random-field Ising model," *Phys. Rev. Lett.*, **52**, 1547 (1984).

[6] T. S. Chow, "Noise and fluctuations of rough surfaces," Phys. Rev. Lett., **79**, 1086 (1997).

[7] T. Delker, D. B. Pengra and P.-Z. Wong, "Interface pinning and the dynamics of capillary rise in porous media," *Phys. Rev. Lett.* **76**, 2902 (1996).

[8] F. Family and T. Viscek, *Dynamics of Fractal Surfaces*, World Scientific, Singapore (1991).

[9] M. E. Fisher, "Renormalization group theory: Its basis and formulation in statistical physics," *Reviews of Modern Physics*, **70**, 653 (1998).

[10] G. Grinstein and S. K. Ma, "Surface tension, roughening and lower critical dimension in the random-field ising model," *Phys. Rev. B*, **28**, 2588 (1983).

[11] S. He, G. L. M. K. S. Kahanda and P.-Z. Wong, "Roughness of wetting fluid invasion fronts in porous media," *Phys. Rev. Lett.*, **69**, 3731 (1992).

[12] H. G. E. Hentschel and F. Family, "Scaling in open dissipative systems," *Phys. Rev. Lett.*, **66**, 1982 (1991). Phys. Rev. Lett., **66**, 703 (1991).

[13] V. K. Horvath, F. Family and T. Viscek, "Dynamic scaling of the interface in two-phase fluid flows," *J. Phys. A*, **24**, L25 (1991).

[14] V. K. Horvath, F. Family and T. Viscek, "Anomalous noise distribution of the interface in two-phase fluid flow," Phys. Rev. Lett., **67**, 3207 (1991).

[15] V. K. Horvath and H. E. Stanley, "Temporal scaling of interfaces propagating in porous media," *Phys. Rev. E*, **52**, 5166 (1995).

[16] J. F. Joanny and P. G. de Gennes, "A model for contact line hysteresis," *J. Chem. Phys.*, **81**, 552 (1984).

[17] L. P. Kadanoff, "Static phenomena near critical points: Theory and Experiment," *Rev. Mod. Phys.*, **39**, 395 (1967).

[18] M. Kardar, "Domain-walls subject to quenched impurities," *J. Appl. Phys.*, **61**, 3601 (1987).

[19] M. Kardar, "Statistical Mechanics of Fields," Unpublished Notes (1998).

[20] D. A. Kessler, H. Levine and Y. Tu, "Interface fluctuations in random media," *Phys. Rev. A*, **43**, 4551 (1991).

[21] J. Krug and P. Meakin, "Kinetic roughening of Laplacian fronts," *Phys. Rev. Lett.*, **66**, 703 (1991).

[22] H. Leschhorn, "Interface depinning in a disordered medium: Numerical results," *Physica A*, **195**, 324 (1993).

[23] K. Maloy, J. Feder and T. Joassang, "Viscous fingering fractals in porous media," *Phys. Rev. Lett.*, **55**, 2688 (1985).

[24] N. Martys, M. Cieplak and M. O. Robbins, "Critical phenomena in fluid invasion of porous media," *Phys. Rev. Lett.*, **66**, 1058 (1991).

[25] O. Narayan and D. S. Fisher, "Threshold critical dynamics of driven interfaces in random media," *Phys. Rev. B*, **48**, 7030 (1993).

[26] T. Nattermann, S. Stepanow, L.-H. Tang and H. Leschhorn, "Dynamics of interface depinning in a disordered medium," *J. Phys. II*, **2**, 1483 (1992).

[27] C. S. Nolle, B. Koiller, N. Martys and M. O. Robbins, "Morphology and dynamics of interfaces in random two-dimensional media," *Phys. Rev. Lett.*, **71**, 2075 (1993).

[28] P. Pelce, *Dynamics of curve fronts*, Academic Press, San Diego (1988).

[29] M. A. Rubio, C. A. Edwards, A. Dougherty and J. P. Gollub, "Self-Affine fractal interfaces from immiscible displacement in porous media," Phys. Rev. Lett., **63**, 1685 (1989).

[30] P. G. Saffman and G. I. Taylor, "The penetration of a fluid into a porous medium or a Hele-Shaw cell containing a more viscous liquid,", *Proc. R. Soc. Lond.*, **A245**, 312 (1958).

[31] S. Stepanow, "Dynamics of growing interfaces in a disordered medium: The effect of lateral growth," *J. Phys. II*, **5**, 11 (1995).

[32] J. P. Stokes, D. A. Weitz, J. P. Gollub, A. Dougherty, M. O. Robbins, P. M. Chaikin and H. M. Lindsay, "Interfacial stability of immiscible displacement in a porous medium," *Phys. Rev. Lett.*, **57**, 1718 (1986).

[33] J. P. Stokes, A. P. Kushnick and M. O. Robbins, "Interface dynamics in porous media: A random-field description," *Phys. Rev. Lett.*, **60**, 1386 (1988).

[34] L.-H. Tang, M. Kardar and D. Dhar, "Driven depinning in anisotropic media," *Phys. Rev. Lett.*, **74**, 920 (1996).

[35] D. A. Weitz *et al.*, "Dynamic capillary pressure in porous media: origin of the viscous fingering length scale," *Phys. Rev. Lett.*, **59**, 2967 (1987).

[36] Y.-C. Zhang, "Non-universal roughening of kinetic self-affine interfaces," *J. Phys. (Paris)*, **51**, 2129 (1990).

Chapter 14

Summary

In this part of the thesis we outlined some salient concepts utilized in the quantitative description of 'self-similar' and 'self-affine' systems. In particular, we claimed that self-similarity and self-affinity requires that the system be identical to itself under appropriate rescalings of the spatial and temporal variables.[1] In such a scenario, the requirement of similarity of the system at all scales constrains the equations governing the rescaled variables to be identical to the original equation, except for possible renormalizations of the coefficients present therein.

We then extended the concept of self-affinity to encompass random fractals, wherein the statistical properties of the fractal satisfy the constraints imposed by self-affinity. This feature enabled us to calculate the statistical properties of random interfaces based on simple scaling analysis. The implementation of these scaling analyses typically required a coarse-graining of the system (or rescaling of the spatial variables), followed by implementation of the constraint arising from the self-affine nature of the functions. *This is in contrast to the rest of the thesis, which required elaborate calculations pertaining to the coarse-graining of the microscale system.*

Subsequently, we elucidated the power of the scaling concepts and the accompanying subtleties by utilizing it for modeling and predicting the roughness exponents of two-phase fluid interfaces in random media. The explicit results derived from such

[1]This rescaling procedure must, of course, be such that the rescaled lengths be greater than a lower cutoff length and smaller than some upper cutoff length.

an analysis represented what we believe to be one of the first theoretical explanations of existing experimental observations. Explicit account was given of the nonlocal dynamics (in a quasistatic approximation) involved in two-phase fluid dynamics quantifying flow through porous media. The results were then used to derive the dynamical equation of motion of a Darcy-scale interfacial fluid front. We then considered the cases of invasion and imbibition separately, and pointed out the features responsible for the different depinning exponents observed in the two cases. A Flory-type scaling analysis was also performed on this model, yielding a roughness exponent $\alpha = 3/4$ in a range of intermediate length scales — in good agreement with experimental observations. Our model possessed a number of features absent in the model widely speculated to be applicable to this scenario, namely the Random Field Ising Model (RFIM). Among other things, our model incorporated physical phenomena existing in two-phase fluid flow phenomena that are not reflected in the RFIM model. Additionally, our model furnishes possible reasons for rationalizing discrepancies observed between experiments and theory.

Appendix A

Scaling in the Inner Region

The following identities are easily obtained (refer [1]; the truncated versions appearing below retain only those terms necessary in the subsequent analysis):

$$\tilde{\nabla} \equiv \frac{\mathbf{i}_1}{\tilde{h}_1}\frac{\partial}{\partial q_1} + \frac{\mathbf{i}_2}{\tilde{h}_2}\frac{\partial}{\partial q_2} + \frac{\mathbf{i}_3}{\delta}\frac{\partial}{\partial \tilde{n}}, \tag{A.1}$$

$$\tilde{\nabla}\cdot\tilde{\boldsymbol{\phi}} \equiv \tilde{h}_1\tilde{h}_2\left[\frac{\partial}{\partial q_1}\left(\frac{\tilde{\phi}_1}{\tilde{h}_2}\right) + \frac{\partial}{\partial q_2}\left(\frac{\tilde{\phi}_2}{\tilde{h}_1}\right) + \frac{1}{\delta}\frac{\partial}{\partial \tilde{n}}\left(\frac{\tilde{\phi}_3}{\tilde{h}_1\tilde{h}_2}\right)\right], \tag{A.2}$$

$$\tilde{\nabla}^2\tilde{\phi} \equiv \tilde{h}_1\tilde{h}_2\left[\frac{\partial}{\partial q_1}\left(\frac{\tilde{h}_1}{\tilde{h}_2}\frac{\partial\tilde{\phi}}{\partial q_1}\right) + \frac{\partial}{\partial q_2}\left(\frac{\tilde{h}_2}{\tilde{h}_1}\frac{\partial\tilde{\phi}}{\partial q_2}\right) + \frac{1}{\delta^2}\frac{\partial}{\partial \tilde{n}}\left(\frac{1}{\tilde{h}_1\tilde{h}_2}\frac{\partial\tilde{\phi}}{\partial \tilde{n}}\right)\right]. \tag{A.3}$$

Further, as a consequence of our requirement that the curvatures be macroscopic, the principal curvatures [2]

$$\kappa_1 = -\frac{1}{\delta h_{10}}\frac{\partial\tilde{h}_1}{\partial\tilde{n}}\bigg|_{\tilde{n}=0}, \tag{A.4}$$

$$\kappa_2 = -\frac{1}{\delta h_{20}}\frac{\partial\tilde{h}_2}{\partial\tilde{n}}\bigg|_{\tilde{n}=0}, \tag{A.5}$$

are assumed to be $O(1)$. (Refer to section 3.5 for the definitions of h_1, h_2.)

The following expressions furnish the leading-order terms for some of the quantities appearing in equations (3.31). Using (A.2) we obtain

$$\mathbf{I} : \mathbf{D} = \tilde{h}_1\tilde{h}_2\left[\frac{\partial}{\partial q_1}\left(\frac{\tilde{v}_1}{\tilde{h}_2}\right) + \frac{\partial}{\partial q_2}\left(\frac{\tilde{v}_2}{\tilde{h}_1}\right) + \frac{1}{\delta}\frac{\partial}{\partial \tilde{n}}\left(\frac{\tilde{v}_3}{\tilde{h}_2\tilde{h}_1}\right)\right], \tag{A.6}$$

$$\boldsymbol{\tau}_v = -\frac{2}{3}\mu\left[\mathbf{i}_1\mathbf{i}_1+\mathbf{i}_2\mathbf{i}_2\right]\frac{1}{\delta}\frac{\partial \tilde{v}_3}{\partial \tilde{n}}+\mu\mathbf{i}_3\mathbf{i}_3\left(2\frac{1}{\delta}\frac{\partial \tilde{v}_3}{\partial \tilde{n}}-\frac{2}{3}\mu(\mathbf{I} : \mathbf{D})\right)+\mu(\mathbf{i}_1\mathbf{i}_3+\mathbf{i}_3\mathbf{i}_1)\left[\tilde{h}_1\frac{\partial \tilde{v}_3}{\partial q_1}-\tilde{v}_1\kappa_1+\frac{1}{\delta}\frac{\partial \tilde{v}_1}{\partial \tilde{n}}\right]$$

$$+\mu(\mathbf{i}_2\mathbf{i}_3+\mathbf{i}_3\mathbf{i}_2)\left[\tilde{h}_2\frac{\partial \tilde{v}_3}{\partial q_2}-\tilde{v}_2\kappa_2+\frac{1}{\delta}\frac{\partial \tilde{v}_2}{\partial \tilde{n}}\right], \tag{A.7}$$

$$\boldsymbol{\tau}_c = -\mathrm{Ca}^{-1}\frac{(\mathbf{i}_1\mathbf{i}_1+\mathbf{i}_2\mathbf{i}_2)}{\delta}\left(\frac{\partial \tilde{c}_o}{\partial \tilde{n}}\right)^2. \tag{A.8}$$

At $O(1/\delta^2)$ the contribution to $\tilde{\nabla}\cdot\tilde{\boldsymbol{\tau}}_v$ is

$$\mathbf{i}_1\frac{\partial}{\partial \tilde{n}}\left(\mu\frac{\partial \tilde{v}_{10}}{\partial \tilde{n}}\right)+\mathbf{i}_2\frac{\partial}{\partial \tilde{n}}\left(\mu\frac{\partial \tilde{v}_{20}}{\partial \tilde{n}}\right)+\mathbf{i}_3\frac{\partial}{\partial \tilde{n}}\left(\frac{4}{3}\mu\frac{\partial \tilde{v}_{30}}{\partial \tilde{n}}\right), \tag{A.9}$$

whereas the corresponding contribution at $O(1/\delta)$ is

$$\mathbf{i}_1\left\{h_{10}h_{20}h_{30}\frac{\partial}{\partial q_1}\left(-\frac{2}{3}\mu\frac{\partial v_{30}}{\partial \tilde{n}}\frac{1}{h_{20}}\right)+\frac{\partial}{\partial \tilde{n}}\left[\mu\left(\frac{\partial \tilde{v}_{11}}{\partial \tilde{n}}+h_{10}\frac{\partial \tilde{v}_{30}}{\partial q_1}-\tilde{v}_{10}\kappa_1\right)\right]+\mu\frac{\partial \tilde{v}_{10}}{\partial \tilde{n}}(\kappa_1+\kappa_2)+\mu\frac{\partial \tilde{v}_{10}}{\partial \tilde{n}}\kappa_1\right\}$$

$$+\mathbf{i}_2\left\{h_{10}h_{20}h_{30}\frac{\partial}{\partial q_2}\left(-\frac{2}{3}\mu\frac{\partial v_{30}}{\partial \tilde{n}}\frac{1}{h_{10}}\right)+\frac{\partial}{\partial \tilde{n}}\left[\mu\left(\frac{\partial \tilde{v}_{21}}{\partial \tilde{n}}+h_{10}\frac{\partial \tilde{v}_{30}}{\partial q_1}-\tilde{v}_{20}\kappa_2\right)\right]+\mu\frac{\partial \tilde{v}_{20}}{\partial \tilde{n}}(\kappa_1+\kappa_2)+\mu\frac{\partial \tilde{v}_{20}}{\partial \tilde{n}}\kappa_2\right\}$$

$$+\mathbf{i}_3\left\{h_{10}h_{20}h_{30}\frac{\partial}{\partial q_1}\left(\frac{\mu}{h_{20}}\frac{\partial v_{10}}{\partial \tilde{n}}\right)+h_{10}h_{20}h_{30}\frac{\partial}{\partial q_2}\left(\frac{\mu}{h_{20}}\frac{\partial v_{20}}{\partial \tilde{n}}\right)+\frac{\partial}{\partial \tilde{n}}\left(2\mu\frac{\partial \tilde{v}_{31}}{\partial \tilde{n}}\right)-\frac{2}{3}\frac{\partial(\mu\chi)}{\partial \tilde{n}}+\right.$$
$$\left.\frac{2}{3}\mu\frac{\partial \tilde{v}_{30}}{\partial \tilde{n}}(\kappa_1+\kappa_2)\right\}. \tag{A.10}$$

In the above, χ denotes the quantity

$$\chi = h_{10}h_{20}\left[\frac{\partial}{\partial q_1}\left(\frac{\tilde{v}_{10}}{h_{20}}\right) + \frac{\partial}{\partial q_2}\left(\frac{\tilde{v}_{20}}{h_{10}}\right) + \frac{1}{h_{20}h_{10}}\frac{\partial\left(\tilde{v}_{31}\right)}{\partial\tilde{n}} + \tilde{v}_{30}\frac{\partial}{\partial\tilde{n}}\left(\frac{1}{\tilde{h}_2\tilde{h}_1}\right)\right]. \tag{A.11}$$

Using the solution of the diffusion equation (3.55) at leading order, we find that the $O(1/\delta^2)$ contribution to $\tilde{\nabla}\cdot\tilde{\boldsymbol{\tau}}_c$ is identically zero, whereas at $O(1/\delta)$ we obtain

$$\tilde{\nabla}\cdot\tilde{\boldsymbol{\tau}}_c = \mathbf{i}_3\mathrm{Ca}^{-1}\left[(\kappa_1+\kappa_2)\left(\frac{\partial\tilde{c}_0}{\partial\tilde{n}}\right)^2\right]. \tag{A.12}$$

Summarized below are the respective forms of the various matching conditions derived within the framework of the singular surface model for the specific geometry chosen to represent the interface [2]. The velocity matching condition for this material interface is

$$\mathbf{v}_0^+ = \mathbf{v}_0^- \quad \text{at } n=0 \tag{A.13}$$

or, equivalently,

$$[[\mathbf{v}_0]] = \mathbf{0}. \tag{A.14}$$

The stress matching condition is

$$\mathbf{n}\cdot[[\mathbf{P}_0]] = -2\sigma\mathcal{H}\mathbf{n} \quad \text{at } n=0, \tag{A.15}$$

where σ denotes the interfacial tension, $\mathbf{n}$ the unit normal to the interface (pointing in the direction from $-$ to $+$), and

$$\mathcal{H} \equiv \frac{\kappa_1+\kappa_2}{2} \tag{A.16}$$

the mean curvature of the interface. In terms of the semi-orthogonal curvilinear

coordinates (q_1, q_2, n) the above conditions can be written as

$$\left[\left[-p_0 + 2\mu\frac{\partial v_{30}}{\partial n}\right]\right] = -2\sigma\mathcal{H}, \tag{A.17}$$

$$\left[\left[\mu\left(h_{10}\frac{\partial v_{30}}{\partial q_1} + \frac{\partial v_{10}}{\partial n} - v_{10}\kappa_1\right)\right]\right] = 0, \tag{A.18}$$

$$\left[\left[\mu\left(h_{20}\frac{\partial v_{30}}{\partial q_2} + \frac{\partial v_{20}}{\partial n} - v_{20}\kappa_2\right)\right]\right] = 0. \tag{A.19}$$

Consistent with our earlier assumptions, surface rheological effects have been assumed absent.

References

[1] J. Happel & H. Brenner, *Low Reynolds Number Hydrodynamics*, Kluwer, Netherlands (1983).

[2] . A. Edwards, H. Brenner and D. T. Wasan *Interfacial Transport Processes and Rheology*, Butterworth-Heinemann, Boston (1991).

Appendix B

Proof of Theorem 1

This section is largely based on Brenner [1]. We use the following identities, proofs of which are left as an exercise for the interested reader.

Identity 1 *A time periodic (or almost time periodic) function ψ possessing a spatially periodic gradient can be decomposed as follows:*

$$\psi = \breve{\psi}(\mathbf{R}, t) + \mathbf{R} \cdot \overline{\mathbf{F}} + \mathbf{R} \cdot \overline{\mathbf{F}'}(t), \tag{B.1}$$

where $\breve{\psi}(\mathbf{R}, t)$ is a spatially- and time-periodic function, and

$$\overline{\mathbf{F}} = \frac{1}{\tau_o} \int_t \oint_{\partial\tau_o} d\mathbf{s}\, \psi, \tag{B.2}$$

$$\overline{\mathbf{F}}' = \oint_{\partial\tau_o} d\mathbf{s}\, \psi - \bar{\mathbf{F}}. \tag{B.3}$$

It follows easily that

$$\int_t \overline{\mathbf{F}}' = \mathbf{0}. \tag{B.4}$$

Identity 2 *For $\breve{\psi}$ a spatially periodic function, the following identity holds:*

$$\int_t \int_{\mathbf{s}_k} d\mathbf{s} \cdot \breve{\psi} = \frac{1}{\tau_o} \mathbf{s}_k \cdot \int_t \oint_{\partial \tau_o} \mathbf{r} d\mathbf{s} \cdot \breve{\psi}. \tag{B.5}$$

In what follows, we outline the proof of Theorem 1.

Proof of Theorem 1

The macroscopic flux density tensor $\overline{\mathbf{M}}$ is defined as

$$\mathbf{s}_k \cdot \overline{\mathbf{M}} = \int_t \int_{\mathbf{s}_k} d\mathbf{s} \cdot \mathbf{M}. \tag{B.6}$$

Using Identity 1 we have that

$$\mathbf{s}_k \cdot \overline{\mathbf{M}} = \int_t \int_{\mathbf{s}_k} d\mathbf{s} \cdot \left[\breve{\mathbf{M}}(\mathbf{R}, t) + \mathbf{R} \cdot \overline{\mathbf{G}} + \mathbf{R} \cdot \overline{\mathbf{G}'}(t) \right], \tag{B.7}$$

where $\overline{\mathbf{G}}$ and $\overline{\mathbf{G}}'$ are defined as in (B.2) and (B.3). Upon using (B.4) and neglecting $O(\|l\|)$ terms [i.e. writing $\mathbf{R} = \overline{\mathbf{R}} + O(\|l\|)$], we obtain

$$\mathbf{s}_k \cdot \overline{\mathbf{M}} = \int_t \int_{\mathbf{s}_k} d\mathbf{s} \cdot \breve{\mathbf{M}}(\mathbf{R}, t) + \mathbf{s}_k \cdot \overline{\mathbf{R}} \cdot \overline{\mathbf{G}}. \tag{B.8}$$

Identity 2 thereby yields

$$\mathbf{s}_k \cdot \overline{\mathbf{M}} = \frac{1}{\tau_o} \mathbf{s}_k \cdot \int_t \oint_{\partial \tau_o} \mathbf{r} d\mathbf{s} \cdot \breve{\mathbf{M}} + \mathbf{s}_k \cdot \overline{\mathbf{R}} \cdot \overline{\mathbf{G}}. \tag{B.9}$$

Using Identity 1 to write $\breve{\mathbf{M}}$ in terms of $\mathbf{M}$, $\overline{\mathbf{G}}$ and $\overline{\mathbf{G}'}(t)$, and upon further neglecting terms of order $O(\|l\|)$, one thereby obtains

$$\mathbf{s}_k \cdot \overline{\mathbf{M}} = \frac{1}{\tau_o} \mathbf{s}_k \cdot \int_t \oint_{\partial \tau_o} \mathbf{r} d\mathbf{s} \cdot \mathbf{M} + \frac{1}{\tau_o} \mathbf{s}_k \cdot \int_t \oint_{\partial \tau_o} \mathbf{r} d\mathbf{s} \cdot \overline{\mathbf{G}}'. \tag{B.10}$$

Subsequent use of (B.4) jointly with the fact that $\mathbf{s}_k$ can be of arbitrary magnitude and direction thereby furnishes a proof of the first part of Theorem 1.

To prove the second part of the theorem we observe that the spatial periodicity of the porous medium requires that $\mathbf{s}_k\{\mathbf{n}\} = \mathbf{s}_k\{\mathbf{n} + d\mathbf{n}\}$, where $\mathbf{n} + d\mathbf{n}$ denotes the face of an adjacent cell. Consequently, (4.32) implies that

$$\mathbf{s}_k \cdot \left[\overline{\mathbf{M}}(\mathbf{R}_{n+dn}) - \overline{\mathbf{M}}(\mathbf{R}_n)\right] = \int_t \int_{\mathbf{s}_k\{\mathbf{n}\}} d\mathbf{s} \cdot \left[\mathbf{M}(\mathbf{s}_k\{\mathbf{n} + d\mathbf{n}\}) - \mathbf{M}(\mathbf{s}_k\{\mathbf{n}\})\right]. \tag{B.11}$$

However, since $\mathbf{R}_n \equiv \overline{\mathbf{R}}$ and $\mathbf{R}_{n+dn} \equiv \overline{\mathbf{R}} + d\overline{\mathbf{R}}$, it follows that

$$\left[\overline{\mathbf{M}}(\mathbf{R}_{n+dn}) - \overline{\mathbf{M}}(\mathbf{R}_n)\right] = \mathbf{l}_k \cdot \bar{\nabla}\overline{\mathbf{M}}.$$

Application of Identity 1 to the right-hand side of (B.11) yields

$$\int_t \int_{\mathbf{s}_k} d\mathbf{s} \cdot \left[\mathbf{M}(\mathbf{s}_k\{\mathbf{n} + d\mathbf{n}\}) - \mathbf{M}(\mathbf{s}_k\{\mathbf{n}\})\right] = \mathbf{l}_k \cdot \overline{\mathbf{G}} \cdot \mathbf{s}_k.$$

Upon combining the above two results, one verifies the second part of Theorem 1. Q. E. D.

References

[1] H. Brenner, "Elements of Transport Processes in Porous Media," 9 folios of unpublished notes (1972).

Appendix C

On the Equivalence of Mass Flux and Momentum Density Definitions of the Macroscale Velocity

Consider (4.36), representing the definition of the macroscopic velocity based upon the mass flux:

$$\varepsilon\overline{\rho}\,\overline{\mathbf{v}} = \frac{1}{\tau_o}\int_t \oint_{\partial\tau_o} \mathbf{r}d\mathbf{s}\cdot\rho\mathbf{v}. \tag{C.1}$$

Gauss's divergence theorem yields

$$\varepsilon\overline{\rho}\,\overline{\mathbf{v}} = \frac{1}{\tau_o}\int_t\int_{\tau_o} \nabla\cdot(\rho\mathbf{v}\mathbf{r})\,d^3\mathbf{r}, \tag{C.2}$$

in which we have utilized the fact that in our diffuse interface model all fields are continuous throughout the unit cell, except at the surface of the solid particle, where $\mathbf{v}=\mathbf{0}$. The right-hand side can be simplified further as

$$\varepsilon\overline{\rho}\,\overline{\mathbf{v}} = \frac{1}{\tau_o}\int_t\int_{\tau_o} \mathbf{r}\nabla\cdot(\rho\mathbf{v})\,d^3\mathbf{r} + \frac{1}{\tau_o}\int_t\int_{\tau_o} \rho\mathbf{v}\,d^3\mathbf{r}, \tag{C.3}$$

which upon using the microscale equation of continuity (3.9) for the mixture can be written alternatively as

$$\varepsilon\overline{\rho}\,\overline{\mathbf{v}} = \frac{1}{\tau_o}\int_t\int_{\tau_o}\mathbf{r}(-\frac{\partial\rho}{\partial t})\,d^3\mathbf{r} + \frac{1}{\tau_o}\int_t\int_{\tau_o}\rho\mathbf{v}\,d^3\mathbf{r}. \tag{C.4}$$

Interchange of the space and time integrations in the first integral gives

$$\varepsilon\overline{\rho}\,\overline{\mathbf{v}} = \frac{1}{\tau_o}\int_{\tau_o}\mathbf{r}d^3\mathbf{r}\int_t(-\frac{\partial\rho}{\partial t}) + \frac{1}{\tau_o}\int_t\int_{\tau_o}\rho\mathbf{v}\,d^3\mathbf{r}. \tag{C.5}$$

The first integral vanishes in view of the assumed steadiness of the macroscale fields, whence (4.26) is obtained. Q. E. D.

Appendix D

On the Definitions of the Macroscopic Pressure and the Stress Tensor

The macroscopic stress tensor is defined in (4.41). Separation of the latter into respective pressure and deviatoric stress contributions is arbitrary. Usually, the quantity of significance is the pressure gradient rather than the pressure itself [1]. Here, we adopt the convention of assigning the mean stress to the pressure term. Thus, we define

$$\overline{p} \stackrel{\text{def.}}{=} -\frac{1}{3}\mathbf{I}:\overline{\mathbf{P}}, \tag{D.1}$$

whence

$$\overline{\boldsymbol{\tau}} = \overline{\mathbf{P}} - \frac{1}{3}\mathbf{I}(\mathbf{I}:\overline{\mathbf{P}}). \tag{D.2}$$

This decomposition furnishes expressions (4.43) and (4.44). Upon applying Identity 1 to (4.44) one obtains, upon neglecting $O(\|l\|)$ terms,

$$\overline{\boldsymbol{\tau}} = -\frac{1}{\tau_o}\int_t \oint_{\partial\tau_o} (\mathbf{r}\mathbf{I} - \frac{1}{3}\mathbf{I}\mathbf{r}) \cdot d\mathbf{s} \cdot (\rho\mathbf{v}\mathbf{v}' + \breve{\mathbf{P}}). \tag{D.3}$$

(The value of the integral multiplying $\overline{\mathbf{R}} \cdot \overline{\mathbf{G}}$ is identically zero.) Since the above quadrature involves averaging spatial- and time-periodic functions respectively over a unit cell and one time period, we find that

$$\bar{\nabla} \cdot \overline{\boldsymbol{\tau}} = \mathbf{0}. \tag{D.4}$$

Thus,

$$\bar{\nabla} \cdot \overline{\mathbf{P}} = -\bar{\nabla}\overline{p}. \tag{D.5}$$

Using Theorem 1 it follows that

$$\bar{\nabla}\overline{p} = -\frac{1}{\tau_o}\int_t \oint_{\partial\tau_o} d\mathbf{s} \cdot \mathbf{P}, \tag{D.6}$$

which requires that

$$\bar{\nabla}\overline{p} = -\frac{1}{\tau_o}\int_t \oint_{\partial\tau_o} d\mathbf{s} \cdot \Big(- p\mathbf{I} + \boldsymbol{\tau}\Big). \tag{D.7}$$

Explicitly,

$$\bar{\nabla}\overline{p} = \frac{1}{\tau_o}\int_t \oint_{\partial\tau_o} d\mathbf{s} p - \frac{1}{\tau_o}\int_t \oint_{\partial\tau_o} d\mathbf{s} \cdot \boldsymbol{\tau}. \tag{D.8}$$

The second integral vanishes in view of the spatial periodicity of $\boldsymbol{\tau}$, whereupon (4.45) is recovered.

References

[1] H. Brenner, "Elements of Transport Processes in Porous Media," 9 folios of unpublished notes (1972).

Appendix E

Generalized Darcy's Law

We assume a general form for the constitutive equations, allowing for coupling between the fluxes. However, recognition that $\overline{\mathbf{J}}_1 + \overline{\mathbf{J}}_2 = \mathbf{0}$ requires that only two of the phenomenological tensors $\mathbf{\Lambda}_{1k}, \mathbf{\Lambda}_{2k}$ $(k = 1, 2)$ be independent quantities. Consequently,

$$\overline{\mathbf{J}}_1 = -\overline{\mathbf{J}}_2 = \mathbf{\Lambda}'_{1a} \cdot \bar{\nabla}\left(\overline{\mu}_1 - \overline{\mu}_2\right) + \mathbf{\Lambda}'_{1b} \cdot \overline{\mathbf{v}} \tag{E.1}$$

and

$$\mathbf{F} = \mathbf{\Lambda}'_{1c}\overline{\mathbf{v}} + \mathbf{\Lambda}'_{1b} \cdot \bar{\nabla}\left(\overline{\mu}_1 - \overline{\mu}_2\right), \tag{E.2}$$

where the symmetry of the coupling tensors has been invoked. Substituting (E.2) into the linear momentum equation (4.54) gives

$$-\bar{\nabla}\overline{p} + \mathbf{\Lambda}'_{1c} \cdot \overline{\mathbf{v}} + \varepsilon \sum_{i=1}^{2} \overline{\rho}_i \mathbf{g}_i + \mathbf{\Lambda}'_{1b} \cdot \bar{\nabla}\left(\overline{\mu}_1 - \overline{\mu}_2\right) = \mathbf{0}; \tag{E.3}$$

equivalently,

$$\overline{\mathbf{v}} = (\mathbf{\Lambda}'_{1c})^{-1} \cdot (\bar{\nabla}\overline{p} - \varepsilon \sum_{i=1}^{2} \overline{\rho}_i \mathbf{g}_i) - (\mathbf{\Lambda}'_{1c})^{-1} \cdot \mathbf{\Lambda}'_{1b} \cdot \bar{\nabla}\left(\overline{\mu}_1 - \overline{\mu}_2\right). \tag{E.4}$$

[When coupling between the fluxes is neglected, the above reduces to the Darcy mixture law (6.7).] Furthermore, use of the relations

$$\overline{\mathbf{J}}_1 = \varepsilon\overline{\rho}_1(\overline{\mathbf{v}}_1 - \overline{\mathbf{v}}); \quad \overline{\mathbf{J}}_2 = \varepsilon\overline{\rho}_2(\overline{\mathbf{v}}_2 - \overline{\mathbf{v}}) \tag{E.5a,b}$$

yields

$$\varepsilon\overline{\rho}_1\overline{\mathbf{v}}_1 = \mathbf{\Lambda}''_a \cdot \bar{\nabla}\left(\overline{\mu}_1 - \overline{\mu}_2\right) + \mathbf{\Lambda}''_b \cdot (\bar{\nabla}\overline{p} - \varepsilon\sum_{i=1}^{2}\overline{\rho}_i\mathbf{g}_i) \tag{E.6}$$

and

$$\varepsilon\overline{\rho}_2\overline{\mathbf{v}}_2 = \mathbf{\Lambda}''_d \cdot \bar{\nabla}\left(\overline{\mu}_2 - \overline{\mu}_1\right) + \mathbf{\Lambda}''_c \cdot (\bar{\nabla}\overline{p} - \varepsilon\sum_{i=1}^{2}\overline{\rho}_i\mathbf{g}_i), \tag{E.7}$$

where the $\mathbf{\Lambda}''_a, \mathbf{\Lambda}''_b, \mathbf{\Lambda}''_d$ and $\mathbf{\Lambda}''_c$ are combinations of $\mathbf{\Lambda}'_{1a}, \mathbf{\Lambda}'_{1b}$ and $\mathbf{\Lambda}'_{1c}$. Knowledge of the explicit forms adopted by $\mathbf{\Lambda}''_a, \mathbf{\Lambda}''_b$, $\mathbf{\Lambda}''_d$, and $\mathbf{\Lambda}''_c$ will prove unnecessary; however, no symmetry in the coupling tensors could be identified despite the fact that only three of the above four phenomenological coefficients are independent. Use of (5.9a,b) gives

$$\bar{\nabla}\left(\overline{\mu}_1 - \overline{\mu}_2\right) = \frac{\overline{\rho}\,\bar{\nabla}\overline{p}_1}{\overline{\rho}_1} - \frac{\overline{\rho}\,\bar{\nabla}\overline{p}_2}{\overline{\rho}_2}, \tag{E.8}$$

which may be written alternatively as

$$\bar{\nabla}\left(\overline{\mu}_1 - \overline{\mu}_2\right) = \left(\frac{\bar{\nabla}\overline{p}_1}{\overline{\rho}_1} - \varepsilon\mathbf{g}_1\right) - \left(\frac{\bar{\nabla}\overline{p}_2}{\overline{\rho}_2} - \varepsilon\mathbf{g}_2\right). \tag{E.9}$$

Substitution into in (E.6) and (E.7) thereby yields

$$\overline{\mathbf{v}}_1 = (\mathbf{\Lambda}'_{11})^{-1} \cdot \left(\bar{\nabla}\overline{p}_1 - \varepsilon\overline{\rho}_1\mathbf{g}_1\right) + (\mathbf{\Lambda}'_{12})^{-1} \cdot \left(\bar{\nabla}\overline{p}_2 - \varepsilon\overline{\rho}_2\mathbf{g}_2\right), \tag{E.10}$$

$$\overline{\mathbf{v}_2} = (\mathbf{\Lambda}'_{21})^{-1} \cdot \left(\bar{\nabla}\overline{p}_1 - \varepsilon\overline{\rho}_1\mathbf{g}_1\right) + (\mathbf{\Lambda}'_{22})^{-1} \cdot \left(\bar{\nabla}\overline{p}_2 - \varepsilon\overline{\rho}_2\mathbf{g}_2\right), \tag{E.11}$$

where, again, the exact forms of the $\mathbf{\Lambda}'_{ij}$ $(i, j = 1...4)$ are unimportant.